IVW - Schriftenreihe Band 143
Institut für Verbundwerkstoffe GmbH - Kaiserslautern

Yves N. Becker

Development and investigation of a thermoplastic composite spinal implant under consideration of the interface between short and endless fibre reinforcement

Bibliografische Information Der Deutschen Bibliothek

Die Deutsche Bibliothek verzeichnet diese Publikation in der Deutschen Nationalbibliografie; detaillierte bibliografische Daten sind im Internet über <http://dnb.dnb.de> abrufbar.

Bibliographic information published by Die Deutsche Bibliothek

Die Deutsche Bibliothek lists this publication in the Deutsche Nationalbibliografie; detailed bibliographic data is available in the Internet at <http://dnb.dnb.de>.

Herausgeber: Institut für Verbundwerkstoffe GmbH
Prof. Dr.-Ing. Ulf Breuer
Erwin-Schrödinger-Straße
TU Kaiserslautern, Gebäude 58
67663 Kaiserslautern
http://www.ivw.uni-kl.de

Verlag: Institut für Verbundwerkstoffe GmbH

Druck: pri-me Printservice & Medienservice
Barbarossastr. 1
67655 Kaiserslautern
D-386

Als Manuskript gedruckt. Printed in Germany.
ISSN 1615-021X
ISBN 978-3-944440-40-8

Development and investigation of a thermoplastic composite spinal implant under consideration of the interface between short and endless fibre reinforcement

Vom Fachbereich Maschinenbau und Verfahrenstechnik
der Technischen Universität Kaiserslautern
zur Erlangung des akademischen Grades

Doktor-Ingenieur (Dr.-Ing.)
genehmigte
Dissertation

von
Herrn
Dipl.-Ing. Yves N. Becker
aus Homburg (Saar)

Tag der mündlichen Prüfung:	25. August 2020
Prüfungsvorsitzender:	Prof. Dr.-Ing. Joachim Hausmann
1. Berichterstatter:	Prof. Dr.-Ing. Ulf P. Breuer
2. Berichterstatter:	Prof. Dr.-Ing. Tilmann Beck

D 386

Vorwort

Die vorliegende Arbeit entstand im Rahmen meiner Tätigkeit als wissenschaftlicher Mitarbeiter an der Institut für Verbundwerkstoffe (IVW) GmbH im Kompetenzfeld Bauweisen der Abteilung Bauteilentwicklung.

Mein besonderer Dank gilt Herrn Prof. Dr.-Ing. Ulf P. Breuer für die Betreuung meiner Arbeit, die fachlichen Diskussionen und die Übernahme des Erstgutachtens. Außerdem danke ich Herrn Prof. Dr.-Ing. Tilmann Beck für die freundliche Übernahme des Zweitgutachtens und dem damit verbundenen Interesse an meiner Arbeit. Herrn Prof. Dr.-Ing. Joachim Hausmann danke ich für die Übernahme des Promotionsvorsitzes.

Ich danke Herrn Indek Raid vom Lehrstuhl für Messtechnik und Sensorik der Technischen Universität Kaiserslautern (TUK) für die Unterstützung bei der Durchführung der Messungen zur Oberflächentopografie, Herrn Prof. Dr.-Ing. Paul L. Geiß von der Arbeitsgruppe Werkstoff- und Oberflächentechnik der TUK für die Unterstützung bei der Durchführung der Kontaktwinkelmessungen und Herrn Dr.-Ing. Daniel Spriestersbach von der Arbeitsgruppe für Werkstoffprüfung der TUK für die Unterstützung bei den rasterelektronenmikroskopischen Aufnahmen. Zudem gilt mein Dank Herrn Cyprian Golebiewski von der Firma Akro-Plastic GmbH für die Materialbereitstellung und die Möglichkeit der Herstellung der Single Lap Shear Probekörper.

Ich danke den Neurochirurgen Herrn Markus Dietrich und Herrn Oscar Godino Martínez für Ihre Unterstützung und Ihr Interesse an der Forschungsarbeit. Ferner bedanke ich mich bei den Projektpartnern Herrn Salvador Llas Vargas, Herrn Ferran Mera Pelaez, Frau Ana Rodríguez Alonso, Frau Alba de los Santos Capdevila und Herrn Marc Serrahima Tornel von der spanischen Firma Neos Surgery S. L. sowie bei den Projektpartnern Herrn Johannes Dell, Herrn Armin Henning, Herrn Sven Pieper und Herrn Etienne Scheiber von der deutschen Firma Schliessmeyer GmbH für die konstruktive und freundschaftliche Zusammenarbeit.

Mein besonderer Dank gilt meiner Vorgesetzten Frau Dr.-Ing. Nicole Motsch-Eichmann für die Betreuung meiner Arbeit, die gewährten Freiräume und die ausgezeichnete Kollegialität. Darüber hinaus bedanke ich mich bei der gesamten Belegschaft der IVW GmbH für die freundschaftliche Zusammenarbeit und den wertvollen Erfahrungsaustausch. Besonders danken möchte ich Constantin Bauer, Christian Becker, Thorsten Becker, Matthias Bendler, Ulrich Blass, Marcel Bücker, Ariane McCauley, Pia Eichert, Stefan Gabriel, Hermann Giertzsch, Werner Gölzer, Benedikt Hannemann, Torsten Heydt, Valentine Kessler, Regina Köhne, Janna Krummenacker, Thomas Pfaff, Heidrun Plocharzik, Vitalij Popow, Jan Rehra, Thomas Rief, Florian Rieger, Florian Schimmer, Stefan Schmidt, Stefan Schmitt, Ralph Schneider, Petra Volk, Harald Weber und Torsten Weick. Der studentisch wissenschaftlichen Hilfskraft Herrn Mertcan Kaya danke ich für die Unterstützung bei Probenvorbereitung und Konstruktion.

Schließlich danke ich meiner Familie für den Rückhalt und die stete Unterstützung.

Homburg, im September 2020

Table of contents

Abstract

In recent years, thermoplastic composites (TPCs) have been increasingly used for aerospace and automotive applications. But also other industrial sectors, such as the medical technology, have discovered the benefits of this material class. Compared to thermoset composites, TPCs can be recycled more easily, remelted, and welded. In addition to that, TPC parts can be produced economically and efficiently. As an example, short cycle times and high production rates of TPCs can be realised with the injection moulding processing technology. Injection moulded parts have the advantage that function integration is feasible with relatively little effort.

However, these parts are characterised by discontinuous fibre reinforcement. Fibres are randomly distributed within the part and fibre orientation can show significant local variations. Whereas the highest stiffness and strength values of the material are achieved parallel to fibre orientation, the lowest values are present in transverse direction. As a consequence, structural mechanical properties of injection moulded discontinuous fibre reinforced parts are lower compared to their continuous fibre reinforced counterparts. Continuous fibre reinforced components show excellent specific mechanical properties. However, their freedom in geometrical product design is restricted.

The aim of this work is to extend the applicability of TPCs for structural mass products due to the realisation of a high-strength interface between discontinuous and continuous fibre reinforced material. A hybrid structure with unique properties is produced by overmoulding a continuous unidirectional endless carbon fibre (CF) reinforced polyether ether ketone (PEEK) insert with discontinuous short CF reinforced PEEK. This approach enables the manufacturing of structural mass products in short cycle times which require both superior structural mechanical properties and sufficient freedom in product design. However, sufficient interface strength between the discontinuous and continuous component is required.

This research is based on the application case of a pedicle screw system which is a spinal implant used for spine stabilisation and fusion. Since the 1990s, CF-PEEK has been successfully used for spinal cages, and recently also for pedicle screws and pedicle screw systems. Compared to metallic implants, CF-PEEK implants show several advantages, such as the reduction of stress shielding, the prevention of artefacts in medical imaging technologies (X-ray, computer tomography scan, or magnetic resonance imaging) or the avoidance of backscattering during radiotherapy. Pedicle screws, which are used in the lumbar spine region, are subjected to high forces and moments. Therefore, a hybrid composite pedicle screw was developed which is based on the overmoulding process described before.

Different adherence tests were conducted to characterise the interface strength between short and endless CF reinforced PEEK. However, no standardised test method existed for interface strength characterisation of overmoulded structures. Sufficient interface strength could only be achieved if a cohesive interface was formed. Cohesive interface formation due to the melting of the surface of the endless CF reinforced PEEK insert after contact with the molten mass required an insert pre-heating temperature of at least 260 °C prior to overmoulding. Because no standardised test method existed for interface strength characterisation of overmoulded structures, a novel test body was developed. This cylinder pull-out specimen did not require any relevant rework steps after manufacturing so that the interface strength could be directly tested after overmoulding. Pre-heating of the endless CF reinforced PEEK inserts resulted in a 73 % increase in interface strength compared to non-pre-heated inserts.

In addition to that, a parametric finite element pedicle screw-bone model was developed. By parametric optimisation, the optimal hybrid composite pedicle screw design in terms of pull-out resistance was found. Within the underlying design space, the difference in screw stability between the worst and the best screw design was approximately 12 %. The resulting design recommendations had to be opposed to the manufacturing requirements to define the final screw design. The moulds of the injection moulding machine were manufactured according to this design so that the hybrid composite pedicle screw could be produced.

The findings of extensive material and interface characterisation were crucial for the achievement of a cohesive interface between insert and overmould so that superior structural mechanical properties of the hybrid composite pedicle screw could be achieved. For example, the bending strength of hybrid composite screws was approximately 48 % higher than the bending strength of discontinuous short CF reinforced PEEK screws. Additionally, fatigue resistance was enhanced by the hybrid screw configuration so that the risk of premature pedicle screw failure could be reduced. In the breaking torque test, hybrid composite screws showed a reduction of 11 % in their breaking torque values compared to their discontinuous fibre reinforced counterparts. However, not only in this test but also in the quasi-static and cyclic bending test, structural integrity of the hybrid composite screws could be maintained which is important for implant components.

Kurzfassung

In den letzten Jahren ist die Nutzung thermoplastischer Verbundwerkstoffe (TPCs) gerade in der Automobilindustrie und im Luftfahrtbereich stark gestiegen. Aber auch in anderen Industriebereichen, wie zum Beispiel in der Medizintechnik, wurden die Potentiale dieser Materialklasse erkannt. Im Vergleich zu duroplastischen Verbundwerkstoffen können TPCs leichter recycelt, wieder aufgeschmolzen und geschweißt werden. Außerdem können TPC Bauteile ökonomisch und effizient hergestellt werden. Als Beispiel sei an dieser Stelle die Spritzgusstechnologie genannt. TPC Spritzgussbauteile können in kurzen Zykluszeiten und in hohen Stückzahlen mit dieser Fertigungstechnologie hergestellt werden. Außerdem besitzen Spritzgussbauteile den Vorteil, dass Funktionsintegration mit vergleichsweise geringem Aufwand realisiert werden kann.

Allerdings bringt die Spritzgusstechnologie neben diesen Potentialen auch einige Nachteile mit sich. Zum Beispiel weisen spritzgegossene TPC Bauteile eine diskontinuierliche Faserverstärkung auf. Die Fasern liegen regellos verteilt im Bauteil vor und die Faserorientierung kann lokal starke Variationen aufzeigen. Während die höchsten Steifigkeits- und Festigkeitswerte des Materials parallel zur Faserorientierung erreicht werden, sind diese quer zur Faserorientierung am niedrigsten. In der Folge sind die strukturmechanischen Eigenschaften dieser spritzgegossenen diskontinuierlich faserverstärkten Bauteile niedriger im Vergleich zu kontinuierlich faserverstärkten Bauteilen. Letztere zeichnen sich durch exzellente spezifische mechanische Eigenschaften aus. Allerdings gibt es Restriktionen hinsichtlich ihrer geometrischen Produktdesignfreiheit.

Das Ziel dieser Arbeit ist die Erweiterung der Verwendungsmöglichkeiten von TPCs für Strukturbauteile in großen Stückzahlen durch die Herstellung eines hochfesten Interfaces zwischen diskontinuierlicher und kontinuierlicher Faserverstärkung. Durch das Überspritzen eines kontinuierlich unidirektional endlos kohlenstofffaserverstärkten (CF verstärkten) Polyetheretherketon (PEEK) Einlegers mit diskontinuierlichem kurz CF verstärktem PEEK wird eine hybride Struktur mit besonderen Eigenschaften hergestellt. Dieser Ansatz ermöglicht die Fertigung struktureller Massenbauteile in kurzen Zykluszeiten, die sowohl hohe strukturmechanische Eigenschaften aufweisen als auch ausreichende geometrische Produktdesignfreiheiten besitzen. Allerdings ist hierfür eine ausreichende Interfacefestigkeit zwischen diskontinuierlicher und kontinuierlicher Komponente erforderlich.

Diese Forschungsarbeit basiert auf dem Anwendungsfall eines Pedikelschraubensystems, das als Spinalimplantat zur Stabilisierung und Fusionierung der Wirbelsäule eingesetzt wird. Seit den 1990er Jahren wird CF-PEEK erfolgreich für Zwischenwirbelkäfige verwendet. Neuerdings findet es auch Anwendung für Pedikelschrauben und Pedikelschraubensysteme. Im Vergleich zu metallischen Implantaten besitzen Implantate aus CF-PEEK einige Vorteile, wie zum Beispiel die Reduktion der Spannungsabschirmung, die Verhinderung von Artefakten bei verschiedenen bildgebenden Verfahren der Medizintechnik (Röntgen, Computertomographie oder Magnetresonanztomographie) oder die Vermeidung von Rückstreuungen bei der Strahlentherapie. Gerade bei Pedikelschrauben, die im lumbalen Wirbelsäulenbereich eingesetzt werden, treten große Kräfte und Momente auf. Daher wird in dieser Arbeit eine hybride Pedikelschraube aus Faserkunststoffverbund entwickelt, die mit dem oben beschriebenen Überspritzungsprozess hergestellt wird.

Verschiedene Anbindungsuntersuchungen wurden durchgeführt, um die Interfacefestigkeit zwischen kurz und endlos CF verstärktem PEEK zu charakterisieren. Allerdings existierte kein standardisiertes Prüfverfahren, zur Bestimmung der Interfacefestigkeit überspritzter Strukturen. Eine ausreichende Interfacefestigkeit konnte nur durch die Herstellung eines kohäsiven Interfaces erreicht werden. Damit sich ein kohäsives Interface ausbilden konnte, musste ein oberflächennahes Aufschmelzen des endlos CF verstärkten PEEK Einlegers nach dem Kontakt mit der Schmelze erfolgen. Hierfür war eine Einlegervorheiztemperatur von mindestens 260 °C vor dem Überspritzungsvorgang erforderlich. Da kein standardisiertes Prüfverfahren für die Charakterisierung der Interfacefestigkeit von überspritzten Strukturen existierte, wurde ein neuartiger Prüfkörper entwickelt. Keinerlei nennenswerte Nachbearbeitungsschritte waren nach der Herstellung dieses Zylinderauszugsprobekörpers erforderlich, sodass die Interfacefestigkeit direkt nach dem Überspritzen geprüft werden konnte. Durch das Vorheizen des endlos CF verstärkten PEEK Einlegers wurde eine Steigerung der Interfacefestigkeit von 73 % gegenüber nicht vorgeheizten Einlegern erreicht.

Darüber hinaus wurde ein parametrisches Pedikelschrauben-Knochen Modell basierend auf der Methode der finiten Elemente entwickelt. Durch eine parametrische Optimierung konnte das optimale Design der hybriden Pedikelschraube aus Faserkunststoffverbund gefunden werden. Die Unterschiede in der Schraubenstabilität zwischen dem schlechtesten und dem besten Schraubendesign unter Beachtung des zugrunde liegenden Designraumes lagen bei etwa 12 %. Die resultierenden Designempfehlungen mussten den Anforderungen aus dem Herstellprozess gegenübergestellt werden, um das endgültige Schraubendesign definieren zu können. Entsprechend diesem Design wurden die Werkzeuge der Spritzgussmaschine gefertigt, sodass die hybride

Faserkunststoffverbundschraube produziert werden konnte.

Die Erkenntnisse umfassender Material- und Interfacecharakterisierung waren von großer Bedeutung für die Erzeugung eines kohäsiven Interfaces zwischen Einleger und überspritztem Material, welches die Voraussetzung für ausgezeichnete Eigenschaften der hybriden Faserkunststoffverbundschraube war. Beispielsweise war die Biegefestigkeit der hybriden Pedikelschrauben aus Faserkunststoffverbund etwa 48 % höher als die der diskontinuierlich kurzfaserverstärkten PEEK Schrauben. Des Weiteren konnte die Dauerfestigkeit der Schraube durch die hybride Schraubenkonfiguration verbessert werden, sodass das Risiko eines vorzeitigen Schraubenversagens reduziert wurde. Bei der Bruchmomentprüfung haben die hybriden Faserkunststoffverbundschrauben im Vergleich zu den diskontinuierlich faserverstärkten PEEK Schrauben ein um 11 % verringertes Bruchmoment aufgezeigt. Die Strukturintegrität der hybriden Faserkunststoffverbundschrauben war allerdings sowohl nach dieser als auch nach der quasi-statischen und zyklischen Biegeprüfung weiterhin gegeben, was für Implantatkomponenten von großer Bedeutung ist.

Nomenclature

Greek symbols

α^T	K^{-1}	Coefficient of thermal expansion
γ_{lv}	$kg \cdot s^{-2}$	Surface energy of liquid in atmosphere
γ_{sl}	$kg \cdot s^{-2}$	Interface energy between solid and liquid
γ_{sv}	$kg \cdot s^{-2}$	Surface energy of solid in atmosphere
$tan\ \delta$		Bending loss factor
ϵ		Strain
ε_{ALLIE}	$kg \cdot m^2 \cdot s^{-2}$	Internal or total strain energy
ε_{ALLSD}	$kg \cdot m^2 \cdot s^{-2}$	Static dissipation or viscous damping energy
Θ	°	Contact angle
κ_{dist}	°	Distal half angle
κ_{prox}	°	Proximal half angle
ν		Poisson's ratio
ξ	°	Cumulated conical shaft angle
ρ	$kg \cdot m^{-3}$	Mass density
ρ_{IL}	$kg \cdot m^{-3}$	Mass density of immersion liquid
σ	$kg \cdot m^{-1} \cdot s^{-2}$	Stress
σ_{Mises}	$kg \cdot m^{-1} \cdot s^{-2}$	Von Mises stress
φ		Fibre mass fraction
φ_V		Fibre volume fraction
Φ	$kg \cdot m^2 \cdot s^{-3}$	Heat flow rate
χ^m		Relative mass change
χ^m_{th}		Theoretical possible relative mass change

χ^T		Relative temperature loss
ψ^{low}	°	Conical angle of lower pedicle screw shaft
ψ^{up}	°	Conical angle of upper pedicle screw shaft

Latin symbols

d	m	Thickness
D	m	Diameter
D_{core}	m	Diameter of pedicle screw core
D_i	m	Inner pedicle screw or shaft diameter
D_o	m	Outer pedicle screw diameter
E	$kg \cdot m^{-1} \cdot s^{-2}$	Young's modulus
E'	$kg \cdot m^{-1} \cdot s^{-2}$	Bending storage modulus
E_{spong}	$kg \cdot m^{-1} \cdot s^{-2}$	Young's modulus of spongious bone
F	$kg \cdot m \cdot s^{-2}$	Force
F_R	$kg \cdot m \cdot s^{-2}$	Reaction force
F_R^{3D90}	$kg \cdot m \cdot s^{-2}$	Reaction force of three-dimensional quarter model
G	$kg \cdot m^{-1} \cdot s^{-2}$	Shear modulus
h_S	$m^2 \cdot s^{-2}$	Specific enthalpy of fusion
h_S^{cryst}	$m^2 \cdot s^{-2}$	Specific enthalpy of fusion of fully crystalline polyether ether ketone
H_S	$kg \cdot m^2 \cdot s^{-2}$	Enthalpy of fusion
l	m	Length
l_{bone}	m	Length of bone block
$l_{cortical}$	m	Length of cortical bone
l_{flank}	m	Length of thread flank
l_{flank}^{low}	m	Length of lower thread flank

l_{flank}^{up}	m	Length of upper thread flank
l_{screw}	m	Length of pedicle screw
L_u	m	Displacement load
m	kg	Mass
m^{900}	kg	Mass at 900 ℃
m^{dipped}	kg	Mass dipped in liquid
m^{dry}	kg	Mass after drying
M	$kg \cdot m^2 \cdot s^{-2}$	Bending moment
M_{in}	$kg \cdot m^2 \cdot s^{-2}$	Insertion torque
M_{out}	$kg \cdot m^2 \cdot s^{-2}$	Removal torque
n_{thread}		Number of threads
N		Number of threads at the transition between upper and lower pedicle screw shaft
p_{thread}	m	Pitch
r_{dist}	m	Distal root radius
r_{head}	m	Radius of spherical pedicle screw head
$r_{head\text{-}shaft}$	m	Fillet radius between pedicle screw head and shaft
r_{prox}	m	Proximal root radius
$r_{shaft\text{-}tip}$	m	Fillet radius between pedicle screw shaft and tip
rot	°	Rotation
R_a	m	Roughness average
R_p	m	Maximum roughness profile peak height
R_z	m	Average maximum height of roughness profile
t	s	Time
t_{CPU}	s	Total CPU time
t_{CPU}^{3D180}	s	Total CPU time of three-dimensional half model

$t_{transfer}$	s	Transfer time
T	K	Temperature
T_{10}	K	Temperature after ten seconds
T_g	K	Glass transition temperature
T_m	K	Melting temperature
u	m	Displacement
u^{cyl}	m	Displacement of cylindrical reference model
V	m^3	Volume
w	m	Width
w_{bone}	m	Width of bone block
W_c		Degree of crystallinity

Accents, subscripts, and superscripts

$\hat{x}$	Maximum value
x_0	Initial property
x_{abs}	Absolute value
x_f	Property of fibre
x_{FRP}	Property of composite
x_m	Property of matrix
x_{PEEK}	Property of polyether ether ketone
x_{rel}	Relative value
x_{sCF}	Property of discontinuous short carbon fibre
$x_{sCF-PEEK}$	Property of discontinuous short carbon fibre reinforced polyether ether ketone
x_{TB}	Property of test body
x_{tot}	Total property

x_{uCF}	Property of continuous unidirectional endless carbon fibre
$x_{uCF-PEEK}$	Property of continuous unidirectional endless carbon fibre reinforced polyether ether ketone
$x^{\|\|}$	Property in longitudinal direction
$x^{\perp}$	Property in transverse direction
x^{d}	Disperse component
x^{p}	Polar component

Coordinates

$1, 2, 3$	Local coordinates
X, Y, Z	Global coordinates

Abbreviations

2D	Two-dimensional
3D	Three-dimensional
3D90	Three-dimensional quarter model
3D180	Three-dimensional half model
3D360	Three-dimensional full model
ASTM	American Society for Testing and Materials
BMD	Bone mineral density
BRM	Bone replacement material
C	Carbon
CF	Carbon fibre
cf.	(to) compare, from Latin “confer”
CFRP	Carbon fibre reinforced polymers

CPSS	Composite pedicle screw system
CPU	Central processing unit
CT	Computer tomography
CTE	Coefficient of thermal expansion
CTSF	Composite transfer squeeze forming
DMTA	Dynamic mechanical thermal analysis
DIN	Deutsche Institut für Normung e. V.
DOF	Degree of freedom
DSC	Differential scanning calorimetry
e. g.	For example, from Latin “exempli gratia”
EN	European standard
EP	Epoxy
et al.	And others, from Latin “et alii” or “et aliae”
FDA	United States Food and Drug Administration
FE	Finite element
FEA	Finite element analysis
FRP	Fibre reinforced polymers
GF	Glass fibre
GFRP	Glass fibre reinforced polymers
HT	High tenacity
IM	Intermediate modulus
IMA	In-mould assembly
IR	Infrared
ISO	International Organization for Standardization
IVW	Institut für Verbundwerkstoffe

LCOS	Local coordinate system
LFT	Long fibre reinforced thermoplastic
LM	Light-optical microscope
MRI	Magnetic resonance imaging
NIS	Nationwide Inpatient Sample
PA	Polyamide
PAEK	Polyaryle ether ketone
PBT	Polybutylene terephthalate
PC	Polycarbonate
PE	Polyethylene
PEEK	Polyether ether ketone
PEI	Polyether imide
PEKK	Polyether ketone ketone
PES	Polyether sulfone
PET	Polyethylene terephthalate
PK	Polyketone
PMA	Post-mould assembly
PMMA	Polymethyl methacrylate
PP	Polypropylene
PS	Polystyrene
PSU	Polysulfone
PUR	Polyurethane
PVC	Polyvinyl chloride
sCF	Discontinuous short carbon fibre reinforced
SEM	Scanning electron microscope

SLS	Single lap shear
ST	Super tenacity
TGA	Thermogravimetric analysis
TMA	Thermal mechanical analysis
TPC	Thermoplastic composite
TUK	Kaiserslautern University of Technology
UHMWPE	Ultra-high molecular weight polyethylene
uCF	Continuous unidirectional endless carbon fibre reinforced
UMS	Unsymmetric matrix storage

1 Introduction

“Any applications where weight, cost, efficiency or performance are critical engineering requirements are a good fit for polyketone composite”, is a quotation of *Tim Herr*, aerospace director at *Victrex plc* [1, p. 238]. This statement highlights some benefits which can be achieved by using polyketone (PK) composites. Polyether ether ketone (PEEK) is one member of this thermoplastic material family. Not only for aerospace but also for other industries, such as the medical technology, PEEK and PEEK composites are materials with outstanding properties. Carbon fibre (CF) reinforced PEEK and other thermoplastic composites (TPCs) are used in various fields of application, for example due to their high specific structural mechanical properties, and their processability in short cycle times and high numbers. Advantageously, TPCs can be remelted, welded, and recycled with reasonable efforts. [1–4]

Since the 1990s, CF-PEEK has been used for implant applications [5]. Due to distinct advantages compared to neat polymers or metals, the number of CF-PEEK implant applications are rising. One of the main advantages of composite implants refers to radiotherapy. In contrast to metallic implants, CF-PEEK does neither attenuate X-rays nor hinder precise dose calculation. Due to the presence of metallic implants close to the region to be treated, backscattering of X-rays can occur so that healthy tissue can be affected. In contrast, backscattering will not be a problem if CF-PEEK implants are present. Thus, radiotherapy is efficient and controllable, and healthy tissue is not disadvantageously affected by the presence of CF-PEEK implants. [6–9]

In addition to that, CF-PEEK is radiolucent [10–13]. As a consequence, medical imaging technologies do not show severe artefacts which can disturb precise system installation during surgery or patient follow-up [6, 14–16]. One additional advantage of CF-PEEK implants mentioned in this chapter refers to the stiffness mismatch between metallic implant materials and bone. Because of the higher stiffness of metallic implant materials, stresses are absorbed by the implant so that bone is unloaded. However, bone will only preserve its strength if stresses above a certain threshold are acting on it. Thus, bone resorption can occur due to the presence of stiff metallic implants [15, 17]. In contrast, stiffness can be tailored with composite implants, so that for example bone strength can be maintained [11, 18–21].

A common problem of elderly people is back pain. However, also younger people can often have back problems. *Banghard et al.* highlight that “up to 80% of the population suffer dorsal pain at some time during life” [22, p. 569]. Approximately half a million spinal fusions were performed only in the United States in 2014[1] [5]. This means around 1370 spinal fusions a day. Certainly, global numbers concerning spinal fusions are much higher and are still rising as a result of population ageing [5, 23]. Additionally, elderly people want to remain more and more physically active which leads to a higher acceptance of surgeries. These facts highlight that there is a huge market for implants and that research in this field is crucial.

Excellent implants are required for successful treatment of patients. Thus, this work focuses on an advantageous material combination used for a hybrid composite pedicle screw to improve its functions, extend its range of application, and improve quality of life. A pedicle screw is one component of a pedicle screw system. Such a system will be implanted into the patient's back to recover spine stability [24] if non-surgical therapies fail [12, 22, 25, 26]. According to *White and Panjabi*, spine stability can be described as "the ability of the spine under physiologic loads to limit patterns of displacement so that the spinal cord and nerve roots are not damaged or irritated and, in addition, to prevent incapacitating deformity or pain caused by structural changes" [23, p. 28]. Nowadays, titanium is the standard material for pedicle screw systems. However, several disadvantages are linked to metallic implants, as mentioned before. These disadvantages have led to the development of CF-PEEK pedicle screws (*Icotec AG*, cf. figure 1.1 on the left) and CF-PEEK pedicle screw systems (*CarboFix Orthopedics Ltd.*, cf. figure 1.1 on the right).

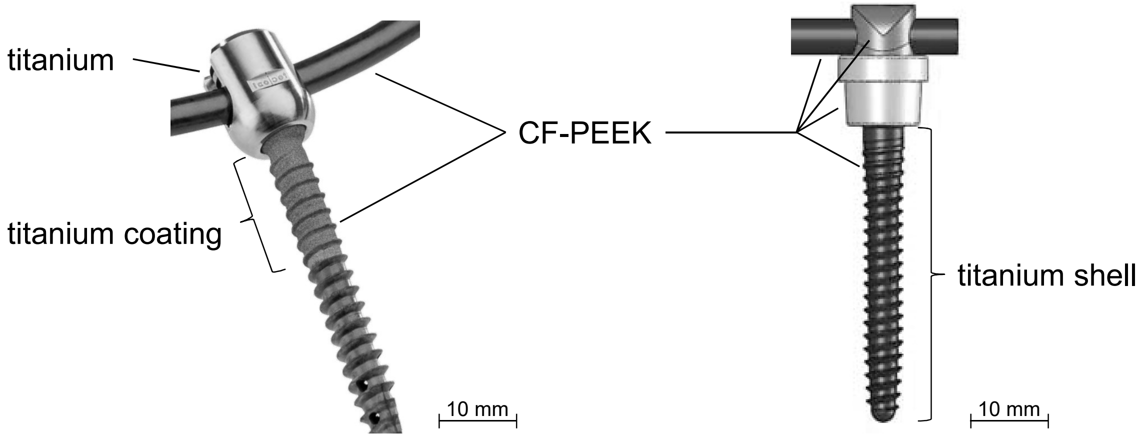

Figure 1.1.: Pedicle screw systems from *Icotec AG* (left) [27] and *CarboFix Orthopedics Ltd.* (right) [28] and their materials

A pedicle screw system used for the stabilisation of the lumbar spine region is subjected to high forces and moments. A fibre reinforcement of the PEEK matrix is required to withstand these loads especially under the consideration of long-term applications. Most composite implants show a discontinuous fibre reinforcement which

[1]data from the *Nationwide Inpatient Sample (NIS)*

enables a production with low cycle times and high freedom in product design. However, discontinuous fibre reinforcement is also linked to some disadvantages, such as a difficult quality assurance due to random fibre distribution. In addition to that, structural mechanical properties are limited due to variations in local short fibre orientation which can also induce some restrictions for the product design. Along the fibre orientation, the material shows high structural mechanical properties, whereas the material properties decrease in the direction perpendicular to the fibre orientation. Parts with discontinuous fibre orientation can be manufactured by injection moulding. With this manufacturing process, a high freedom in product design and a high degree of function integration can be achieved. In addition to that, the injection moulding manufacturing technique is characterised by an economical part production with short cycle times [29, 30].

The limitations of discontinuous fibre reinforcement can be overcome by material combinations. By using *the right material at the best place*, the structural mechanical properties of a product can be significantly enhanced while its material costs remain constant or can even be reduced. Furthermore, the freedom in product design can be efficiently increased with material combinations. Hybrid structural parts with superior material properties can be produced by overmoulding endless fibre reinforced inserts with discontinuous fibre reinforced material. This technique combines the advantages of the high freedom in design of injection moulded products with the excellent structural mechanical properties of endless fibre reinforced composites. However, sufficient interface strength between the two components has to be ensured to benefit from the superior properties.

2 State of the art

Selective information about metallic, polymeric and composite implant materials is given in the beginning of this chapter. A focus is laid on PEEK and CF-PEEK because the material combination for the composite pedicle screw system (CPSS), studied in this work, is based on CF-PEEK composites. The need for implanting a pedicle screw system, its functions and typical materials used for this system are introduced in the following as well. Ceramic implants are not considered within this work. Selective information about the interface formation between materials is given at the end of this chapter. The overmoulding technology is focused in that section because the material combination of the hybrid composite pedicle screw is realised with this technique.

2.1 Materials for medical applications

Materials used for medical applications have to fulfil particular requirements. For example, these materials have to be biocompatible and should have sufficient cell adhesion capability to promote the building of functional connections between implant and bone (osseointegration).

According to *Williams*, “biocompatibility refers to the ability of a biomaterial to perform its desired function with respect to a medical therapy, without eliciting any undesirable local or systemic effects in the recipient or beneficiary of that therapy, but generating the most appropriate beneficial cellular or tissue response in that specific situation, and optimising the clinically relevant performance of that therapy” [31, p. 2951]. This means that a biomaterial, which is foreign to the host, is in contact with the human body without causing unacceptable harm [31]. A biocompatible material is non-toxic, non-immunogenic, non-thrombogenic, non-carcinogenic, non-mutagenic, and non-irritant [5, 31].

Besides biocompatibility, sufficient long-term stability of the implant is required [31]. Long-term stability can be achieved by osseointegration [23, 32] which is dependent on the implant surface properties [23]. Few months after surgery, bridging trabeculations begin to form from bone to implant [33]. Relative movements between bone and implant can lead to implant loosening [34] but can be effectively restricted by osseointegration [5]. In addition to the dependency on implant surface properties, osseointegration is dependent on cell adhesion capability [10, 34–40].

Materials for long-term implant applications are required to have sufficient structural mechanical properties to resist biomechanical loads [19, 31, 41]. In addition to that, material deteriorations, such as corrosion, degradation, water uptake, or wear, have to be minimal and within the acceptable limits [31, 42].

2.1.1 Metals

Advantageously, the strength of metallic implants is high [11] so that the risk of implant failure or implant component failure is low. Compared to polymeric implants, metallic implants composed of stainless steel or titanium typically show a higher cell proliferation [39].

However, the application of metallic implants can lead to allergic tissue reactions [14]. Additionally, the high mass density of titanium or stainless steel contributes to a high implant weight which can lead to patients' discomfort [14]. Due to the radiopacity of metals, artefacts in medical imaging technologies, such as X-ray, computer tomography (CT) scan or magnetic resonance imaging (MRI), arise [6, 7, 11, 15, 22, 23, 25]. These artefacts prevent precise assessment during surgery, for example during the usage of computer-assisted navigation with fluoroscopic guidance [5], and during post-operative patient follow-up [6, 7, 43]. In addition to that, problematic scattering effects of ionising radiation in the presence of metallic implants are typically observed during radiotherapy [6–8]. As a consequence, radiation can hit neighbouring healthy tissue so that less radiation dose reaches the tumour [8]. Metallic implants still increase the degree of uncertainty during radiotherapy because they affect the precision of delivered particles and of dose calculation although modern treatment planning systems and new artefact reduction methods are available nowadays [8, 9].

Another disadvantage of metallic implants is the difference in physical and mechanical properties compared to bone. The stiffness of metallic implants is much higher compared to the stiffness of human bone. As a consequence, the stresses are absorbed by the implant, bone is unloaded, and bone resorption can occur [15, 17]. According to *Wolff's law* of 1892, "every change in the form and function of bone or of their function alone is followed by certain definite changes in their internal architecture, and equally definite alteration in their external conformation [...]" [44, p. 175], which means that bone will only maintain its structure if mechanical stimuli above a certain threshold are acting on it [23, 34, 44–46]. Bone resorption due to the presence of implants can lead to the loss of implant stability and to failure which results in pain for patients and the need for reoperation [11, 22, 34, 47]. This phenomenon, called *stress shielding* [11, 15, 22, 45], has to be avoided by biomedical engineering [46].

Stainless steel is still used for implants. However, its stiffness is higher than that of titanium which can lead to even more severe stress shielding effects. In addition to that, medical imaging is complicated, and the risk of infections and allergic reactions is high [23]. Compared to titanium, the corrosion resistance of stainless steel is inferior [23]. These are some reasons why stainless steel has been widely replaced by other materials, such as titanium [23], for implant applications.

Titanium is one of the standard and most important material for implants nowadays [41]. It has been in medical use since the 1950s [41]. Among different titanium alloys, the biocompatible alloy Ti6Al4V is mainly used for implant applications [41, 48, 49]. Titanium implants show superior osseointegration behaviour [23]. Their strength, fatigue limit, and corrosion resistance are excellent [13, 41, 48, 49]. There are various applications of titanium implants, such as bridging rods for pedicle screw systems [13], locking plates, or intramedullary nails [15]. However, the disadvantages of metallic implants mentioned before can also be applied to titanium implants.

2.1.2 Polymers

For more than 50 years, polymers have been used for medical applications [19, 41]. In the early years of application, polymers were only used for sterilised medical disposables, such as syringes or cannulae [19, 41]. Today, polymers are used for various applications and also for short- and long-term implants [19]. The widespread of polymeric medical products is based on easy availability, processing with low-cost, high freedom in design, and a broad property range [41].

Without claim of completeness, different polymeric materials like polyether ether ketone (PEEK), polysulfone (PSU), polybutylene terephthalate (PBT), polyamide (PA), and polystyrene (PS) were studied for potential implant applications [5, 15]. However, only PEEK showed the requisite combination of structural mechanical properties, biocompatibility, manufacturability, and consistent availability [5]. Table 2.1 summarises different applications for a selection of polymers.

2.1.2.1 Polyether ether ketone

Semi-crystalline thermoplastic PEEK was first introduced by *Imperial Chemical Industries plc* in 1978 [41, 51, 52] and has been used as a biomaterial since the 1990s [11, 14, 15]. *PEEK-OPTIMA™* for long-term implant applications was introduced by *Victrex plc* in 1998 [5]. The chemical repeat unit of PEEK can be seen in figure 2.1.

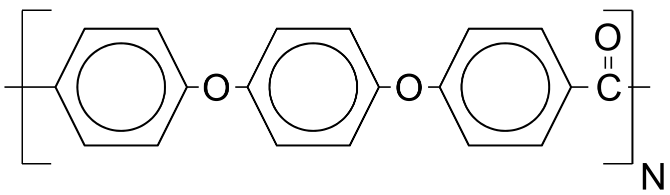

Figure 2.1.: Chemical repeat unit of PEEK according to [35, 51, 53–58]

Table 2.1.: Medical polymeric applications according to [41, 50]

Polymer	Application
Polyamide (PA)	Ankle foot orthoses based on additive manufacturing
Polycarbonate (PC)	Components for kidney dialysis, syringes, packagings, tubes
Polyethylene (PE)	Joint sockets for hip endoprosthesis, knee prosthesis, syringes, packagings
Polyether ether ketone (PEEK)	Spinal cages, pedicle screws, pedicle screw systems, scaffolds, abutments, prosthetic frameworks
Polyethylene terephthalate (PET)	Artificial blood vessels, ligament replacements
Polymethyl methacrylate (PMMA)	Bone cement, artificial teeth, tooth fillings
Polypropylene (PP)	Components for kidney dialysis, heart valves, packagings
Polyurethane (PUR)	Artificial blood vessels, skin implants, heart valves, membranes for kidney machines
Polyvinyl chloride (PVC)	Blood bags, bags for intravenous solutions, disposables

The aromatic rings of the PEEK polymer contribute to excellent thermal properties, such as a glass transition temperature of 143 ℃ or a melting temperature of 343 ℃. PEEK is typically processed at temperatures of about 380 ℃. At temperatures above 400 ℃, the sensitivity of PEEK to oxygen rapidly increases and its thermal stability is limited. [10, 15, 36, 51, 54, 56, 59–64]

Compared to other polymers, PEEK is characterised by superior structural mechanical properties [19, 36, 56, 59, 60, 64] and fatigue resistance [22, 52, 65]. PEEK still shows high stiffness and strength values at temperatures well above the glass transition temperature [15, 65]. Its Young's modulus is approximately 4 GPa, its tensile strength 98 MPa [66], and its tendency to creep is low [65]. Due to a stiffness in the range of human bone, stress shielding is alleviated [46]. This is one significant advantage over metallic implants. Compared to commonly used metals for implant applications, PEEK has a lower density of approximately 1.3 g/cm^3 so that the implant weight can be significantly reduced which can contribute to patients' comfort [14, 67]. However, PEEK implant components can be more expensive than titanium components [13], and strength can be insufficient for implants subjected to high biomechanical loads.

PEEK shows a high chemical and radiation resistance [15, 36, 52, 56, 59, 63–65, 68], and low water uptake [14, 60, 65, 69]. The chemical stability of PEEK contributes to its poor adhesion to soft tissue or bone [10], as described more in detail below, and enables the application of common sterilisation methods which are based on heat, low-temperature gas, ionising radiation, or liquid disinfection [5, 14, 36, 41]. Material ageing in vitro and in vivo is insignificant [17] as well as the chemical damage by water exposure [15]. There are neither toxic effects [40, 70] nor significant allergic reactions linked with PEEK implants [14].

Another advantage of PEEK implants over metallic ones refers to their radiolucency [10–13]. As a consequence, severe artefacts in medical imaging technologies will be prevented if PEEK implants are used [6, 14–16]. By this improvement of medical imaging quality, patient assessment becomes more secure [6, 19, 71]. To locate metal-free implant components during surgery or follow-up, integrated radio-opaque markers composed of titanium, tantalum, or barium sulphate ($BaSO_4$) are commonly used [5, 14, 19, 71–73]. In the event of implant failure, these markers also enable the location and removal of all system components [73]. The problem of backscattering in the presence of metallic implants during radiotherapy can be avoided by using PEEK implants [6, 8, 9, 73]. Therefore, accurate planning of radiotherapy is possible and the efficiency of radiotherapy is improved [8, 9]. With small titanium markers or thin coatings used for improving implant visibility, no significant artefacts arose and no significant effect on radiotherapy was observed [9].

PEEK can be processed without additives [36, 38] which is important for implant materials. Several processing techniques for polymers, such as injection moulding, compression moulding, extrusion, or laser sintering can be used to process PEEK [5, 12, 14, 15, 52, 74]. However, additional requirements, such as a high temperature equipment for the processing machine, have to be considered due to the high melting point of PEEK [75]. Dependent on the processing technique, amorphous or semi-crystalline material characteristics, which influence the material properties, are obtained [5, 76–78]. The lower the cooling rate, the higher the degree of crystallinity [55, 56, 76, 78].

The bioactivity and bone bonding properties of PEEK are poor because PEEK is an inert material [14, 15, 40, 79, 80] with low surface energy [5]. However, bone bonding properties can be enhanced either with surface modification techniques, such as ion bombardments [81], or with coatings composed of calcium phosphate (hydroxyapatite) [5, 11, 14, 15, 23, 31, 32, 38, 79] or titanium [5, 7, 15, 22, 41]. Bone ingrowth can be promoted by the creation of a porous surface texture [15, 32]. Concerning coating thickness, significant variations exist in the literature. *Banghard et al.* inform about a titanium coating thickness of 0.24 µm [22]. Others report 0.03 µm to 0.12 µm coating thickness [9, 32, 41], *Kurtz* recommends a maximum peak height from 65 µm to 400 µm [5], and *Nevelsky et al.* of less than 100 µm [9]. Nevertheless, these studies show that coating thickness is in the nanometre to micrometre range. A titanium coating can also be used to improve the adhesion between a calcium phosphate coating and a PEEK substrate [82].

Biocompatible PEEK for implants is mainly manufactured by *Invibio Ltd.*, *Solvay GmbH*, and *Evonik Industries AG* [5]. *Invibio* offers radio-opaque PEEK[1] to improve implant visibility. In March 2019, *Evonik* introduced radio-opaque PEEK into their product portfolio as well[2]. In addition to that, an implantable polyether ketone ketone (PEKK) grade is available from *Oxford Performance Materials, Inc.*[3]

PEEK as an implant material is mainly used for orthopaedic and traumatologic implant applications [15, 83]. Typically, PEEK is used for spinal (e. g. spinal cages) [5, 12, 15], cranial (e. g. scaffolds) [15, 84], and dental implants (e. g. implant fixtures, healing caps, abutments, and prosthetic frameworks) [5, 14]. One example for a cervical total disc replacement device is the *NuNec system* from *RTI Surgical Holdings, Inc.* (former *Pioneer Surgical Technology, Inc.*) [72], which however is no longer available on the market. From the same company, the PEEK nucleus replacement device *NUBAC* was developed with similar low wear rates compared to common systems [85]. PEEK was also used for arthroscopic anchors [5] and the isoelastic *Epoch II hip stem* from *Zimmer, Inc.*, with an original development dating back to the mid-1980s [5].

2.1.3 Composites

Polymeric implants subjected to high loads need fibre reinforcements to have sufficient stiffness and strength properties [19]. The stiffness of composite implants can be tailored, e. g. by variations in the fibre volume fraction, fibre orientation, fibre lengths, materials, or design to optimise stress distribution in bone [47]. In contrast, the stiffness of metallic implants can only be changed by modifying the implant design [86]. The optimisation of implant stiffness can reduce the effect of stress shielding and can enhance screw stability [11, 18–21]. If the implant stiffness is too low, stress shielding will be eliminated but micromotions between bone and implant will increase. This will prevent successful osseointegration and will cause pain [47]. Compared to metallic implants, a higher freedom in design can be achieved by composite ones [14].

Continuous unidirectional endless CF reinforced carbon (uCF-C) composite screws for osseosyntheses were studied by *Błażewicz et al.* [87] They found that uCF-C screws obtained from machining uCF-C semi-finished products were superior to screws with a uCF-C core and wound endless CFs forming the thread [87]. Concerning the latter, shear failure between thread and core was observed leading to a 50 % less holding force compared to steel screws [87].

[1] https://invibio.com/materials/peek-optima-image-contrast; accessed 21 November 2019
[2] https://medical.vestakeep.com/product/medical/de/medien/pressemitteilungen/pages/article.aspx?articleId=109404; March 12th, 2019; accessed 23 October 2019; press release
[3] http://oxfordpm.com/cmf-orthopedics; accessed 29 October 2019

Thermoset composite implants, such as an CF reinforced epoxy (CF-EP, trade name *Caproman®* from *MAN-Ceramics Corp.*) hip endoprosthesis [5, 19], were examined in clinical studies as well. However, compatibility problems [17] and contouring difficulties arose [5, 15, 42]. Thermoset composites have the disadvantage that they cannot easily be contoured to the shape of bone in contrast to metallic or thermoplastic materials [5]. In addition to that, toxic additives can remain on the implant surface [41].

Schulte et al. studied a vertebral body replacement device composed of a bioglass-PUR composite with an integrated CF-PEEK plate [6]. It improved prognosis and showed similar in-vivo test results compared to the titanium counterpart [6]. However, the variability in clinical outcome was higher [6].

Besides the usage of CFs for the reinforcement of polymeric matrices, glass fibre reinforced polymers (GFRP) are used for different medical applications as well. GFRP can be used for example in dentistry [32] or in combination with bioactive glass for cranial implants [88].

2.1.3.1 Carbon fibre reinforced polyether ether ketone

For implant applications subjected to high loads, neat PEEK implants increase the risk of pseudoarthrosis due to insufficient stiffness [13]. The addition of CFs improves the structural mechanical properties of PEEK [5, 22, 61, 74]. Simultaneously, its ductility [74] and tendency to creep [89] are reduced. In contrast to titanium, the stiffness of CF-PEEK can be tailored so that it is closer to the stiffness of human bone and stress shielding is alleviated [90].

CF influence the crystallisation process [61] because they act as nucleating agents [91]. As a consequence, the crystallisation starts at higher temperatures and the degree of crystallinity is typically higher for composites than for neat polymers [57]. In contrast, no significant difference in the glass transition and melting temperature is found for CF-PEEK compared to neat PEEK [42, 57]. The same as PEEK, CF-PEEK is radiolucent [7, 20, 21, 73], sterilisation resistant [47], biocompatible [5, 11], bioinert [5, 20], chemically inert [42], does neither attenuate radiotherapy nor lead to the disturbance of healthy tissue [8, 9, 19, 21], and shows radiation stability [42]. The material cost is high [20] but it can be processed by common processing technologies used for plastic materials, such as extrusion or injection moulding [74]. By using CF-PEEK as an implant material, a similar foreign body response to metallic implants was found besides no signs of infection or adverse tissue reactions [20, 88, 92]. Only uncritical tissue irritations were reported due to composite wear particles [19].

CF-PEEK as an implant material was introduced with the *Brantigan I/F lumbar fusion* *cage*[4] in the 1990s [5]. Besides spinal cages [20, 73], CF-PEEK is used nowadays for heart valves [31], hip joint endoprosthesis [93], orthopaedic trauma (fracture fixation plates [20, 41, 92, 94] or intramedullar nails [20]), dentistry [20], and cranioplasty [5, 20]. Due to suitable tribological properties, CF-PEEK is used as a bearing material for joint arthroplasty [15], such as in knee replacements [67, 95]. Another medical application of CF-PEEK refers to surgical instruments [19].

Implantable discontinuous short CF reinforced PEEK (sCF-PEEK) and continuous unidirectional endless CF reinforced PEEK (uCF-PEEK) is produced by *Invibio Ltd.* under the trade name *PEEK-OPTIMA™ Reinforced* and *PEEK-OPTIMA™ Ultra-Reinforced*. The uCF-PEEK materials from *Invibio* were previously named *Endolign Tape* and *(pultruded) Endolign Rod* [5].

In [41], sCF-PEEK screws for osteosynthesis were produced by injection moulding. This study has shown that structural mechanical properties of these discontinuous reinforced screws were not sufficient for osteosynthesis [41]. sCF-PEEK specimens are characterised by fibre discontinuity, random fibre distributions, and variations in the fibre orientation. Moreover, fibre distribution and orientation can change dependent on part geometry and process parameters. With discontinuous fibre reinforcement, the fibre distribution and orientation is difficult to control, and variations in structural mechanical properties can be observed so that the achievement of a constant product quality may be challenging.

Tognini et al. produced cortical CF-PEEK bone screws with CF volume fractions up to 61 vol.-% by composite transfer squeeze forming (CTSF) [96]. For this process, a composite rod was heated and axially pushed into a mould [96]. The fatigue properties were superior and notch sensitivity was less compared to titanium screws [96]. Compared to injection moulded screws, structural mechanical properties were higher [96]. However, discontinuous fibre distribution was still present [41].

2.2 Pedicle screw systems

Pedicle screw fixation was popularised in Europe by *Roy-Camille* starting in the 1960s [49]. Today, it is one of the standard surgical methods in the thoracic and lumbar spine region [25]. The components of a pedicle screw system can be seen in figure 2.2.

Pedicle screws are the central element of spinal fusion [25], and the success of bone fixation is highly dependent on the screw holding power [45]. Pedicle screws have the function of anchoring the system in the vertebrae. Their threads typically show a buttress shape [97]. In contrast to monoaxial pedicle screws with a fixed connection

[4] FDA approval in 2001

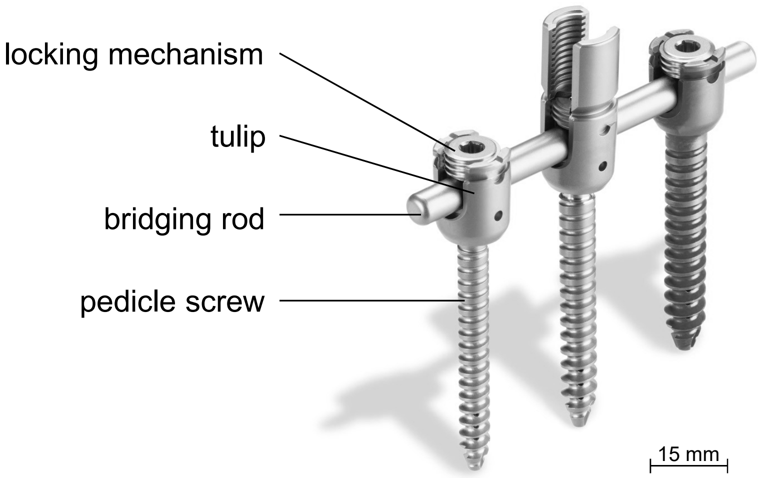

Figure 2.2.: Components of a pedicle screw system; image reference: *Ulrich GmbH & Co. KG*

between screw and tulip, polyaxial screws have a spherical head on which the tulip can rotate and tilt prior to fixation [26, 98]. The tulip connects the screw with the bridging rod which can slide in the tulip. These movements are restricted after the activation of a locking mechanism. In metallic systems, the fixation between bridging rod and tulip, and tulip and screw is typically achieved by tightening set screws or nuts [23, 98]. The fixation is dependent on the friction in between the components and has to be realised without the introduction of surface defects which could lead to reduced fatigue life of the system [23, 99].

With polyaxial pedicle screw systems, screw alignment and system installation during surgery is easier compared to monoaxial systems [26, 98]. Additionally, the risk of pedicle screw or bridging rod breakage is reduced [98], and there is less need to bend and adapt the bridging rods during surgery [26] so that operation time can be reduced [26].

This research on the material combination of continuous and discontinuous fibre reinforced PEEK is based on a one-level pedicle screw system. A one-level pedicle screw system consists of four screws which are connected by two bridging rods. Figure 2.3 illustrates such a system with its components, relevant anatomical structures, and the direction of the pull-out force which is acting on the pedicle screw head. Pull-out forces can lead to implant loosening. This critical loading case is mainly a result of spine bending and lifting of heavy objects. Pull-out forces lead to shear stresses in bone which have to be lower than bone shear strength to prevent implant failure. Pedicle screw systems can also stabilise more than one spine level.

Patients with spondylolisthesis, spondylolysis, degenerative arthritis, tumours, scoliosis, degenerative disc disease (spinal stenosis), or spinal bone fractures can be treated

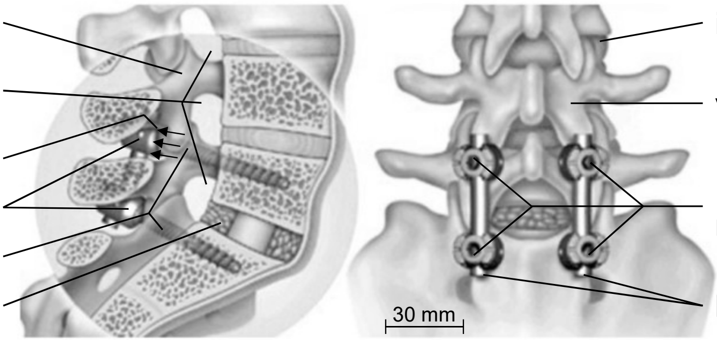

Figure 2.3.: One-level spinal fixation; image reference: [100]

by implanting pedicle screw systems [6, 101]. By the use of these systems, spine instabilities can be effectively decreased so that abnormal displacements or rotations between vertebrae under physiological loads can be eliminated [24]. If non-surgical, less invasive therapies fail to heal these pathologies and to recover spinal stability, invasive spinal fusion (arthrodesis) will be required [12, 22, 25, 26]. The prevention of abnormal movements of vertebrae leads to the reduction of painful pressure on nerves and the spinal cord [97].

Typically, a drill or an awl is used to open cortical bone and to drill a pre-hole into bone so that screw insertion is eased [23, 43, 102, 103]. In spongious bone, no prehole should be drilled to achieve bone compaction during insertion so that sufficient fixation strength is promoted [23]. Based on the experience with metallic screws, the pre-hole diameter should be smaller than the inner screw diameter [23]. If the pre-hole is tapered [104], pedicle screws will typically not require a cutting edge to cut the thread into bone [102]. Two screws are inserted for each affected vertebra [43]. The upper part of the screw is located in cortical bone, and the lower part in spongious bone. Five to twelve minutes are typically needed to implant one pedicle screw [25] as long as there are no complications. Dependent on the pedicle size, different pedicle screw diameters are used [43]. During computer assisted surgery, medical images are taken to confirm correct screw positioning [71, 73] so that misalignments and complication rates can be significantly reduced [25].

The main functions of pedicle screw systems are the correction of spine alignment and the recovery of spine stability [101]. Pedicle screw systems are typically installed from the patient's back, aiming at vertebral fusion and the restriction of mobility [23, 49] following the statement *no movement, no pain*. With metallic pedicle screw systems, a rigid fixation is typically achieved [23]. However, ideal spine fixation means ensuring sufficient stability without excessive rigidity of the system [16]. Vertebral fusion occurs after approximately six months after surgery [23]. During this time, the pedicle screw system has to withstand about one million cycles [23]. Pedicle screw systems shall provide short-term stability of the human spine which means that they have to fulfil their function for about two years [105]. After this time, implants can be removed [26] or remain in the patient's body.

Several studies have been published concerning the optimisation of metallic pedicle screws. Typically, screw design optimisation yields the improvement of screw stability in bone and the resistance against pull-out [45].

Besides an optimal pedicle screw design, a material stiffness comparable to bone is important to decrease stress shielding and to improve implant stability, as described before. Pedicle screw stability is also influenced by its structural stiffness defined as a product of material stiffness and implant cross-section [45]. In addition to that, it depends on the design of the screw and the thread profile [23, 45, 101, 106–109], the properties of bone [23, 101, 107, 108, 110], the structural mechanical properties of the screw material [110], the surgical technique [101], and the size of the pre-hole [108, 110].

Research on metallic pedicle screws confirms that screw stability can be improved by design optimisation, such as the increase of outer screw diameter [23, 45, 106, 107, 109–112], the decrease of pitch [109, 110, 112], the decrease of inner screw diameter [23, 48, 111, 112], the decrease of half angle[5] [112], and the increase of screw purchase length [97, 107, 110, 111]. However, the risk of screw failure is increased by decreasing the inner diameter [23]. Threads with less sharp edges lead to a more homogeneous stress distribution, less notch effects, and a higher fatigue limit of pedicle screws [49, 113, 114]. Besides design optimisation, screw stability can be improved by optimising screw trajectory in vertebrae, by augmentation with bone cement, or by using expandable pedicle screws [106]. The stability of the entire pedicle screw system depends on the fixation of rod, screw, and potential cross-links [48].

In addition to cylindrical screw shafts, pedicle screws can also have a tapered/conical shape to compact bone during insertion [48, 108, 114]. By the compaction of bone material, conical screws can improve pull-out strength in specific situations [103, 108]. Dual core or dual shafted screws with a fixed outer or inner radius and two different inner or outer radii are further commercially available screw designs [114]. These screws ease screw insertion while having superior screw stability [103, 106]. Additionally, due to their thicker upper screw shaft diameter, the risk of screw neck breakage is reduced [103]. Dual shafted screws avoid the problem of losing bone contact in contrast to conical screws when turned back during surgical procedure [103]. Additionally, the danger of pedicle breakage especially in osteoporotic bone can be reduced [106].

[5]design parameter of a buttress thread (cf. figure 4.19); no distinction between proximal and distal half angle was made in [112]

Gefen introduced the concept of a *graded-stiffness* screw having a “reduced-stiffness-titanium core and outer polymeric threads” [45, p. 337] to improve stress transfer from screw to bone. Stress transfer can also be improved by increasing the number of threads [45].

2.2.1 Medical background

Bone properties depend on species, race, region, gender, age, and state of health [115, 116]. Additionally, bone is an anisotropic material [41]. It is composed of cortical and spongious bone, also known as cancellous or trabecular bone [18, 41]. Bone has to be stiff to withstand physiological forces as well as strong and tough to prevent easy breakage [46]. The flexural strength of human bone varies but is typically in the range of 80 MPa to 180 MPa [92, 115]. Cortical and spongious bone differ in the degree of porosity which is dependent on loading, disease, and age [115]. The stiffness of cortical bone varies in the range from 12 GPa to 20 GPa [15, 17, 18, 92, 115] whereas spongious bone has a stiffness in the range from 0.01 GPa to 3 GPa [18, 24, 117, 118]. Spongious bone has a higher strain before failure and a higher energy storage capacity than cortical bone [115]. The transition between cortical and spongious bone is continuous [116].

Figure 2.4 shows the anatomical Cartesian coordinate system of the human spine. Instead of the terms *dorsal* and *ventral*, the terms *posterior* and *anterior* are often used. On each of the three axis, translational and rotational movements can occur.

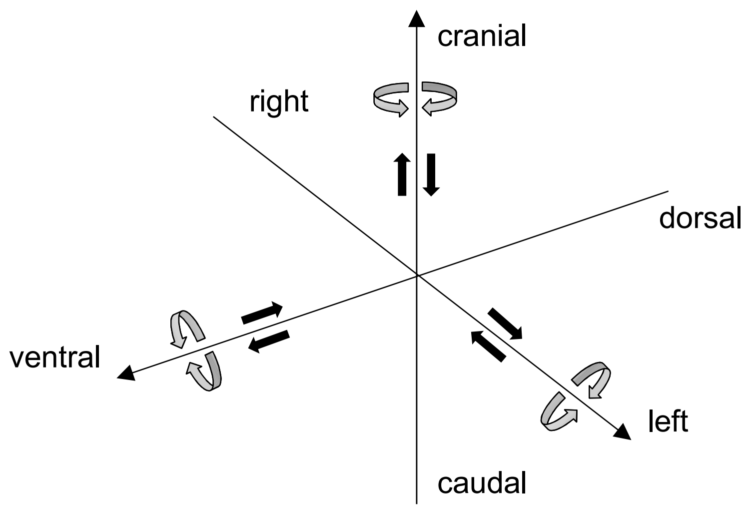

Figure 2.4.: Anatomical Cartesian coordinate system of the human spine according to [23, 119]

The spine is loaded by the upper body weight. Therefore, one main function of the spine is to provide structural support for the upper body. The majority of this load is carried by the vertebrae [23]. Width, height, and volume of vertebrae increase from cranial to caudal to resist the increasing body weight [23, 119]. The lumbar vertebrae are the biggest and strongest vertebrae [119]. Figure 2.5 illustrates the structure of vertebrae schematically with the Latin names of their components. In between the vertebrae, intervertebral discs (*discus intervertebralis*) enable and restrict spine movements [23].

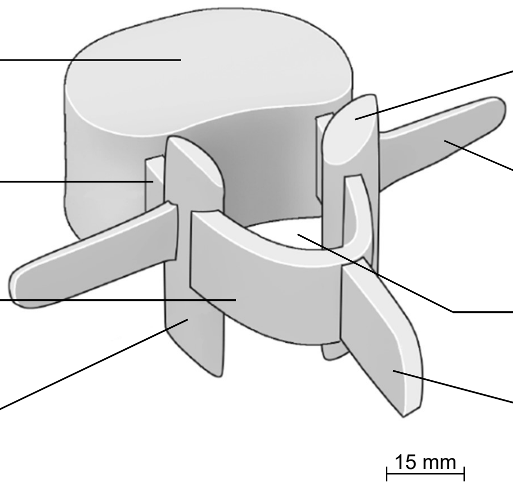

Figure 2.5.: Structure of vertebra [119]

Most of the pull-out strength of the pedicle screw depends on the pedicle and not on the vertebral body [23, 101]. The pedicle is a bone cylinder between the lamina and the vertebral body [101], as shown in figure 2.5. It is composed of cortical bone surrounding little spongious bone [49]. Similarly, the vertebral body consists of inner spongious bone surrounded by cortical bone [86]. The more the screw thread is located in cortical bone, the higher the screw stability is [110]. Pedicle size differs along the spine [43], and its dimensions limit the maximum outer diameter of the pedicle screw [49, 97]. Its bone mineral density (BMD) and its cortical to spongious bone ratio are higher than that of the vertebral body [23, 101] which indicates the pedicle as one of the strongest spine elements [97]. *Hohn et al.* found that the BMD of the pedicle is in the range of $(0.303 \pm 0.076)\,\mathrm{g/cm^3}$ [120]. In this study, the highest BMD of the non-osteoporotic pedicle of a 35 year old male was approximately $0.42\,\mathrm{g/cm^3}$ [120]. BMD positively correlates with pedicle screw stability [120, 121]. Furthermore, a higher BMD typically observed with younger patients decreases the risk of bone failure [23, 120].

Osteoporotic bone has a lower BMD than healthy bone [101] so that screw fixation is critical in osteoporotic bone [23, 122]. Therefore, expandable pedicle screws or cement augmentation, for example with PMMA, is used to enhance screw stability [21, 106, 122, 123]. For cement augmentation, pedicle screws have to be cannulated and fenestrated [106, 120, 124]. Disadvantageously, neurologic injury due to cement leakage into foramina and spinal canal (cf. figure 2.3 and 2.5) can occur [106, 123].

Cannulated screws enable minimal invasive surgery [123].

The human spine is subjected to one to three million cycles a year [23, 42]. Certainly the load levels and the number of cycles differ dependent on the activity level of the patient. Stress concentrations are a common reason for implant failure under static or cyclic loading [11, 23, 25]. Implant failure can also occur due to an incorrect operation method or erroneous post-operative management [110]. Screw fatigue fracture is often located at the inner screw diameter [125]. During service life, high bending forces are acting on the screw whereas torsion forces are typically irrelevant [23]. Screw breakage is more often observed than bridging rod breakage [48]. Another common complication, which has to be avoided, is screw loosening [21]. Besides implant failure, failure at the screw-bone interface can occur due to bone fracture [23, 106]. It is important to achieve a reliability of implants, especially for long-term applications, to prevent reoperations [11].

Expensive cadaveric bones are often used for biomechanical tests. However, significant variations in bone properties are common [112, 114]. Additionally, bone can deform or break during loading [114]. Therefore, bone replacement materials (BRMs), such as ultra-high molecular weight polyethylene (UHMWPE) or PUR foam, are often used to biomechanically test implants [114]. BRMs are standardised in ASTM F 1839 [126]. Their mechanical properties are uniform and consistent so that they are recommended for comparative biomechanical studies [48, 102, 104, 107, 108]. However, the results obtained by tests with BRM should not be directly transferred to in-vivo situations because the mechanical properties and the geometry of human bone are approximated [48, 102, 107, 112]. PUR foams are purchasable in different densities to represent different bone qualities [126].

2.2.2 Materials

As mentioned before, titanium is one of the standard materials for implants. Also for pedicle screw systems, titanium is widely used. The majority of pedicle screws, bridging rods, tulips, and locking mechanisms on the market is composed of titanium. Some of the big manufacturers of titanium pedicle screw systems are *B. Braun Melsungen AG*[6], *Ulrich GmbH & Co. KG*[7], *Zimmer Biomet Spine, Inc.*[8], *Medtronic plc*[9], *DePuy*

[6]www.bbraun.com/en/products-and-therapies/product-catalog/spine-surgery.html; accessed 25 November 2019

[7]www.ulrichmedical.de/en/products/spinal-systems/rod-screw-systems/; accessed 25 November 2019

[8]www.zimmerbiomet.com/medical-professionals/spine.html; accessed 25 November 2019

[9]www.medtronic.com/us-en/patients/treatments-therapies/spinal-fusion-scoliosis-surgery.html; accessed 25 November 2019

Synthes[10], and *Globus Medical, Inc.*[11]

The pedicle screw systems *VADER®* and *LightMore®* from *Icotec AG* are composed of CF-PEEK screws with titanium tulips, titanium set screws, and CF-PEEK or titanium bridging rods[12] (cf. figure 1.1 on the left). The *Icotec* composite pedicle screws are composed of CFs embedded in a PEEK matrix. However, the fibres are discontinuously distributed due to manufacturing by composite flow moulding [21]. Composite flow moulding is a manufacturing technique with which a pultruded rod is heated above the melting temperature, and is pushed under pressure into a cavity which contains the geometry of the final product [5]. This process is very similar to the CTSF of cortical bone screws mentioned before.

In [21], CF-PEEK pedicle screws resisted similar numbers of load cycles until loosening compared to titanium screws. However, especially for non-metallic implants, stress concentrations could lead to early implant failure [11]. These stress concentrations existed at pedicle screw threads which change stress distribution and cause discontinuities [11]. Thus, pedicle screw design will have to account for the reduction of stress concentrations especially if composite materials are considered [11].

CarboFix Orthopedics Ltd. distributes a pedicle screw system which is entirely non-metallic, except of the titanium shell of the pedicle screw (cf. figure 1.1 on the right) [8, 9]. No artefacts arise with this system [8]. It is comparable to standard metallic pedicle screw systems in terms of intraoperative complications and recovery of spine stability [8]. However, several disadvantages concerning this system were reported, such as a difficult positioning, a fix bridging rod contour, and a special tool which is required for system installation [8]. According to *Tedesco et al.*, the surgical procedure is not user-friendly [8]. Due to a reduced torsional resistance of the *CarboFix* CF-PEEK screws, a proper pre-hole preparation with tapping should be considered [8].

For about one decade, PEEK and CF-PEEK have been successfully used for bridging rods of pedicle screw systems [5, 16, 127–129]. These non-metallic rods are semi-rigid components which restore normal kinematic behaviour of the spine while ensuring sufficient stabilisation [13]. Major manufacturers are *DePuy Synthes*[13], *Medtronic plc*[14], and *Invibio Ltd.*[15] The increase in flexibility compared to metallic bridging rods contributes to less implant failure. Stress is beneficially reduced at the screw-bone inter-

[10] www.jnjmedicaldevices.com/en-US/product/expedium-verser-spine-system; accessed 25 November 2019

[11] www.globusmedical.com/solution/spine/posterior-lumbar/; accessed 25 November 2019

[12] www.icotec-medical.com/de/implantate/lumbale-wirbelsaeule/pedicle-systems.html; accessed 30 October 2019

[13] *Expedium® PEEK Rod* [16]

[14] *CD Horizon® Legacy™* [5]

[15] https://invibio.com/components/spinal-rods; accessed 4 November 2019

face, and the risk of adjacent segment disease, which is a propagating disease due to abnormal loads on adjacent segments to the fused level, is reduced [16, 33, 127, 128, 130–132]. Despite the advantages of using PEEK or CF-PEEK bridging rods in specific surgical situations, the usage of these rods together with metallic screws and ordinary locking mechanism, e. g. set-screws or nuts, can lead to rod damage [129]. Typically, only a limited number of spine segments can be fused with purchasable CF-PEEK bridging rods due to their limited length [73]. These rods typically have a pre-bended shape [73]. In addition to rigid and semi-rigid pedicle screw systems, several dynamic systems exist on the market [23, 71, 127, 130, 132].

2.3 Material combinations

Nowadays, functional requirements can often not be met by a single material [133]. However, a hybrid structure, which is composed of two or more materials, can have properties that one part cannot fulfil [134]. Two parts or materials can be joined together to benefit from the advantages of each component [133, 135, 136]. However, a weak boundary layer can exist between two substrates and can decrease their interface strength [30]. It can be caused by surface contaminations, air or gas enclosures, or chemical reaction products [30]. For structural applications of material combinations, a sufficiently high interface strength has to be achieved [30].

2.3.1 Interface

The term *interface strength* describes the strength of the contact region of two materials or components. Cohesive failure of a hybrid structure occurs within the adherend and indicates excellent interface strength [137]. The term *cohesion* refers to attraction forces between atoms and molecules due to chemical primary and secondary valency bondings within the material [30, 138]. These types of bondings are illustrated in figure 2.6.

Adhesion is based on complex interdependencies across the interface [30]. Adhesive failure occurs at the interface between the adherends [137]. In this case, the failure surface is typically smooth [30]. Besides cohesive and adhesive failure, failure due to a combination of both is also possible [139]. *Kisin* informs about the empiric rule of adhesion: “The adhesion between two surfaces will be high if they show similar surface energies and low if there is a large discrepancy between the two” [140, p. 2]. Three types of adhesion can be differentiated [138]:

- *specific adhesion* due to chemical, molecular physical, and thermodynamic theories

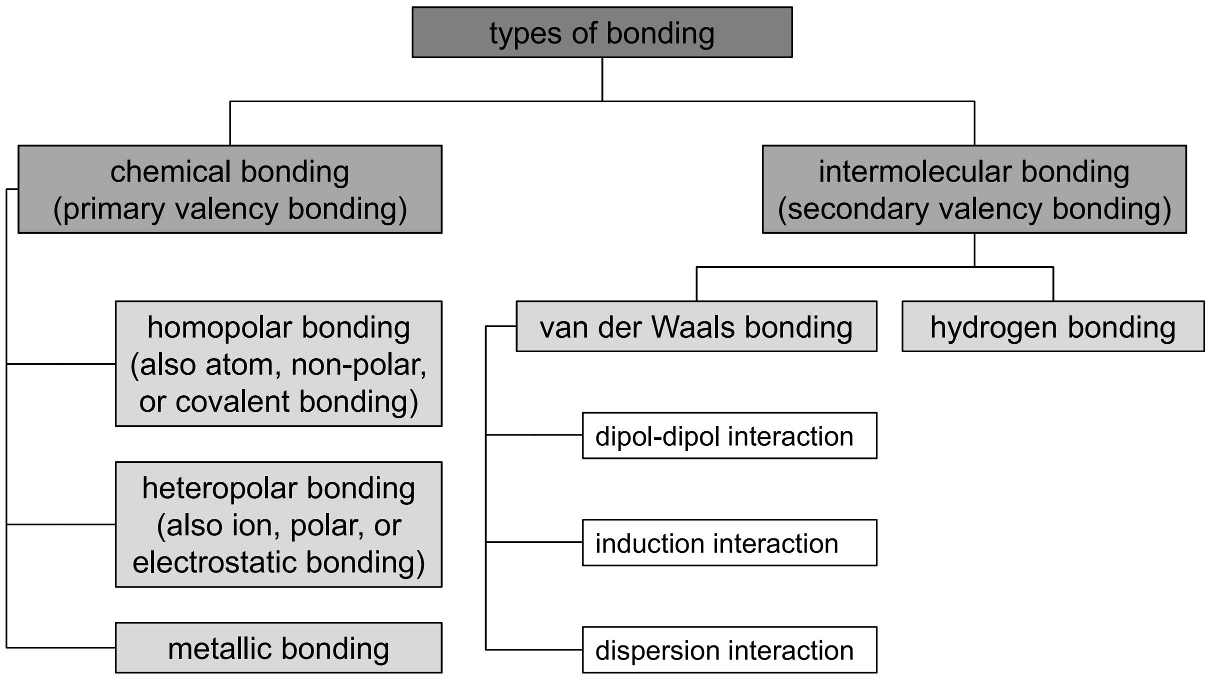

Figure 2.6.: Types of bonding according to [138]

- *mechanical adhesion* due to form fit of molten material and substrate
- *autohesion* due to diffusion and entanglements of chain segments across the interface

These models for the interpretation of adhesion and corresponding theories are shown in figure 2.7.

If molten polymers have close contact, interdiffusion of molecular polymer chain segments across the interface will occur leading to excellent interface strengths [142–145]. In the case of chemically identical materials, this process is called *autohesion* [30, 146] or *healing* because of the possibility of crack closure [143, 147, 148]. Healing of polymer interfaces is characterised by surface approach, wetting, diffusion, and randomisation [148]. Chains of one polymer, which cross the interface, interpenetrate the other polymer, and form entanglements with chains of the other polymer [147]. Healing is dependent on several processing parameters, such as time, temperature, pressure, or polymer characteristics, e. g. its mass. In 1971, *de Gennes* formulated the *reptation model* which is based on a three-dimensional (3D) network. This model describes that neighbouring chains, which represent obstacles, cannot be crossed by a polymeric chain but the chain can move in between [146]. For amorphous polymers, the glass transition temperature has to be exceeded for a sufficient time to enable healing processes [143, 147]. In contrast, semi-crystalline polymers typically require temperatures close to the melting temperature so that healing can occur because polymer chain mo-

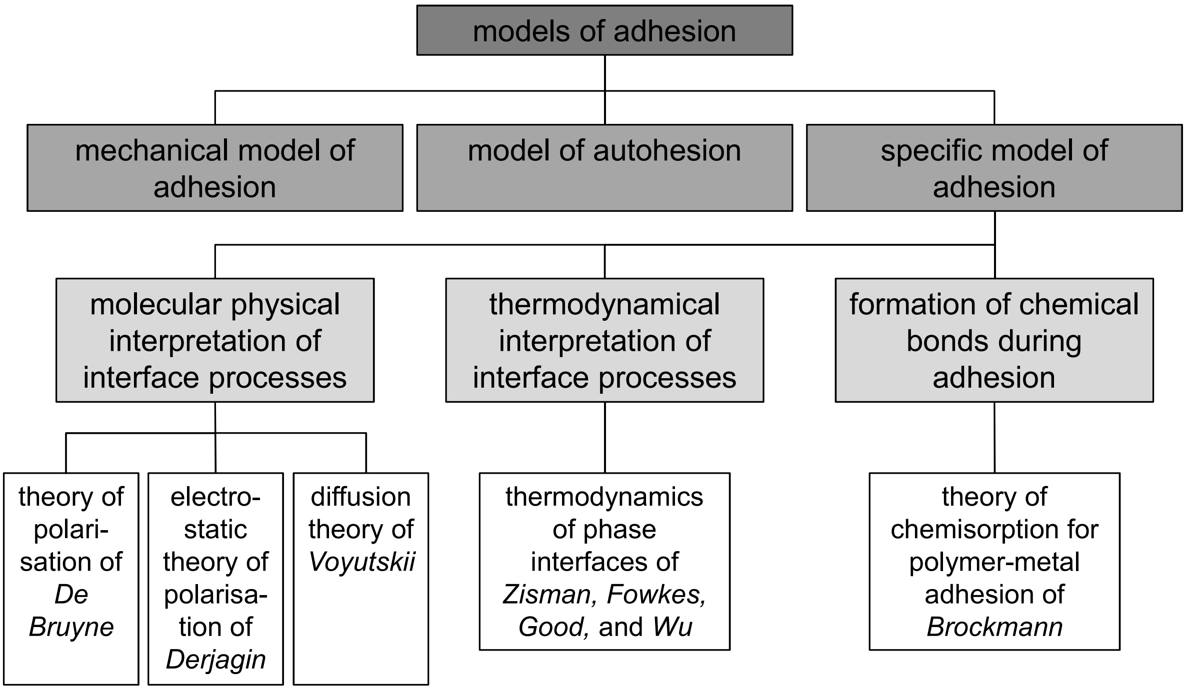

Figure 2.7.: Models of adhesion and corresponding theories according to [141]

bility is hindered by the presence of crystalline regions [143]. With sufficient healing time, and a constant healing temperature, the healed structure can reach the properties of the virgin material [148]. Increasing heating time leads to an improvement of chain mobility so that a deeper penetration of chain segments into the opposing surface is promoted [149]. *Lamèthe*, *Beauchêne* and *Léger* report that for PEEK specimens pre-heated at 250 ℃, 0.25 s are sufficient for chain interdiffusion under the application of pressure [149]. A detailed discussion about other theories of adhesion is beyond scope of this work but further literature can be considered.

One example of the interface formation by interdiffusion between a thermoset prepreg (e. g. bismaleimide or cyanate ester with woven fibres) and a thermoplastic part (e. g. polyether imide (PEI) or polyether sulfone (PES) with chopped GF) is described in [150]. Both matrices should be partially miscible so that the interface between the two parts can be formed by “bringing the parts into mutual contact and heating the parts at a temperature and pressure for a period of time sufficient to promote mutual miscibility” [150, p. 1]. This co-curing process leads to molecular diffusion of thermoplastic into the thermoset or vice-versa while the thermoset has still not fully cured. For this process, the cure temperature does typically not exceed the glass transition temperature of the matrix of the thermoplastic, and the cure time is about 0.5 h to 24 h. After curing, a structural joint between the thermoset and thermoplastic can be established with this technique. [150]

If two surfaces are in close contact with each other, surface forces will lead to the attraction of both surfaces [151]. A clear distinction exists between the *effective contact surface* and the *geometrical surface*. Whereas the geometrical surface only depends on the dimensions of the part, the effective contact surface influences interface strength [138]. The lower the viscosity of the molten mass or of the adhesive, the better the wetting and the bigger the effective contact surface [30, 152]. The viscosity of the molten mass can be decreased by increasing its temperature [152], but material degradation has to be avoided [145]. In addition to the effective contact surface and the geometrical surface, the *real surface* exists. It considers the roughness of the geometrical surface [138]. A rough material surface promotes mechanical interlocking of two surfaces in close contact [136, 153]. Figure 2.8 illustrates the three different types of material surfaces.

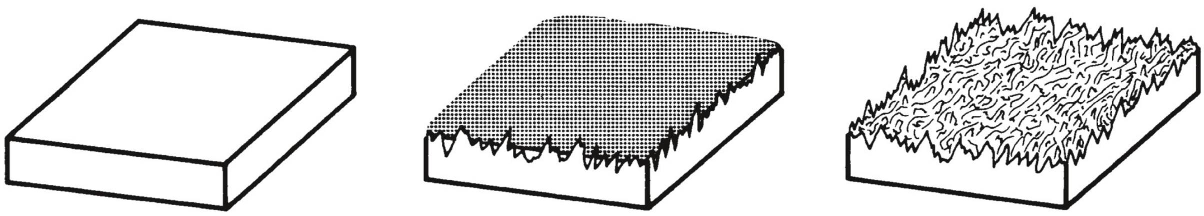

Figure 2.8.: Types of material surfaces [138]

A joint which relies on the mechanical interlocking between a phenolic thermoset and a GF-PC is described in [154]. To establish the joint between the two materials, the thermoplastic is heated above its melting temperature by a laser so that it can flow onto the surface of the thermoset and preferably into a notch or groove. After solidification of the thermoplastic, a sufficiently strong joint can be established. This technique can also be used to join thermoplastics with other non-thermoplastic materials. [154]

Another possibility to mechanically interlock thermosets with thermoplastics is described in [155] and is based on *a fibre reinforced thermoplastic hybrid interlayer*. For this process, a woven cloth was partially impregnated by the thermoplastic. One side of the cloth was not impregnated but was co-cured with a wet lay-up of a thermoset composite. During curing, the thermoplastic remelted and mixed with the thermoset matrix so that the dry parts of the woven cloth were impregnated, and mechanical interlocking occurred. In addition to mechanical interlocking, the interface strength was promoted by the interdiffusion of polymeric chains. With this technique, a lap shear strength of 20 MPa was achieved for a GF reinforced PEI-EP hybrid. [155]

2.3.2 Joining technologies

Hybrid structures can be manufactured by different joining technologies, such as mechanical fastening, adhesive bonding, welding, compression moulding, overmoulding, or as a combination of those [156, 157].

Mechanical fastening, adhesive bonding, and welding are post-mould assembly (PMA) technologies which are based on separate steps for forming of the product and assembly [134, 135, 156]. PMA technologies enable a higher freedom in product design [134]. Disadvantageously, process time is typically higher compared to in-mould assembly (IMA) technologies, such as compression moulding or overmoulding [135]. In contrast to PMA technologies, the assembly step is integrated into the forming step of the product for IMA technologies [30, 133, 134, 156]. The integration of the joining process in the compression or injection moulding step is a promising alternative for the production of structural parts with a high level of function integration [30, 143, 158]. Expensive assembly steps can be eliminated. However, thermal distortions and residual stresses can result [156]. Despite of this fact, several disadvantages of mechanical, adhesively bonded, and welded joints can be avoided with IMA technologies [158].

2.3.2.1 Mechanical fastening

Advantageously, mechanical fastened joints can be recycled and disassembled with little efforts [157]. In addition to that, different materials can be joined and quality can easily be controlled [4]. However, mechanical joints also have some disadvantages. The strength of the components is reduced due to the required holes [4]. Furthermore, high stress concentrations arise near the joining points [157, 159], contact corrosion can occur [158], and potential damage or delamination of composites can be the result of self-piercing joining [158].

In [157], strong mechanical joints between metal and polymer could be manufactured with the collar joining method in which annular collars were punched into a metal sheet which was then cold-pressed into a polymeric component. Another mechanical fastening technique to join metals and polymers is friction riveting [157, 159]. High rotation speeds of the metallic rivet lead to the melting of the polymeric region around the tip of the rivet [157, 159]. The rivet is then pushed into the molten polymeric base material [157]. Finally, a forging pressure is applied so that the tip of the rivet plasticises and a strong joint is established [157].

2.3.2.2 Adhesive bonding

Adhesive bonding strength is based on adhesion between adhesive and substrates, and on cohesion within the adhesive and substrates [156]. With this technique, dissimilar materials can be effectively joined, especially in the case of thin and flat components [4, 157]. Stress is more homogeneously distributed due to a large effective contact surface and the lack of holes, structural damping is improved, and there is less risk of corrosion problems compared to mechanical fastened joints [4]. In contrast to welding, no thermal residual stresses arise, and there is no warpage of the joined structure [4]. However, adhesive bonding is a time consuming and expensive joining process [4, 136]. Other disadvantages are the difficult recycling of adhesively bonded joints [144], the limited chemical, temperature and environmental stability of the adhesive [4, 136], and the existence of dimensioning shear stress peaks [4].

Due to their low surface energy [5], thermoplastic materials typically show poor conditions for adhesive bondings. Therefore, their surface is typically treated prior to bonding. Functional groups, which are prone to build covalent bonds, can be created with plasma or corona exposure, or with flame treatment [30, 155]. Roughening of the surface increases the effective contact area while it simultaneously cleans and activates the surface to achieve higher interface strengths [138, 144]. For metallic substrates, primers can be used to promote interface strength [144]. Concerning metallic adhesively bonded joints, interface strength is mainly dependent on adhesive properties, surface preparation, and the primer used [144]. Disadvantageously, surface pretreatments require additional cost, energy and time [30], and can also lead to specimen weakening [160].

2.3.2.3 Welding

A high number of welding techniques exists but for TPCs, ultrasonic, induction, and resistance welding are most common [144]. Temperatures within the welding zone and applied pressures are important factors for interface strength [160]. Although there are no stress concentrations due to holes within the part, residual stresses can exist after welding [144]. Welding of carbon fibre reinforced polymers (CFRP) can induce uneven heating spots and delaminations due to a high thermal and electrical conductivity [144].

In addition to common welding materials, thermoplastic films can be used to join different parts [144, 155]. In [155], thermoplastic films were co-cured with a thermoset composite. The thermoplastic showed a good chemical and mechanical compatibility with the thermoset composite [155]. The thermoplastic films could be used to join thermoset structures with each other so that acceptable joint strengths could be achieved [155]. With this technique, time and cost can be saved because the application of the thermoplastic films can be done prior to welding [144].

2.3.2.4 Compression moulding

In [161], a continuous GF-PP fabric was bonded to a long GF reinforced PP material in a single compression moulding step. Two mechanisms mainly contributed to interface strength: (1) interdiffusion of molecular chains, and (2) mechanical adhesion which is based on surface roughness. Insert pre-heating temperatures below but close to the melting point were chosen to achieve sufficient interface strength, to be able to handle the preform easily, and to maintain the initial preform geometry [161]. However, with such high pre-heating temperatures, fibre reorientation in the outer shell of the insert could occur due to insert surface melting and flow induced shear forces [161, 162] which may result in decreased mechanical properties of the hybrid structure [162].

The interface strength is highly dependent on the manufacturing parameters of the joint. *Cantwell et al.* inform about interface strengths of CF-PEEK specimens between 5 MPa and 50 MPa [163]. Additionally, they applied a 100 µm thick PEEK film in between two CF-PEEK adherends and achieved interface strengths in excess of 50 MPa by compression moulding. However, if the joining temperature is below the melting temperature of PEEK, interface strengths of less than 10 MPa will be observed. In their study, single lap shear (SLS) tests were conducted to determine the interface strength. [163]

2.3.2.5 Overmoulding

Overmoulding enables the production of lightweight parts in low cycle times and in an economic way [30, 160]. The interface strength of the overmoulded structure is dependent on the processing parameters [142]. If the molten mass and insert are in close contact, heat will be transferred from the molten mass to the insert [142]. If the interface temperature exceeds the melting temperature of the insert, the surface of the insert will melt, and molecular interpenetration across the interface will occur so that excellent interface strengths can be achieved [142, 145]. Afterwards, cooling leads to a solidification of the interface [142] and to a demouldable hybrid product. Both thermal energy and shrinkage of the molten mass can contribute to interface strength [30].

Sufficient high temperatures at the interface are typically required for excellent interface strengths because diffusion is enhanced and the viscosity of the molten mass decreases so that insert wetting is promoted [30, 152]. The interface temperature is dependent on the temperature of the molten mass, the mould, and the insert [152]. However, degradation of the molten mass will occur if its temperature is too high [145]. Increasing the mould temperature reduces insert cooling before overmoulding so that interface strength can be enhanced [30, 162], but cycle time can increase [160].

Overmoulding is based on the injection moulding technology. Injection moulding is one of the most common polymer processing technologies [164]. Mainly three stages exist for this process: plasticising, forming and demoulding [30]. Complex parts can be produced economically and with high function integration, accuracy, and quality [15, 29, 30]. Not only neat polymers, but also short and long fibre composites like CF-PEEK can be processed with this technology. Injection moulding of PEEK requires processing temperatures of about 400 ℃, and mould temperatures of 175 ℃ to 205 ℃ [5]. Fibre orientation, fibre distribution and fibre length vary dependent on processing parameters [74]. Additionally, mould design is a significant factor concerning fibre orientation [74]. Due to discontinuous fibre distributions, structural mechanical properties are lower than for unidirectional fibre reinforced composites [74]. Cooling of the molten mass leads to solidification and shrinkage [5, 164]. Residual stresses and warpage can be the result of non-uniform cooling [29, 143, 164]. Polymer shrinkage can even lead to the separation of the overmould from a metallic substrate [153]. However, by using composite overmoulds, thermal shrinkage can be reduced [153].

No standardised test method exists for overmoulded structures. In [156], a flat metal insert was partially overmoulded with long fibre reinforced thermoplastics (LFTs). The resulting flat hybrid pull-out specimen was tested under tension [156]. *Epple and Bonten* modified a mould for dog bone specimens so that an insert could be positioned and partially be overmoulded [3]. For interface characterisation between a resin and a composite, the Iosipescu specimen geometry was used in [143]. Another test specimen for hybrid structures was described in [158]. Here, a hybrid plate was cut and notches were milled into the specimen to conduct compression shear tests [158]. Finally, *Tanaka*, *Fujita* and *Katayama* describe a process in which a composite laminate was pressed, and a rib structure was overmoulded [165]. After cutting, T-shape specimens were tested in tension to characterise interface strength [165].

Overmoulding of metals

One of the first relevant examples of the implementation of a metal structure overmoulded with a fibre reinforced thermoplastic polymer is the front end of the Audi A6 from 1996 [136]. For this hybrid product, a sheet steel was deep-drawn and overmoulded with GF-PA so that a hybrid rib structure could be produced which benefited from the properties of both materials [136, 166]. In addition to the lightweight potential, the overmoulding of metals with polymers can lead to electrical conductivity of polymeric products [133].

The interface strength, which results from the overmoulding of metals with polymers, is typically based on form fit and mechanical adhesion [30, 136, 156]. The polymer melt solidifies in cuts and indentations within the metal insert [156]. If the metal surface is rough, micromechanical interlocking between metal insert and molten polymer mass will be promoted [156]. Heating the metal insert before overmoulding improves micromechanical interlocking and interface strength because the polymer can penetrate more easily the microroughness of the insert [136, 137, 153]. Without pre-heating of the adherend, a solidified skin layer of the overmould can restrict microroughness penetration [167]. However, even if the adherend is cold, the macroroughness of the metal adherend can be penetrated by the polymer by applying high pressures [167].

In addition to form fit and mechanical adhesion, interface interdependencies, such as covalent bonds, dipole-dipole interactions, or hydrogen bonds between polymer and metal (cf. figure 2.6), can contribute to interface strength [139]. Adhesion can be improved by etching, anodising, plasma spraying, abrasive blasting, pre-heating, or laser structuring of the adherend [136, 158]. Additionally, primers can be used which should adhere well to both the substrate and the overmould [136]. The combination of adhesion and interlocking can redundantise holes for form fit so that a reduction of structural properties can be avoided [136].

Overmoulding of polymers and composites

A typical application of the overmoulding technology in terms of overmoulding thermoplastic endless fibre reinforced structures (laminates) is their reinforcement by ribs. These overmoulded ribs can increase the geometrical stiffness and resistance of laminates, for example against buckling loads [143, 145]. Overmoulding of thermoplastic laminates combines the superior mechanical properties of endless fibre reinforced composites with the high freedom in design of injection moulded parts [1, 168]. If a cohesive interface due to surface melting is achieved, excellent interface strengths will result. Otherwise, an adhesive interface between insert and overmould exists. The laminates can be formed by closing the mould, and can be functionalised by overmoulding additional elements like ribs, hooks, or bosses [2, 145]. For this process, the global players concerning injection moulding, *KraussMaffei Group GmbH* and *Engel Austria GmbH*, developed special technologies[16, 17] with which heating of semi-finished parts, thermoforming, and overmoulding can be automatically realised in one production facility.

To join a thermoset CF-EP prepreg with thermoplastic PP, a similar approach can be

[16]www.kraussmaffei.com/de/unsere-verfahren/fiberform-technologie; *FiberForm-Technology*; accessed 9 January 2020

[17]www.engelglobal.com/de/at/verfahren/leichtbau/organomelt.html; *ENGEL organomelt*; accessed 18 February 2020

used. The prepreg is pre-heated with a pre-heating time lower than its cure time. It is then transferred to the mould, the mould closes, and the thermoplastic is injected. Besides of the overmoulding, the thermoset is drawn and formed into the shape of the cavity. The materials remain in the mould until the thermoset is completely cured. [169]

A different approach is the selective local reinforcement along the main load paths of injection moulded structures by endless fibres. In [170], a production technique is presented with which a hybrid product was manufactured, based on an overmoulding process of endless fibre inserts. As a result of this process, injection moulded parts were locally reinforced by unidirectional fibre reinforced tapes, and metallic inserts were used as load introduction elements [170]. Compared to completely discontinuous fibre reinforced products, higher specific structural mechanical properties could be achieved [170]. Another example of a locally reinforced structure is published by *Menovsky et al.* in the patent US20180008275A1 which describes a hybrid clip for aneurysm [171]. For this clip, a thin biocompatible unidirectional CF-PEEK spring insert used for tight closure of the aneurysm was overmoulded with CF-PEEK [171]. No artefacts in medical imaging technologies were created with this clip [171]. In addition to that, *DePuy Synthes* patented a polymeric PEEK bridging rod with a local internal unidirectional CF-PEEK reinforcement (patent US9232968B2) to enhance bridging rod strength and fatigue properties [172]. The hybrid bridging rod can be produced by pressing or overmoulding [172].

Thermoplastic polymeric or composite inserts should be heated prior to overmoulding to increase the interface temperature and to promote interface strength [143, 145, 152]. Dependent on the insert pre-heating temperature, handling and fixation can be difficult [166]. An appropriate insert fixation in the mould is important for successful overmoulding [166]. If the surface of the polymeric insert melts, a cohesive interface will be formed. In this case, excellent interface strengths can be achieved due to molecular interdiffusion and entanglements across the interface [145, 166]. Therefore, the melting temperature of the insert should be smaller than or equal to the melting temperature of the molten mass [166]. For example, this can be achieved by using the same matrices for insert and overmould [143]. Geometric stability of the pre-heated insert prior to overmoulding has to be ensured which means that ideally only the surface of the insert should melt but not the bulk material [152].

Similarly to adhesive bondings, surface preparation methods can lead to an improvement of interface strength of polymeric or composite overmoulded structures. As an example, plasma treatment can be used to effectively increase interface strength by the activation and the cleaning of the surface of the polymeric insert [166].

Overmoulding of polyaryle ether ketones (PAEKs) is eased by the use of low-temperature processing PAEK inserts [1]. With these kind of inserts, the heat required for achieving a high-strength interface is reduced. In [168], a low-melt multi-layer PAEK composite laminate was overmoulded with PEEK without pre-heating of the insert, and an interface with sufficient strength could be established.

3 Research objectives and procedure

The majority of polymeric products is manufactured by processes which typically show a high level of automation, such as injection moulding. With these processes, low cycle times and high production rates can be achieved. These attributes will still be maintained if different materials are joined within the manufacturing process, e. g. by overmoulding. The overmoulding technology enables the production of hybrid structures which consider that the most expensive material with the best structural mechanical properties is only used where it is actually needed. Thus, the lightweight potential of these structures is utilised while cost is kept low. With hybrid TPC structures, which satisfy both the aspects of *low cost* and *high performance*, new fields of applications can be unlocked. In this work, an advantageous material combination with a high-strength interface is realised under the consideration of a hybrid composite pedicle screw.

It has been shown that composite implants are characterised by distinct advantages compared to their metallic counterparts (cf. chapter 2.1). However, failure of radiolucent composite implants can lead to the loosening of implant parts within the patient's body which are difficult to locate by medical imaging technologies. Additionally, micromotions due to the reduced stiffness of discontinuous CF reinforced composite pedicle screws hinder osseointegration and can lead to screw loosening [47]. Therefore, the concept of a hybrid composite pedicle screw, which is based on the material combination of discontinuous short CF reinforced PEEK (sCF-PEEK) and continuous unidirectional endless CF reinforced PEEK (uCF-PEEK), was developed. This concept aims at the structural integrity of the pedicle screw in the case of screw breakage, and at the possibility to tailor the stiffness of the hybrid composite screw to its application by varying the thickness of its core or the fibre volume fraction. Additionally, the risk of pedicle screw breakage, for example under bending loads, can be decreased by this concept because the strength of the hybrid composite screw is superior compared to their discontinuous fibre reinforced counterparts.

In the following, a focus is laid on the stiffness assessment of the hybrid composite pedicle screw. The Young's modulus of the injection moulded sCF-PEEK material highly depends on the fibre distribution and fibre orientation. According to the material data sheet of the manufacturer *Invibio Ltd.*, it is assumed to be 18 GPa in the following [173]. The stiffness of cortical bone is similar to this value but depends on several factors, such as age, gender, or the patient's health condition. *Bader et al.* described the need for lowering the stiffness of the implant to reduce stress shielding [19]. Discontinuous CF reinforced PEEK pedicle screws can efficiently reduce stress shielding.

However, higher micromotions between bone and implant can exist due to the reduced implant stiffness. These micromotions can hinder osseointegration and reduce screw stability [47], as mentioned before. Furthermore, implanting a pedicle screw system results in pull-out forces which are acting on the pedicle screw head. These loads motivate the need of high screw stiffness in longitudinal direction so that the bone stress distribution around the screw thread is more homogeneous and micromotions between screw and bone are reduced.

Under the assumption of a sufficient strong interface between core and overmould, the stiffness components of the hybrid composite screw are connected parallel in longitudinal direction. The total longitudinal stiffness of the hybrid composite pedicle screw $E_{tot}^{||}$ can be calculated by using the rule of mixture [4] with the corresponding volumes $V_{uCF-PEEK}$ and $V_{sCF-PEEK}$ of the uCF-PEEK core and the sCF-PEEK overmould, related to the total volume V_{tot} of the hybrid composite pedicle screw:

$$E_{tot}^{||} = \frac{V_{uCF-PEEK}}{V_{tot}} \, E_{uCF-PEEK}^{||} + \frac{V_{sCF-PEEK}}{V_{tot}} \, E_{sCF-PEEK} \tag{3.1}$$

In this equation, $E_{uCF-PEEK}^{||}$ is the stiffness of the uCF-PEEK core in fibre direction, and $E_{sCF-PEEK}$ is the stiffness of the sCF-PEEK material which is assumed to be isotropic. For the calculation, a pedicle screw with common dimensions (length of 51 mm, outer diameter of 6.5 mm) was considered. The total volume of this screw was determined with 1154 mm^3. Additionally, a central and cylindrical uCF-PEEK core was assumed which had a diameter D of 2.5 mm and covered the whole length l of the pedicle screw of 51 mm. The volume $V_{sCF-PEEK}$ of the sCF-PEEK overmould can then be calculated by

$$V_{sCF-PEEK} = V_{tot} - V_{uCF-PEEK} = V_{tot} - \pi \left(\frac{D}{2}\right)^2 l \approx 904 \, mm^3 \, . \tag{3.2}$$

With the stiffness of the uCF-PEEK core in fibre direction[1] and the stiffness of the sCF-PEEK material of 18 GPa [173, 174], equation 3.1 yields approximately 50 GPa for the total longitudinal stiffness $E_{tot}^{||}$ of the hybrid composite pedicle screw.

The patient's weight represents a natural loading case in which transverse forces are acting on the pedicle screw. For the calculation of the total transverse stiffness $E_{tot}^{\perp}$ of the hybrid composite pedicle screw, the isotropic stiffness $E_{sCF-PEEK}$ of the sCF-PEEK material of 18 GPa [173, 174] and the transverse stiffness $E_{uCF-PEEK}^{\perp}$ of the uCF-PEEK core[2] are connected in series [4]. The resulting total transverse stiffness is

[1] 170.2 GPa; material data of *Invibio PEEK-OPTIMA™ Ultra-Reinforced* provided by *Neos Surgery S. L.*
[2] 9.4 GPa; material data of *Invibio PEEK-OPTIMA™ Ultra-Reinforced* provided by *Neos Surgery S. L.*

then calculated by inverting

$$\frac{1}{E_{tot}^{\perp}} = \frac{1}{E_{uCF-PEEK}^{\perp}} \frac{V_{uCF-PEEK}}{V_{tot}} + \frac{1}{E_{sCF-PEEK}} \frac{V_{sCF-PEEK}}{V_{tot}} \ . \tag{3.3}$$

Inverting this equation yields a total transverse stiffness $E_{tot}^{\perp}$ of approximately 15 GPa which fits well to the stiffness of human bone.

Both the total longitudinal and transverse stiffness of the hybrid composite pedicle screw are much lower than the stiffness of a titanium implant of approximately 114 GPa [18, 48, 114, 124, 175]. The stiffness of the hybrid composite screw in transverse direction is lower than that of a discontinuous CF reinforced screw because the uCF-PEEK core has inferior structural mechanical properties perpendicular to the fibre direction. Thus, stress shielding can be effectively reduced. In addition to that, the stiffness of the hybrid composite screw in longitudinal direction is higher compared to discontinuous CF reinforced screws to prevent micromotions so that osseointegration can be promoted. Besides, the compression stiffness component of the hybrid composite screw is close to that of bone as well.

Based on this motivation, the primary aim of this work is to develop and analyse a function optimised design of a hybrid composite pedicle screw. This function optimisation yields (1) the possibility of tailoring the pedicle screw stiffness to prevent stress shielding, to maximise screw stability and to increase the applicability of composite screws, (2) the prevention of artefacts in medical imaging technologies, (3) a decreased weight compared to metallic screws, and (4) an increased bending strength compared to discontinuous fibre reinforced screws.

For this purpose, the methodology shown in figure 3.1 is followed. This work aims at a profound material and interface characterisation of the underlying materials, the comparison of different interface characterisation methods, the development of a suitable specimen for interface characterisation, the comprehension of the interface formation, the numerical investigation of the hybrid composite pedicle screw, the determination of an optimal hybrid composite pedicle screw design, the realisation of the manufacturing process of the hybrid composite pedicle screw considering the possibility of automation, and the biomechanical characterisation of the hybrid composite pedicle screw.

Profound know-how about the interface strength between a continuous endless CF-PEEK insert and discontinuous short CF-PEEK overmoulding material is of crucial importance for this research. Therefore, a special focus was laid on the development of comprehension concerning the interface strength.

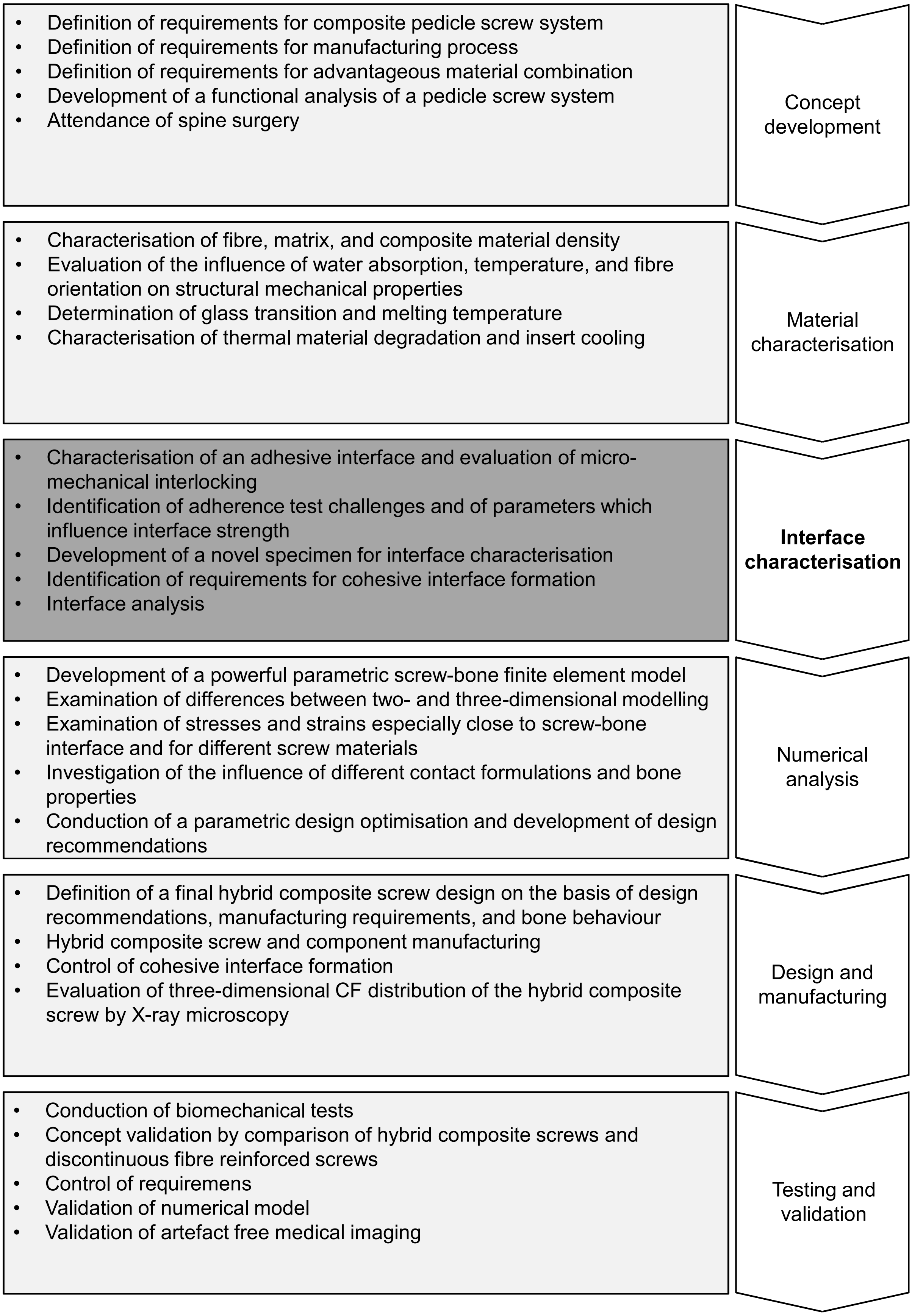

Figure 3.1.: Methodology and objectives of this work

4 Material and interface characterisation, modelling, design, and verification

The specifications of the CPSS are defined in the beginning of this chapter. Additionally, profound material and interface characterisations are presented which were conducted to successfully realise the concept of the hybrid composite pedicle screw. In parallel, finite element (FE) models were developed in *Abaqus 2018* from *Simulia* (*Dassault Systèmes SE*) to simulate the interaction between pedicle screw and bone, and to perform a design optimisation of the hybrid composite pedicle screw. For these studies, two- and three-dimensional (2D and 3D) FE models were generated in the programming language *Python*. Based on the design recommendations, the manufacturing requirements and the bone characteristics, a final design of the hybrid composite pedicle screw was developed and the screw could be manufactured. Additionally, the other components of the CPSS were designed and manufactured. At the end of this chapter, biomechanical tests and other validations emphasise the advantages of the hybrid composite pedicle screw and the CPSS.

4.1 Specification

The requirements, which the CPSS has to fulfil, were defined in the beginning of this research. A focus was laid on a one-level pedicle screw fixation system (cf. figure 2.3).

Figure 4.1 illustrates the functions of a pedicle screw system based on the modelling times *during surgery* and *after surgery*, and shows that the manufacturing process induces additional requirements to the CPSS components. Functions, which are only important after surgery, are shown with dashed arrows. The four components of the pedicle screw system (cf. figure 2.2) were analysed together with two head system components namely *surgeon* and *patient*. The term *spine segment* refers to the region of the spine which is treated.

As mentioned in chapter 2.2, the main function of the pedicle screw system is the restriction of the motion of the affected spine segment and the correction of spine alignment. On the one hand the system has to withstand forces which appear during the installation of the system and the alignment of the spine during surgery. On the other hand pull-out, bending, and torsional forces act on the system during its service time. For the hybrid composite pedicle screw, 1 kN was specified as the required pull-out force the screw has to withstand, based on the literature [106, 107, 122]. Additionally, the screw insertion torque should be less than 3 Nm [110, 123]. Concerning cyclic

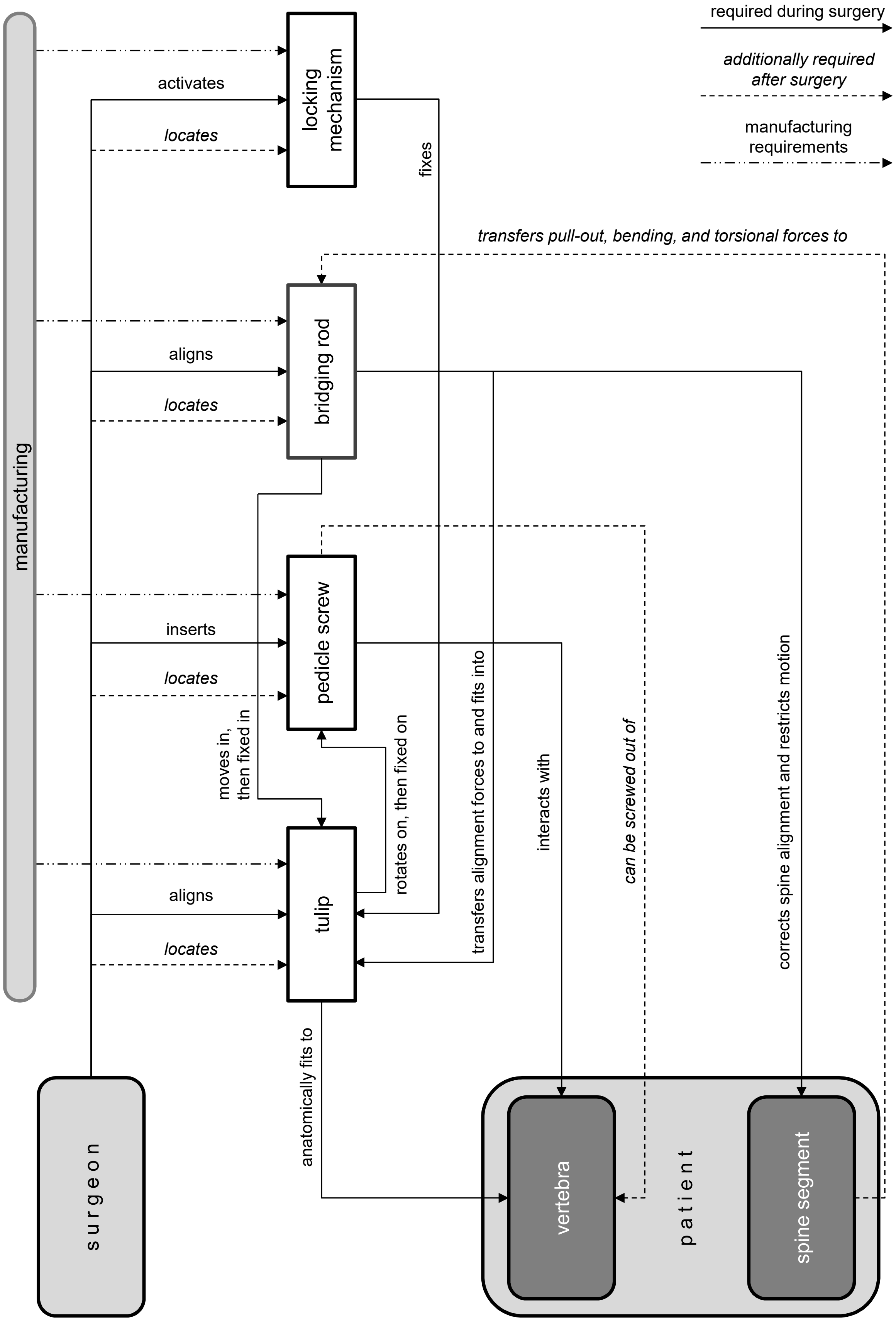

Figure 4.1.: Functional analysis of a pedicle screw system

testing, the hybrid composite pedicle screw has to resist 2.5 million cycles at a specific load [176].

The design of the CPSS had to consider the spine anatomy and the surgical procedure for the installation of the system. The basic dimensions of the composite pedicle screw were defined in the specifications in order to standardise certain variables a priori and to decrease the number of design variations. With this standardisation, the outer shape of a *master screw* was specified. The design space for the screw shaft was defined as a cylinder with a length of 45 mm and a diameter of 6.5 mm. Within this design space, the optimum design in terms of structural mechanical properties, stability, and manageability of the pedicle screw had to be found. The head of the polyaxial screw had to allow a multi-axial rotation of the tulip of at least 15° to ease system installation. Concerning the reinforcing uCF-PEEK insert of the hybrid composite pedicle screw, a compromise of its diameter had to be found considering both conflicting aspects: (1) increasing the structural mechanical properties of the screw in longitudinal direction (favoured by a big insert diameter), and (2) ensuring flowability of the molten mass to form the screw head and thread (favoured by a small insert diameter). The design of the CPSS had to account for the composite material properties. Compared to titanium, the structural mechanical properties of sCF-PEEK and of uCF-PEEK in transverse direction are lower. On the one hand a reduced material stiffness is beneficial because stress shielding is reduced. On the other hand the design of the system has to account for reduced material strength, creep, and potential micromotions between implant and bone due to reduced stiffness.

Additional requirements existed due to the manufacturing process of the CPSS components. For the manufacturing of the hybrid composite pedicle screw, the uCF-PEEK insert was overmoulded with sCF-PEEK material. The concept of the overmoulding process is illustrated in figure 4.2.

The injection moulding of the hybrid composite pedicle screw and other potential injection moulded CPSS components required a tool design which avoided material agglomerations and undercuts so that demoulding was feasible. PEEK is a high temperature resistant thermoplastic material which is processed at approximately 380 ℃ (cf. chapter 2.1.2.1). Therefore, an injection moulding machine with a high temperature equipment and suitable temperature control was required. In addition to that, a sealed fixation of the uCF-PEEK insert within the mould was required for precise overmoulding. The complete filling of the mould cavity by the molten mass had to be ensured, and rework of the injection moulded parts had to be as low as possible. If the inserts are heated prior to overmoulding, the heating and transfer time to the mould will have to be in-line with the injection moulding cycle. As a consequence, efficient production was

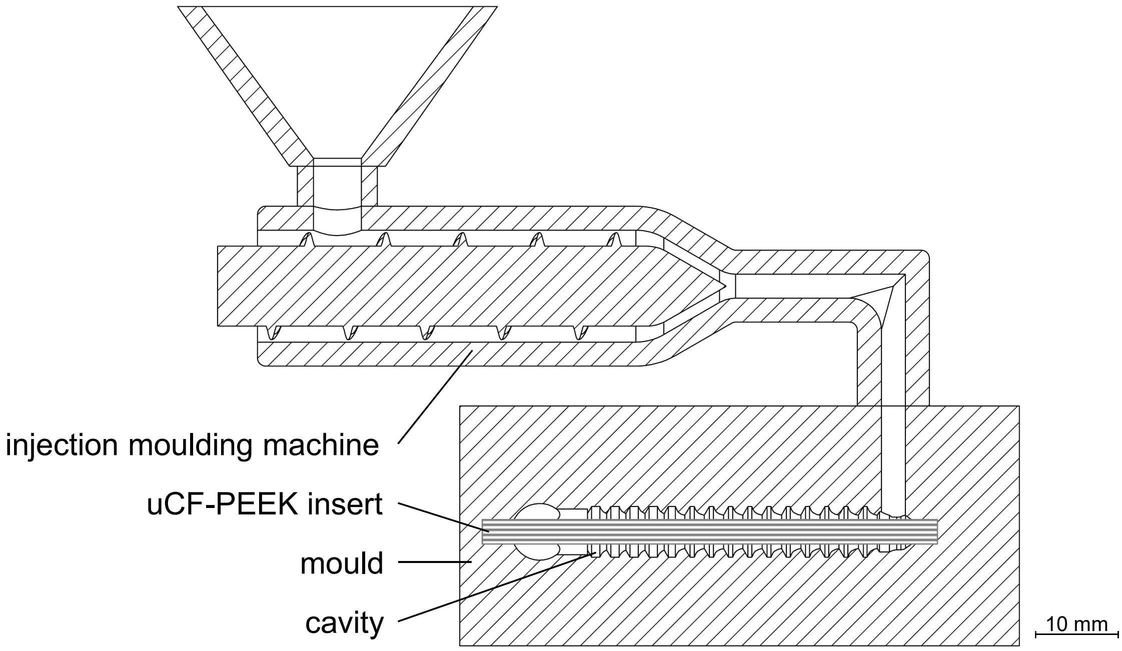

Figure 4.2.: Overmoulding concept of the composite pedicle screw core

feasible. Since the bridging rod was a purchased and licensed part, no manufacturing requirements existed for this component.

An excellent adhesion between the uCF-PEEK core and the overmoulding material of the hybrid composite pedicle screw had to be achieved due to

- the preservation of the structural mechanical properties of the screw also for long time application,
- the prevention of the core from disassociating from the overmould to ensure structural integrity during transport, assembly and service life,
- the transfer of shear forces from the overmould to the core which arise due to pull-out loads, and
- the increase in applicability and the extension of the freedom in design meaning the realisation of smaller screw diameters and smaller screw lengths while still having sufficient structural mechanical properties.

To better understand the requirements that a pedicle screw system has to fulfil during implantation, a spine surgery was attended at the *Westpfalz-Klinikum GmbH*. For this research, it was considered important to know how surgeons treat a pedicle screw system and which difficulties have to be faced during surgery. By the attendance of the spine surgery, the procedures during operation were better understood. Additionally, the psychological and physiological stresses of the surgeon and its assistants could be assessed. Long operation times are common for spine surgeries. These times must not increase due to complicated system design or alignment difficulties due to insufficient degrees of freedom (DOFs) of the system. In the development process of an implant, the conditions during surgery have to be reflected. Easy manageability and installation of an implant has to be ensured so that surgeons can focus on its precise installation. During implantation, the surgeon has only few possibilities to align the pedicle screw system due to limited space and anatomic restrictions. System misalignments or breakage typically require the removal of the pedicle screw system which also has to be considered for the design of the CPSS. The surgeon who installed the system is not necessarily in charge of its removal. Additionally, special systems typically require special tools for installation and removal. However, not every tool is available in every operating theatre. Considering these aspects, the possibility to remove the CPSS with ordinary tools was defined as one additional requirement. Finally, sharp edges should be avoided in the design of the CPSS components to prevent the operating staff and the patient from injuries.

The CPSS had to be sterilised according to the international standard DIN EN ISO 14630 [177] to prevent infections. Since CF-PEEK was used for the CPSS, the system could be sterilised by common sterilisation methods (cf. chapter 2.1.2.1).

The CPSS had to be artefact-free in order to neither affect medical imaging technologies, such as X-ray, CT scan or MRI, nor to attenuate radiotherapy. However, the screw had to be visible up to a certain degree so that the surgeon is able to locate it at any time during and after surgery. Talking to surgeons, it is sufficient to locate the outer edges of the screw thread and its tip. The surgeon can then be sure that the pedicle entirely surrounds the screw, and that the tip of the screw does not protrude the cortical shell of the vertebra. Visibility of the CPSS components can be ensured by a titanium coating and radio-opaque markers (cf. chapter 2.1.2.1). By a titanium coating, not only the visibility but also the osseointegration of the hybrid composite pedicle screw can be enhanced.

4.2 Material and interface characterisation

In this work, the material combination of the hybrid composite pedicle screw was realised by overmoulding a uCF-PEEK insert with sCF-PEEK material. To be able to deeply understand this process and the resulting product, relevant physical, thermal, and mechanical properties have to be known. However, only the material manufacturer typically knows all relevant material data. Therefore, a profound material and interface characterisation was conducted to determine relevant properties for the materials used.

Three materials were studied: uCF-PEEK plate material from *Haufler Composites GmbH & Co. KG*, uCF-PEEK rod material *PEEK-OPTIMA™ Ultra-Reinforced* from *In-*

vibio Ltd., and sCF-PEEK injection moulding material *Victrex® PEEK 450CA30* from *Victrex plc*.

4.2.1 Mass density measurement

The mass densities were of interest to evaluate the weight saving potential of the CPSS compared to metallic systems. In addition to that, the densities were used in the rule of mixture in chapter 4.2.4 to determine the fibre volume fraction of the material and to compare these results with the results obtained by thermogravimetric analysis (TGA). To determine the mass densities of the underlying materials, density measurements by the principle of liquid displacement on the basis of DIN EN ISO 1183 [178] were conducted.

1.25 ml wetting agent[1] was mixed with 250 ml demineralised and degassed water to obtain the immersion liquid. Nine sCF-PEEK specimens with the dimensions of 25 mm × 25 mm × 2 mm (length l × width w × thickness d), three uCF-PEEK plate specimens with the dimensions of 25 mm × 25 mm × 2 mm ($l \times w \times d$), and three uCF-PEEK rod specimens with a diameter of 2.5 mm and a length of about 15.5 mm were examined in this study. The precision scale *Ohaus DV214C* was used for the measurements, and the study was conducted at room temperature. In accordance with the standard, no conditioning of the specimens was required because the determination of the density up to the second position after the decimal point was sufficient. It was assumed that the lift of the copper wire, which was used for the fixation of the specimen in the liquid, was negligible.

To determine the density of the composite materials, the density ρ_{IL} of the immersion liquid was determined first. For this purpose, a standard test body with a volume V_{TB} of 10 ml was used. The mass m_{TB}^{dry} of the test body was measured in dry conditions for ten times. Additionally, its mass m_{TB}^{dipped} was measured for ten times when dipped in the immersion liquid. The density of the immersion liquid was calculated by using the formula [178]

$$\rho_{TB} = \frac{m_{TB}^{dry}}{m_{TB}^{dry} - m_{TB}^{dipped}}\, \rho_{IL} \tag{4.1}$$

in which ρ_{TB} is the density of the test body. Reordering of equation 4.1 for ρ_{IL} and using $V_{TB} = \frac{\rho_{TB}}{m_{TB}^{dry}}$ yields

$$\rho_{IL} = \frac{m_{TB}^{dry} - m_{TB}^{dipped}}{V_{TB}}\,. \tag{4.2}$$

Using this formula, the density of the immersion liquid was determined to be 1.00 g/cm^3.

[1] *WAC Wetting Agent* from *Compard AG*

With this value, the density of the different materials could be determined. The mass of each specimen was measured several times when dipped in liquid. The density of the fibre reinforced polymers (FRP) could be calculated by using equation 4.1. For the sCF-PEEK material, the density was $(1.41 \pm 0.001)\,g/cm^3$, and for both the uCF-PEEK plate and uCF-PEEK rod material $(1.58 \pm 0.004)\,g/cm^3$. *Victrex plc* informs about an sCF-PEEK density of $1.40\,g/cm^3$ in the corresponding data sheet [179], and *Invibio Ltd.* specifies the density of the uCF-PEEK rod material with $1.59\,g/cm^3$ [180]. These values are in good accordance with the measurements. The density of the sCF-PEEK material is dependent on the processing condition of the injection moulding process and the resulting fibre volume fraction. The fibre volume fraction also varies dependent on the location at which the specimen is taken from. The theoretical fibre mass fraction calculated with the mass densities is presented in chapter 4.2.4.

Table 4.1 summarises the data of the densities ρ_{FRP}, ρ_m and ρ_f of the composites, matrices and fibres, and informs about the CF type of the materials.

Table 4.1.: Densities of the composites, their matrices, and fibres

Material	ρ_{FRP} in g/cm^3	ρ_m in g/cm^3	ρ_f in g/cm^3	CF type
uCF-PEEK plate	1.58 ± 0.004	1.30 [66, 181]	1.79 [182]	ST [a)] [182]
uCF-PEEK rod	1.58 ± 0.004	1.30 [66, 181]	1.74 [4]	IM [b)]
sCF-PEEK	1.41 ± 0.001	1.30 [66, 181]	1.74 [4]	HT [c)] [183]

[a)] super tenacity carbon fibre, *HexTow® AS4A* from *Hexcel Corp.*

[b)] intermediate modulus carbon fibre

[c)] high tenacity carbon fibre

No information about the CF type of the uCF-PEEK rod material was available. However, assuming a Young's modulus of 294 GPa for intermediate modulus (IM) CF in fibre direction [4], a Young's modulus of 4 GPa for the PEEK matrix [66], and a fibre volume fraction of 62 vol.-% [180], a theoretical stiffness of the uCF-PEEK rod material of approximately 184 GPa was obtained. This value is slightly higher but still in good accordance with the data sheet[2]. Conducting the same calculation with other fibre types resulted in higher differences compared to the composite material stiffness listed in the data sheet. In addition to that, the theoretical density of the composite of $1.57\,g/cm^3$ will fit well to the material density determined in this study and to the material data sheet [180] if the density of $1.74\,g/cm^3$ of the IM CF [4] and the density of $1.30\,g/cm^3$ of the PEEK matrix [66, 181] are used for calculation. Consequently, IM

[2] 170.2 GPa; material data of *Invibio PEEK-OPTIMA™ Ultra-Reinforced* provided by *Neos Surgery S. L.*

CFs were assumed to be used for the uCF-PEEK rod material. The fibre density of the uCF-PEEK rod material listed in table 4.1 is based on this assumption.

With this study, the mass of the CPSS could be approximated and compared with a titanium pedicle screw system[3] which consisted of tulip, set-screw, and a pedicle screw with similar dimensions to the hybrid composite pedicle screw. For both systems, a bridging rod with a length of 70 mm and a diameter of 6 mm was considered. Although the titanium pedicle screw was cannulated and fenestrated, the mass of the CPSS (8.4 g) was less than half of the mass of the titanium system (17.3 g). This mass difference will be significant especially if several spine levels have to be stabilised by the pedicle screw system.

4.2.2 Liquid absorption analysis

Because the CPSS will be subjected to humid environment when implanted in the human body, the effect of the immersion in saline environment on the structural mechanical material properties was determined. Additionally, the mass changes of the uCF-PEEK plate and sCF-PEEK material due to liquid absorption were investigated. Six uCF-PEEK plate specimens, six sCF-PEEK specimens, and five sCF-PEEK screws were dried in a convection oven at 50 ℃ for 20 days and 17 hours. After this time, drying did not result in any further significant mass loss. The dimensions of the uCF-PEEK plate and sCF-PEEK specimens were 80 mm $\times$ 20 mm $\times$ 2 mm ($l \times w \times d$). Three uCF-PEEK plate specimens and three sCF-PEEK specimens were placed in a basin with 9 l distilled water. The remaining specimens and the screws were placed in a basin with 19.5 l saline solution (9 g sodium chloride (NaCl) per litre). The liquid absorption analysis was conducted at room temperature.

The relative mass changes χ^m of the specimens and the screws were calculated by relating their absolute mass change to their mass after drying m^{dry}:

$$\chi^m = \frac{m - m^{dry}}{m^{dry}} \tag{4.3}$$

In this equation, m represents the mass of the specimen or the screw at a specific time after immersion. The relative mass change of the specimens and the screws over the immersion time t is shown in figure 4.3.

No difference between the mass change of the specimens immersed in water and in saline solution could be observed. As expected, the maximum mass change decreased with increasing CF volume fraction because CFs do not significantly absorb any liquid. The sCF-PEEK material showed a relative mass change of (0.36 $\pm$ 0.006) % which is

[3] *Spineart Romeo® 2 MIS*

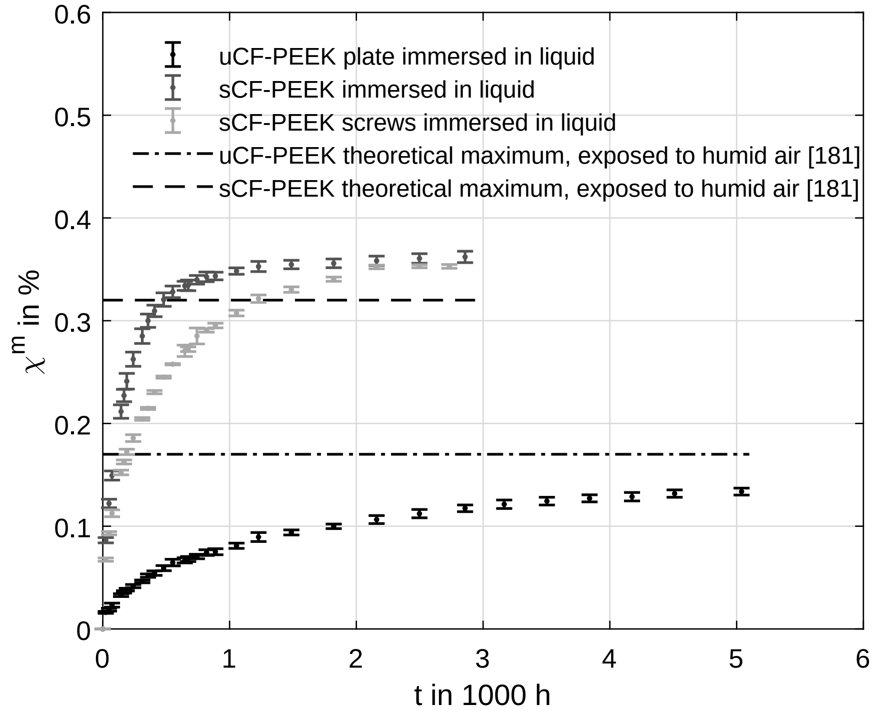

Figure 4.3.: Relative mass change χ^m of uCF-PEEK plate specimens, sCF-PEEK specimens, and sCF-PEEK screws over immersion time t

in good accordance to the data provided by the manufacturer [179]. After the immersion, the relative mass change of the uCF-PEEK plate material was (0.13 ± 0.003) % and of the sCF-PEEK screws (0.35 ± 0.002) %. The effect of liquid absorption on the structural mechanical properties of the screw is described in chapter 4.6.2.

The results were compared to data from the literature. According to *Wang* and *Springer* [184], the theoretical relative maximum mass change $\hat{\chi}^m_{FRP,\ th}$ of a composite when exposed to humid air can be calculated by

$$\hat{\chi}^m_{FRP,\ th} = \left(\frac{1}{1 + \frac{\varphi_V}{1-\varphi_V} \, \frac{\rho_f}{\rho_m}} \right) \hat{\chi}^m_{PEEK} \, . \tag{4.4}$$

Here, $\hat{\chi}^m_{PEEK}$ is the relative maximum mass change of neat PEEK, which is 0.45 % according to [66], and φ_V is the fibre volume fraction. The equation is based on the assumption that fibres do not absorb any moisture [184]. Figure 4.3 shows the theoretical relative maximum mass change for the two materials with horizontal lines. When immersed in liquid, the mass change of the specimen is typically higher compared to its mass change when exposed to humid air [184]. Thus, the mass changes of sCF-PEEK specimens and the sCF-PEEK screws are higher compared to the theoretical literature value. During the underlying immersion time, the final relative mass change of the uCF-PEEK plate specimens when immersed in liquid was lower than the theoretical relative maximum mass change when exposed to humid air. However, referring to figure 4.3, a slight increase of the relative mass change of the uCF-PEEK specimens could still be observed at the end of the analysis, and the difference between the experimental and theoretical literature value was small.

4.2.3 Differential scanning calorimetry

The differential scanning calorimetry (DSC) aimed at the determination of the glass transition temperature T_g and the melting temperature T_m of the PEEK matrices. Additionally, information about the degree of crystallinity W_c was gained. The *DSC 1* from *Mettler-Toledo GmbH* was used for the DSC which was based on the principle of a heat flux difference. The reference was a aluminium pan. Two heating and two cooling phases with a rate of 10 ℃/min were studied so that in total four segments per specimen existed. The temperature increased from 25 ℃ to 380 ℃. The maximum temperature was chosen so that on the one hand no crystalline phases existed anymore and on the other hand the molecules of the PEEK matrix did not decompose. Up to a temperature of 380 ℃, the thermal properties of the composite materials is mainly governed by the thermal properties of the PEEK matrix. The temperatures are too low to significantly affect the CF. The cooling phase started at 380 ℃ and ended at 25 ℃. Liquid nitrogen was used for cooling. During the analysis, nitrogen flushing gas with a rate of 30 ml/min prevented the material from significant degradation.

The specimens were cut into small pieces with a maximum extension of 5 mm so that they fitted into the 70 µl pans of the DSC instrument. Two uCF-PEEK plate, two uCF-PEEK rod, and two sCF-PEEK specimens were used for the DSC. The DSC diagrams of the specimens for both heating segments can be seen in figure 4.4. In the figure, the heat flow rate Φ is plotted against the temperature T.

One main melting region can be identified for all specimens. In addition to that, small initial melting peaks in front of the main melting region can be observed for several specimens. The peaks existed in the first segment, for the uCF-PEEK plate specimens at approximately 270 ℃, and for the uCF-PEEK rod specimens at approximately 215 ℃. Pairs of endothermic peaks in the first heating segment were also described by others [55, 56, 68, 77]. Typically, these initial peaks are a result of the thermal characteristics of the manufacturing process. During manufacturing, different crystal formations can arise. After controlled cooling during DSC, these manufacturing effects can be eliminated, and the crystal size distribution can be homogenised. Therefore, relevant thermal material properties, which should be independent of manufacturing effects, were extracted from the second heating in the third segment (cf. table 4.2).

All specimens show a homogeneous and little distinct glass transition area which is typical for TPCs. As can be seen in table 4.2, the glass transition and melting temperature

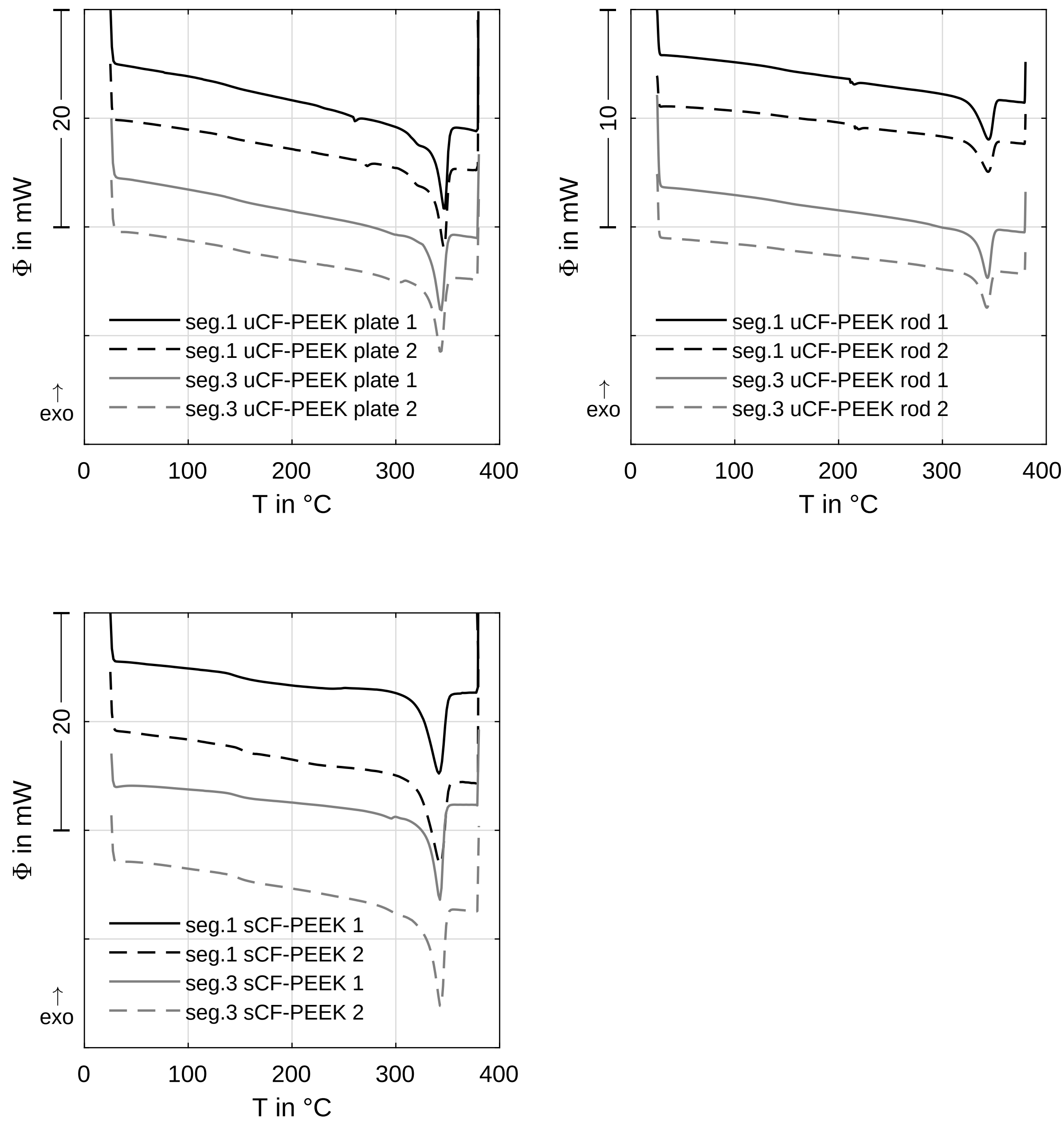

Figure 4.4.: DSC diagrams for the heating segments of two uCF-PEEK plate (upper left), uCF-PEEK rod (upper right), and sCF-PEEK specimens (lower left)

Table 4.2.: Glass transition temperature T_g, melting temperature T_m, and degree of crystallinity W_c of the PEEK matrices of the uCF-PEEK plate, uCF-PEEK rod, and sCF-PEEK specimens

	uCF-PEEK plate	uCF-PEEK rod	sCF-PEEK	Mean
T_g in ℃	143.01 $\pm$ 0.34	143.66 $\pm$ 0.61	147.06 $\pm$ 0.12	144.58 $\pm$ 1.82
T_m in ℃	342.09 $\pm$ 0.04	342.74 $\pm$ 0.19	341.73 $\pm$ 0.36	342.18 $\pm$ 0.48
W_c in %	44.53 $\pm$ 2.27	45.65 $\pm$ 0.47	34.43 $\pm$ 0.65	n/a

of the PEEK matrices of the uCF-PEEK plate, uCF-PEEK rod, and sCF-PEEK specimens were very similar after controlled cooling and the elimination of manufacturing effects in the third segment.

The degree of crystallinity affects the glass transition temperature of the specimen [56]. It was determined for the sCF-PEEK material of the composite screw, the uCF-PEEK plate, uCF-PEEK rod, and sCF-PEEK material. *Wunderlich* informs about the specific enthalpy of fusion h_S^{cryst} of fully crystalline PEEK of 37.4 kJ/mol [185]. With a molar mass of PEEK of 288 g/mol [186], the specific enthalpy of fusion of fully crystalline PEEK can also be expressed by 130 J/g [5, 75]. The degree of crystallinity W_c can then be calculated by the fraction of the specific enthalpy of fusion h_S of the specimen and the specific enthalpy of fusion h_S^{cryst} of fully crystalline PEEK [75]:

$$W_c = \frac{h_S}{h_S^{cryst}} = \frac{\frac{H_S}{m_{PEEK}}}{h_S^{cryst}} \tag{4.5}$$

Here, the specific enthalpy of fusion h_S is calculated by the fraction of the enthalpy of fusion H_S of the specimen and the mass m_{PEEK} of its PEEK matrix. The mass of the PEEK matrix can be calculated by using the formula

$$m_{PEEK} = (1 - \varphi)m \tag{4.6}$$

in which φ represents the fibre mass fraction.

To determine the degree of crystallinity, four specimens were extracted from the sCF-PEEK screw material and two specimens from each of the other materials. They were examined by DSC and TGA (cf. chapter 4.2.4) so that the fibre mass fraction could be determined for each specimen and used to calculate the corresponding degree of crystallinity. The mean degree of crystallinity of the sCF-PEEK material of the composite screw was (32.05 $\pm$ 1.76) % in the first segment of the DSC. The first segment was chosen here, because the influence of the manufacturing process was of interest for the degree of crystallinity of the screw overmoulding material. The degree of crystallinity obtained for the uCF-PEEK plate, uCF-PEEK rod, and sCF-PEEK material after controlled cooling (third segment) can be seen in table 4.2. These values are in accordance with the findings of other authors [35, 51, 53, 55, 75].

4.2.4 Thermogravimetric analysis

The aim of the TGA was the determination of the fibre volume fraction φ_V of the uCF-PEEK plate, uCF-PEEK rod, and sCF-PEEK material. Additionally, the material degradation behaviour was of interest because the overmoulding and insert material were exposed to high temperatures during the overmoulding process. Like for the DSC, the maximum extension of the specimens was lower than 5 mm so that they fitted into the 70 µl pans.

In a pre-study, it was observed that even at a temperature of 900 ℃, the PEEK matrix did not completely decompose in nitrogen atmosphere. Instead, a plateau was reached at which the mass of the specimen remained constant. In contrast, a simultaneous degradation of matrix and fibre until complete dissolution would be observed when heated up to 900 ℃ in air atmosphere. During this process, it was neither possible to determine the beginning of the fibre degradation nor to distinguish between the degradation of matrix and fibre. Scanning electron microscope (SEM) examinations of the specimen shortly before complete dissolution showed that matrix material still surrounded the fibres due to the excellent thermal stability of PEEK.

As a result of this pre-study, the following procedure was used to determine the fibre volume fractions of the underlying materials, and to examine their degradation behaviour:

1. heating up to 900 ℃ with a rate of 20 ℃/min in nitrogen atmosphere
2. holding the temperature for a time of 20 min in nitrogen atmosphere
3. cooling down to 400 ℃ with a rate of 10 ℃/min in nitrogen atmosphere
4. switching to air atmosphere with/without holding time
5. heating up to 900 ℃ with a rate of 10 ℃/min in air atmosphere
6. holding the temperature for a certain time in air atmosphere

In total, three specimens were analysed for each material. Their original specimen mass was measured before TGA. The differences in the behaviour of the specimens of one material were insignificant. Figure 4.5 shows the temperature T and the relative mass $1 - \chi^m$ over time t for one of the uCF-PEEK plate (upper left), uCF-PEEK rod (upper right), and sCF-PEEK specimens (lower left). Furthermore, the characteristics of one neat PEEK specimen (*Victrex® PEEK 450G*) during TGA are illustrated on the lower right. The TGA of the neat PEEK material was needed for the characterisation of the fibre volume fraction of the uCF-PEEK and sCF-PEEK materials.

In nitrogen atmosphere, the decomposition of the PEEK matrix could be divided into two parts: (1) a region characterised by rapid degradation after reaching a temperature of approximately 550 ℃, and (2) a plateau region at which material degradation was insignificant. These observations are in accordance with the findings of other authors [51, 53, 58, 59, 187, 188]. The mass m_{PEEK}^{900} of the neat PEEK specimen at the plateau region was determined ten minutes after first reaching the holding time at a temperature

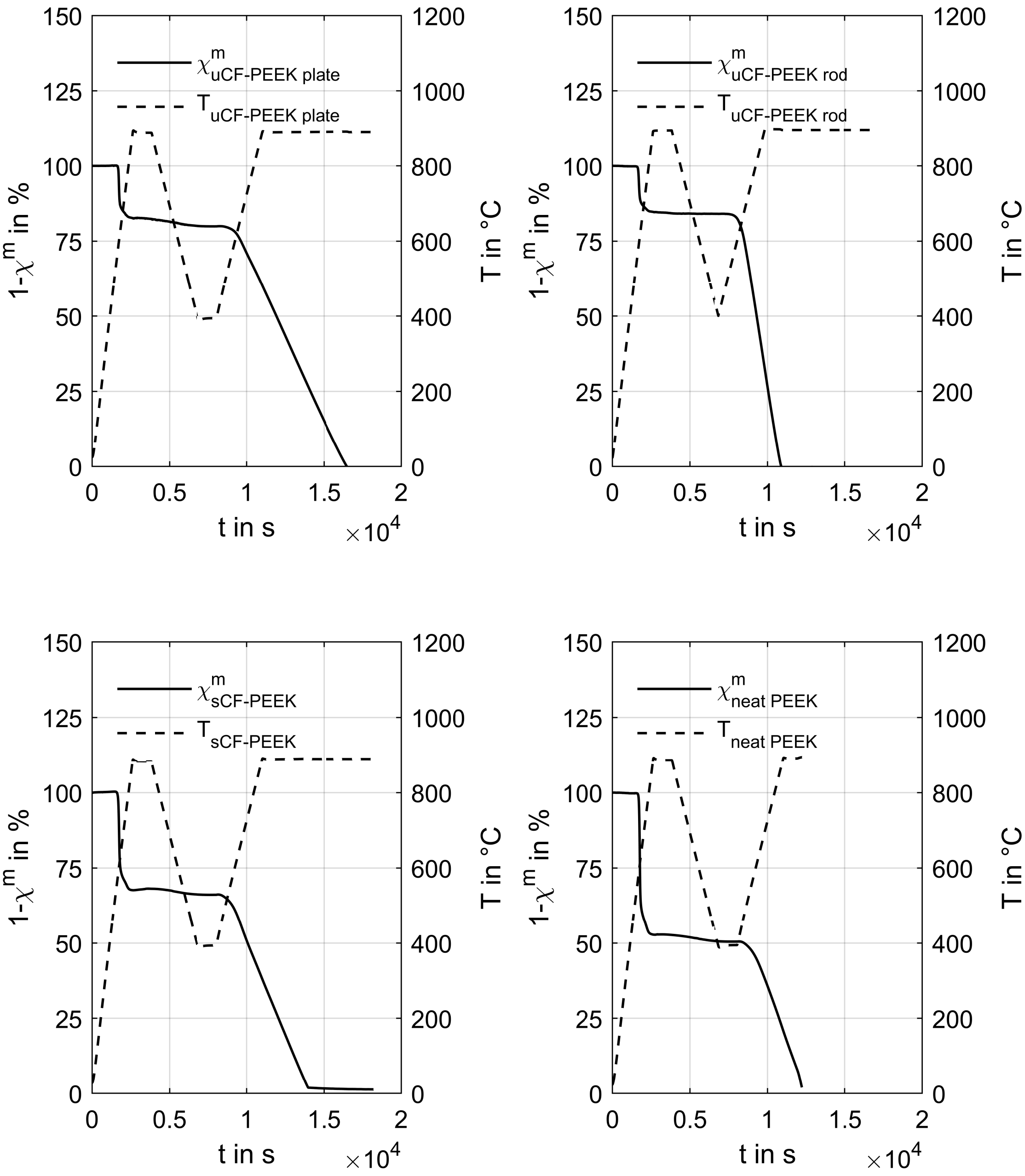

Figure 4.5.: TGA diagrams of a uCF-PEEK plate (upper left), uCF-PEEK rod (upper right), sCF-PEEK (lower left), and neat PEEK specimen (lower right)

of 900 ℃. With this value, the relative mass change χ^m_{PEEK} of the neat PEEK specimen in nitrogen atmosphere was calculated by

$$\chi^m_{PEEK} = \frac{m_{PEEK} - m^{900}_{PEEK}}{m_{PEEK}} \tag{4.7}$$

in which m_{PEEK} is the mass of the neat PEEK specimen prior to TGA. The resultant mass change was (46.60 ± 0.57) % which is in good accordance with the findings of others [51, 53, 58, 59, 62, 189]. Generally, processed CF-PEEK can have slightly different thermal properties than unprocessed neat PEEK material. However, these differences are typically negligible [51]. As a consequence, it was assumed that for all analysed materials, the first plateau region corresponded to a matrix mass loss of 46.60 %. After this plateau, any further decomposition occurred due to oxidation processes caused by switching from nitrogen to air atmosphere during TGA.

By knowing the matrix mass loss at the plateau region, the matrix mass loss of the composites determined by TGA could be extrapolated to 100 %. This value corresponds to the mass m_m of the matrix of the composites:

$$m_m = \frac{m_{FRP} - m^{900}_{FRP}}{\chi^m_{PEEK}} \tag{4.8}$$

Here, m_{FRP} is the mass of the composite specimens prior to TGA, and m^{900}_{FRP} is the mass of the composite specimens at the plateau region ten minutes after first reaching the holding time at a temperature of 900 ℃. The fibre mass fraction φ was then calculated by

$$\varphi = \frac{m_f}{m_f + m_m} = 1 - \frac{m_m}{m_{FRP}} \tag{4.9}$$

in which m_f is the mass of the fibres. The resulting fibre mass fraction was (63.43 ± 1.12) % for the uCF-PEEK plate, (66.63 ± 0.12) % for the uCF-PEEK rod, and (29.54 ± 1.46) % for the sCF-PEEK material. The fibre mass fraction of the sCF-PEEK material is in good accordance with the data from the manufacturer (cf. table 4.3) and from other authors [54, 179].

Referring to table 4.1, the densities of fibre and matrix, which were determined by the method of liquid displacement described in chapter 4.2.1, are known. Thus, the fibre volume fraction φ_V could be calculated by [4]

$$\varphi_V = \frac{1}{1 + \frac{1-\varphi}{\varphi}\,\frac{\rho_f}{\rho_m}}\,. \tag{4.10}$$

The resulting fibre volume fraction was (55.75 ± 0.82) vol.-% for the uCF-PEEK plate, (59.87 ± 0.09) vol.-% for the uCF-PEEK rod, and (23.85 ± 1.10) vol.-% for the sCF-

PEEK material.

To check these values, another method to determine the fibre volume fraction is presented in the following. The fibre volume fraction φ_V can also be determined by reordering the rule of mixture expressed in the form to calculate the density of the composite ρ_{FRP} [4]:

$$\rho_{FRP} = \varphi_V \rho_f + (1 - \varphi_V)\rho_m \tag{4.11}$$

As mentioned before, the densities of the matrices and fibres are known (cf. table 4.1). In addition to that, the densities of the composites were determined in chapter 4.2.1. Therefore, the fibre volume fractions were calculated with 57.82 vol.-% for the uCF-PEEK plate material, 63.23 vol.-% for the uCF-PEEK rod material, and 24.08 vol.-% for the sCF-PEEK material. Solving equation 4.10 for the fibre mass fraction φ resulted in

$$\varphi = \frac{\rho_f}{\frac{\rho_m}{\varphi_V} + \rho_f - \rho_m}\,. \tag{4.12}$$

With this equation, the fibre mass fraction could be determined for the underlying materials. It was 65.37 % for the uCF-PEEK plate material, 69.71 % for the uCF-PEEK rod material, and 29.80 % for the sCF-PEEK material.

A verification analysis was conducted for two sCF-PEEK specimens by using the *MaxRes-function* during TGA. With this function, the heating rate was automatically adjusted as a function of the mass change of the specimen [190]. By slowing down the heating rate with this technique, the degradation of fibre and matrix could be successfully separated after the plateau region. By using the *MaxRes-function*, a similar fibre mass fraction was obtained for the sCF-PEEK specimens compared to the fibre mass fraction obtained by using the relative mass change χ_m^{PEEK} of neat PEEK, as described before.

The fibre volume and mass fractions obtained by using the mass density data of the composites, and the fibre volume and mass fractions obtained by TGA were very similar. Furthermore, the values are in good accordance with the data provided by the manufacturers [179, 180, 191]. Table 4.3 summarises the data of the fibre volume and mass fractions of the three materials and includes the data provided by the manufacturer.

After TGA and before complete decomposition of the specimens, information about the fibre diameter and the fibre length was obtained by SEM examinations. Table 4.4 summarises the resulting length l_{sCF} and diameter D_{sCF} of the short CFs of the sCF-PEEK specimens, and the diameter D_{uCF} of endless CFs of the uCF-PEEK plate specimens.

Table 4.3.: Fibre mass φ and volume fraction φ_V of uCF-PEEK plate, uCF-PEEK rod, and sCF-PEEK specimens

	uCF-PEEK plate		uCF-PEEK rod		sCF-PEEK	
	φ in %	φ_V in vol.-%	φ in %	φ_V in vol.-%	φ in %	φ_V in vol.-%
Liquid displacement	65.37	57.82	69.71	63.23	29.80	24.08
TGA	63.42	55.75	66.63	59.87	29.54	23.85
Data from manufacturer	n/a	60 [191]	n/a	62 [180]	30 [54, 179]	n/a

Table 4.4.: Length l and diameter D of sCF and uCF

l_{sCF} in µm	D_{sCF} in µm	l_{uCF} in µm	D_{uCF} in µm
145.91 ± 19.81	7.52 ± 0.44	n/a	6.24 ± 0.50

Patel et al. inform about a short CF length of *Victrex® 450CA30* of approximately 200 µm and a short CF diameter of this material of approximately 7 µm before processing [51]. Dependent on the processing conditions used for the manufacturing of the sCF-PEEK specimens, the fibre length can be reduced within the manufacturing process. Under this consideration, the values found in the literature are in good accordance with the values of this study.

4.2.5 Dynamic mechanical thermal analysis

Specimens were examined by dynamic mechanical thermal analysis (DMTA) to determine temperature dependent flexural stiffness properties. Additionally, the influence of the fibre orientation on the stiffness properties of the sCF-PEEK specimens was analysed.

For DMTA, specimens were tested by three point bending. A constant testing frequency of 1 Hz was used for the analysis. During the three point bending test, the temperature constantly increased by 2 ℃/min from 20 ℃ to 300 ℃. The testing machine *Eplexor 100 N* from *Erich Netzsch GmbH & Co. Holding KG* was used and the test was performed in air atmosphere. In total, eight specimens with a length of 48 mm and a width of 10 mm were examined: two uCF-PEEK plate specimens with their main extension in fibre direction (uCF-0), two uCF-PEEK plate specimens with their main extension perpendicular to the fibre direction (uCF-90), two sCF-PEEK specimens with their main extension parallel to the injection direction (sCF-0), and two sCF-PEEK specimens with their main extension perpendicular to the injection direction (sCF-90). The thickness of the sCF-PEEK specimens was 1.8 mm and of the uCF-PEEK plate specimens

2 mm. No uCF-PEEK rod specimen could be studied by DMTA because the dimensions were inappropriate. However, flexural properties of the uCF-PEEK rod material can be assumed to be similar to the uCF-PEEK plate material. The bending storage modulus E' and the bending loss factor $tan\ \delta$ of the uCF-0 and sCF-0 specimens over the temperature T are illustrated in figure 4.6. In figure A.1 listed in appendix A.1, the corresponding results of the uCF-90 and sCF-90 specimens are shown.

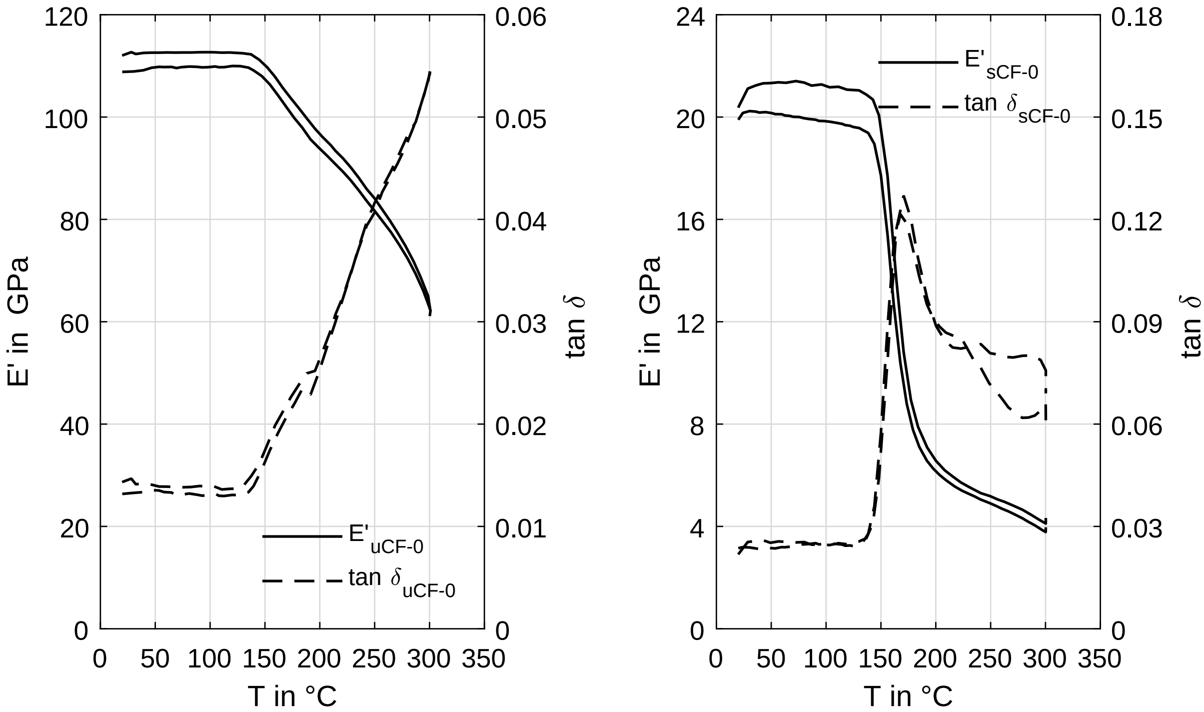

Figure 4.6.: DMTA diagrams of uCF-PEEK plate specimens parallel to fibre direction (left) and sCF-PEEK specimens parallel to injection direction (right)

Figure 4.6 shows that the bending storage modulus is rather constant up to a temperature of 136 ℃. The stiffness decrease of the uCF-0 specimens is rather linear. Reasons for this are the high fibre volume fraction of the uCF-PEEK plate specimens, and the fibre dominated stiffness properties in 0-direction. Increasing the temperature mainly influences the mechanical properties of the PEEK matrix. The bending storage modulus at room temperature was (110.43 $\pm$ 1.60) GPa for the uCF-0 specimens, (9.03 $\pm$ 0.04) GPa for the uCF-90 specimens, (20.13 $\pm$ 0.24) GPa for the sCF-0 specimens, and (7.98 $\pm$ 0.05) GPa for the sCF-90 specimens. As can be seen, not only for the uCF-PEEK specimens but also for the sCF-PEEK specimens, stiffness properties are dependent on the fibre orientation which results from the manufacturing process. At a body temperature of 37 ℃, the difference in bending stiffness is negligible for all CF-PEEK specimens in comparison to their bending stiffness at room temperature. However, if the pre-heating temperature of the inserts before overmoulding is significantly higher than the glass transition temperature, structural mechanical properties will be reduced. Therefore, careful handling of the pre-heated inserts is required.

4.2.6 Cooling characterisation

Investigating the decrease of temperature of the CF-PEEK material over time after pre-heating was important to approximate the insert temperature just before overmoulding (cf. chapter 4.2.8.3 and 4.5.1), and to determine the temperature distribution of the insert surface. For the achievement of a cohesive interface, a homogeneous temperature distribution is favourable so that a homogeneous melting of the insert surface can occur. Additionally, on-line temperature control is beneficial for quality assurance. However, due to limited space in and around the moulds, it was not possible to measure the temperature on-line in the process which motived the studies listed in the following.

The temperature T was recorded over time t with the infrared (IR) camera *thermoIMAGER TIM 450* from *Micro-Epsilon Messtechnik GmbH & Co. KG*. The specimens were heated in the convection oven *TR 120* from *Nabertherm GmbH*. After heating, they were rapidly placed on a wooden support close to the oven to start the measurement of the temperature decrease with the IR camera. It was assumed that the support had a minor influence on the cooling characteristics of the specimens. The temperature was recorded by the IR camera under an angle of 20° to avoid heat ray reflection. Two specimens were analysed: (1) a specimen called *plate* with the dimensions of 80 mm $\times$ 80 mm $\times$ 2 mm ($l \times w \times d$) representing the overmoulded uCF-PEEK plate of the compression shear test described in chapter 4.2.8.1, and (2) a uCF-PEEK plate specimen called *insert* with the dimensions of 68 mm $\times$ 3 mm $\times$ 2 mm ($l \times w \times d$) representing the insert of the cylinder pull-out specimen described in chapter 4.2.8.3 and of the hybrid composite pedicle screw. Due to restricted availability, limited stock, and high cost of uCF-PEEK rod inserts, the uCF-PEEK plate material with similar dimensions was used for the representation of the uCF-PEEK rod material in this analysis.

In a first study, the absolute temperature of the specimens at a specific time was determined. For this study, an emission tape from *Testo SE & Co. KGaA* was bonded to the uCF-PEEK plate. The temperatures of tape and plate were measured with the IR camera and compared. Specimens were heated in the oven with a temperature of 280 °C. The relation between the real absolute temperature T_{abs} of the tape and the temperature T measured with the IR camera on the uCF-PEEK plate yields the linear equation

$$T_{abs} = 1.10\, T - 1.84\, °C \tag{4.13}$$

of the form $y = mx + n$. With this expression, the real absolute temperature of the uCF-PEEK specimens could be determined.

In a second study, the absolute specimen temperature was compared with the oven target temperature which was 300 ℃ in this study. After ten minutes, the absolute uCF-PEEK plate temperature inside the oven showed no significant changes anymore. Thus, a pre-heating time of ten minutes will be required for insert pre-heating if this oven is used. The heating characteristics of the specimens are dependent on the type of oven used, the position in the oven, and the target temperature.

For uCF-PEEK plate and insert, the temperatures at two spots were measured simultaneously. At the first spot, the temperature was measured in the middle of the largest surface of the plate and insert. At the second spot, the temperature was measured at one corner of the plate, and at one edge of the insert. Certainly, the measurement start temperature T_0 was lower than the oven temperature of 300 ℃, because the specimens cooled from the instance of opening the oven at the time $t = t_0 - t_{transfer}$ until the measurement start at t_0. The variable $t_{transfer}$ describes the time in between the instance of opening the oven and the start of the measurement.

Figure 4.7 shows the temperature-time diagram of the uCF-PEEK plate and insert. The solid and dashed curves show the absolute temperature T_{abs} over time t for the measurement spot at the middle and at the corner/edge of each specimen. Due to a smaller mass to surface ratio of the insert, the uCF-PEEK insert cooled faster than the uCF-PEEK plate, as expected. After ten seconds, the plate temperature decreased by approximately 15 ℃ which corresponds to 7 % of the measurement start temperature T_0. In contrast, the insert temperature was approximately 45 ℃ or 20 % lower than the measurement start temperature at this time. Further studies have shown that with higher measurement start temperatures, the difference to the temperature after ten seconds was even higher.

Cooling was significantly faster at the corner of the uCF-PEEK plate compared to cooling in its middle. For the insert, the difference between the cooling characteristics at its edge and in its middle was insignificant. The temperature distribution was more homogeneous which is beneficial for controlling the overmoulding process.

To study the influence of forced convection during insert transfer from the oven to the mould, a ventilator was placed next to the IR camera. In addition to that, the influence of a heated aluminium support was analysed which was used during transport of the hot uCF-PEEK specimens from the mould to the IR camera and during their examination. The support was heated in the oven together with the specimens. Due to the relatively high specific heat capacity of 900 J/(kg K) and the thermal conductivity of 125 W/(m K) of aluminium[4], thermal energy could be transferred to the specimens to

[4] https://www.thyssenkrupp-materials.ch/de/downloads/werkstoffdatenblaetter-aluminium; aluminium alloy EN AW - 5083 (3.3547); accessed 16 January 2020

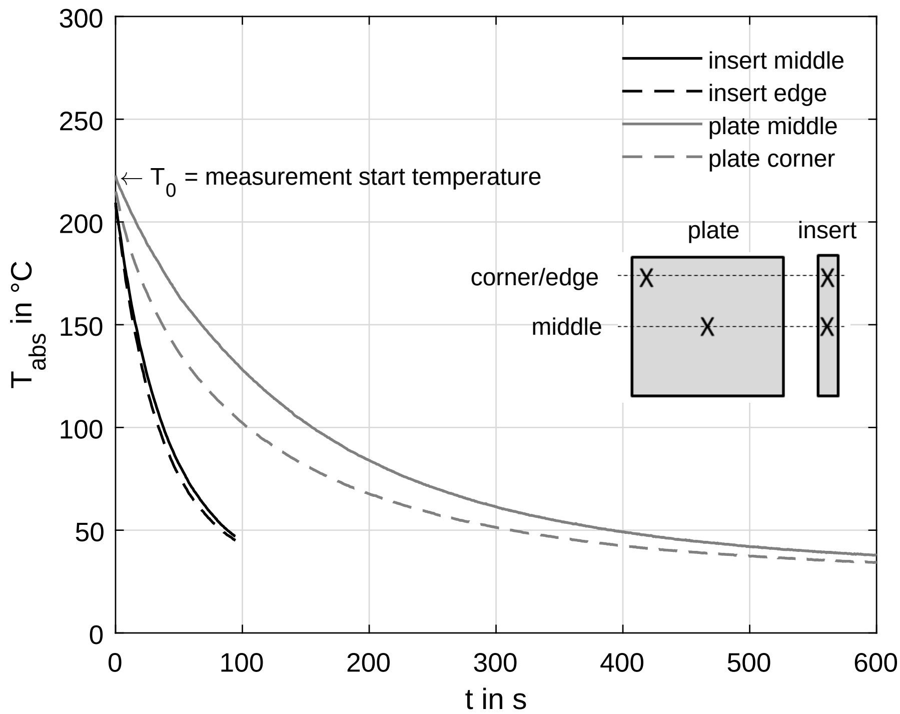

Figure 4.7.: Temperature-time diagram of insert and plate at the measuring spots in the middle and at the edge/corner

decrease their cooling. The relative temperature loss χ^T of the uCF-PEEK inserts between the measurement start temperature T_0 and the temperature T_{10} after ten seconds was calculated with

$$\chi^T = \frac{T_0 - T_{10}}{T_0}, \tag{4.14}$$

and was studied for different combinations:

- forced convection and no hot support: χ^T = 33 %
- free convection and no hot support: χ^T = 20 %
- forced convection and hot support: χ^T = 14 %
- free convection and hot support: χ^T = 7 %

This study shows that the insert temperature prior to overmoulding is dependent on the specimen pre-heating temperature, the transfer time, and the transfer condition. Furthermore, the uCF-PEEK plate showed a similar cooling behaviour compared to the uCF-PEEK insert. However, the relative temperature loss of the plate was lower than the one for the insert. This study also shows that the temperature loss of the insert will be significantly increased if the inserts are subjected to forced convection and if no hot support is used for their transport from the oven to the mould. Therefore, forced convection should be avoided during transport of the hot inserts within the overmoulding manufacturing process, and the hot inserts should be transported on or preferably in a heated support. To additionally keep the temperature loss of the inserts between opening of the oven and start of injection sufficiently low, transfer has to be fast.

4.2.7 Thermal expansion analysis

Due to thermal contraction, the hot overmoulded material can shrink onto the insert surface during cooling, and interface strength can be promoted, especially in the case of adhesive interface formation. For the analysis of thermal contraction, measurements of the coefficient of thermal expansion (CTE) were conducted by thermal mechanical analysis (TMA) with the instrument *TMA/SDTA 2+* from *Mettler-Toledo GmbH*. Three uCF-PEEK plate specimens were used for the determination of the CTE α_{11}^{T} in longitudinal fibre direction, and three more specimens for the determination of the CTEs α_{22}^{T} and α_{33}^{T} in transverse fibre direction. A differentiation between longitudinal and transverse fibre direction was also made for the sCF-PEEK material. Injection moulded sCF-PEEK screws without insert were cut perpendicularly to their axis so that these specimens, showing preferable dimensions, could be used for the determination of the longitudinal CTE of the sCF-PEEK material. Additionally, specimens taken from injection moulded plates were used for the determination of the transverse CTE of the sCF-PEEK material. Due to the fact that the exact fibre distributions of injection moulded parts are complex and typically unknown, isotropic thermal expansion behaviour of the sCF-PEEK material was assumed for the simulation described in chapter 4.2.8.3. Thus, the average of the longitudinal and transverse CTE of the sCF-PEEK material was determined.

Typically, the material data sheets from the manufacturers inform about the CTEs only below and above the glass transition temperature. In contrast, several temperature intervals were defined for the CTE data in this study so that simulation accuracy could be improved. Table 4.5 informs about the CTE data of the uCF-PEEK and sCF-PEEK material.

Table 4.5.: CTE data of uCF-PEEK and sCF-PEEK specimens

	uCF-PEEK			sCF-PEEK	
Temperature in ℃	α_{11}^{T} in 10^{-6} K^{-1}	α_{22}^{T} in 10^{-6} K^{-1}	α_{33}^{T} in 10^{-6} K^{-1}	Temperature in ℃	α^{T} in 10^{-6} K^{-1}
23 to 145	-0.17	27.01	27.01	23 to 120	36.61
145 to 160	-2.64	-5.63	-5.63	120 to 160	36.21
>160	0.77	101.19	101.19	160 to 200	81.46
				200 to 230	105.76
				>230	155.20

4.2.8 Adherence tests

To evaluate the strength of the interface between a uCF-PEEK insert and sCF-PEEK overmoulding material, different standard adherence test methods were initially compared. The compression shear test is described in the following. As mentioned in chapter 2.3.2.5, the compression shear test is also used in [158] for interface characterisation. However, due to several disadvantages of this adherence test, interface characterisation was also conducted with SLS specimens. With the specific specimen preparation for SLS tests, interface strength between the insert and the overmould could be significantly improved. Interface strength was so high that the sCF-PEEK adherend failed earlier than the interface. Consequently, interface strength could not be determined with this test. Therefore, a novel test body was developed which is ideal for interface characterisation of overmoulded structures. This cylinder pull-out specimen was invented at the *Institut für Verbundwerkstoffe GmbH* within this work, and was registered with a utility patent (cf. chapter 4.2.8.3).

As mentioned in chapter 2.3.1, there are two possibilities to describe the interface:

1. If the heat transfer from the molten mass to the insert is insufficient to melt the insert surface, an *adhesive interface* will be formed.
2. If the heat transfer from the molten mass to the insert is sufficient to melt the insert surface, and close contact between insert and molten mass is ensured for a sufficiently long time, a *cohesive interface* will be formed.

4.2.8.1 Compression shear test

The first test which was used to determine the interface strength between a uCF-PEEK insert and sCF-PEEK overmould was the compression shear test. In contrast to the tension shear test [192], the compression shear test has the advantage of a more favourable stress distribution [193] because the compression stiffnesses of the two materials were more similar than their corresponding tension stiffnesses. To promote the formation of a sufficiently strong interface, the inserts were pre-heated.

To characterise the contribution of micromechanical interlocking between a uCF-PEEK plate insert and sCF-PEEK overmould, a confocal topography measurement was conducted. Additionally, contact angle measurements were performed prior to compression shear testing to evaluate the surface energy of the uCF-PEEK plate insert.

Confocal topography measurement

If two specimens are in close contact with each other, micromechanical interlocking will be one mechanism which contributes to interface strength. To evaluate the interlocking capability between a uCF-PEEK plate insert and sCF-PEEK overmould, the surface roughness of the insert with dimensions of 80 mm $\times$ 79.5 mm $\times$ 2 mm ($l \times w \times d$) was optically measured with a confocal topography measurement system from *NanoFocus AG* at the *Institute for Measurement and Sensor Technology* at the *Kaiserslautern University of Technology*.

In a first study, the specimens were cleaned with isopropanol, and the topography was analysed by using two different measuring lengths in the centre both at the front and the back of the specimen, and in each corner at the front. The positions of the measuring lengths in the centre of the specimen were slightly different to avoid measuring at the same spot. The measured lengths were orthogonal to the fibre orientation of the uCF-PEEK plate. The mean roughness values of the uCF-PEEK plate specimen R_a (roughness average), R_p (maximum profile peak height) and R_z (average maximum height of profile) were (1.34 $\pm$ 0.56) µm, (3.21 $\pm$ 0.91) µm and (10.18 $\pm$ 3.88) µm.

To illustrate the surface topography, figure 4.8 shows two SEM images of the uCF-PEEK plate surface. The images were taken with a cathode voltage of 20 kV. The SEM images indicate that small cavities exist on the surface. Furthermore, the fibre orientation is visible due to the high fibre volume fraction.

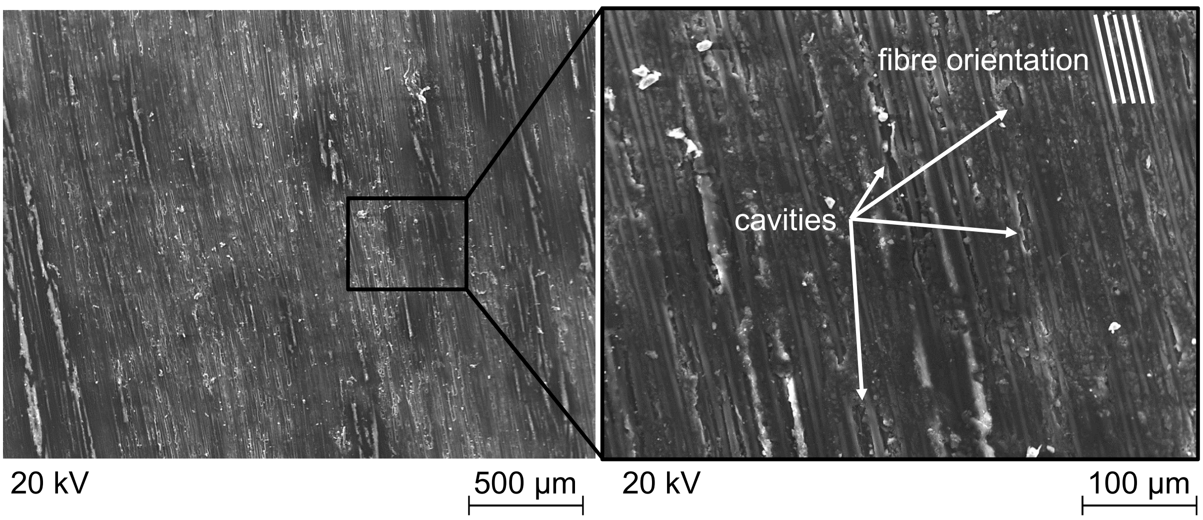

Figure 4.8.: SEM image of the surface of a uCF-PEEK plate specimen

In a second study, a uCF-PEEK plate was heated in an oven at 250 ℃ for about one hour to examine the influence of a pre-heating process step on the surface roughness. This pre-heating temperature is well above the glass transition temperature of the PEEK matrix but still far below its melting temperature. After cooling of the plate, the same procedure as described before was used for measuring its surface roughness. The roughness values R_a, R_p, and R_z of the pre-heated uCF-PEEK plate were not significantly different from the corresponding values of the non-heated plate. Therefore, with a pre-heating temperature of 250 °C only micromotions of molecular chains of the PEEK matrix were relevant so that the surface topography of the uCF-PEEK insert was not significantly changed.

Contact angle measurement

The surface energy of the specimens influences the adhesion strength of the interface. To evaluate the surface energy of the uCF-PEEK plate, a contact angle measurement [138, 194] was performed with two liquids: (1) distilled water[5] (H_2O) and (2) diiodomethane[6] (CH_2I_2). Figure 4.9 illustrates the shapes of a distilled water drop (left) and a diiodomethane drop (middle) on the surface of the uCF-PEEK plate. More than five drops were analysed for each liquid.

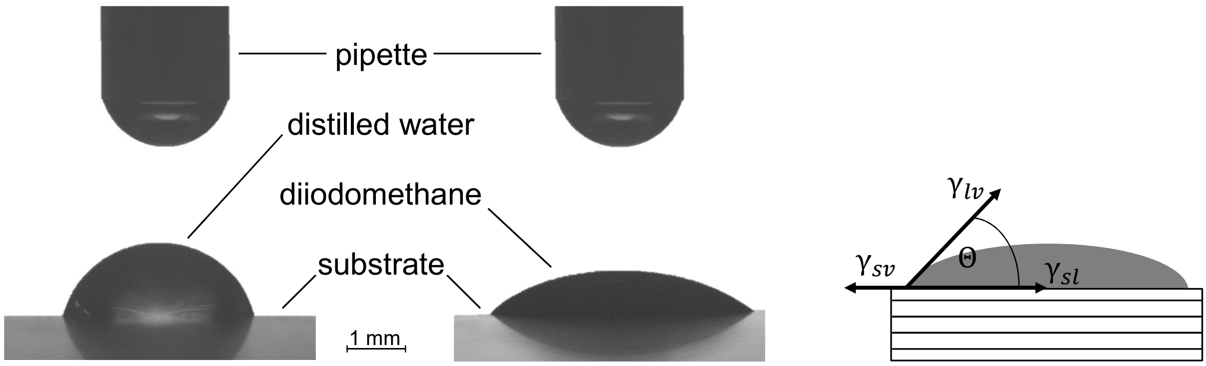

Figure 4.9.: Drop of distilled water (left) and diiodomethane (middle) used for contact angle measurements on the uCF-PEEK plate surface, and geometric dependence of surface energies (right)

The surface energy γ_{sv} of a solid (s) in atmosphere (v) is defined by the sum of its polar (p) and disperse (d) component γ_{sv}^p and γ_{sv}^d. It can also be expressed by the *Young-equation* [39, 139]:

$$\gamma_{sv} = \gamma_{sl} + \gamma_{lv}\ cos\ \Theta \tag{4.15}$$

Here, the interface energy between a solid and a liquid (l) is described by γ_{sl}, the surface energy of the liquid in atmosphere by γ_{lv}, and the contact angle by Θ (cf. figure 4.9 right). The interface energy γ_{sl} can be described by the sum of the surface energies γ_{sv} and γ_{lv} of the solid and liquid phases decreased by the double of the sum of the

[5]surface energy γ_{lv} of 72.8 mN/m with a polar component γ_{lv}^p of 51.0 mN/m and a disperse component γ_{lv}^d of 21.8 mN/m [36, 194]

[6]surface energy γ_{lv} of 50.8 mN/m with a polar component γ_{lv}^p of 0 mN/m and a disperse component γ_{lv}^d of 50.8 mN/m [194]

geometrical means of the disperse and polar components of the phases:

$$\gamma_{sl} = \gamma_{sv} + \gamma_{lv} - 2\left(\sqrt{\gamma_{sv}^{d}\gamma_{lv}^{d}} + \sqrt{\gamma_{sv}^{p}\gamma_{lv}^{p}}\right) \tag{4.16}$$

Reordering equation 4.15 for γ_{sl} and using it in equation 4.16 yields the linear equation

$$\frac{\gamma_{lv}}{2\sqrt{\gamma_{lv}^{d}}}(1 + cos\,\Theta) = \sqrt{\gamma_{sv}^{p}}\,\frac{\sqrt{\gamma_{lv}^{p}}}{\sqrt{\gamma_{lv}^{d}}} + \sqrt{\gamma_{sv}^{d}} \tag{4.17}$$

of the form $y = mx + n$ [35].

By contact angle measurements, the surface energy of the uCF-PEEK plate was determined with 46.6 mN/m. No significant difference was found for a pre-heated specimen subjected to 250 °C for one hour. Other authors have shown that the surface energy of neat PEEK was approximately 34 mN/m [35, 36]. In addition to that, a plasma activated neat PEEK surface, which promotes adhesion, showed a surface energy of more than 70 mN/m [35, 36]. Also for this study, plasma pre-treatment of the composite inserts could beneficially increase surface energy and adhesion capabilities. However, it was not considered at this stage because the question if adhesive or cohesive interface formation is required to achieve sufficient interface strength has not been answered yet. This study shows that the adhesion capability of uCF-PEEK is poor so that the formation of an adhesive interface with sufficient interface strength is difficult.

Test procedure

Five uCF-PEEK plate specimens with the dimensions of 80 mm $\times$ 79.5 mm $\times$ 2 mm ($l \times w \times d$) were used as inserts for overmoulding. The width of the specimens was orthogonal to the fibre direction and considered the thermal expansion of the specimens (cf. chapter 4.2.7) due to pre-heating so that they fitted into the mould of the injection moulding machine *Arburg 320 S Allrounder 500-150*. The mould dimensions were 80 mm $\times$ 80 mm $\times$ 4 mm ($l \times w \times d$) so that the insert volume filled half of the volume of the mould cavity. The specimens were cleaned with isopropanol prior to overmoulding.

The convection ovens used for insert pre-heating were placed close to the injection moulding machine to keep the transfer time and the temperature loss of the pre-heated inserts low (cf. chapter 4.2.6). Two uCF-PEEK plates at room temperature and three pre-heated uCF-PEEK plates were overmoulded with sCF-PEEK after manual transfer. Considering the pre-heating temperature of the convection ovens, the transfer times, and transfer conditions of the inserts, the pre-heated inserts had a temperature of approximately 170 °C just before overmoulding. The overmoulding was conducted with a temperature of the molten mass of 395 °C and a mould temperature of 200 °C. The mould temperature was chosen that high to prevent further heat loss of the pre-heated inserts due to conduction. After overmoulding, the specimens were prepared for testing according to ASTM D 695 [195] and ASTM D 3846 [196].

Figure 4.10 illustrates the geometry of the compression shear test specimens on the right. The hybrid plates composed of insert and overmould were cut into specimens with a width of 12.7 mm. A hand milling tool was used to mill the two required grooves into the specimens. It was ensured that the depth of the grooves was just higher (approximately 0.3 mm) than the thickness of the corresponding adherend. Otherwise, the compression strength of the adherend and not the strength of the interface was tested [197]. The end faces of the compression shear test specimens were ground parallel and plane to enable a homogeneous load introduction.

The compression shear tests were conducted with a *Hydropuls Längszylinder PL 10 kN* from *Instron Structural Testing Systems GmbH*. The testing speed was 1 mm/min and the tests were performed at room temperature. In accordance with the standards, the specimens were not clamped by the testing machine. Two small metallic supports with a slightly bigger thickness compared to the specimens were aligned by an in-house developed positioning tool and clamped by the testing machine. For the compression shear test, the specimens were placed onto these supports so that the specimens were in contact with the support but not with the clamps of the testing machine. Consequently, the compression force was only applied at the end faces of the specimens and not simultaneously at the side faces. In accordance with the standards [195, 196], a buckling support was used for the compression shear test to prevent buckling of the specimen. The test set-up is shown in figure 4.10 on the left.

Several specimens have already failed during the preparation steps so that no statistically relevant results about the interface strength could be achieved by compression shear testing. The interface strength between the uCF-PEEK insert and the sCF-PEEK overmould was insufficiently low. The main potentials for improvement refer to:

- **Curvature:** After overmoulding, the hybrid plates showed a curvature which was the result of thermal stresses that arose during cooling. A reason for this curvature lies in the different thermal contraction of the uCF-PEEK plate and sCF-PEEK materials due to different CTEs (cf. chapter 4.2.7).
- **Pre-stresses:** Due to the curvature of the specimens, the interface was prestressed during the clamping process, which was needed for cutting the specimens and milling the grooves, and during the installation of the buckling support prior to testing. Additionally, many preparation steps, such as cutting or milling, were required to conduct the compression shear test. These preparation steps

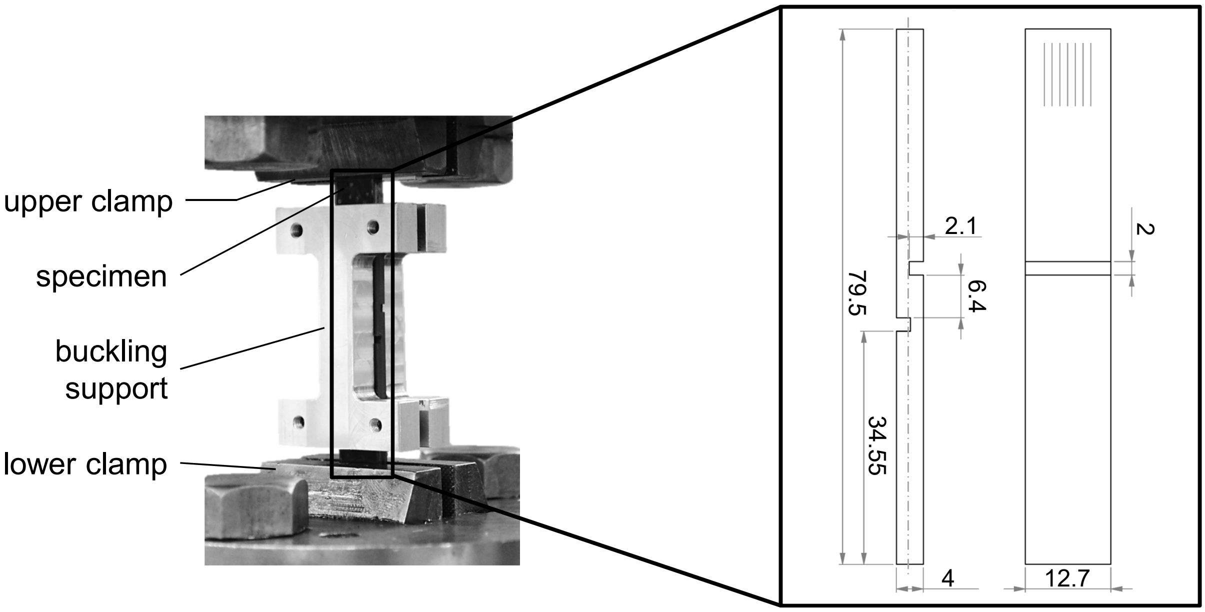

Figure 4.10.: Compression shear test set-up (left) and specimen geometry (right)

contributed to interface weakening, e. g. due to induced vibrations.

- **Plane and parallel specimen end faces:** The end faces of the specimens had to be plane and parallel to achieve valid test results. However, excellent planarity and parallelism were difficult to achieve.
- **Cooling:** The pre-heated inserts rapidly cooled down between opening the oven and start of overmoulding. As mentioned in chapter 4.2.6, it is important to ensure fast insert transfer, and to provide a hot support to decrease cooling.
- **Adhesive interface:** Insert pre-heating temperatures of approximately 170 °C just before overmoulding were not sufficient to achieve adequate interface strengths. An adhesive interface was formed. It is assumed that by the realisation of a cohesive interface, higher interface strengths can be achieved. The surface temperature of the insert has to be close to the melting temperature of the PEEK matrix to enable insert surface melting, and the formation of a cohesive interface. However, form stability of the insert has to be maintained during transfer particularly under the consideration of the material stiffness reduction at these high temperatures (cf. chapter 4.2.5).
- **Low matrix content:** The uCF-PEEK plate had a fixed fibre volume fraction of about 60 vol.-%. Thus, only little matrix material was located at the insert surface. If a cohesive interface is to be established, the molten mass will only form a cohesive interface with the matrix material of the insert. Therefore, increasing the matrix content of the insert would contribute to higher cohesive interface strength but would disadvantageously decrease the structural mechanical properties of

the hybrid composite pedicle screw. Only few biocompatible semi-finished uCF-PEEK products are available on the market. The biocompatible uCF-PEEK rods, required for the manufacturing of the hybrid composite pedicle screw, could only be bought from *Invibio Ltd.* with a fixed fibre volume fraction of 60 vol.-% so that this parameter could not be changed.

Examination of the smooth failure surface of the specimens confirmed that adhesive failure occurred. Compared to the temperature of the molten mass, the insert surface temperature was too low. Consequently, a solidified skin layer of the molten mass could be provoked which prevented the penetration of the molten mass into the microroughness of the insert surface. As a consequence, micromechanical interlocking between uCF-PEEK plate insert and sCF-PEEK overmould was insufficient and did not significantly contribute to interface strength.

Contact angle measurements have shown that the surface energy of the uCF-PEEK plate insert is low so that its adhesion capability is poor. Low surface energy can further be a reason for poor wettability of the insert surface by the molten mass, and for poor molecular interaction between insert and overmould.

Due to insert pre-heating, less heat has to be transferred from the molten mass to the insert to achieve the melting of the insert surface so that cohesive interface formation can occur. However, the heat transfer from the molten mass to the insert surface was insufficient to form a cohesive interface in this case. This study underlines the necessity of the formation of a cohesive interface between the uCF-PEEK insert and the sCF-PEEK overmould material so that sufficient interface strength can be achieved. The insert temperature has to be above a certain threshold so that heat transfer from the molten mass is sufficient to melt the insert surface. With sufficient time in this melting state, interdiffusion of molecules of the PEEK matrices can occur, and the formation of a cohesive interface can take place. In addition to that, different test methods with less specimen preparation steps are required to successfully characterise interface strength.

Despite of the fact that the compression shear test specimens showed insufficient interface strength, several parameters, which influence interface strength, could be determined with this study. Figure 4.11 summarises these parameters, and their interdependencies. The know-how gained with this first adherence test was used for additional tests and improvements.

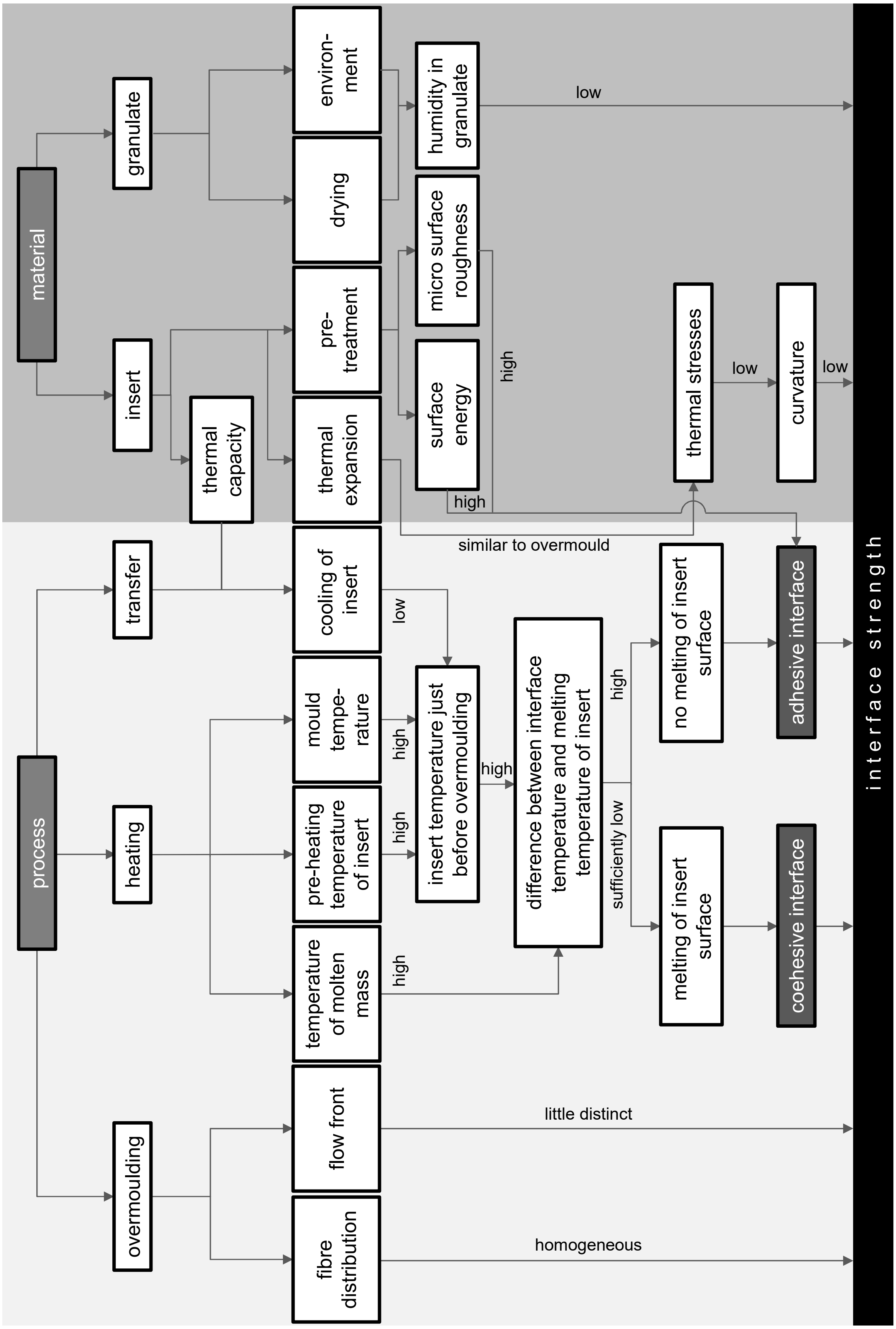

Figure 4.11.: Parameters, which influence the interface strength, and their interdependence

4.2.8.2 Single lap shear test

For the manufacturing of the SLS specimens, uCF-PEEK plate inserts with the dimensions of 100 mm $\times$ 25 mm $\times$ 2 mm ($l \times w \times d$) were overmoulded with sCF-PEEK material. Half of the inserts were surface ground with abrasive paper P120 at the overmould area to increase surface roughness, and all inserts were cleaned with isopropanol prior to overmoulding. The overmoulding region of the insert had a length of 12.5 mm and a width of 25 mm. Only this region was heated above 300 °C with the heating plate *IKA C-MAG HP*. At this temperature, partial melting and recrystallisation of the PEEK matrix can already occur [55], and structural mechanical properties are low (cf. chapter 4.2.5). However, insert handling was still possible because only the overlap region was pre-heated. Nevertheless, careful handling of the hot inserts during transfer was required. In addition to that, transfer times were below ten seconds so that cooling of the pre-heated insert region was low. As a consequence, the insert temperature just before overmoulding was more than 260 °C. In this study, the sCF-PEEK material *Akrotek PEEK CF30* from *Akro-Plastic GmbH* with a fibre mass fraction of 30 % [198] was used for overmoulding. This material is similar to *Victrex® PEEK 450CA30* from *Victrex plc*. The overmoulding procedure was conducted with the injection moulding machine *Sumitomo (SHI) DEMAG Systec 100-310*. The resulting sCF-PEEK overmould adherend had a thickness of 4 mm, a width of 25 mm, and a length of 100 mm. After the overmoulding process, aluminium cap strips were applied to the specimens to decrease the bending moments during the SLS tests. The SLS specimen is shown in figure 4.12.

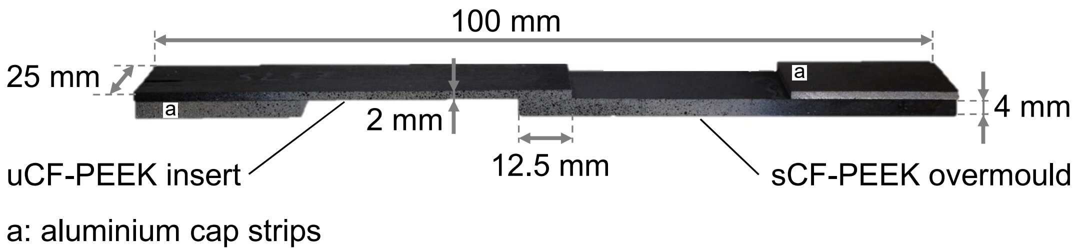

Figure 4.12.: SLS specimen

The tests were conducted in tension with the testing machine *Hydropuls Längszylinder PL 10 kN* from *Instron Structural Testing Systems GmbH* with a testing speed of 1 mm/min, and at room temperature. Figure 4.13 shows the stress-strain diagram of the SLS specimens. The term *SLS - rough* represents specimens with partial surface grinding, as described before.

No significant differences in the stress-strain characteristics between SLS specimens with a smooth and a rough overlap region could be observed. Specimen failure occurred at the sCF-PEEK adherends close to the edge of the overlap region. In this

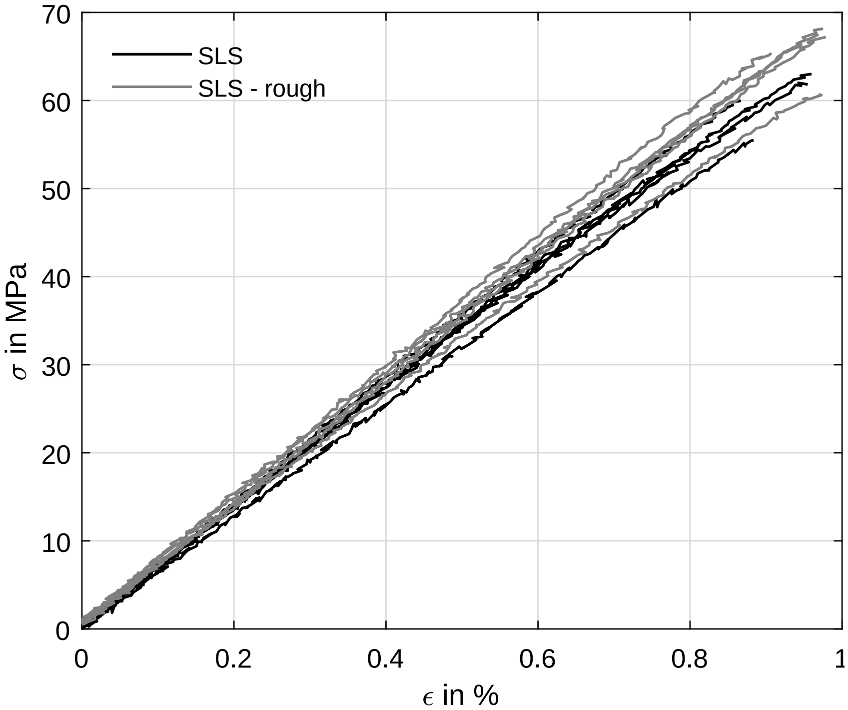

Figure 4.13.: Stress-strain diagram of SLS specimens

area, stress concentrations were located which contributed to this failure mechanism. Complete fracture at the interface was not observed. The stress values illustrated in figure 4.13 were obtained by dividing the force values by the cross-section of the sCF-PEEK adherends. With a thicker sCF-PEEK adherend or a smaller overlap region, interface failure could have been achieved. However, the mould design could not be changed for this study.

Several polished sections of the interface after testing were examined. Four exemplifying polished sections are shown in figure 4.14.

The upper left image shows no distinct visible border between the sCF-PEEK and uCF-PEEK material. In the case of insert surface melting, matrix accumulations and fibre reorientations can emerge at the interface (cf. upper right). However, these phenomena were not critical in this case, because the regions in which matrix accumulation or fibre reorientation occurred were very limited. Although interface failure was not the final failure mechanism of the SLS specimens, local interface cracks developed. The lower left image shows a local crack along the interface. The crack path indicates that both adhesive and cohesive failure mechanisms occurred at this location. Cohesive cracks can also be seen in the lower right image. In this case, the interface strength between the uCF-PEEK plate insert and the sCF-PEEK overmould exceeded the inter-fibre strength of the uCF-PEEK plate component. These findings indicate the successful formation of a cohesive interface. For cohesive interfaces, surface roughness plays a minor role.

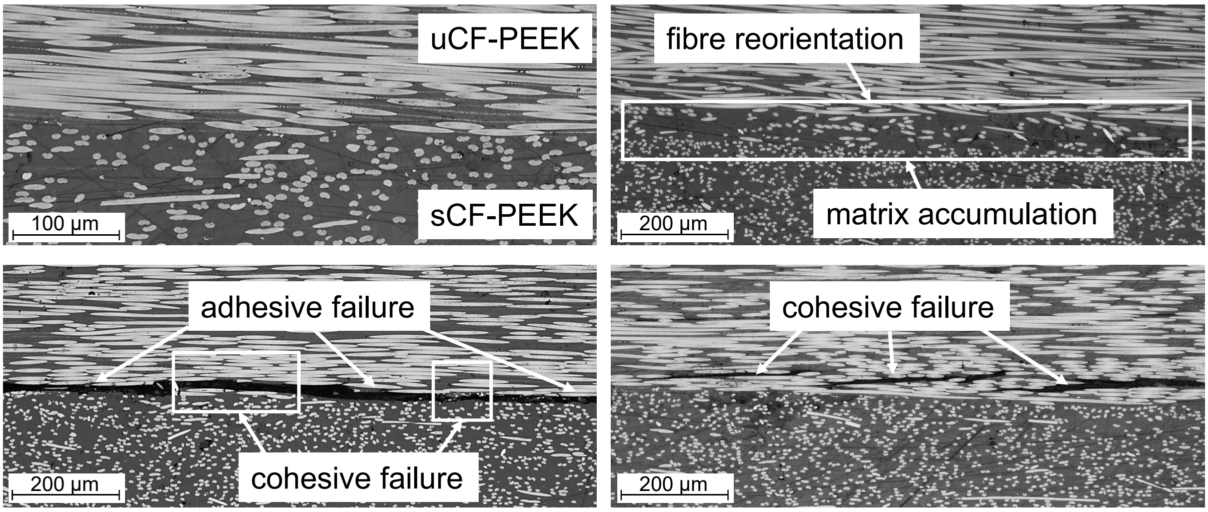

Figure 4.14.: Polished sections of the interface after SLS testing: interface detail (upper left), matrix accumulation at the interface (upper right), adhesive and cohesive failure mechanisms (lower left), and cohesive cracks (lower right)

The SLS adherence test shows that with a pre-heating temperature of more than 260 °C just before overmoulding a cohesive interface between uCF-PEEK plate and sCF-PEEK material could be established. A cohesive interface contributed to higher interface strengths than an adhesive interface (cf. chapter 4.2.8.1). However, sCF-PEEK adherend tensile failure was observed during the SLS tests due to specimen geometry and stress concentrations at the edge of the overlap so that no information about interface shear strength could be achieved. Therefore, the SLS test was not appropriate for interface strength characterisation. Consequently, research on a suitable specimen for interface strength characterisation was conducted.

4.2.8.3 Cylinder pull-out test

To account for the hybrid composite pedicle screw design and to investigate the interface strength between uCF-PEEK and sCF-PEEK material, a novel cylinder pull-out specimen was developed. Within this work, the utility patent DE202019102255.8 was registered for this specimen. Following the hybrid composite screw structure, the cylinder pull-out specimen consisted of a uCF-PEEK rod insert which was cylindrically overmoulded with sCF-PEEK material. Compared to the compression shear or SLS specimens, this cylinder pull-out specimen showed distinct advantages, such as no negative influences of specimen preparation on the interface, easy manufacturability, low rework, low material cost, and a simple test set-up. In addition to that, the mould costs were kept low due to the simple geometry of the cylinder pull-out specimen.

An FE model was built up in *Abaqus* to ensure that with a certain cylinder diameter no significant disturbing edge effects influence the interface strength even at a theoretical pull-out force of 10 kN. These edge effects are a result of the compression stress due to pull-out loads at the region of the cylinder which is in contact with the steel support. The bigger the cylinder diameter is, the lower is the influence of these edge effects on the interface. The cylinder diameter was defined with 14.5 mm so that a proper load introduction into the specimen during the pull-out test was ensured as well. Under the consideration of the maximum injection volume of the injection moulding machine, the overmoulding length was maximised to 34 mm. Approximately five times more material was injected for the cylinder compared to the injected volume of the hybrid composite pedicle screw. Figure 4.15 shows the cylinder pull-out test set-up on the left and the geometry of the cylinder pull-out specimen on the right.

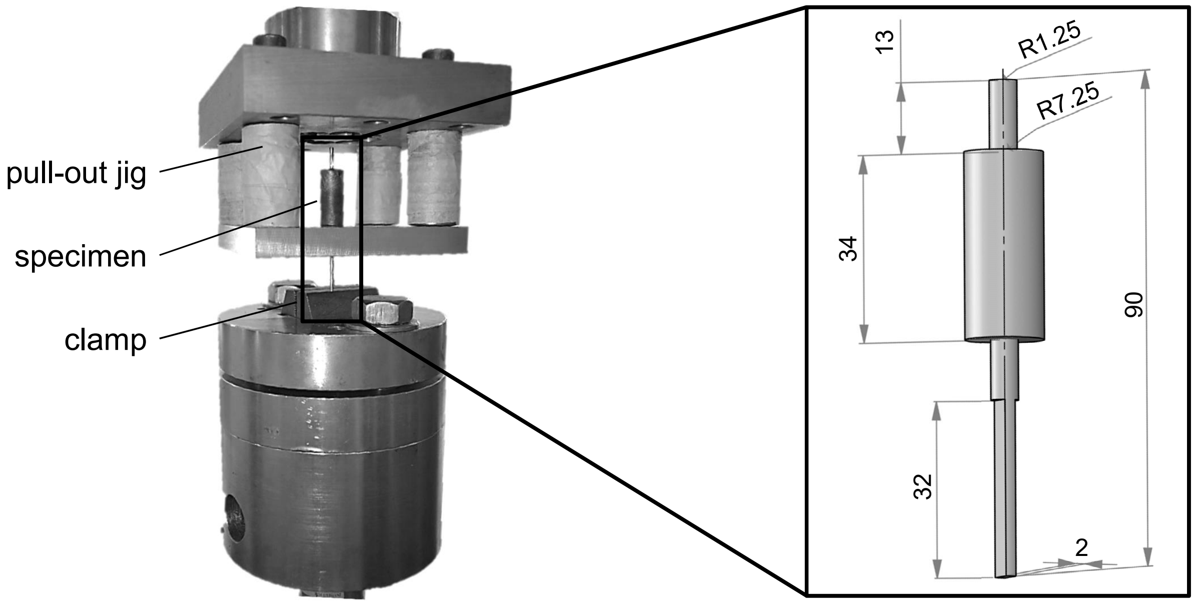

Figure 4.15.: Cylinder pull-out test set-up (left) and specimen geometry (right)

Ten uCF-PEEK rod inserts with a diameter of 2.5 mm were overmoulded with sCF-PEEK and tested in a special pull-out testing jig. The injection moulding machine *Babyplast type 6/10 PT* was used for manufacturing. During the overmoulding process, the mould temperature was 215 °C. With the underlying mould design, the molten sCF-PEEK material with a temperature of 400 °C hit the insert perpendicularly and flowed along the longitudinal axis of the insert during injection. This mould design was realised because of economic aspects. However, the composite inserts could slightly bend during overmoulding due to the high injection pressure of the molten mass, and a significant distance from the injection point to the insert fixation points in the mould. The number of specimens, which could be produced, was limited because only a certain number of uCF-PEEK rods could be purchased from the manufacturer. With the available uCF-PEEK rods, both the cylinder pull-out specimens and the hybrid composite pedicle screws had to be manufactured.

Prior to overmoulding, the inserts were pushed through small perforated metal jigs which were fixed in the mould. These jigs ensured a proper fixation of the inserts during overmoulding. The outer diameter of the inserts needed to be within a small tolerance range so that a proper fixation of the inserts in the injection moulding machine could be realised. If the insert diameter was out of tolerance, the insert would either not fit through the hole of the jigs, or it would be pushed out of place by the injection pressure. Besides a correct insert diameter, a minimum insert length of 100 mm was required to ensure an appropriate fixation in the injection moulding machine. After turning and cutting of the uCF-PEEK rod inserts and after the injection process, two flat faces were ground at the lower ends of the inserts to facilitate clamping in the testing machine.

Five out of ten uCF-PEEK rod inserts were not pre-heated prior to overmoulding. The other five inserts were heated up to 290 ℃ in the convection oven *Heraeus RL 200* after cleaning with isopropanol. Trials have shown that the target temperature of this oven was close to the actual temperature of the inserts. A pre-heating temperature of 290 ℃ of the entire insert decreased the required heat which has to be transferred from the molten mass to the insert to form a cohesive interface, while sufficient form stability during insert transfer to the injection moulding machine was ensured. Nevertheless, the stiffness properties of the uCF-PEEK rod inserts were significantly reduced at 290 ℃ (cf. chapter 4.2.5) so that careful handling of the inserts during transfer was required to prevent insert damage. Several inserts were pre-heated simultaneously to keep the time in between the injections low and to prevent degradation of the sCF-PEEK material. As a result of the study of the cooling characteristics described in chapter 4.2.6, a heated metal cask was used for the manual transport of the pre-heated inserts to the injection moulding machine to decrease cooling, and to prevent the specimens from forced convection. Transfer times were kept lower than ten seconds so that the temperature of the inserts just before overmoulding was higher than 260 ℃. This value was calculated on the basis of the results of chapter 4.2.6. After overmoulding, the cylinder pull-out specimens were demoulded by ejector pins, and sprue and runner were manually cut off. No other steps were required to prepare the specimens for testing.

The tests were conducted with the testing machine *Hydropuls Längszylinder PL 10 kN* from *Instron Structural Testing Systems GmbH*. The testing speed was 0.5 mm/min, and the tests were performed at room temperature. In figure 4.16, the results of the cylinder pull-out specimens with non-heated uCF-PEEK rod inserts are shown on the left and with pre-heated uCF-PEEK rod inserts on the right. The force values F are plotted after the running-in regions of the pull-out tests against the pull-out displacements u.

The specimens with pre-heated uCF-PEEK inserts showed significantly higher maxi-

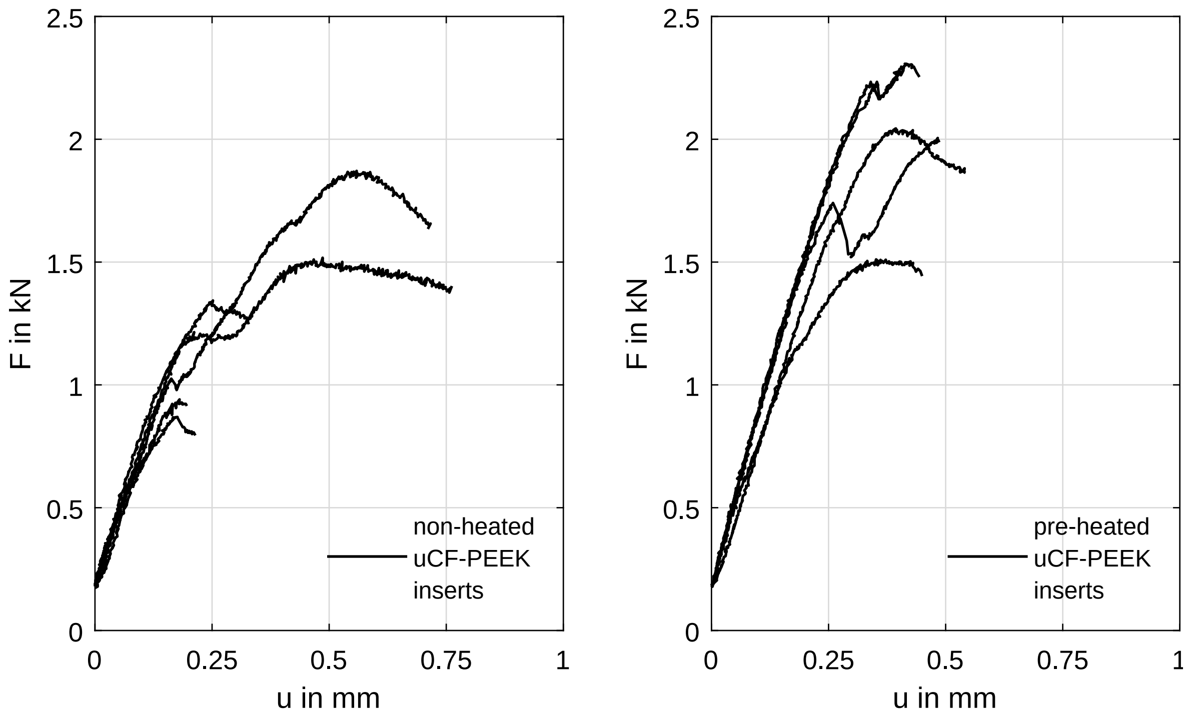

Figure 4.16.: Force-displacement diagrams of cylinder pull-out specimens with non-heated uCF-PEEK inserts (left) and pre-heated uCF-PEEK inserts (right)

mum pull-out forces than the specimens with non-heated inserts. First failure of the specimens was characterised by a sudden force drop. Afterwards, the forces further increased to their maximum at which total failure of the specimens occurred. This increase in force after first failure can be explained by the slight insert curvature which is a result of injection position, as described before. Additionally, thermal contraction can lead to a strong locking between uCF-PEEK rod insert and sCF-PEEK overmould. The forces at first failure, and the maximum forces for each specimen are listed in table 4.6.

The interface strength between the uCF-PEEK rod insert and the sCF-PEEK overmould is highly dependent on the insert temperature. Three significant heat fluxes can be identified which influence interface strength: (1) cooling of the pre-heated inserts during transfer from the oven to the injection moulding machine, (2) heating of the non-heated inserts and cooling of the pre-heated inserts after contact with the mould, and (3) heating of the inserts by the molten mass. Because of significant differences in the interface strength between specimens with non-heated and pre-heated uCF-PEEK inserts, it is assumed that the heat transfer from the molten mass to the non-heated uCF-PEEK inserts was insufficient to form a cohesive interface. Any further increase of the temperature of the molten mass would promote the formation of a cohesive interface also at lower pre-heating temperatures. However, the sCF-PEEK material would degrade rapidly (cf. chapter 4.2.4). Under the assumption of the formation of an adhesive interface for the specimens with non-heated uCF-PEEK inserts, surface roughness

Table 4.6.: Force F at first failure and maximum force $\hat{F}$ of cylinder pull-out specimens

Specimen	F at first failure in N	$\hat{F}$ in N
Non-heated insert 1	1044	1876 [a)]
Non-heated insert 2	877	877
Non-heated insert 3	1348	1348
Non-heated insert 4	1216	1524 [a)]
Non-heated insert 5	958	958
Mean	1089 ± 172	1318 ± 369
Pre-heated insert 1	2237	2318
Pre-heated insert 2	2077	2221
Pre-heated insert 3	1761	2049 [a)]
Pre-heated insert 4	1524	1524
Pre-heated insert 5	1681	2010
Mean	1856 ± 262	2024 ± 274

[a)] pull-out force exceeded clamping force

linked to micromechanical interlocking and thermal contraction of the overmould can significantly contribute to interface strength.

The shear stress at first failure was used to characterise and compare the interface strength of the different cylinder pull-out specimens. An FE model was built up in *Abaqus* in which a *tie constraint*[7] was assumed between insert and overmould to represent sufficient interface strength. The mean forces at first failure of the specimens with non-heated and pre-heated uCF-PEEK rod inserts were used for the pull-out loads in the FE model. The results showed that the region of highest shear stress was located in the lower part of the cylinder close to the interface (cf. figure 4.17). The shear stress at first failure of the specimens with pre-heated uCF-PEEK rod inserts was approximately 64 MPa which was 73 % higher than the average shear stress at first failure of approximately 37 MPa of the specimens with non-heated uCF-PEEK inserts.

Thermal contraction

Two FE models were built up in *Abaqus* to compare the contact pressures on the uCF-PEEK rod due to thermal contraction at different insert pre-heating temperatures: (1) the cylinder pull-out specimen (cf. figure 4.15), and (2) the hybrid composite pedicle screw. For this study, the linear elastic material data was extended by the CTE data shown in table 4.5. Under the assumption of an adhesive interface, the interaction

[7]translational and rotational DOFs are equal for a pair of surfaces

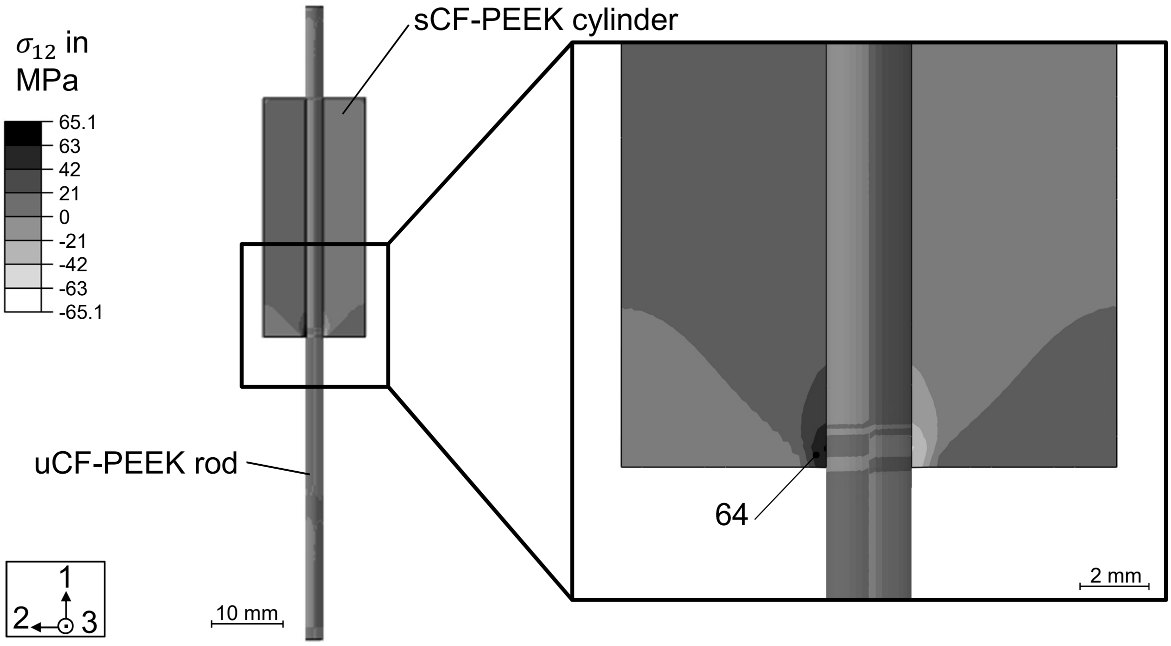

Figure 4.17.: Shear stress distribution of the cylinder pull-out specimen with pre-heated uCF-PEEK rod insert

between insert and overmould was approximated with a friction coefficient of 0.2[8]. For this FE analysis, no pull-out load was modelled but the thermal conditions of the manufacturing process were implemented.

Considering the scenario of a uCF-PEEK rod insert at room temperature, a contact pressure of about 348 MPa was achieved due to thermal contraction of the hot overmould and linear elastic material properties. The contact pressure on the insert was highest in the middle of the overmoulded region and slightly decreased towards its edges. It slightly decreased in the interval of insert temperatures from 23 °C to 100 °C, slightly increased in the interval from 100 °C to 160 °C where it reached its maximum of 353 MPa, and decreased to 142 MPa in the interval from 160 °C to 290 °C.

In addition to the finite element analysis (FEA) of the cylinder pull-out specimen, the hybrid composite pedicle screw was analysed. The same behaviour as for the cylinder pull-out specimen was observed while insignificantly higher maximum contact pressures for different insert pre-heating temperatures were achieved due to a different geometry. However, contact pressure was not as evenly distributed as in the case of the cylinder pull-out specimen. The contact areas below thread peaks showed higher contact pressures than the areas below thread valleys. This observation emphasises that the contact pressure is highly sensitive on the volume and the location of the overmoulded material. Dependent on the material distribution local variations in contact

[8]This value will often be used as a standard value to model friction interaction especially if no exact friction data is available. A friction coefficient of 0.2 was also used in [111, 121, 199].

stress arise. Despite of the fact that approximately five times more material was injected for the cylinder pull-out specimen compared to the hybrid composite screw, the same behaviour of thermal contraction was observed, and similar maximum contact pressures were achieved.

It can be concluded that for insert pre-heating temperatures in the interval of approximately 23 °C to 160 °C, contact pressure due to thermal contraction was highest. For higher insert pre-heating temperatures, contact pressure decreased. The analysis was based on linear elastic material properties so that absolute contact stresses were relatively high. In reality, plastic deformations of the material occur which reduce these contact pressures. Furthermore, the sCF-PEEK material was assumed to be isotropic. However, the fibre orientation of real specimens can vary which influences contact stresses. Nevertheless, the contact stress development for different temperatures could be determined for the cylinder pull-out specimen and the hybrid composite pedicle screw. Thermal shrinkage will contribute to interface strength especially if non-heated inserts are considered. However, an adhesive interface is formed in this case with a lower strength compared to the strength of a cohesive interface which will develop if inserts are adequately pre-heated. Therefore, it is important to ensure cohesive interface formation for the hybrid composite pedicle screw.

Interface formation

To further investigate the interface between insert and overmould, and to prove the assumptions of adhesive and cohesive interface formations, stereo microscopy was used. The cylinder of a specimen with a pre-heated uCF-PEEK insert was cut in half after the insert was completely pulled-out of the cylinder. Figure 4.18 illustrates an image of the cylinder cut on the left and of the corresponding insert on the right.

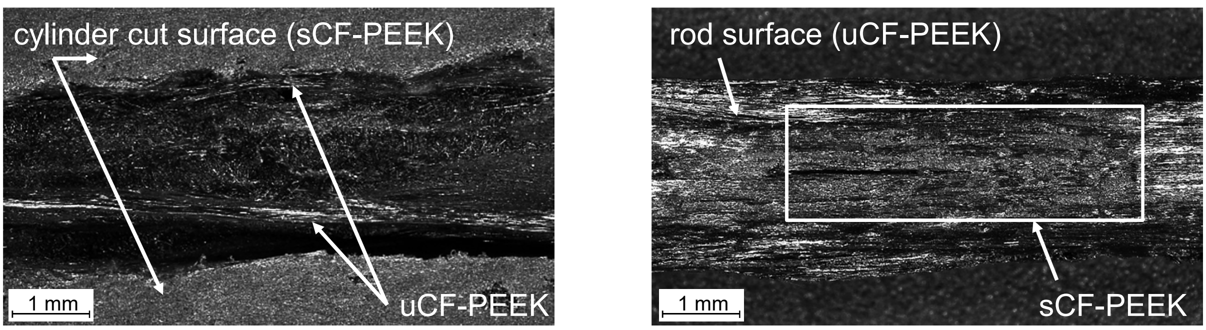

Figure 4.18.: Stereo microscope images of the sCF-PEEK cylinder cut (left) and the corresponding uCF-PEEK rod insert (right) after pull-out testing

The image on the left shows a bunch of endless fibres which stick to the sCF-PEEK material of the cylinder. Similarly, the uCF-PEEK rod surface was studied. Short CFs on the rod surface were present and can be seen in the image on the right. These findings underline that a cohesive interface between the uCF-PEEK material of the pre-heated insert and the sCF-PEEK material of the overmould was formed. The rough insert surface after pull-out testing is a result of cohesive failure.

4.2.8.4 Concluding remarks

The previously described adherence tests highlight that several requirements have to be fulfilled in order to successfully test the interface strength of hybrid overmoulded composite structures. For interface testing, the geometry of the specimen should be directly obtained by means of a representative manufacturing process. As a consequence, only few preparation steps will be required for the conduction of the interface test. Advantageously, the interface is not influenced by specimen preparation. As an example, the compression shear test required several preparation steps after overmoulding to receive the final specimen geometry. Each step affected the interface. In contrast, minor preparation steps were required for the cylinder pull-out specimen after overmoulding so that the influence on the interface strength was insignificant.

During injection, the molten mass should flow along the main extension of the insert. As a consequence, transverse forces on the insert, which can lead to insert deformation, are significantly reduced. Especially if the insert bulk material is pre-heated up to temperatures close to the melting point, the risk of insert deformation during transfer and overmoulding is high. Preferably, only the insert surface melts due to heat transfer from the molten mass so that a cohesive interface is formed while the risk of insert deformation is low.

In addition to that, the set-up of the production cell should allow efficient and reproducible overmoulding. This means that heating sources should be placed close to the injection moulding machine to keep transfer times of pre-heated inserts low. During the transfer itself, forced convection should be prevented. Preferably, the pre-heated inserts are transferred in a hot cask, or the heating is further applied to the inserts during transfer. Most accurate control of pre-heating temperature will be achieved if the heating of the inserts is realised in the injection moulding machine. However, sufficient machine extensions are required to pre-heat the inserts inside of the injection moulding machine which was not the case for this study.

The automation of insert pre-heating, insert transfer, and overmoulding contributes to manufacturing efficiency, and can lead to economic benefits. Pre-heating and transfer times can be easily controlled in an automated process so that the reproducibility of hybrid composite structures is favoured.

4.3 Finite element analysis

FE models were built up in *Abaqus* to primarily investigate pedicle screw stability. Experimental test efforts could be significantly reduced by numerical simulation. In general, reproducible in vivo test results are difficult to obtain due to a large variety of geometry and mechanical properties of human bone [121]. However, these problems can be eliminated with numerical models.

Parametric FE models written in *Python* were developed for the numerical analysis and design optimisation of the hybrid composite pedicle screw. The FE solver *Abaqus* was used for calculation. Due to the parametric character of the FE models, variations of various model features could be realised fast and efficiently. By executing the parametric script, 2D or 3D models of a pedicle screw embedded in bone were automatically generated.

4.3.1 2D model

2D FE models typically contain much lower numbers of elements and nodes than the corresponding 3D counterparts [45, 46, 102, 200]. Therefore, efficient simulations can be conducted with 2D models due to low computation times. However, the results of the 2D analysis should only be used for comparative investigations [45, 197]. For the 2D problems, symmetric matrix storage was used for the solver.

4.3.1.1 Geometry

For the numerical model, bone geometry was simplified. Bone was assumed to be a rectangular block with a length l_{bone} of 45 mm and a width w_{bone} of 65 mm, and was divided into two parts: (1) the upper part which represented cortical bone, and (2) the lower part which represented spongious bone. With the experience of cooperating surgeons, the length $l_{cortical}$ of cortical bone was defined with 11 mm in the model to represent an average value for the length of cortical bone of pedicle and lumbar vertebra. The 2D screw could be modelled axisymmetric or with an offset of the half of the pitch between the left and right thread edges. The thread helix was indicated with this offset. A buttress thread was used for the thread design.

Certain variables were standardised to decrease the number of possible design variations. The total screw length l_{screw} was defined with 50.74 mm from the top to the tip of the screw, and the outer diameter D_o of the screw with 6.5 mm. The screw consisted of a thread number n_{thread} of 15, and the pitch of the thread p_{thread} was standardised with 2.4 mm. Fillets were applied between screw head and shaft, and shaft and tip to avoid sharp edges. The screw tip had a length of 2.2 mm and was modelled sharp. The head of the screw was modelled spherically, and showed a radius r_{head} of 3.55 mm. All other variables, which were required to build up the geometry of the FE model, could be modified. Figure 4.19 illustrates the buttress thread of the screw with its significant design parameters on the left. Besides the outer diameter D_o and the standardised pitch p_{thread}, the modifiable variables are shown: inner screw diameter D_i, distal half angle κ_{dist}, proximal half angle κ_{prox}, distal root radius r_{dist}, proximal root radius r_{prox}, and the length of the thread flank l_{flank}.

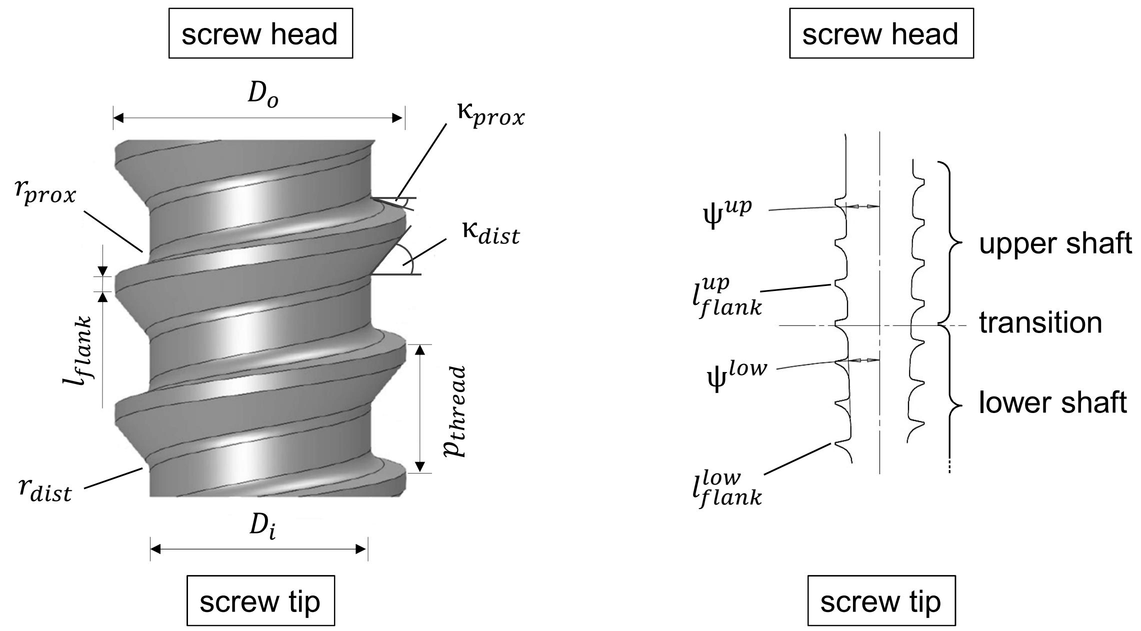

Figure 4.19.: Design parameters which describe the buttress thread (left) and the partitioned pedicle screw shaft (right)

The thread was partitioned into an upper and a lower part separated by the variable N. This variable defined the number of threads at which the partition was realised. Because the screw shaft length in between four threads corresponds to the length of cortical bone, the variable N was standardised with the value of 4 for this study. Both the upper and lower screw shaft could be independently designed conically or cylindrically. The variables ψ^{up} and ψ^{low} symbolise the conical angles of the upper and lower screw shaft. In addition to that, two different lengths of the thread flanks l^{up}_{flank} and l^{low}_{flank} could be used independent of the two parts (cf. figure 4.19 on the right).

The dimensions of the overmoulded insert were also defined in the script. The insert could be modelled shorter than the screw by defining its start and end position. However, the models used for the studies presented in the following were built up with an insert which covered the whole length of the screw. The variable D_{core} describes the diameter of the uCF-PEEK insert located in the centre of the hybrid composite pedicle screw. The standardised and modifiable geometry variables of the parametric FE models are listed in table 4.7.

Table 4.7.: Geometry variable definition

Standardised		Modifiable
D_o	6.5 mm	κ_{dist}
l_{bone}	45 mm	κ_{prox}
$l_{cortical}$	11 mm	ψ^{low}
l_{screw}	50.74 mm	ψ^{up}
n_{thread}	15	D_{core} a)
N	4	D_i
p_{thread}	2.4 mm	l_{flank}^{low}
r_{head}	3.55 mm	l_{flank}^{up}
$r_{head\text{-}shaft}$	0.3 mm	r_{dist}
$r_{shaft\text{-}tip}$	1 mm	r_{prox}
w_{bone}	65 mm	

a) only used for hybrid composite screw

Several partition lines were needed for the screw-bone model to define the geometry of the screw core, the edges at which the pull-out load was applied, the geometry of the cortical bone, a vertical edge from the tip of the bone cavity to the lower bone edge to apply local seeds, and an area around the bone cavity in which a free mesh was applied (cf. chapter 4.3.1.4).

To investigate the influence of increasing osseointegration (cf. chapter 4.3.1.3) and of better bone properties, nine 2D screw-bone models with different conical shaft angles were modelled and are shown in table 4.8. In the table, the sum of the upper and lower conical angles ψ^{up} and ψ^{low} is represented by the cumulated conical angle ξ.

Table 4.8.: Model overview of conical shaft study

	Model-1	Model-2	Model-3	Model-4	Model-5	Model-6	Model-7	Model-8	Model-9
ψ^{up} in °	0	0	0	0.5	0.5	1.0	1.0	1.5	1.5
ψ^{low} in °	0	1.0	2.5	0.5	1.0	1.0	1.5	1.5	2.0
ξ in °	0	1.0	2.5	1.0	1.5	2.0	2.5	3.0	3.5

Model-1 represented a pedicle screw with a completely cylindrical screw shaft whereas for model-2 and model-3 the upper part of the screw shaft was cylindrical and the lower part was conical. All other models had completely conical screw shafts.

The geometry of the model is based on the assumption that the bone cavity perfectly fits to the outer shape of the pedicle screw. In reality, surgeons use special drills or other instruments to drill pre-holes into the vertebrae. The pull-out resistance of pedicle screws is dependent on the size and quality of these pre-holes, especially shortly after surgery. However, these dependencies were not considered in the numerical models because they were used for comparative studies only. Nevertheless, laboratory tests were performed in which different pre-hole diameters were tested for different BRMs (cf. chapter 4.6.1 and 4.6.2).

4.3.1.2 Properties

To account for the different bone properties of cortical and spongious bone, two bone materials were defined. In addition to that, three pedicle screws with different materials were considered to examine the differences in screw pull-out resistance: (1) a titanium screw, (2) an injection moulded sCF-PEEK screw, and (3) a hybrid composite screw. The load magnitudes were chosen in the way that linear elastic material behaviour could be assumed for screw and bone materials.

The parametric script enables isotropical or anisotropical modelling of cortical bone. In many studies [46, 102, 107, 111, 121, 124, 125], there was no differentiation between cortical and spongious bone, or isotropic material properties of bone were assumed, especially in the case of simplified bone geometries. However, anisotropic cortical bone properties account for a more realistic material behaviour. Therefore, elastic anisotropic behaviour was assumed for cortical bone in this study. To properly assign the anisotropy of cortical bone and uCF-PEEK, local coordinate systems (LCOSs) were defined. For the uCF-PEEK material, the 1-axis of the LCOS was oriented along the fibre direction. Compared to the radial or transverse direction, cortical bone is stiffer along the diaphyseal axis (longitudinal direction) so that transverse isotropic behaviour could be assumed for cortical bone [118]. The 1-axis of the cortical bone material was assumed to be collinear with the screw axis. The Young's moduli E_{11}, E_{22} and E_{33}, the Poisson's ratios ν_{12}, ν_{13} and ν_{23}, and the shear moduli G_{12} and G_{13} were defined for the anisotropic material description. Additionally, the shear modulus G_{23} was calculated by

$$G_{23} = \frac{E_{22}}{2(1+\nu_{23})}\,. \tag{4.18}$$

As mentioned in chapter 2.2.1, bone properties differ dependent on several factors. The main difference between good and poor bone quality lies in the stiffness value of spongious bone. To analyse the influence of healthier and stronger bone on the pull-out characteristics, the Young's modulus E_{spong} of the spongious bone was increased from 0.1 GPa (poor bone quality) to 1 GPa (good bone quality). Relative variations of spongious bone stiffness are typically higher than for cortical bone [18, 24, 117]. It was assumed that increasing the spongious bone stiffness by a factor of 10 significantly changes the pull-out behaviour of the hybrid composite pedicle screw. The stiffness of cortical bone remained constant to clearly evaluate the effect on the pull-out behaviour and to promote the comparability of results. Table 4.9 informs about the material properties of screw and bone used for the comparative analyses of this study.

Table 4.9.: Material properties

	E_{11} in GPa	E_{22} in GPa	E_{33} in GPa	ν_{12}	ν_{13}	ν_{23}	G_{12} in GPa	G_{13} in GPa	G_{23} in GPa	Ref.
Cortical bone	17.9	10.1	10.1	0.40	0.40	0.62	3.30	3.30	3.12	[118]
uCF-PEEK	170.2	9.4	9.4	0.34	0.34	0.40	5.46	5.46	3.36	[a)]

	E in GPa	ν	Ref.
Spongious bone	0.1 or 1[b)]	0.20	[18, 24, 117, 118, 121]
Titanium	114	0.30	[18, 48, 114, 124, 175]
sCF-PEEK	18	0.33	[173, 174]

a) material data of *Invibio PEEK-OPTIMA™ Ultra-Reinforced* provided by *Neos Surgery S. L.*

b) a stiffness value of 0.1 GPa was chosen to represent poor bone quality, and 1 GPa was chosen to represent good bone quality

4.3.1.3 Interactions

As mentioned in chapter 2.1.2.1, the osseointegration capability of PEEK and CF-PEEK implants is typically poor, but coatings can be applied to promote osseointegration. In this study, three different contact states between pedicle screw and bone were modelled, dependent on the time after surgery:

1. Short time after surgery (hours): There is neither significant osseointegration nor significant friction interaction between screw and surrounding bone. The tangential contact behaviour was assumed to be frictionless in the model [201].
2. Medium time after surgery (days, weeks): Osseointegration and friction interaction between screw and surrounding bone are relevant. The tangential contact behaviour was based on a friction coefficient of 0.2 in the model [111, 121, 199].[9]
3. Long time after surgery (several months): The level of osseointegration is high so that functional connections between screw and surrounding bone exist. The interaction was based on a tie constraint in the model [90, 201].

[9] This value was assumed for a medium osseointegration state in between no and full osseointegration. In [111, 121, 199], a friction coefficient of 0.2 was used between bone and a stainless steel implant.

A friction coefficient of 0.2 was assumed for a medium osseointegration state in between no osseointegration (frictionless contact) and full osseointegration (tie constraint). Numerous osseointegration states exist, but only three states were relevant for this study. This approach is widely accepted in the literature, and the modelling techniques listed before were also used by others [46, 201–203].

In the model, a surface-to-surface contact with a finite sliding formulation was implemented between screw (master) and bone (slave). There was neither a need for slave adjustment nor for surface smoothing. If short or medium time after surgery is modelled, the tangential contact behaviour will be defined. It could either be frictionless to represent the state of short time after surgery, or it was based on a penalty formulation to represent the state of medium time after surgery. In both cases, the normal contact behaviour was assumed to be a hard contact based on a penalty formulation with a normal contact stiffness of 8 GPa and a linear behaviour. This normal contact stiffness was chosen to be lower than the stiffness of sCF-PEEK to promote convergence while still having minor contact penetrations. Separation after contact was allowed.

4.3.1.4 Mesh

The *Abaqus* 8-node quadratic quadrilateral plane stress elements *CPS8R* and the 6-node quadratic triangular plane stress elements *CPS6* were used for the mesh of the 2D models. If the hybrid composite screw is modelled, the core of the screw will be structurally meshed with local seed assignment whereas the remaining screw parts will be meshed freely. A slightly coarser mesh was used for the screw core compared to the mesh at the outer edges of the screw. Titanium and sCF-PEEK screws were entirely meshed freely. Concerning bone, the area close to the screw cavity showed a free mesh with small elements to account for the screw-bone interaction. The remaining bone parts were structurally meshed with coarser elements towards the left and right outer edges. Figure 4.20 highlights edges and partition lines used for mesh control on the left. In the figure, a hybrid composite pedicle screw with the reinforcing uCF-PEEK core (a) and sCF-PEEK material for thread and head (b) is shown. The screw is embedded in bone which consists of a cortical shell (c) and a spongious bone part (d). A detailed view of the mesh is shown in figure 4.20 on the right. The boundary conditions, which will be described more in detail in chapter 4.3.1.5, are shown as well.

Due to the 2D character of the model, the number of elements was quite low. Approximately 16000 elements were used for the mesh of screw and bone so that the 2D model consisted of approximately 32000 elements and 100000 nodes. Roughly 98 % of the mesh consisted of *CPS8R* elements. Certainly, these numbers depend on the specific screw and bone geometry.

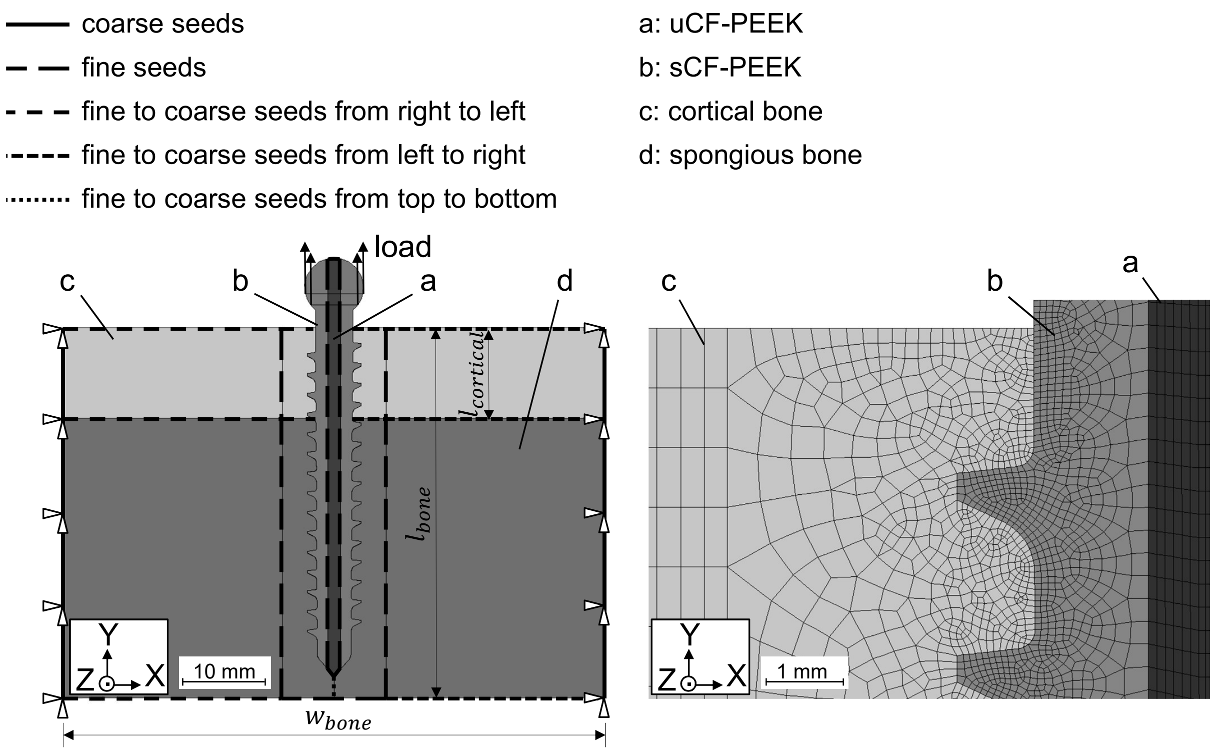

Figure 4.20.: Local seeds with boundary conditions for the pull-out loading case (left) and mesh detail (right)

4.3.1.5 Loads and boundary conditions

To study the hybrid composite screw numerically, a pull-out loading case was modelled. This loading case does not replicate the complex and multidirectional in vivo loads, the human spine is subjected to. However, pull-out is a suitable loading case to evaluate screw fixation strength and to compare numerical studies [204]. Because thread design is crucial for screw stability in bone under pull-out loads, this loading case was chosen for the numerical studies including screw thread design optimisation.

The pull-out load was applied to the lower edges of the screw head. The model could be constructed with a displacement or a force load. The load magnitude was chosen in the way that the material behaviour of screw and bone has been in the linear elastic region. Additionally, the left and right bone edges were clamped so that the displacements u_X and u_Y in the global coordinate system were restricted (cf. figure 4.20 on the left).

4.3.2 3D model

A 3D FE model is a more realistic representation of the real scenario compared to a 2D model [201]. However, it is also based on several assumptions so that it is still a simplification of the reality. Disadvantageously, computation time is typically higher compared to 2D models. In addition to the 2D screw-bone model, an axisymmetric 3D model was developed. It could be modelled as a quarter (3D90), half (3D180) or full model (3D360), dependent on the revolve angles used. The thread helix angle can influence the pull-out behaviour of pedicle screws. Thus, by the simplification of axisymmetric modelling, some limitations to the interpretation of the results have to be applied, but this approach is widely used in the literature [45, 46, 102, 107, 200]. A comparison of the load distribution between an axisymmetric 3D model and a model, which considered the thread helix, was made in [205]. In that study, the helical effect did not significantly influence load distribution. Due to the broad acceptance of axisymmetric models in the literature, the significant increase in complexity concerning parametrisation, and uncertain increase in accuracy, the helical angle was neglected in the models used for this study. Furthermore, the modelling of the 3D geometry of a vertebra was beyond scope of this work so that bone geometry was simplified.

Basically, most of the commands used for building up the 2D model were adopted for the 3D case. The mesh of the 3D models was slightly coarser than in the 2D case to keep the number of elements in a reasonable range. Additionally, the material definition accounted for the third dimension. The *Abaqus* elements used for the 3D model were the 20-node quadratic brick element *C3D20R* with reduced integration and the 10-node quadratic tetrahedron element *C3D10*. The 3D90 model consisted of approximately 33000 elements and 147000 nodes, the 3D180 model of 68000 elements and 300000 nodes, and the 3D360 model of 133000 elements and 572000 nodes. These numbers were dependent on the specific screw and bone geometry, as for the 2D case. The 3D90 model showed an X-symmetry boundary condition in the ZY-plane, and a Z-symmetry boundary condition in the XY-plane. Only the Z-symmetry boundary condition was used for the 3D180 model.

To promote convergence, an automatic contact stabilisation scheme could be implemented for the 3D models. A constant damping factor based on the dissipated energy fraction (default value 0.0002) was used [206]. If an unstable region exists in the model, local velocities will arise which will be artificially damped so that part of the strain energy will be consumed by the damper. This static dissipated energy should only be a small fraction of the total strain energy. In addition to that, the option of adaptive stabilisation was activated, and the allowable accuracy tolerance for the ratio of dissipated energy to total strain energy in each increment was 5 % which is also the *Abaqus* default value [206]. Besides contact stabilisation, the solver option of unsymmetric matrix storage (UMS) was activated [206]. With these options, excellent accuracy could be maintained and numerical errors could be prevented while convergence was promoted. Concerning the 3D90 and 3D180 model, the symmetry boundary conditions had a stabilisation effect so that the convergence of these models was faster than the convergence of the 3D360 models. Therefore, contact stabilisation and UMS were only used for the 3D360 models.

If contact stabilisation is used, it will be important to check the ratio of static dissipation or viscous damping energy ε_{ALLSD} and the internal or total strain energy ε_{ALLIE} of the solution. As an example, the energy ratio $\varepsilon_{ALLSD}/\varepsilon_{ALLIE}$ of a 3D360 model with a displacement load L_u of 0.6 mm was

$$\frac{\varepsilon_{ALLSD}}{\varepsilon_{ALLIE}} = \frac{4.17 \cdot 10^{-3}\, J}{3.64\, J} = 0.115\,\%\,. \tag{4.19}$$

The energy ratios of other models with different loads were in the same range. Additionally, the ratio of the maximum nodal viscous damping force to the maximum reaction force was in the range of 0.004 %. These numbers show that contact stabilisation did not significantly influence solution accuracy.

4.3.3 Simulation results

Because several studies were based on the simplified but time efficient 2D screw-bone model, the correlation between 2D and 3D models is examined in this chapter. In addition to that, stresses and strains of pedicle screws and bone are investigated. Finally, a study is presented in which the contact formulations between screw and bone were changed.

4.3.3.1 Differences between 2D and 3D modelling

To decrease the number of elements and to increase computational efficiency, symmetry planes should be identified in an FE model. The screw-bone model was constructed as a 2D model, or as a 3D quarter, half or full model (cf. chapter 4.3.2) to see the differences in simulation time and accuracy.

For this study, a hybrid composite screw was modelled with a frictionless contact definition between screw and bone, and with the displacement pull-out load of 0.6 mm. As mentioned in chapter 4.3.2, the options of contact stabilisation and UMS for the equation solver were used for the 3D360 model to promote convergence. For a better comparison of the 2D model with the 3D models, the thread was modelled axisymmetric in this study. In addition to that, the relative reaction force $F_{R,rel}$ was defined as the ratio of reaction forces F_R of the corresponding models related to the reaction force

F_R^{3D90} of the 3D90 reference model:

$$F_{R,rel} = \frac{F_R}{F_R^{3D90}} \tag{4.20}$$

In figure 4.21, the relative reaction forces $F_{R,rel}$ are plotted against the node numbers of the corresponding models. The node (element) numbers were 99824 (32228) for the 2D, 147339 (32633) for the 3D90, 299802 (68276) for the 3D180, and 572286 (133460) for the 3D360 model.

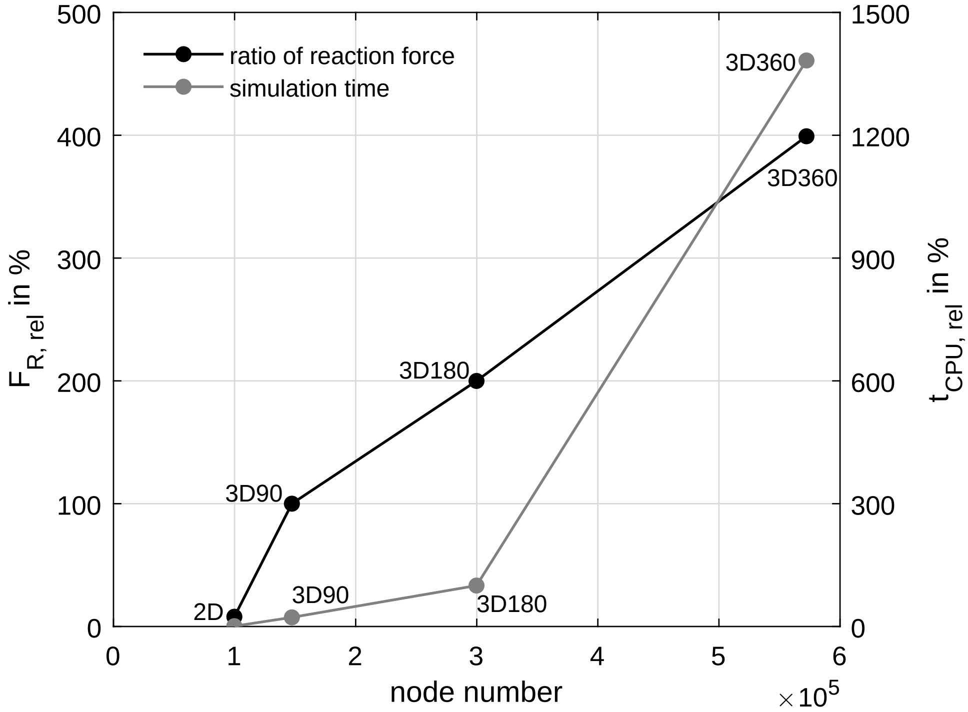

Figure 4.21.: Comparison between 2D and 3D models by the ratio of reaction force $F_{R,rel}$ and simulation time $t_{CPU,rel}$

As expected, the 3D180 model shows twice the reaction force of the 3D90 model, and the 3D360 model shows four times the reaction force of the 3D90 model. The same observations were also obtained with other pull-out displacement loads.

To compare the simulation time of the models, the total central processing unit (CPU) times t_{CPU} of the corresponding models were related to the total CPU time t_{CPU}^{3D180} of the 3D180 model based on a displacement load of 0.6 mm:

$$t_{CPU,rel} = \frac{t_{CPU}}{t_{CPU}^{3D180}} \tag{4.21}$$

Only relative values are presented here because the simulation time depends on the computational resources available. The relative CPU time was 0.86 % for the 2D model, 22.28 % for the 3D90 model, and 1382.67 % for the 3D360 model. As mentioned before, the 3D360 model was modelled with the solver options of contact stabilisation and UMS which promoted convergence but additionally increased simulation time. Figure 4.21 shows the relative CPU times $t_{CPU,\ rel}$ of the different models over the corresponding node numbers.

The possibility of saving simulation time by the 3D90 model without losing accuracy compared to the 3D180 and 3D360 model is proven by this study. With the 2D model, efficient simulations can be conducted. However, this model should only be used for comparative analyses.

4.3.3.2 Stress and strain analysis

To analyse the stresses and strains of the hybrid composite pedicle screw and bone, a 3D90 model was subjected to a pull-out displacement load of 0.1 mm in this study so that the material behaviour of screw and bone has still been in the elastic region. Moreover, the interaction between screw and bone was modelled as frictionless, and a tie constraint between the uCF-PEEK core and the overmoulded sCF-PEEK material was assumed which represented a sufficient strong interface. The equivalent von Mises stress σ_{Mises} was used to investigate the material behaviour (cf. figure 4.22).

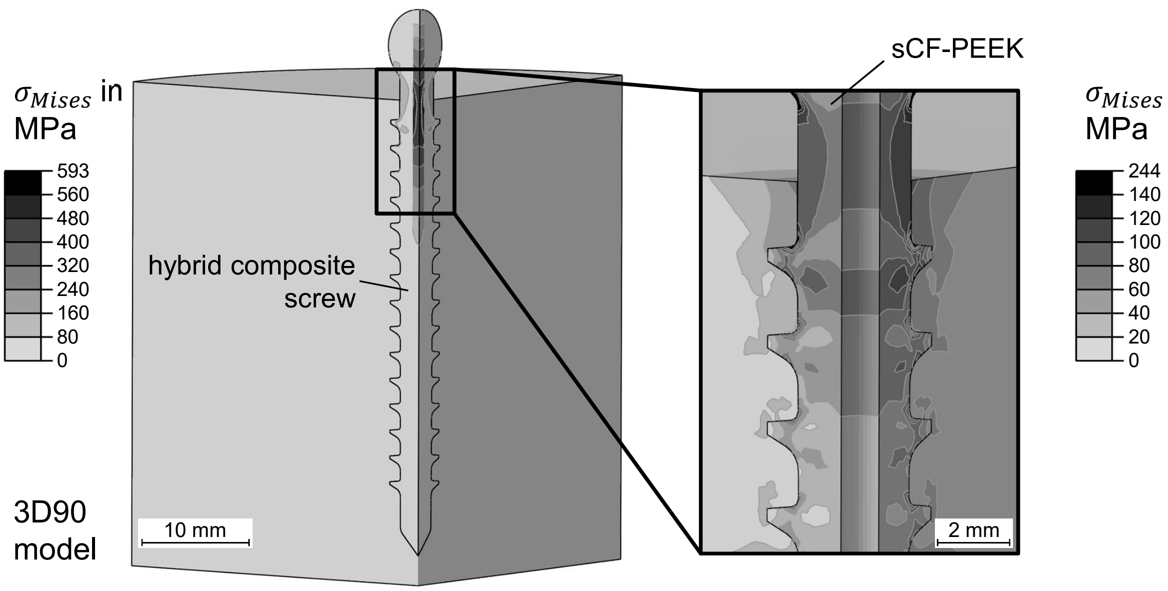

Figure 4.22.: Von Mises stress analysis of hybrid composite pedicle screw-bone model with detailed view without screw core

Concerning the hybrid composite pedicle screw, high stress values were located at areas close to the proximal root radii. The stress was transferred from the screw head to the uCF-PEEK core which was subjected to high stresses σ_{11} in fibre direction. Sufficient interface strength has to be ensured to guarantee proper load transfer. Generally, stiffer cortical bone showed higher stresses and lower strains than spongious bone.

The regions of highest von Mises stresses in the bone were located in the cortical part around the first thread which is in accordance with the findings of others [23, 45, 121]. The regions of highest strains were located in the spongious bone part close to the thread flanks.

Three 3D90 models with different screw materials were defined to study their differences in stress distribution: (1) a titanium screw, (2) an sCF-PEEK screw, and (3) a hybrid composite screw. The model geometry and all other parameters used for the analysis were the same for all models. The pull-out load was 100 N. Figure 4.23 illustrates the contour plots of the three models and compares von Mises stress values σ_{Mises} at distinct locations. The underlined numbers refer to bone stresses.

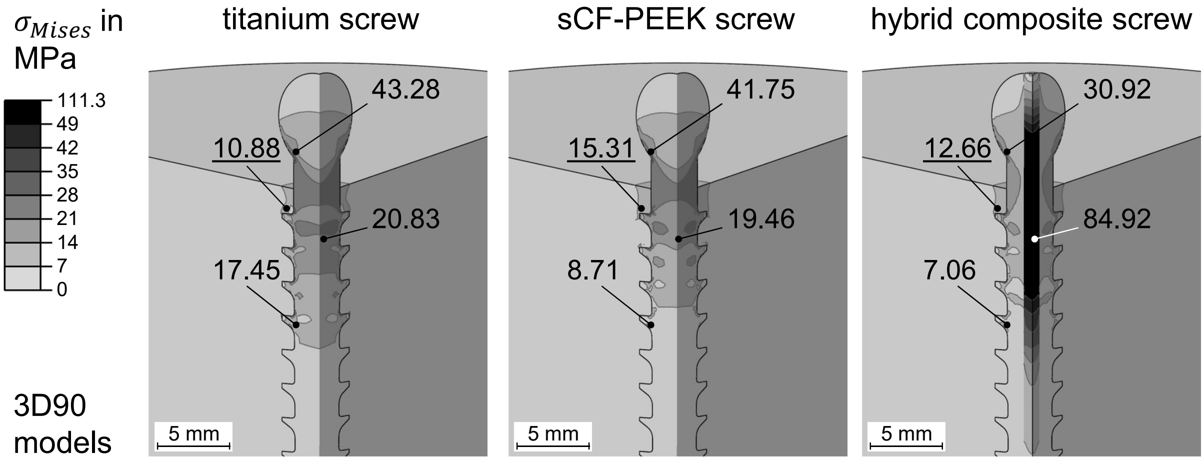

Figure 4.23.: Comparison of von Mises stress σ_{Mises} of models with different screw materials

The bone stress of the sCF-PEEK and hybrid composite pedicle screw model was approximately 40.7 % and 16.4 % higher than the bone stress of the titanium pedicle screw model. Therefore, the risk of stress shielding can be reduced for both composite and hybrid composite pedicle screws. The stiffer titanium screw showed higher von Mises stresses than the sCF-PEEK screw and the discontinuous CF reinforced parts of the hybrid composite screw. The uCF-PEEK core of the hybrid composite screw shows high stresses. However, there is only a minor risk of core failure due to its high strength. In addition to that, the stresses in the overmoulding material are comparatively low. Compared to the entirely discontinuous CF reinforced PEEK pedicle screws, the hybrid composite screws showed a reduction of approximately 22 % of the pull-out displacements at the specified pull-out load of 100 N.

This study shows that an excellent adhesion between core and overmould is important to guarantee proper load transfer, that screw purchase of cortical bone is important for pedicle screw stability, and that stress shielding can be reduced with hybrid composite pedicle screws.

4.3.3.3 Contact formulations

In this study, pedicle screws were subjected to a pull-out load of 100 N. Figure 4.24 shows the results of the contact study under the consideration of different spongious bone qualities (cf. chapter 4.3.1.2) and different contact formulations (cf. chapter 4.3.1.3). The absolute displacement value u_{abs} of each model listed in table 4.8 was related to the absolute displacement value u_{abs}^{cyl} of the cylindrical reference model-1 for each contact formulation to analyse relative displacements u_{rel}:

$$u_{rel} = \frac{u_{abs}}{u_{abs}^{cyl}} \tag{4.22}$$

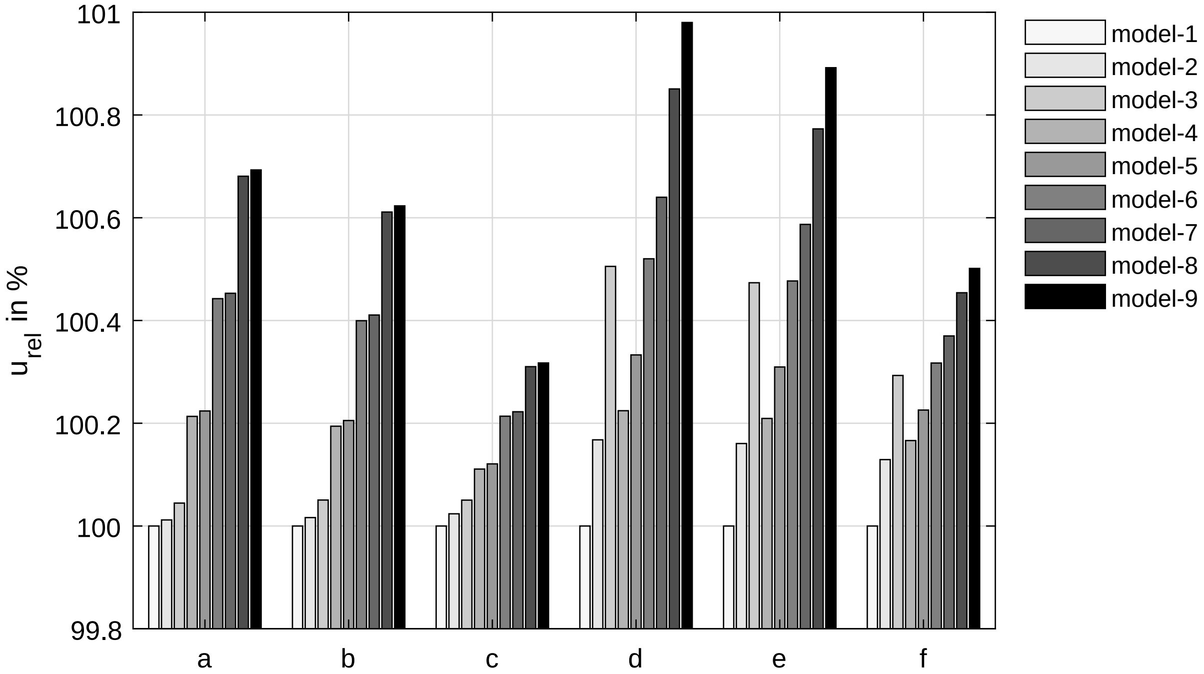

Figure 4.24.: Relative pull-out displacements u_{rel} in axial screw direction: a) short time after surgery with poor bone quality, b) medium time after surgery with poor bone quality, c) long time after surgery with poor bone quality, d) short time after surgery with good bone quality, e) medium time after surgery with good bone quality, f) long time after surgery with good bone quality

A cylindrical screw showed the lowest displacement values independently of bone quality or contact formulation. The differences in relative pull-out displacements between the models were below 1 %. Typically, the optimisation of one design parameter only contributes to small improvements. However, the sum of the improvements of all parameters can contribute to significant changes (cf. chapter 4.3.4).

In the case of *poor bone quality*, the relative displacements will increase if the conical angles increase. Screws with the same upper conical angle (cf. table 4.8) showed the same level of relative displacement. If the upper conical angle increases, the relative displacement will increase as well. Contrarily, the lower conical angle played a minor role in case of poor bone quality. This means that the conical angle ψ^{up} of the upper screw part located in cortical bone had a bigger influence on the screw pull-out characteristics than the conical angle ψ^{low} of the lower screw part located in spongious bone. Most forces between screw and bone were transferred in the upper screw part which is in interaction with cortical bone. The lower screw part, which was embedded in spongious bone, transferred much less forces. Therefore, the influence of the conical angle of the upper screw part on pedicle screw stability was higher compared to the conical angle of the lower screw part. The results of the short time (frictionless contact) and medium time (friction contact) studies with poor bone quality were very similar. In the long time studies (tie constraint) with poor bone quality, the influence of conicity on the relative displacement was significantly smaller.

In the case of *good bone quality*, one relative displacement level for each model was reached. This means that not only the upper but also the lower conical angle had a significant influence on the pull-out characteristics in the case of good bone quality. Here, the cumulated conical shaft angle ξ can be chosen as an indicator. As an example, model-3 had a cumulated angle of 2.5°. The displacement of model-3 rather fitted to the displacements of model-6 and model-7 which had a cumulated angle of 2° and 2.5° (cf. table 4.8). More pull-out forces will be transferred in the lower screw part if the stiffness of spongious bone increases. This study highlights that a special attention will have to be given to the design of the lower pedicle screw part if screws for patients with good bone properties, such as healthy youths, are to be developed.

To investigate the differences in absolute axial screw displacements among the studies with different contact formulations, the absolute axial screw displacement $u_{abs,\ model\text{-}1}^{frictionless,\ 0.1}$ of model-1 of the frictionless contact study, modelled with a spongious bone stiffness of 0.1 GPa (poor bone quality), was taken as the reference model. The absolute displacement values $u_{abs,\ model\text{-}1}$ of model-1 of the other contact studies were related to this reference:

$$\text{Ratio of axial screw displacements} = \frac{u_{abs,\ model\text{-}1}}{u_{abs,\ model\text{-}1}^{frictionless,\ 0.1}} \tag{4.23}$$

The corresponding percentage values of the ratio of axial screw displacements are shown in table 4.10.

Both the interaction definition and the spongious bone quality significantly influence the pull-out characteristics of hybrid composite pedicle screws. The higher the interaction between screw and bone, the lower the axial screw pull-out displacement. More inter-

Table 4.10.: Comparison of different contact studies

Contact	E_{spong} in GPa	Ratio of axial screw displacements in %
Frictionless	0.1	100
Friction	0.1	98.60
Tie	0.1	60.77
Frictionless	1	36.03
Friction	1	35.72
Tie	1	27.71

action corresponds to a better osseointegration between screw and bone. The degree of osseointegration increases with increasing time after surgery. The most critical state of the patient with the highest risk of pulling-out the hybrid composite pedicle screw is shortly after surgery when osseointegration is still poor. The pull-out displacements were significantly increased in the case of poor spongious bone quality. This means that poor spongious bone quality highly increased the risk of pedicle screw pull-out.

4.3.4 Parametric optimisation

The parametric script written in *Python* enabled the use of the optimiser *LS-OPT 5.2.1* from *Dynamore GmbH* for parametric optimisation. The aim of the optimisation was the determination of a hybrid composite screw shaft and thread design which showed the highest resistance against a specified pull-out force of 100 N. With this load, the material behaviour of screw and bone was in the elastic region. The pull-out loading case was chosen here because the screw shaft and thread design highly affect the pull-out characteristics. Dependent on the pedicle screw design, the resultant screw pull-out displacements vary. The higher the resistance against pull-out loads is, the lower the pull-out displacements are. Lower pull-out displacements correspond to reduced micromotions between screw and bone so that osseointegration can be promoted and long-term screw stability enhanced. An excellent thread and shaft design is crucial to prevent the pedicle screw from pulling-out [23, 45, 97, 106–108, 199, 207].

As mentioned in chapter 4.3.1.1, some variables were standardised and were not included in the optimisation process. For the optimisation, the screw was modelled with the uCF-PEEK core, the cortical bone was modelled anisotropic, and the interaction between screw and bone was modelled as frictionless. The screw head geometry as well as the fillet between head and body, body and tip, and at the tip itself did not change within the optimisation procedure.

The parametric script was adapted so that the optimiser could identify the variables which should be changed within the specific optimisation procedure. The point selection and the design space were full factorial to see the influence of each parameter combination. The script was read by *Abaqus*, the calculation was conducted, and output was produced. Irrelevant data, such as the big output data base (.odb), was automatically deleted to avoid the accumulation of a huge amount of data. The absolute axial displacement of one specific node, which was located at the uppermost point of the screw head, was analysed for the optimisation. A file (.txt) with the resulting displacement value was automatically written after the calculation. It was read by the optimiser as a response file, parameters were changed, and the process could start again. This loop continued until all defined screw designs were calculated. After the optimisation procedure, the results could be post-processed and visualised by other programs. Figure 4.25 illustrates this process of optimisation.

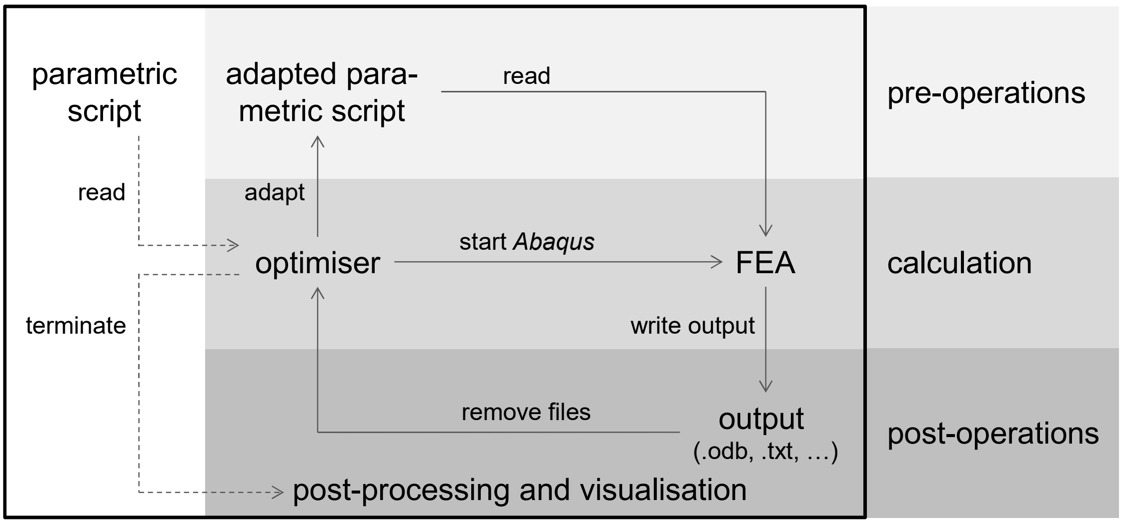

Figure 4.25.: Process of optimisation

In the following, the results of the parametric optimisation are presented. As an introductive example, the distal root radius and the proximal root radius were studied in equidistant intervals from 0.1 mm to 1.2 mm and from 0.1 mm to 0.4 mm. Simultaneously, the distal and proximal half angles were changed. In figure 4.26, the relative axial screw pull-out displacements u_{rel} are plotted against the two root radii r_{dist} and r_{prox}. The relative axial screw pull-out displacement was calculated by the division of the absolute displacement of each model with the lowest absolute displacement within the analysed set of models.

To illustrate this optimisation curve, the distal half angle κ_{dist} was fixed at 35°. The surface plot shows that for each pair of root radii and one specific distal half angle four data points with different z-coordinates were obtained, dependent on the proximal half angle. Therefore, four surfaces for each proximal half angle could be drawn. Referring

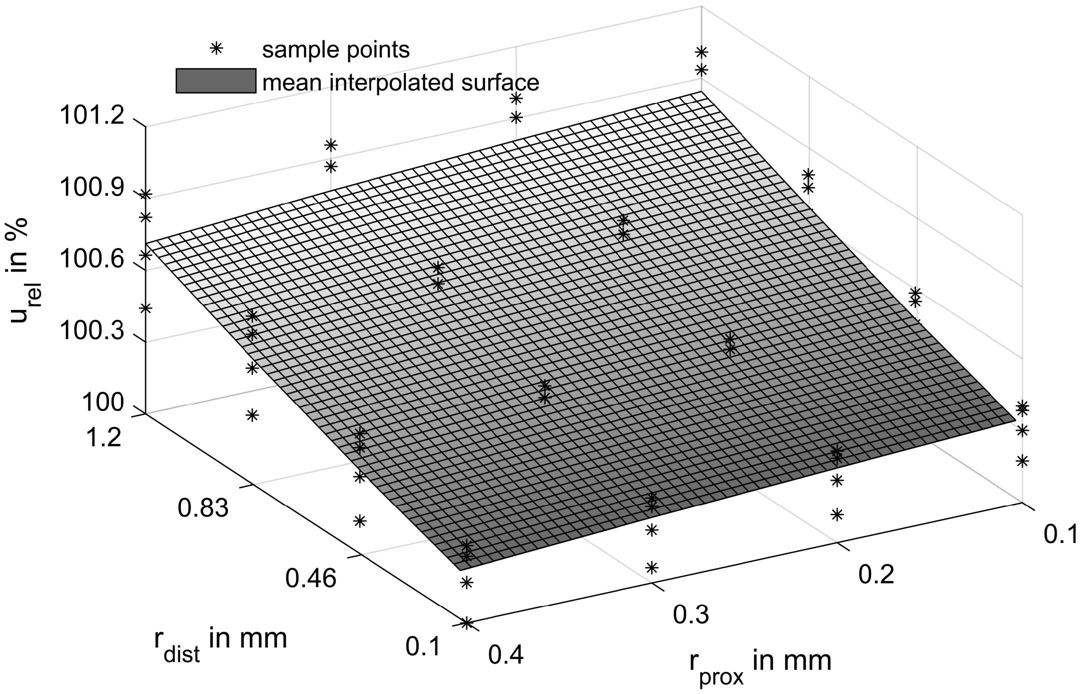

Figure 4.26.: Mean surface plot of the relative axial screw displacements u_{rel} dependent on the thread root radii r_{dist} and r_{prox} with a fixed distal half angle κ_{dist} of 35°

to figure 4.26, the data points are shown by asterisks, and the illustrated surface is the surface showing the mean displacement values.

If the results for one specific proximal half angle are chosen, only one surface will result. In figure 4.27, the relative screw pull-out displacements u_{rel} are plotted against the distal and proximal root radii r_{dist} and r_{prox} for a distal half angle κ_{dist} of 35° and a proximal half angle κ_{prox} of 0°. The area in between the data points was interpolated.

To extend the study presented in chapter 4.3.3.3, the variables ψ^{up} and ψ^{low}, which describe the conicity of the upper and lower screw shaft, were varied from 0° to 1.5° and from 0° to 2° in equidistant intervals according to table 4.11.

Table 4.11.: Parameter range of the upper and lower conical shaft angle ψ^{up} and ψ^{low} used for design optimisation

ψ^{up} in °	0	$\frac{3}{14}$	$\frac{6}{14}$	$\frac{9}{14}$	$\frac{12}{14}$	$\frac{15}{14}$	$\frac{18}{14}$	$\frac{21}{14}$
ψ^{low} in °	0	$\frac{2}{7}$	$\frac{4}{7}$	$\frac{6}{7}$	$\frac{8}{7}$	$\frac{10}{7}$	$\frac{12}{7}$	$\frac{14}{7}$

The relative displacement u_{rel}, introduced in equation 4.22, was also used for this study. The resulting surface plot of the relative displacement values for the poor bone quality case (E_{spong} of 0.1 GPa) is illustrated in figure 4.28.

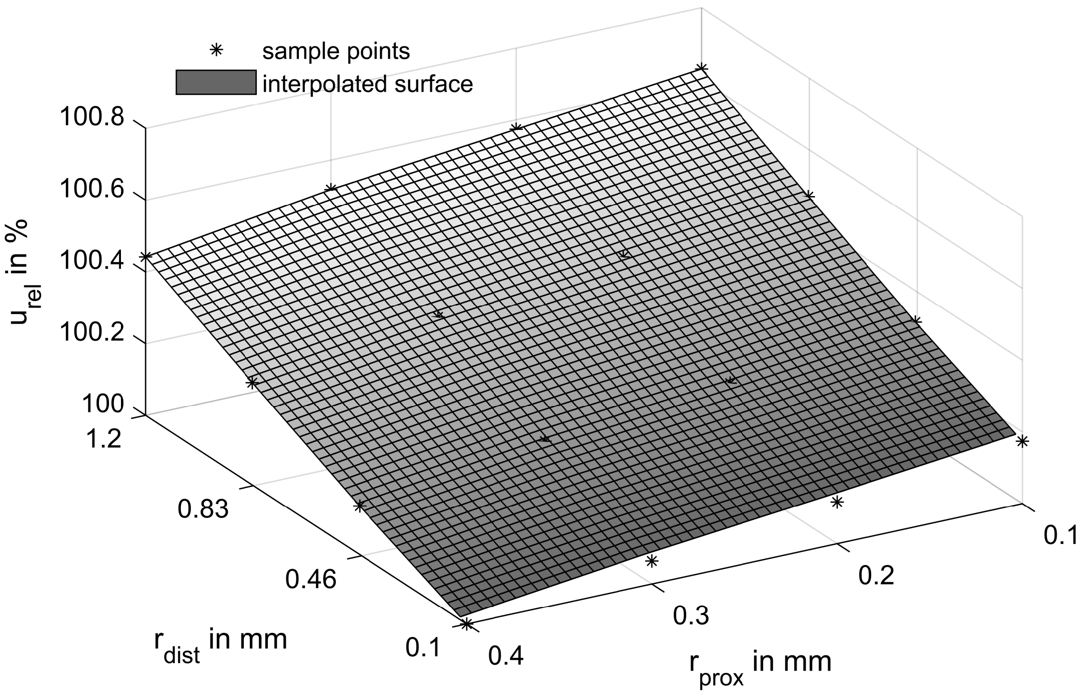

Figure 4.27.: Surface plot of the relative axial screw displacements u_{rel} dependent on the thread root radii r_{dist} and r_{prox} with a fixed distal half angle κ_{dist} of 35° and a fixed proximal half angle κ_{prox} of 0°

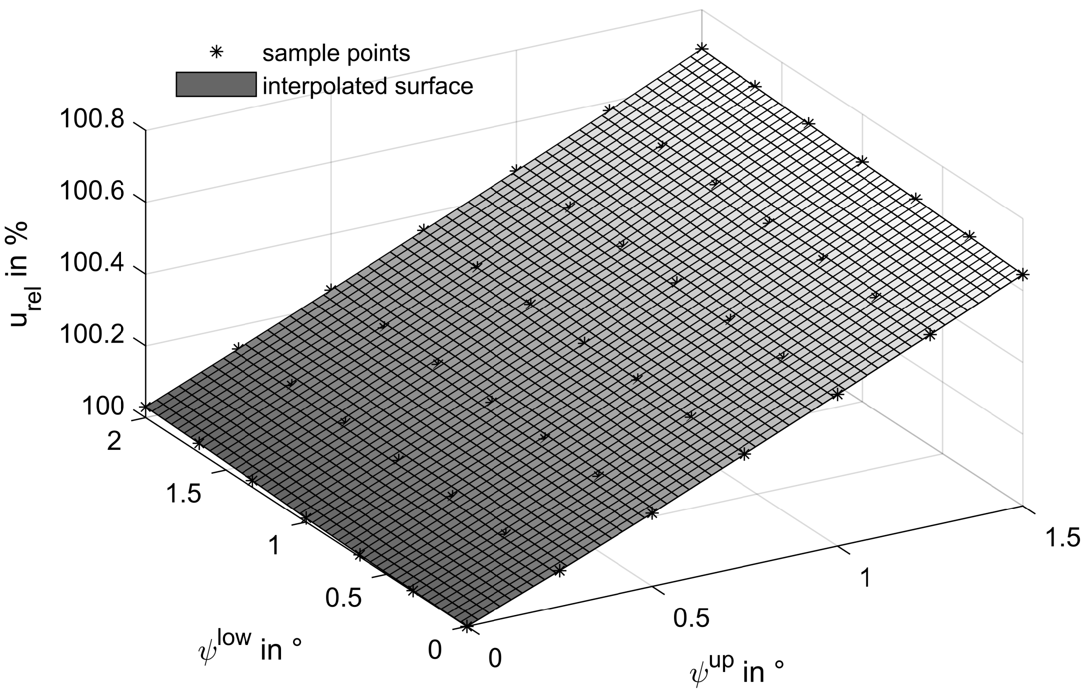

Figure 4.28.: Surface plot of the relative axial screw displacements u_{rel} dependent on the conicities ψ^{up} and ψ^{low} of the screw shaft in the case of poor bone quality

Verifying the results of chapter 4.3.3.3, the completely cylindrical screw showed the lowest displacement values. The displacement values increased with a higher degree of conicity. Referring to figure 4.28, the slope of the upper conical angle ψ^{up} was significantly steeper than the slope of the lower conical angle ψ^{low} in the case of poor bone quality. This means that the influence of the upper conical angle on the pull-out behaviour of the hybrid composite pedicle screw was bigger than the influence of the lower conical angle as far as poor bone properties were assumed for spongious bone.

The same model was built up with a spongious bone stiffness E_{spong} of 1 GPa to account for the case of good bone quality. The corresponding results are shown in figure 4.29. Compared to figure 4.28, the surface has turned clockwise. This means that the influence of the conical angle ψ^{low} of the lower thread part has become more important in the case of younger and healthier bone (cf. chapter 4.3.3.3).

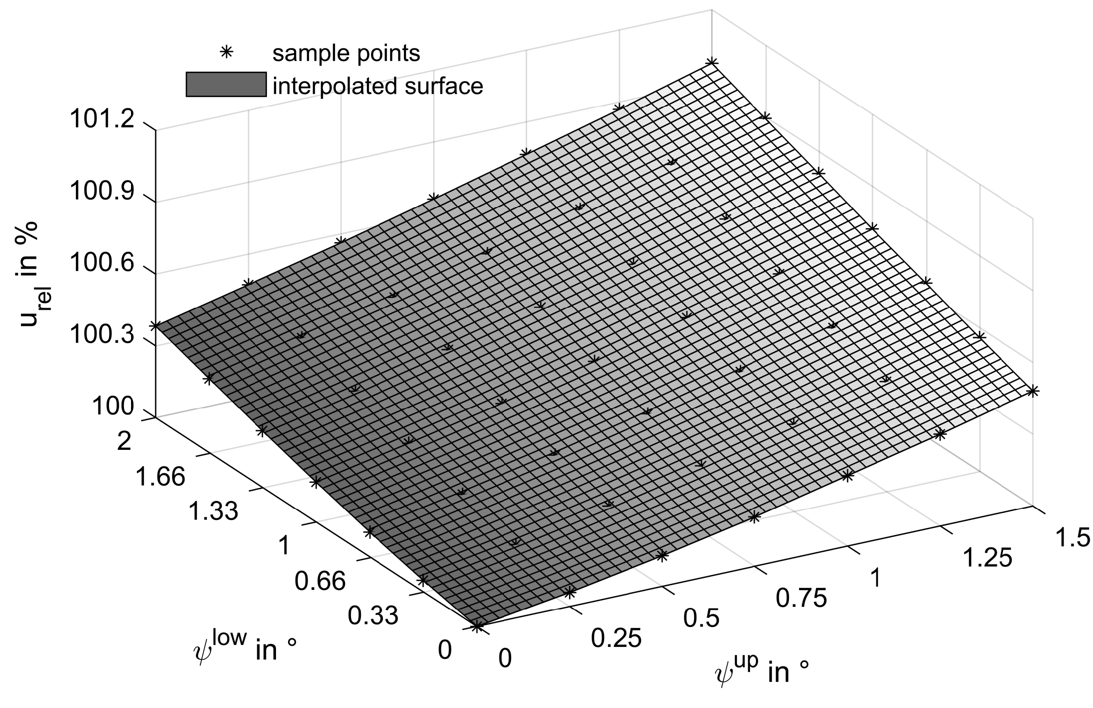

Figure 4.29.: Surface plot of the relative axial screw displacements u_{rel} dependent on the conicities ψ^{up} and ψ^{low} of the screw shaft in the case of good bone quality

The different influences of geometry parameters on the pull-out characteristics of the hybrid composite pedicle screw can also be shown by analysing the diameter D_{core} of the uCF-PEEK core together with the conical angles ψ^{up} and ψ^{low} of the upper and lower screw shaft. Figure 4.30 shows two surfaces. Each surface corresponds to one specific value of the diameter of the screw core. The lower surface shows the relative axial screw displacement for a hybrid composite pedicle screw dependent on the conical shaft angles with a core diameter of 1.8 mm and the upper surface for a core diameter of 0.4 mm. The influence of the core diameter was significantly higher than the influence of the conical shaft angles because the levels of relative axial screw displacements of each surface are different.

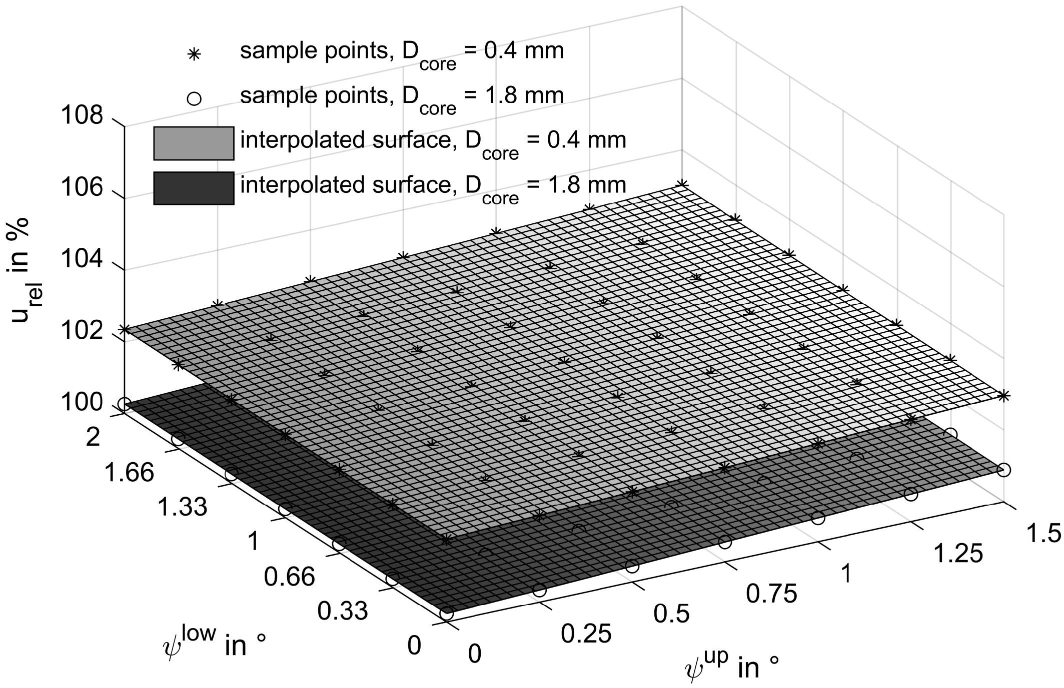

Figure 4.30.: Surface plot of the relative axial screw displacements u_{rel} dependent on the conicities ψ^{up} and ψ^{low} of the screw shaft and the diameter D_{core} of the screw core

The analyses presented before showed some examples of how the hybrid composite pedicle screw optimisation was conducted, the results were examined, and interpreted. In the same manner, the optimisation has been performed for the variables distal and proximal half angle κ_{dist} and κ_{prox}, the inner screw diameter D_i, and the upper and lower thread flank l^{up}_{flank} and l^{low}_{flank}. The corresponding figures A.2 and A.3 of the optimisation study for these variables are listed in appendix A.2. With these studies, the effect of different parameters on the pull-out behaviour of the hybrid composite pedicle screw could be identified. Based on the optimisation results, the recommendations, if either a high (↑) or a low value (↓) for the specific design variable should be used, are shown in table 4.12. Because screw stability was most critical shortly after surgery, the screw shaft and thread design have been optimised for this worst-case scenario (frictionless contact).

Increasing the screw core diameter can increase interface strength because the interface is established over a bigger area. In addition to that, lower shear stresses will

Table 4.12.: Recommendations for screw design variables

	Variable	Parameter range	Design recommendation
Primary effects	D_i	3.2 mm to 5.0 mm	↑
	D_{core}	0.4 mm to 2.5 mm	↑
Secondary effects	κ_{dist}	5° to 35°	↑
	κ_{prox}	0° to 10°	↓
	r_{dist}	0.1 mm to 1.2 mm	↓
	r_{prox}	0.1 mm to 0.4 mm	↑
	l_{flank}^{up}	0.05 mm to 0.4 mm	↑
	l_{flank}^{low}	0.05 mm to 0.4 mm	↑
	ψ^{up}	0° to 1.5°	↓
	ψ^{low} a)	0° to 2°	↓

a) lower conical angle becomes more important with healthier/younger bone (cf. chapter 4.3.3.3)

develop at the interface if the pedicle screw is subjected to bending or torsional forces. With the specific parameter ranges listed in table 4.12, the difference between the best and the worst screw design in terms of pull-out resistance was approximately 11.91 %. Each parameter optimisation only contributed to a small improvement of screw stability. However, the sum of the contributions of all parameters led to a significant improvement of screw stability.

Figure 4.31 shows two hybrid composite screws. The screw at the top was designed according to the design recommendations so that a high resistance against pull-out forces was achieved. A cylindrical screw shaft was used for its design because the highest resistance against pull-out could be obtained with this shaft design (cf. chapter 4.3.3.3). However, differences in pull-out resistance between screws with conical and cylindrical shafts were low. The screw at the bottom shows a poor resistance against screw pull-out. As mentioned before, these composite screw designs are based on the assumptions of linear elastic material properties of screw and bone, a simplified bone geometry, and simplified bone characteristics, e. g. no bone resorption or bone compaction. Conical screws will compact spongious bone if pre-holes are sufficiently small [108]. However, due to a reduced torsional stiffness of hybrid composite pedicle screws (cf. chapter 4.6.6), pre-holes have to be sufficiently large to insert these screws without damage. Therefore, the effect of bone compaction was supposed to be insignificant and was not considered for this study. For the final hybrid composite screw design, manufacturing requirements and bone characteristics have to be taken into account.

For a first consistency check, a 3D90 design study was performed. Qualitatively, the same behaviour as in the 2D case was observed. For a second consistency check, a

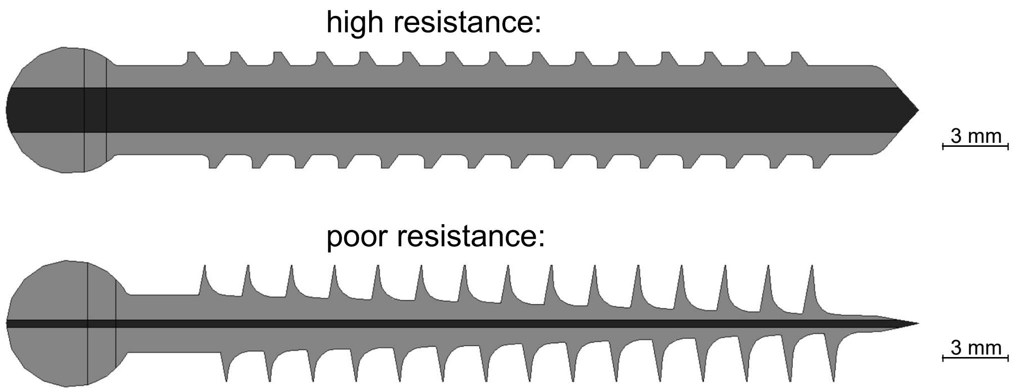

Figure 4.31.: Theoretical screw designs (assumptions applied) with a high (top) and poor resistance against pull-out forces (bottom)

tie constraint was used to describe the interaction between screw and bone instead of the description with a frictionless contact. The design recommendations still counted for this case. However, the influence of the uCF-PEEK core diameter and the proximal half angle on the pull-out characteristics were of less significance.

The stability of hybrid composite pedicle screws subjected to pull-out loads has been improved by this design optimisation. Enhanced screw stability may contribute to less failure of the CPSS. The stiffness of the screw may further be increased by optimising the adhesion between the uCF-PEEK core and the sCF-PEEK material. Certainly, the manufacturing technique and the requirements of the manufacturing process of the screw (cf. chapter 4.1) limit the design space and the feasible parameter range. Concluding, the parametric optimisation results in recommendations, which have to be checked, up to which limit they can be realised for the manufacturing of the hybrid composite pedicle screw.

4.4 Design

A simple substitution of the materials of already existing products by FRP does not typically lead to the fulfilment of the requirements. Different material properties have to be considered to achieve an ideal product design with sufficient structural mechanical properties. In this work, the design of metallic pedicle screw systems was not simply substituted but thoroughly adapted so that the combination of the sCF-PEEK and uCF-PEEK material was used in an ideal way. In addition to that, a new concept for the CPSS was developed. The new system consisted of several parts (cf. figure 4.32): a screw (a), a tulip (b), an upper clamp ring (c), a lower clamp ring (d), and a bridging rod (e). The bridging rod was a purchased part. For all other components, a design was realised which optimally considered the mechanical properties of TPCs.

Pedicle screw systems are used to stabilise at least two adjacent vertebrae. A one-level

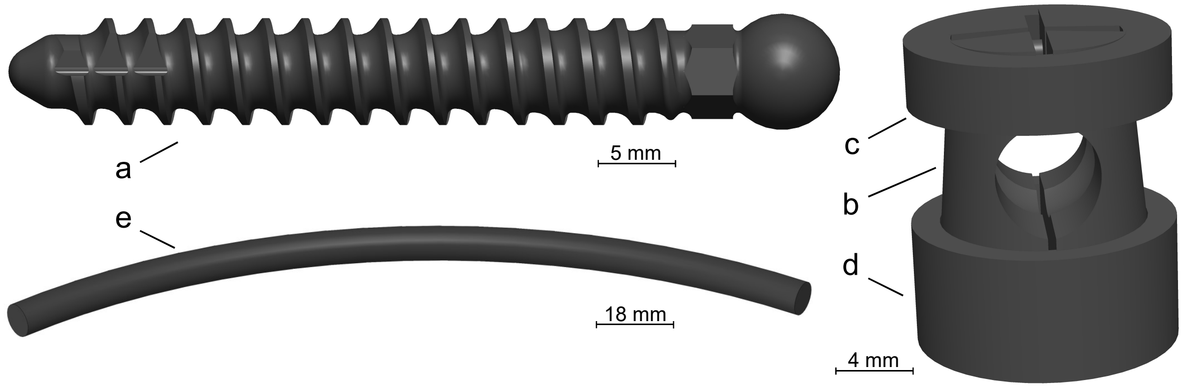

Figure 4.32.: Components of the CPSS

fixation system is used for such a fixation, and is focused in this work, as described in chapter 2.2. To ease the installation of the CPSS, and to reduce handling efforts of the surgeon and his assistants during surgery, the system can be pre-assembled by the manufacturer or by the assistants prior to surgery. For easier installation, a special holding device was designed to hold the CPSS components in the correct pre-assembly position. Consequently, the surgeon only has to perform the final assembly steps so that the effort for installation is comparable to metallic pedicle screw systems. Due to limited scope of this work, a focus is laid on the final design of the CPSS components and neither on the development process itself nor on the developed instrumentations needed for system installation. During the research process, several design refinements were realised especially for screw, tulip, and clamp rings.

4.4.1 Pedicle screw

Some important dimensions of the hybrid composite pedicle screw were defined in the specifications (cf. chapter 4.1). A master screw was specified with certain pre-defined dimensions. In the beginning of the design process, standard titanium pedicle screws were examined to gain information about commonly used shaft lengths and tip angles. The length of the shaft of the hybrid composite pedicle screw was fixed with 45 mm from the top of the hexagon to the screw tip. The tip of the hybrid composite pedicle screw had an angle of approximately 60° and was rounded with a radius of 1.5 mm. The optimisation results of chapter 4.3.4 were used to further specify the hybrid composite pedicle screw design. Several recommendations for the screw design were summed up in table 4.12. As mentioned before, each variable had to be checked, up to which limit the recommendations could be realised in order to successfully mould the screw. For example, under the consideration of manufacturing requirements, undercuts had to be avoided in the hybrid composite screw design to enable demoulding. As a consequence, the smallest feasible proximal half angle was 10°.

A *double shafted screw* with 16 threads was finally developed (cf. figure 4.32, component a) to account for both the design of completely cylindrical screws with the highest pull-out resistance (cf. chapter 4.3.3.3), and the characteristics and properties of human bone which were simplified for simulation. The outer diameter of the screw is constant. The upper screw shaft, which is located in the cortical bone region, shows a slightly bigger inner diameter than the lower shaft. Both shaft parts were designed cylindrically. In between, there is a small transition zone in which the inner diameter decreases from the value of the inner diameter of the upper shaft to the value of the inner diameter of the lower shaft. The transition between upper and lower screw shaft takes place after thread number four, counted from the screw head. The length from first to fourth thread is about 9.6 mm which approximately corresponds to the length of the cortical bone cylinder of the pedicle of an adult[10]. The inner screw diameter is bigger in the upper screw part than in the lower part to improve screw strength because most of the forces are transferred in the upper screw part which is in contact with cortical bone. Not only the inner screw diameter but also the thread flanks are bigger in the upper than in the lower part to improve their resistance against existing forces. As described in chapter 2.1, sufficient pedicle screw stability can only be achieved by osseointegration. Therefore, increasing the surface of the hybrid composite screw by a smaller lower shaft diameter is beneficial because functional connections to the screw can be built over a bigger surface area providing that osseointegration is feasible, e. g. due to a titanium coating. Additionally, the load can be transferred from the lower threads to a bigger volume of spongious bone. Therefore, the risk of local spongious bone shear fracture can be decreased.

Typically, a small set screw is used for common metallic pedicle screw systems to fix the bridging rod to the screw and the tulip. Furthermore, these screws have a small recess between the screw head and the first thread to account for the required rotational DOFs of the tulip. However, this recess promotes failure of metallic screws in this region (*weak neck*). In contrast, the required DOFs of the tulip could be realised without recess between screw head and shaft for the CPSS. Thus, the hybrid composite pedicle screw design does not show a weak neck so that the risk of screw neck failure is reduced.

A cutting edge was realised in the lower part of the screw thread so that the screw can actively cut the thread into bone during insertion. By this feature, friction forces are reduced, and the insertion of the hybrid composite pedicle screw into bone is eased. For many metallic pedicle screw systems, the instrumentation connection is realised on the screw head. However, for the CPSS, it is beneficial to have as much contact area as possible between the tulip and the spherical head of the hybrid composite

[10]information provided by surgeons in contact

pedicle screw. Therefore, the instrumentation connection of the screw was realised underneath its spherical head. As a consequence, friction forces needed for system fixation could develop over a bigger area. A hexagon connection between screw and instrument was realised to enable screw insertion into bone. The strength of the screw neck was increased by the design of the hexagon because additional material was used in the upper part of the screw which is subjected to high forces.

Conversations with surgeons in contact have confirmed that the variety of available implants is huge and there are already lots of different special tools for implantation on the market. If pedicle screw systems have to be removed, surgeons will not always know prior to surgery which kind of system is implanted. Thus, if the implant can only be removed by a special tool, which is not on hand, surgery will be complicated and operation times will increase. Considering this aspect, the instrumentation connection of the CPSS was realised by an ordinary hexagon so that no special tools are required to insert or remove the hybrid composite pedicle screw.

4.4.2 Tulip

The main functions of the tulip were analysed in the beginning of the design phase:

- enable the fixation of the screw
- enable the fixation of the bridging rod
- ease the installation of the pedicle screw system by rotational DOFs of the tulip in relation to the pedicle screw

On this basis, different conceptual tulip designs were developed. For the two fixations of bridging rod with tulip and screw with tulip, three different possibilities were considered: fixation by a snap connection, by a screw or a nut, or by a cable strap or a clamp ring. The combination of these fixation possibilities resulted in a number of new concepts which were evaluated. Different criteria, such as achievable fixation forces, assembly and disassembly difficulty, or long-term stability, were defined to converge to a final concept. Due to limited scope, only the final concept is presented in the following.

A sphere joint connects the tulip with the screw to account for the required DOFs of the system and to ease its installation (cf. chapter 4.4). This joint enables the tulip to rotate for some degrees relatively to the screw to ease system installation. As a consequence, the difficulty of bridging the pedicle screws by the rod is reduced so that correct system alignment in the human body can be achieved faster.

The height of the tulip of the CPSS was kept as small as possible to ensure that the system anatomically fits and does not negatively influence the patient's well-being. The tulip consists of two identical halves (cf. figure 4.32, component b). Therefore, only one injection moulding tool was required so that the tool costs could be reduced. Each tulip half has a small pin at the upper right inner vertical face. It fits into the corresponding hole of the counterpart to ease the positioning between the two tulip halves. The tulip consists of two conical faces: one in the upper and one in the lower part. Special clamp rings (cf. chapter 4.4.3) are pushed over these faces to fix the system. To allow some deformity during fixation, several cuts were realised in the tulip design.

4.4.3 Locking mechanism

As mentioned in chapter 2.2, set screws or nuts are typically used to restrict the DOFs of metallic pedicle screw systems. However, these fixations are inappropriate for the long-term fixation of composite pedicle screw systems. Therefore, the fixation of the CPSS was achieved by pushing two clamp rings (cf. figure 4.32, components c and d) into their final position. The fixation is based on friction and clamping forces. The outer dimensions of the rings were kept as small as possible because space is limited close to the pedicle. The final inner clamp ring diameters and conicities were determined by FE simulations and assembly trials during which the required forces for system fixation were recorded.

4.4.4 Bridging rod

The bridging rod was bought from the manufacturer *Invibio Ltd.* as a semi-finished product so that only little information is of interest here. Bridging rods out of PEEK or CF-PEEK should be used for the CPSS to prevent artefacts and to reduce stress shielding. Both straight and bended bridging rods (cf. figure 4.32, component e) can be used with the CPSS.

4.5 Manufacturing

The manufacturing of most parts of the CPSS was realised by injection moulding. The horizontal injection moulding machine *Babyplast type 6/10 PT* was used for the manufacturing of the injection moulded CPSS components. During the injection moulding process, the material should not remain too long in the cylinder of the injection moulding machine to prevent degradation.

In this chapter, information is mainly provided about the manufacturing of the hybrid composite pedicle screw and the clamp rings. The tulip halves were manufactured with a standard injection moulding process which was based on the typical requirements concerning the injection moulding of high temperature resistant TPC materials. The bridging rod was a semi-finished part bought from the manufacturer.

4.5.1 Pedicle screw

The manufacturing of the hybrid composite pedicle screw was based on the overmoulding of the uCF-PEEK rod inserts with sCF-PEEK material. The sCF-PEEK material was dried for at least three hours at 150 ℃ prior to overmoulding. The overmoulding procedure of the hybrid composite pedicle screws was similar to the one used for the manufacturing of the cylinder pull-out specimens. The gained experience and know-how during the overmoulding and testing of the compression shear, SLS, and cylinder pull-out specimens (cf. chapter 4.2.8) were required for a fast and successful start of production of the hybrid composite pedicle screws. For the manufacturing of the hybrid composite screw, straight uCF-PEEK rods were bought from the manufacturer *Invibio Ltd.* They were cut into pieces of approximately 74 mm length. The uCF-PEEK rod diameter of 2.5 mm needed to be within the tolerance range of approximately ± 0.1 mm so that the rod could be properly fixed in the injection moulding machine. Trials have shown that the roughness of the insert surface had to be sufficiently smooth in order to completely fill the screw cavity. On the one hand a certain minimum insert length had to be ensured to realise an appropriate fixation in the injection moulding machine. On the other hand the length should not be longer than needed due to limited stock, material cost, and material savings. The mould temperature was 200 ℃, and the temperature of the molten mass was approximately 400 ℃. Like for the manufacturing of the cylinder pull-out specimens, the chosen temperature of the molten mass was high to promote cohesive interface formation, although the risk of material degradation of the molten mass increased. The inserts were cleaned with isopropanol before overmoulding and were heated up to their target temperature in the oven *Heraeus RL 200*. Trials have shown that with this type of oven the target temperature was close to the actual temperature of the insert after at least six minutes. The inserts were handled with care due to reduced structural mechanical properties at this temperature (cf. chapter 4.2.5). The inserts were rapidly transferred to the injection moulding machine in a manual process, and the overmoulding with sCF-PEEK was performed. During transfer, careful handling of the hot inserts was required. As a result of the study of the cooling characteristics described in chapter 4.2.6, a heated metal cask was used for the transport of the inserts to decrease the influence of forced convection so that the cooling of the specimens was decreased. Between opening of the oven and start of injection approximately five seconds elapsed. This time was sufficient to prevent the inserts from critical cooling (cf. chapter 4.2.6) so that an insert pre-heating temperature of at least 260 ℃ was ensured prior to overmoulding. For the fixation of the inserts in the injection moulding machine, two small metal parts with centred holes were used through which the heated inserts were pushed. These fixation jigs prevented the uCF-PEEK rod insert from being pushed out of place during injection. For the hybrid composite pedicle screw production, the main flow direction of the molten mass was aligned with the longitudinal axis of the screw. In addition to that, the injection was next to one fixation jig. By these considerations, forces on the insert, which could lead to insert curvature, were alleviated. After overmoulding, ejector pins demoulded the hybrid composite pedicle screw. The upper end of the uCF-PEEK core was cut at the surface of the screw head, and the screw tip was ground to its final shape. Furthermore, sprue and runner were cut off.

The CF alignment of the hybrid composite screw as a result of the manufacturing process can be seen on an X-ray microscope scan. For this study, the 3D X-ray microscope *Zeiss Xradia 520 Versa* was used. Figure 4.33 illustrates one cut view through the screw centre in which the uCF-PEEK core can clearly be distinguished from the sCF-PEEK overmould material.

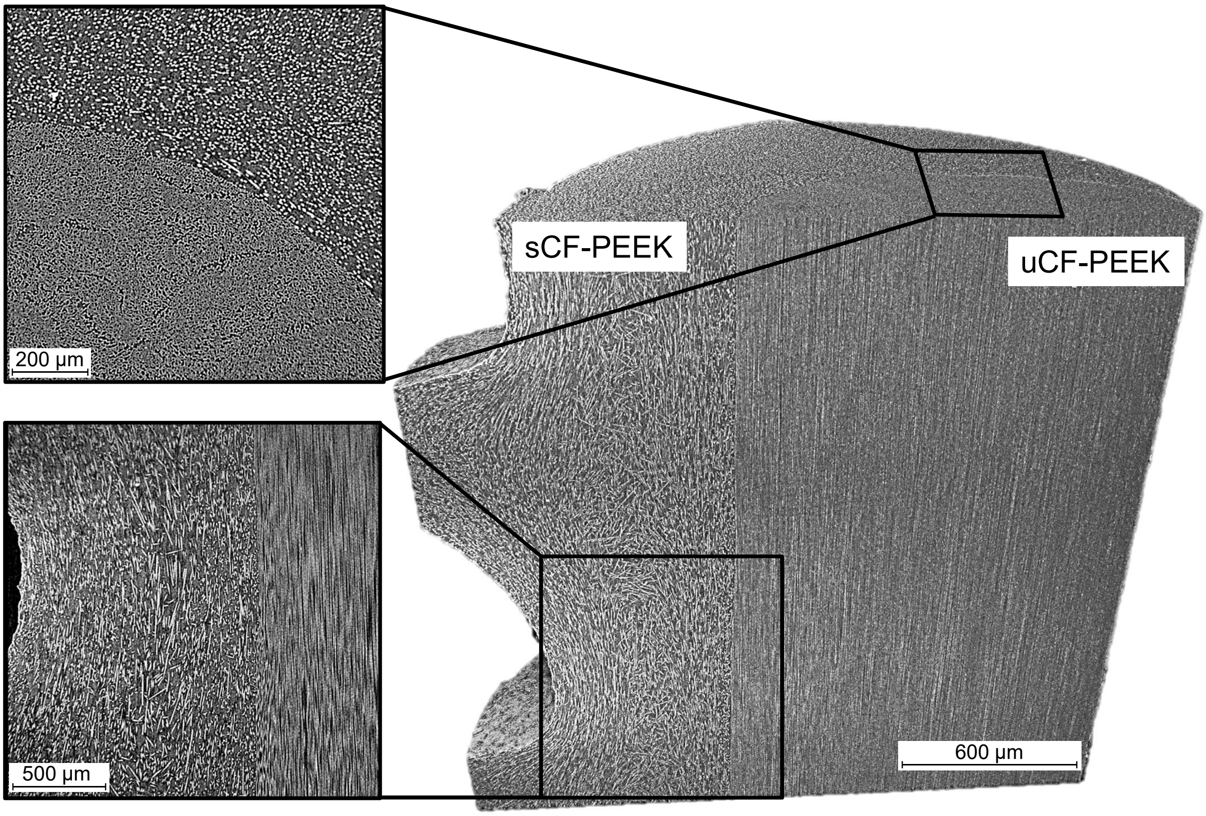

Figure 4.33.: X-ray microscope scan of the fibre orientation of the hybrid composite pedicle screw

The interface of the hybrid composite pedicle screw was further examined by a light-optical microscope (LM). Polished sections were prepared for different screw regions. Figure 4.34 shows examples of the interface between the sCF-PEEK overmould and the uCF-PEEK core.

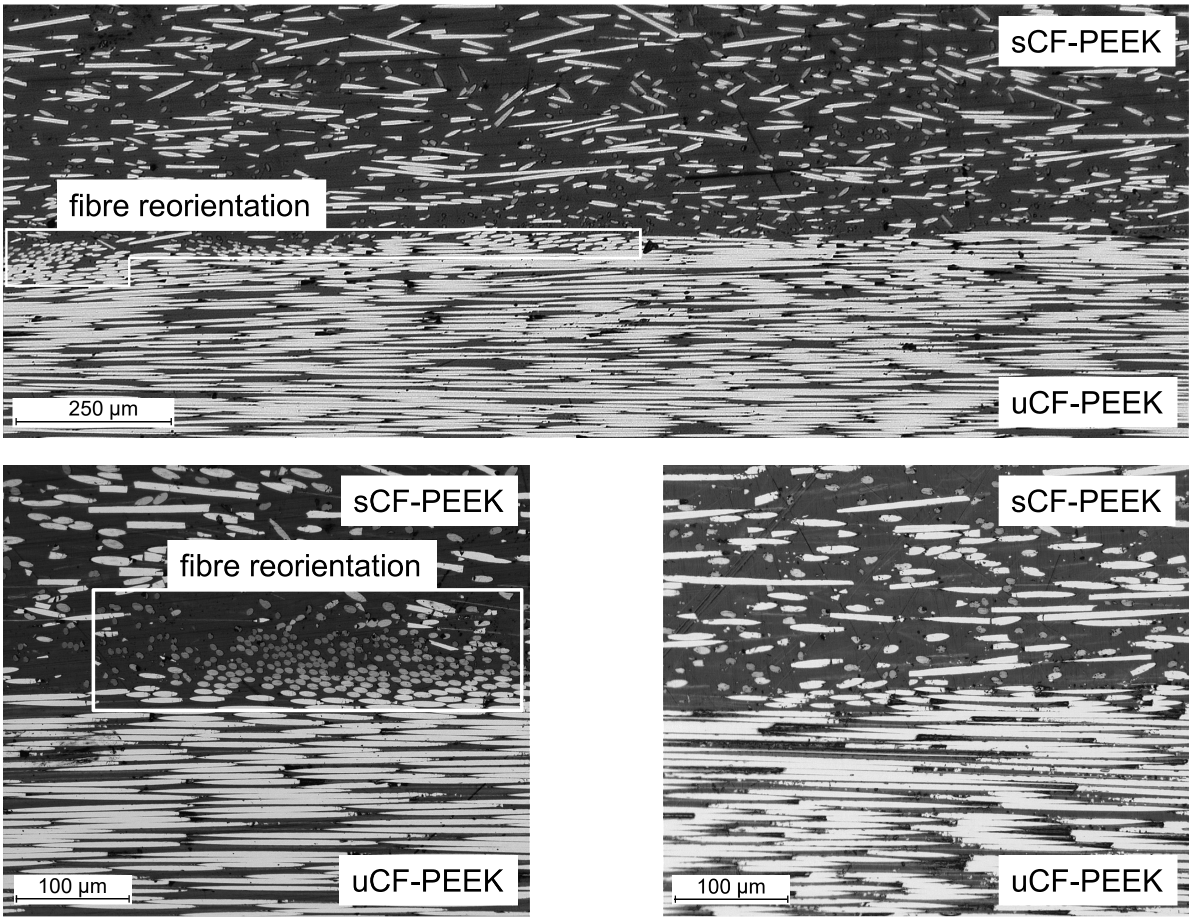

Figure 4.34.: LM images of micrographs of the hybrid composite pedicle screw interface

A clear distinction between the two materials close to the interface is difficult which already indicates the formation of a cohesive interface. A reorientation of CFs at the surface of the uCF-PEEK rod is shown in the upper micrograph on the left. This phenomenon is shown with a smaller scale in the lower left micrograph. Prior to overmoulding, the uCF-PEEK inserts were turned to their final diameter. During this turning process, unidirectional endless CFs located at the surface were cut. Fibre reorientation will only be possible if the matrix at the insert surface is in a molten state. It can occur in the instant when the molten sCF-PEEK mass fills the cavity of the mould and contacts the molten uCF-PEEK rod insert surface at which cut unidirectional CFs are present. Here, fibre reorientation only occurs in a narrow region so that it does not significantly influence the structural mechanical properties of the insert. These findings are evidences for the successful formation of a cohesive interface for the hybrid composite pedicle screw, similar to the SLS and cylinder pull-out specimens. Violating the requirements for achieving a cohesive interface led to the formation of a weak interface. Figure 4.35 illustrates a gap between the sCF-PEEK and uCF-PEEK rod material due to poor overmoulding. In this case, the difference between the interface temperature and the melting temperature of the insert was not sufficiently low (cf. figure 4.11).

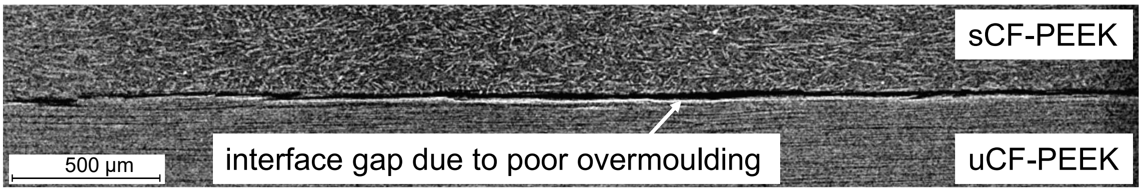

Figure 4.35.: X-ray microscope scan of an interface gap due to poor overmoulding

Not only the creation of a strong interface between core and overmould is crucial for the structural mechanical properties of the hybrid composite pedicle screw, but also the fibre orientation along the thread. The fibre orientation is mainly a result of mould design and process parameters. The hybrid composite pedicle screw thread was analysed by the 3D X-ray microscope *Zeiss Xradia 520 Versa* (cf. figure 4.36). The illustrated region of interest is taken from a thread in the centre of the screw. The fibres close to the thread roots are oriented parallel to the plane of view. The sCF orientation around the outer thread region is in good accordance with the theoretical load paths which can develop in the screw under pull-out loading conditions. The numerical stress and strain analysis of chapter 4.3.3.2 highlights that high stresses are located at the thread roots in the pull-out loading case. As can be seen in figure 4.36, the fibre orientation at the thread roots is advantageous to transfer stress, and to improve the strength of the screw in this area.

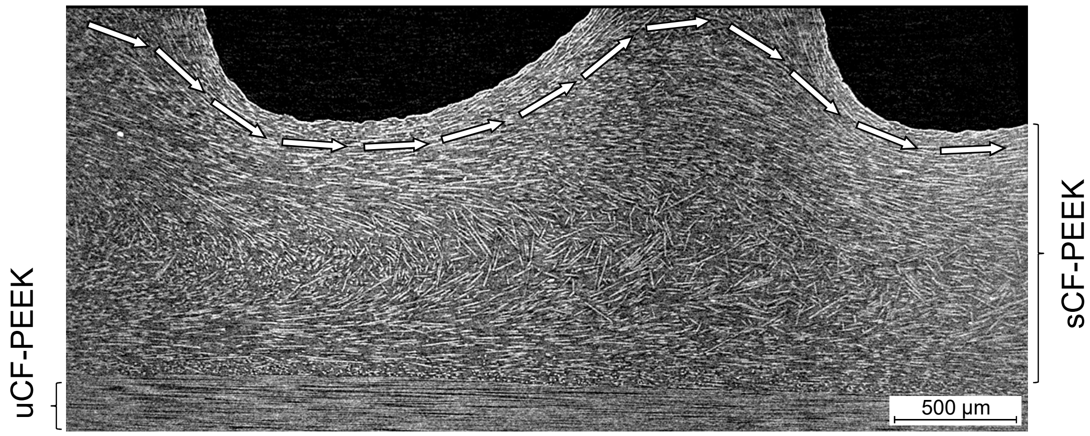

Figure 4.36.: X-ray microscope scan of the hybrid composite pedicle screw thread

4.5.2 Locking mechanism

The clamp rings have to resist the forces which develop during their lateral movement over the conical tulip faces to fix the system. The rings are required to maintain their dimensions during service life so that system failure is prevented. Therefore, a winding process was chosen for the manufacturing of the clamp rings to achieve the required high structural mechanical properties in circumferential direction. The rings were produced with the endless uCF-PEEK tape *Sulzer Suprem*™ with a fibre volume fraction of 60 vol.-%. The tape was heated and wound under tension onto a mandrel with a diameter of 8 mm. The wound CF-PEEK tube was cut into small rings which were turned to their final shape. In general, the dimensions of the upper and lower clamp ring were different. Not only the outer but also the inner conical shape of the rings was machined. The outer diameter of the tube was slightly bigger than the final outer diameter of the clamp rings. Care had to be taken during machining and during the removal of burrs to avoid any delamination. Afterwards, the rings were cleaned with isopropanol. The relevant data of the winding process is listed in table 4.13.

Table 4.13.: Parameters of the manufacturing process of wound clamp rings

Tape width	5 mm
Tape thickness	0.25 mm
Yarn tension	15 N to 20 N
Core temperature before winding	200 °C
Tape width at deposition	8 mm
Feed	8 mm
Winding speed	5 m/min to 10 m/min

4.6 Testing

Different biomechanical and visibility tests were performed to study the properties of the hybrid composite pedicle screw, to prepare the process of certification, and for validation. The biomechanical tests described in the following are standardised and are based on one-axial loads. However, a complex loading of pedicle screws is present in real situations [114]. Nevertheless, biomechanical tests are useful to compare results, and to estimate the performance of implants and implant components in real situations. Tests were conducted at room temperature because the influence of body temperature on testing results is insignificant (cf. chapter 4.2.5).

4.6.1 Quasi-static pull-out test

The quasi-static pull-out test was conducted in accordance with ASTM F 543 [208] to evaluate the stability of hybrid composite pedicle screws and to validate the FE analysis. Pull-out tests are highly sensitive to screw design variations [97]. The maximum achievable pull-out force is an indicator of pedicle screw fixation strength [102, 107]. However, pure pull-out forces are unlikely to be seen in vivo [97, 107]. Typically, they are superposed with other forces and moments which act on the implant in vivo

[97, 122]. In this study, BRM blocks from *Sawbones* were used for the pull-out tests. These rigid PUR foams are commonly used for biomechanical tests for orthopaedic devices and instruments, and are standardised in ASTM F 1839 [126].

The pull-out tests were conducted on a *Hydropuls Längszylinder PL 10 kN* from *Instron Structural Testing Systems GmbH*. The testing speed was 1 mm/min. A specific testing device was designed and manufactured for the pull-out tests. Several clamps and supports were used to sufficiently fix the BRM to the testing machine. The upper clamps, which prevented the BRM block from moving in the loading direction, were fixed with four hexagon socket screws. For the pull-out tests, four different BRM grades were used to simulate different bone properties. Lower BRM grades represent poor bone properties, e. g. of osteoporotic bone. The properties of the used BRM grades are summarised in table 4.14.

Table 4.14.: Properties of solid rigid PUR foams [209]

Grade	Density in g/cm^3	Compression strength in MPa	Compression modulus in MPa	Tensile strenght in MPa	Tensile modulus in MPa	Shear strength in MPa	Shear modulus in MPa
15	0.24	4.9	123	3.7	173	2.8	33
25	0.40	12.9	317	8.8	399	5.9	68
30	0.48	18.0	445	12.0	592	7.6	87
40	0.64	31.0	759	19.0	1000	11.0	130

As mentioned in chapter 2.2.1, the BMD of the pedicle is typically in the range of (0.303 ± 0.076) g/cm^3 with a maximum of 0.42 g/cm^3 which is lower than the nominal density of BRM grade 30. This means that grade 40 is a BRM with an artificially high density.

The BRMs were cut in blocks with dimensions of 65 mm $\times$ 65 mm $\times$ 40 mm ($l \times w \times d$). A pre-hole was drilled into the centre of the BRM blocks. A separate study was conducted in which different pre-hole diameters were examined for composite pedicle screw insertion. In the case of high BRM densities, high friction forces will develop when the screw is inserted. Starting with a small drill, the drill size was increased until an appropriate pre-hole diameter was found to insert the screw without damaging it. As a result of this study, pre-holes with a diameter of 6.0 mm were used for BRM grade 25 and grade 30. In addition to that, a pre-hole with a diameter of 4.9 mm was used for the porous BRM grade 15 to ensure proper fixation. For grade 40, high friction forces required a pre-hole with a diameter of 6.2 mm. As mentioned before, the BMD of the pedicle is typically lower than the density of BRM grade 30 and 40. Thus, the friction forces were artificially high during insertion of the composite screw in the case of BRM grade 40. In reality, pre-hole size can be smaller dependent on the patient's bone characteristics. Besides, pre-hole size is also dependent on the evaluation and experience of the surgeon.

The entire thread of the hybrid composite pedicle screws was inserted with a 5 mm wrench for the pull-out test. It was ensured that the screw tip did not cross the backside of the BRM block. The test set-up for the quasi-static pull-out test is shown in figure 4.37.

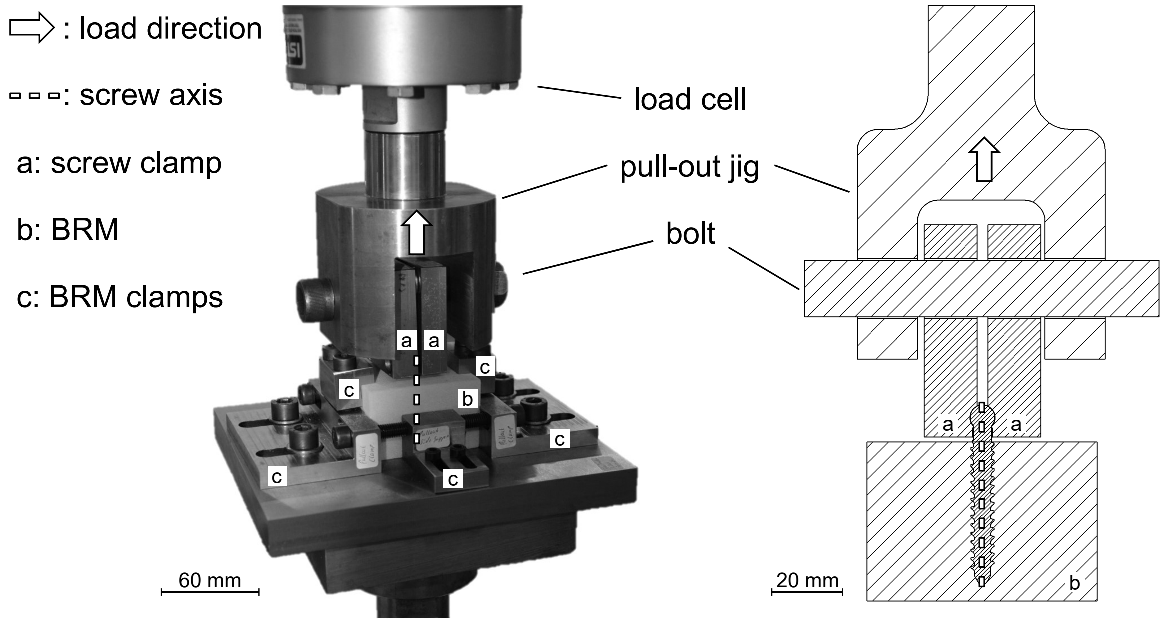

Figure 4.37.: Test set-up for quasi-static pull-out test

The pull-out test results of the hybrid composite pedicle screws for the BRM grades 15 (upper left), 25 (upper right), 30 (lower left) and 40 (lower right) can be seen in figure 4.38. For each BRM grade, five tests were conducted. To neglect the effect of running-in and the initial alignment of the testing jig, the force values are illustrated from 300 N onwards for all specimens.

As can be seen in figure 4.38, the pull-out behaviour of composite pedicle screws is quite different dependent on the BRM grade. The pull-out resistance significantly depends on the density of the BRM and the specific pre-hole diameter used for the test. The very porous grade 15 shows a mean maximum force value of (1.43 ± 0.08) kN at approximately 0.7 mm displacement. The force-displacement curves continuously declined to low force values after reaching their maximum. This means that for grade 15, screw stability was lost after reaching the maximum force peak at which failure of the BRM occurred. Concerning grade 25, the pull-out behaviour of the hybrid com-

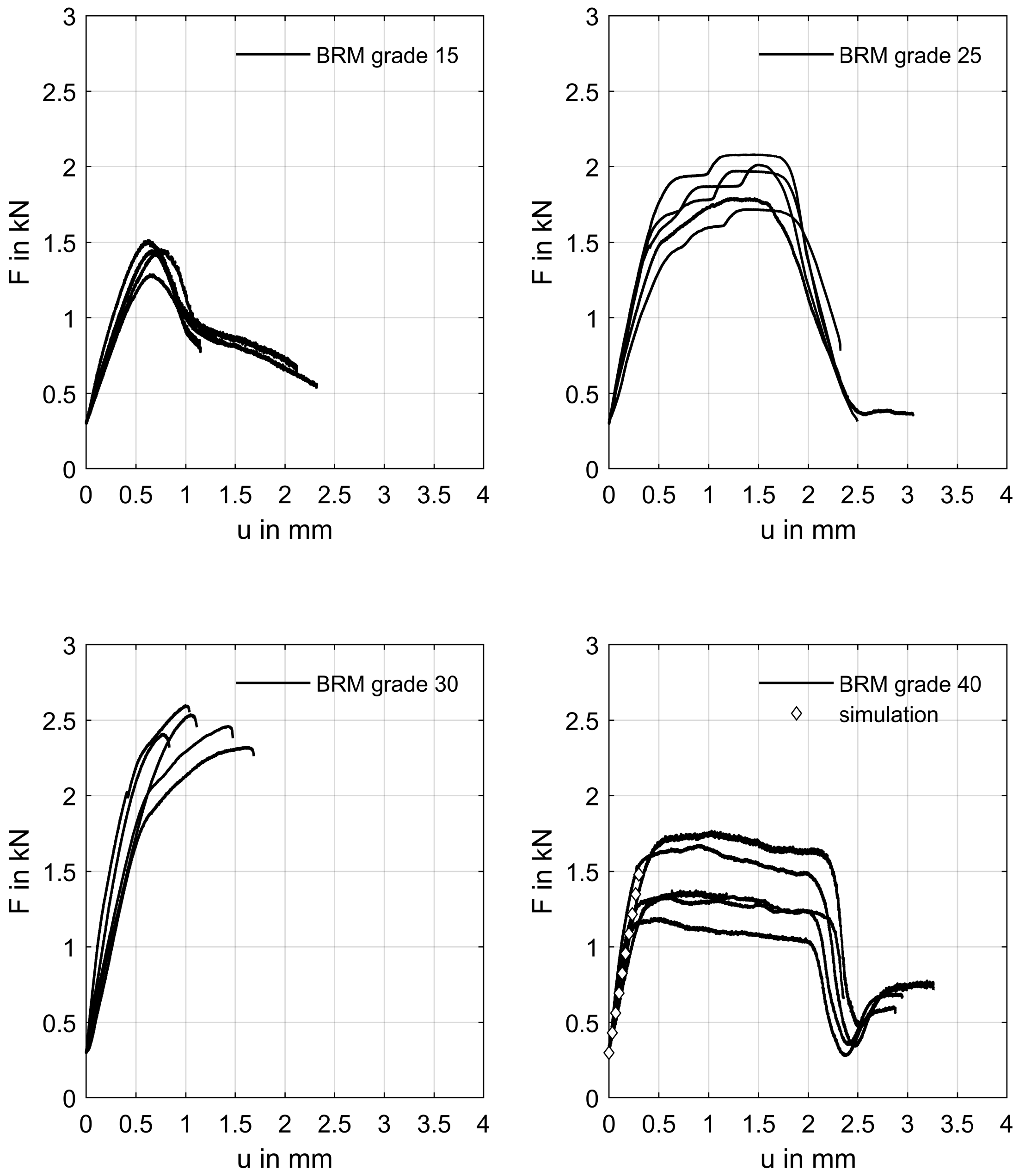

Figure 4.38.: Force-displacement diagrams for the quasi-static pull-out test of hybrid composite pedicle screws for BRM grade 15 (upper left), 25 (upper right), 30 (lower left), and 40 (lower right)

posite screws was different. In four out of five cases, the force continuously rose to a first plateau before it reached another plateau region and finally decreased. The BRM grade 25 maintained its strength for a longer time compared to grade 15 due to its increased structural mechanical properties (cf. table 4.14), but finally BRM failure was observed. The mean maximum pull-out force of the hybrid composite pedicle screws for BRM grade 25 was (1.91 ± 0.15) kN. The force values of grade 30 continuously rose up to their maximum. A sudden force drop was the result of pedicle screw failure. The pull-out strength of BRM grade 30 exceeded the hybrid composite pedicle screw strength in the area of the screw neck. The mean maximum force of BRM grade 30 was (2.47 ± 0.11) kN. Concerning BRM grade 40, the thread was in direct contact with the BRM in the beginning of the pull-out test. With increasing displacements, the pull-out force increased until the breakaway force was reached. At this force, the screw was pulled through the pre-hole with a relatively constant force due to friction. A reason for this behaviour lies in the bigger required pre-hole diameter of BRM grade 40 compared to the pre-hole diameters of the other BRM grades. The force level, which was highly dependent on the pre-hole quality and screw insertion, was constant over a broad pull-out displacement range until the displacements equalled approximately one thread pitch. Afterwards, the screw threads were pulled over the next initial screw thread location of the BRM. The region of the BRM which was initially in contact with the screw thread was subjected to friction forces during screw insertion and time dependent plastic deformation. As a consequence, a sudden force drop will be observed if the screw is pulled over the next thread indentation. After the screw thread is completely pulled over the indentation, the unaffected BRM region is in contact with the screw thread again, and a second increase in pull-out force values occurs. However, the initial force plateau was not reached anymore. For the BRM grade 40, the mean maximum pull-out force was approximately (1.47 ± 0.24) kN.

An FE model (3D90) was built up with the final hybrid composite pedicle screw design to compare the experimental to the numerical results (cf. chapter 4.3). For this comparison, a displacement pull-out load of 0.3 mm was applied to the screw neck. The bone was modelled linear elastic with the properties of BRM grade 40 (cf. table 4.14), but any other BRM grade could have been chosen for this comparison as well. The shear modulus was used as the bone stiffness for the numerical simulation because screw pull-out mainly results in shear stresses in the BRM. The resulting linear force-displacement curve corrected by the running-in force of 300 N is shown in figure 4.38 on the lower right. It can be seen that the numerical results fit well to the experimental data in the elastic region.

Summing up the pull-out test results, the pull-out characteristics of composite pedicle screws are highly dependent on the density of the BRM and the pre-hole diameter. The pedicle screw resistance against pull-out increased with increasing BRM density up to grade 30. Failure of the BRM was observed in the case of the porous BRM grades 15 and 25. As mentioned in chapter 2.2.1, expandable pedicle screws or cement augmentation can be used to improve screw stability in osteoporotic bone. Additionally, a smaller pre-hole diameter can contribute to a higher compaction of osteoporotic bone. Pull-out resistance was very high for BRM grade 30 so that screw neck failure was observed. The very dense BRM grade 40 required a big pre-hole diameter which led to screw pull-out without significant damage of the BRM. The screw was pulled through the pre-hole after reaching its breakaway force. These findings are supported by examining the pre-holes of the BRM blocks with different grades after the pull-out tests. Figure 4.39 shows that screw thread indentations of BRM grades 15 and 25 are barely visible due to the failure of BRM. In contrast, the thread indentations of BRM grade 30 can be clearly seen which means that there was no significant failure of BRM, and that screw stability was high. Due to the required big pre-hole diameter of the dense BRM grade 40, only small thread indentations are visible which supports that screw stability was poor in this case.

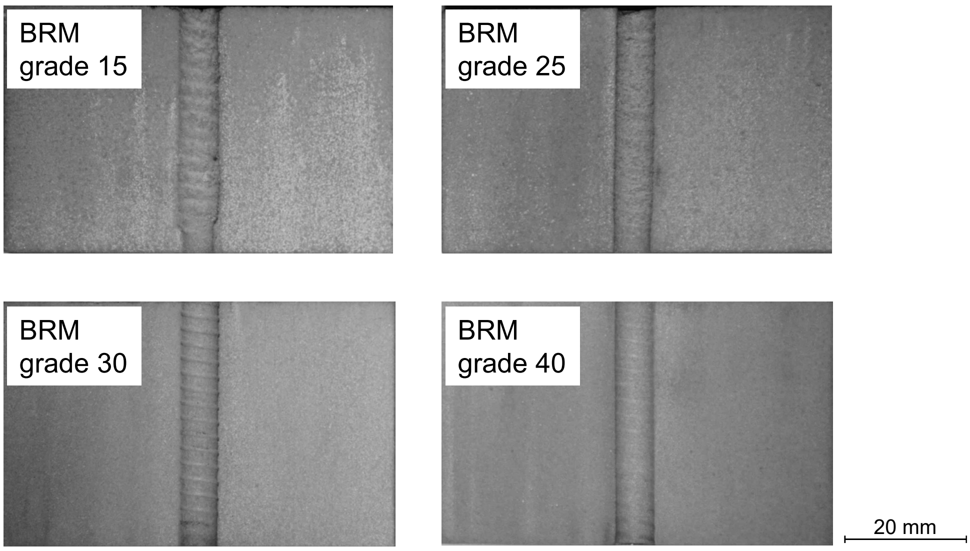

Figure 4.39.: BRM blocks grade 15 (upper left), grade 25 (upper right), grade 30 (lower left), and grade 40 (lower right) after pull-out test

4.6.2 Quasi-static bending test

The quasi-static bending test was conducted to evaluate the resistance of the hybrid composite pedicle screw against bending loads and to compare entirely discontinuous sCF-PEEK pedicle screws with hybrid composite pedicle screws. For this test, the screws were inserted in UHMWPE cylinders with lengths of 45 mm and outer diameters of 30.8 mm. As already described in chapter 4.6.1, a separate study was performed to define the smallest pre-hole diameter possible for the UHMWPE material. As a result, a pre-hole diameter of 5.4 mm was defined to enable composite pedicle screw insertion without the risk of screw damage. In accordance with the standard ASTM F 2193 [176], the screw was inserted with a 5 mm wrench from the tip to thread number five which corresponds to an insertion length of approximately 12 mm.

Five sCF-PEEK pedicle screws, five hybrid composite pedicle screws, five gamma radiation sterilised sCF-PEEK pedicle screws, and five conditioned sCF-PEEK pedicle screws (maximum level of liquid absorption, cf. chapter 4.2.2) were tested in bending to evaluate the improvement of bending properties due to the uCF-PEEK core and to determine potential differences in the mechanical behaviour due to sterilisation or conditioning. Concerning the conditioned screws, tests were conducted within one hour after taking the screws out of the basin with saline solution to prevent them from significant drying. For all tests, the load was introduced by a stainless steel cylinder with a diameter of 14 mm whose longitudinal axis was aligned perpendicular to the longitudinal axis of the pedicle screw. The distance between load introduction and screw tip was 5 mm so that the load introduction point was located at the half of the thread insertion length. The screw head was fixed to the testing jig with four hexagon socket screws. The length measured from the clamp of the screw head to the load introduction point was 31.4 mm. The quasi-static bending tests were conducted with a *Hydropuls Längszylinder PL 10 kN* from *Instron Structural Testing Systems GmbH*, and the testing speed was 3 mm/min. The test set-up for the quasi-static bending test is shown in figure 4.40.

The test results of the hybrid composite pedicle screws (upper left), the sCF-PEEK pedicle screws (upper right), the sterilised sCF-PEEK pedicle screws (lower left), and the conditioned sCF-PEEK pedicle screws (lower right) can be seen in figure 4.41. Five tests were performed for each screw configuration. With a length l of 31.4 mm measured from the clamp of the pedicle screw head to the load introduction point, the bending moment M was calculated by

$$M = F\,l \tag{4.24}$$

in which F symbolises the force values.

The hybrid composite pedicle screws show a higher resistance against bending than the entirely discontinuous sCF-PEEK pedicle screws. The mean maximum bending moment of the hybrid composite screws of (6.67 ± 0.36) Nm was approximately 48 % higher than the one of the sCF-PEEK screws which was (4.50 ± 0.16) Nm. This means

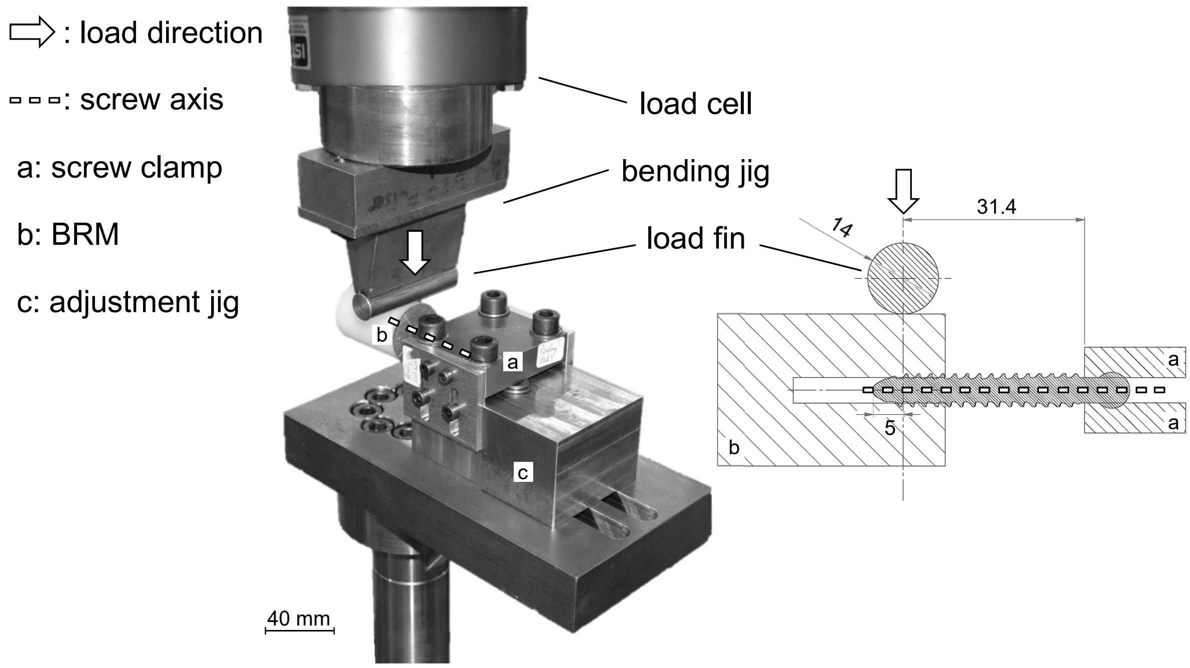

Figure 4.40.: Test set-up for quasi-static bending test

that the uCF-PEEK rod insert significantly contributes to a higher bending stiffness and bending strength of composite pedicle screws. The sterilised and conditioned sCF-PEEK pedicle screws show no significant difference in bending properties compared to standard sCF-PEEK pedicle screws. The mean maximum bending moments of the sterilised and conditioned sCF-PEEK pedicle screws were (4.16 ± 0.34) Nm and (4.55 ± 0.16) Nm. In addition to that, all tested composite pedicle screws showed no significant differences concerning their mean displacement at failure.

The quasi-static bending test results show that sterilisation by gamma radiation and liquid absorption do not significantly influence the bending properties of sCF-PEEK screws. The same behaviour can be assumed for hybrid composite pedicle screws. In addition to that, the bending properties were successfully improved by reinforcing the discontinuous CF reinforced pedicle screws with the uCF-PEEK rod inserts. For the hybrid composite screws, some bending strength was still present after first failure so that structural integrity could be maintained. These screws showed a gradual failure, and maintained their structural integrity for higher displacements which is important in the event of pedicle screw failure within the human body. This was not the case for sCF-PEEK pedicle screws. For sCF-PEEK screws, sudden and catastrophic failure led to a separation between screw head and shaft. Consequently, screw removal would also be complicated, because locating the composite screw parts within the human body is difficult.

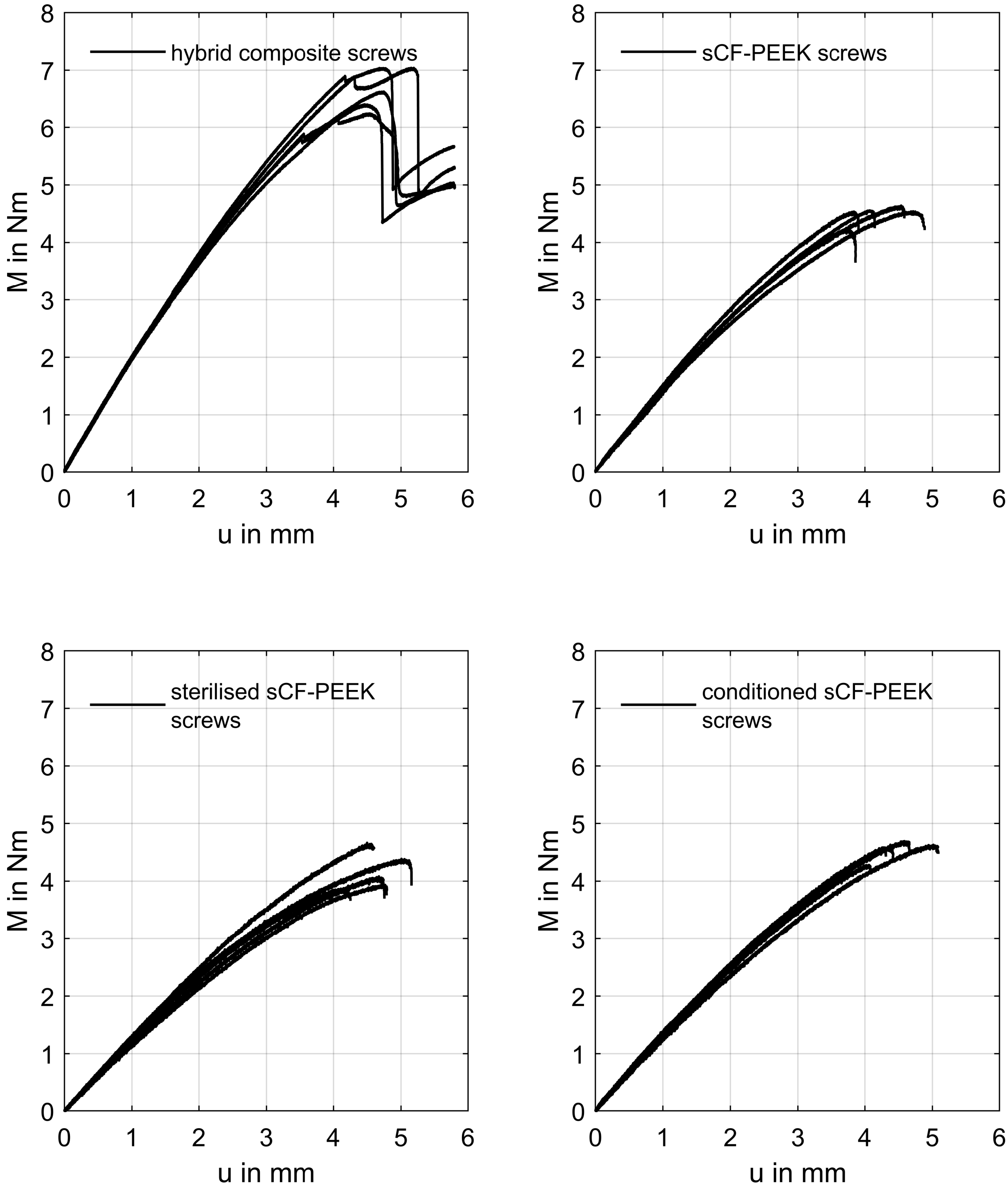

Figure 4.41.: Bending moment-displacement diagrams for the quasi-static bending test of hybrid composite pedicle screws (upper left), sCF-PEEK pedicle screws (upper right), sterilised sCF-PEEK pedicle screws (lower left), and conditioned sCF-PEEK pedicle screws (lower right)

4.6.3 Cyclic bending test

As mentioned in chapter 2.2.1, one to three million load cycles a year are acting on the human spine dependent on the individual level of activity [23, 42]. The aim of the cyclic bending test was to compare the fatigue behaviour between hybrid composite pedicle screws and sCF-PEEK pedicle screws.

The cyclic tests were conducted on a *Hydropuls Längszylinder PL 10 kN* from *Instron Structural Testing Systems GmbH* with a testing frequency of 5 Hz, an R-ratio of 0.1, and a maximum number of test cycles of 2.5 million which is in accordance with the standard ASTM F 2193 [176]. As for the quasi-static bending test, the screws were inserted in UHMWPE cylinders over a length of 12 mm. A diameter of 5.4 mm was used for the pre-holes of the UHMWPE cylinders. The test set-up of the quasi-static bending test shown in figure 4.40 was also used for the cyclic bending test. Rotation of the testing jig during the testing time was prevented.

The maximum loads for the hybrid composite pedicle screws were 50 N, 100 N and 150 N which corresponds to the load levels of approximately 23.5 %, 47.1 % and 70.6 % of their mean maximum force of the quasi-static bending test. The same load levels were used for testing the sCF-PEEK pedicle screws which resulted in maximum loads of 33.7 N, 67.4 N and 101.2 N. Additionally, cyclic bending tests with the maximum loads of the hybrid composite screws mentioned before were conducted for the sCF-PEEK pedicle screws.

Under the consideration of the load level of 70.6 % of the mean maximum force of the quasi-static bending test, screw failure below 31000 cycles was observed for the hybrid composite pedicle screws and below 22000 cycles for the sCF-PEEK pedicle screws. In addition to that, the maximum number of load cycles was reached for the medium (47.1 %) and the lowest (23.5 %) load level for both types of screws. Considering the case that the maximum loads of the hybrid composite screws were applied for the sCF-PEEK pedicle screws, 2.5 million cycles could only be reached for sCF-PEEK screws tested with the lowest load level. Figure 4.42 illustrates the number of cycles, which were reached for the hybrid composite pedicle screws and the sCF-PEEK pedicle screws, dependent on the load level. In the figure, only one data point is illustrated at 2.5 million cycles for each type of pedicle screw. These data points represent the highest loads for which 2.5 million cycles were reached. For the sCF-PEEK screw, the load levels of 100 N and 101.2 N and the corresponding numbers of cycles were merged for illustration.

The cyclic bending test shows that fatigue properties of discontinuous fibre reinforced TPC parts can be significantly improved by local unidirectional endless fibre reinforce-

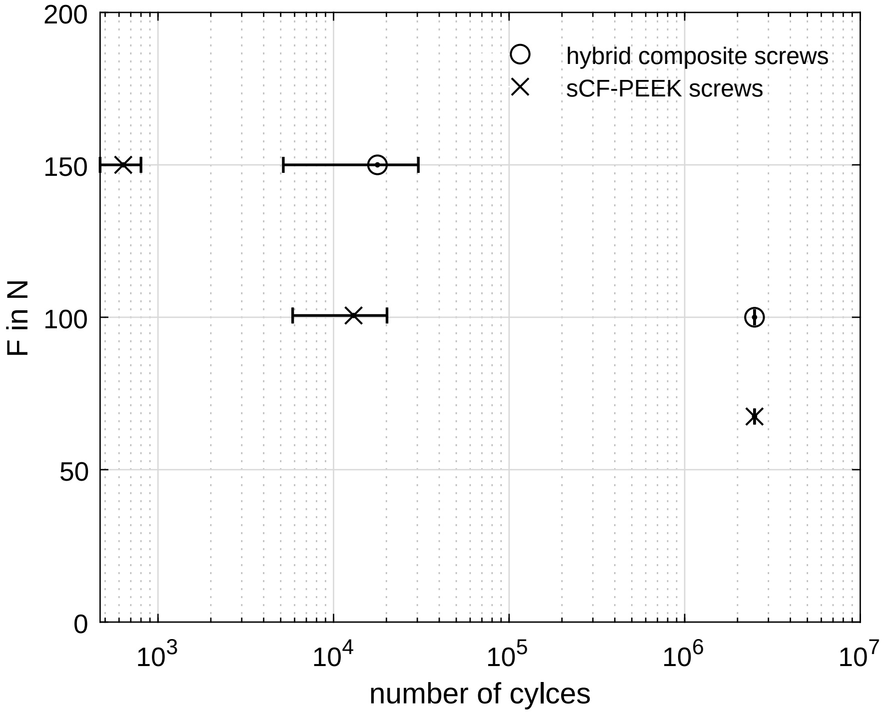

Figure 4.42.: Cyclic bending test results for hybrid composite and sCF-PEEK pedicle screws

ments.

4.6.4 Insertion torque test

PUR blocks grade 15, 25, 30, and 40 from *Sawbones* with dimensions of 40 mm $\times$ 40 mm $\times$ 40 mm ($l \times w \times d$) were used for the insertion torque tests in accordance with ASTM F 543 [208]. In a separate study, a pre-hole diameter of 6.2 mm was determined for grade 40, a diameter of 6.0 mm for grade 25 and 30, and a diameter of 4.9 mm for grade 15 (cf. chapter 4.6.1). The testing machine was an *ElectroForce® 3550* from *TA Instruments, Inc.* (former *Bose Corp.*). Due to a limited maximum number of machine turns, the insertion torque was studied for two rotation intervals:

1. From thread number three to thread number twelve in order to characterise the development of the insertion torque (initial insertion).
2. From thread number six to thread number 15.5 in order to quantify the maximum insertion torque (final insertion).

The composite pedicle screw has in total 16 threads as described in chapter 4.4.1.

For the insertion torque tests, the screw head was fixed in a testing jig so that the rotational DOFs of the pedicle screw were restricted. Minor translations of the pedicle screw were allowed to compensate differences in the alignment of screw and pre-hole axis. The BRM block was restricted in its rotational DOFs around the pre-hole axis by two counter bearings. The screw was inserted with a constant rotation speed of 30°/s, and no axial displacement of the machine was needed. The BRM block was lifted due to screw rotation and contact of the BRM block with the counter bearings. The test set-up of the insertion torque test is shown in figure 4.43. The same set-up was used for the removal torque test (cf. chapter 4.6.5).

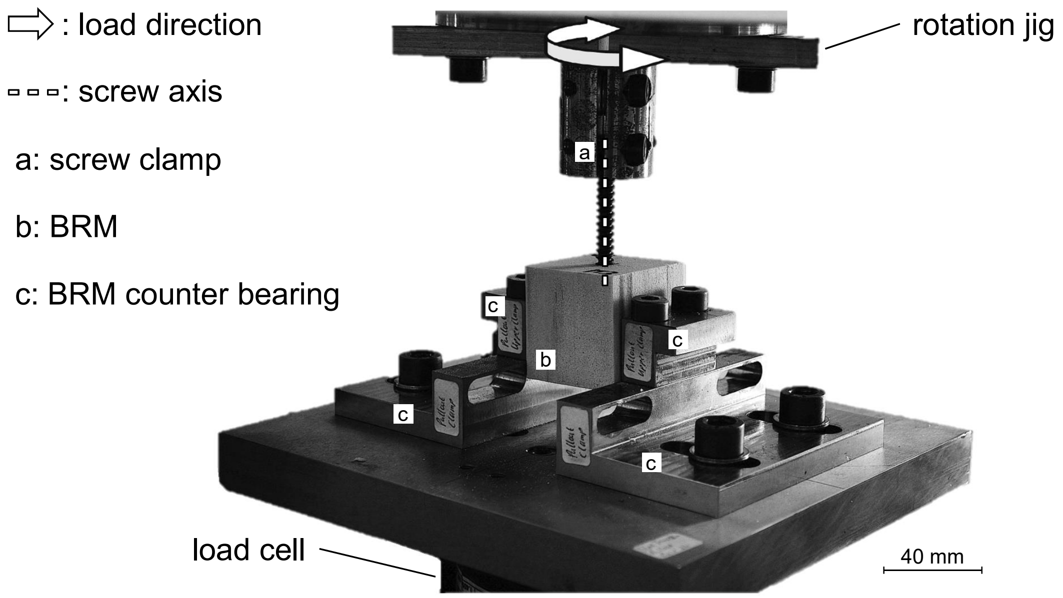

Figure 4.43.: Test set-up for insertion and removal torque test

For the initial insertion, the composite pedicle screws were manually inserted into the BRM blocks up to thread number three to ensure a stable position of the screw within the BRM prior to testing. The insertion torque was analysed during the insertion from thread number three to thread number twelve. In figure 4.44 on the left, the insertion torque M_{in} is plotted over the rotation rot. One representative curve is shown for each BRM grade. The first local maximum insertion torque values are marked with asterisks for each BRM grade.

After contact between BRM block and counter bearing and after reaching the first local insertion torque maxima, a general trend can be observed: torque values rise with increasing rotation. With linear approximations of the test curves, the slope would be smallest for BRM grade 15 and highest for BRM grade 30. The mean torques of the insertion from thread three to twelve were examined to compare different BRM grades concerning their initial insertion behaviour. They are shown in figure 4.45 on the upper left. The mean insertion torque is lowest for BRM grade 15 and highest for BRM grade 30. In between, a similar mean insertion torque is reached for BRM grade 25 and 40.

As mentioned before, a second test (final insertion) was conducted to quantify the maximum insertion torques. For this study, screws were manually inserted up to thread number six prior to testing. The testing machine performed 9.5 turns to insert nearly

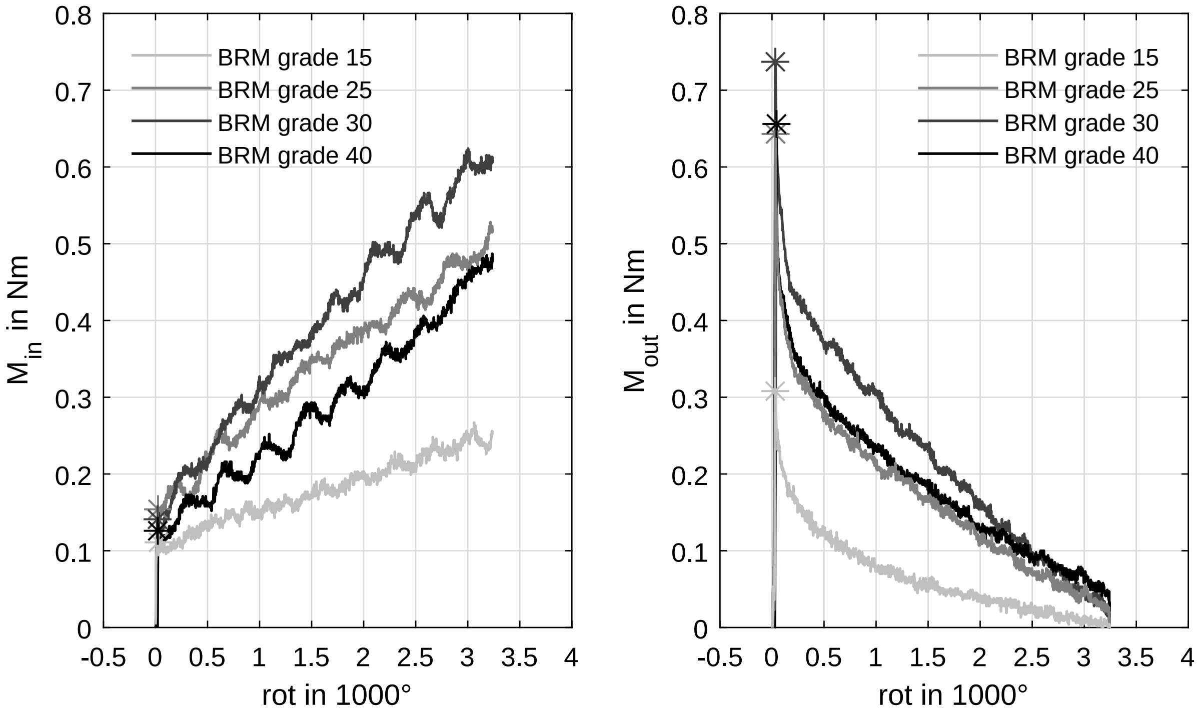

Figure 4.44.: Torque-rotation diagrams for insertion (left) and removal torque test (right) for thread number three to thread number twelve

the entire thread of the composite pedicle screws. A similar insertion torque-rotation behaviour was observed compared to figure 4.44. However, the initial insertion torques after contact between BRM and counter bearing were higher. The mean maximum insertion torques are shown in figure 4.45 on the upper right. The highest mean maximum insertion torque was reached for BRM grade 40 with (0.87 ± 0.15) Nm, followed by BRM grade 30 with (0.85 ± 0.06) Nm, BRM grade 25 with (0.59 ± 0.01) Nm, and BRM grade 15 with (0.34 ± 0.06) Nm. Fulfilling the requirements, these insertion torques were below the required maximum insertion torque of 3 Nm (cf. chapter 4.1).

As mentioned in chapter 4.6.1, the highest mean maximum pull-out force was achieved for BRM grade 30, a medium force for BRM grade 25, and the lowest force for BRM grade 15. This trend correlates well with the trend observed for the insertion torque test for the BRM grades 15, 25, and 30. However, there was no correlation between the pull-out and insertion torque behaviour of BRM grade 40. The highest insertion torques were measured for BRM grade 40, and these torques were significantly higher than the ones observed for BRM grade 15. In contrast, the maximum pull-out forces of BRM grade 40 were not significantly higher than the ones obtained for BRM grade 15. Therefore, a general relation between pull-out strength and maximum insertion torque cannot be established for composite pedicle screws. This is in accordance with the findings of other authors concerning metallic pedicle screws [110, 210, 211].

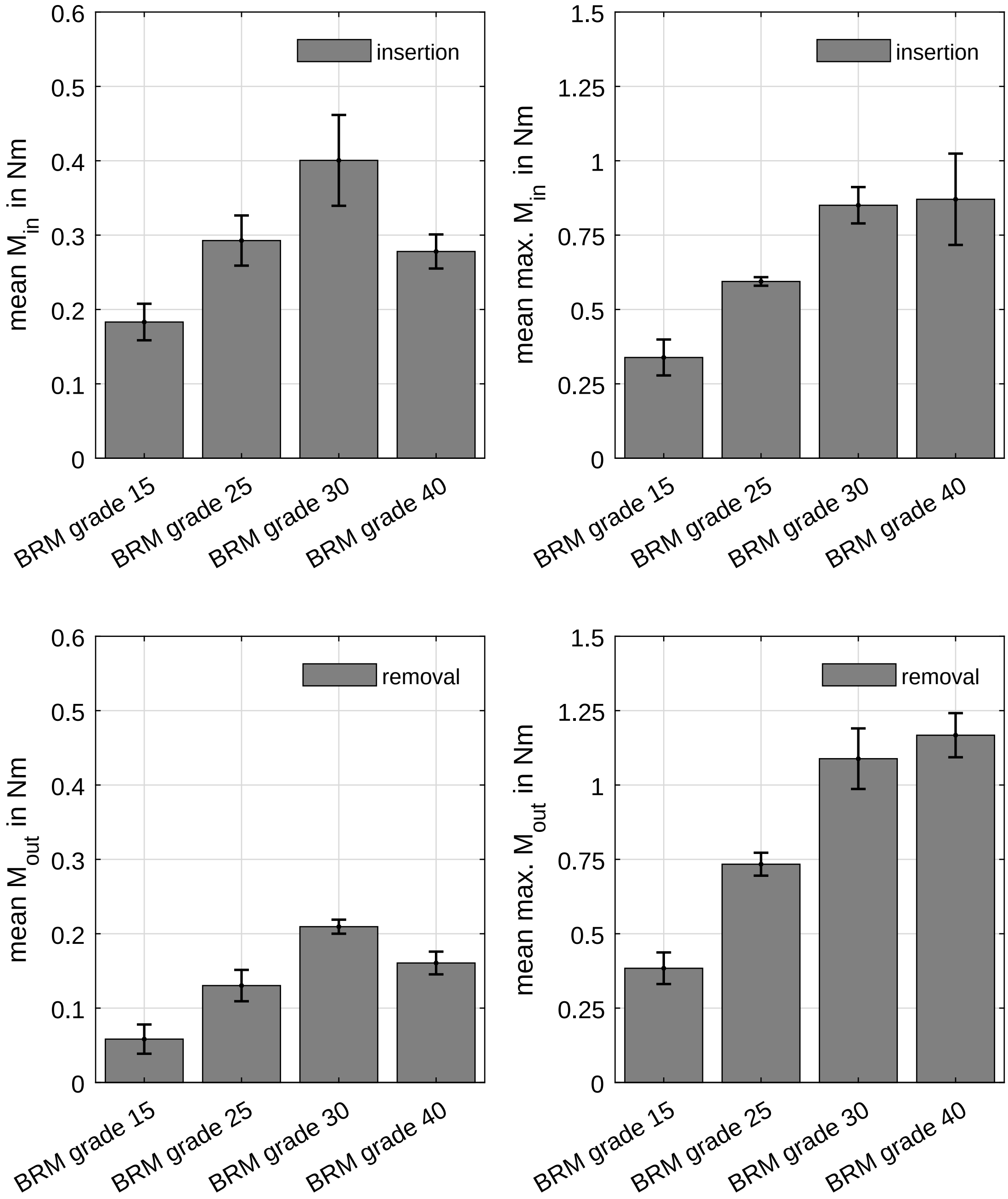

Figure 4.45.: Mean torques (thread number three to twelve, left) and mean maximum torques (thread number six to 15.5, right) for insertion (upper) and removal torque test (lower)

4.6.5 Removal torque test

The test set-up and rotation speed of the insertion torque test mentioned before were also used for the removal torque test. The removal of the composite pedicle screw was performed immediately after screw insertion, and in accordance with the standard ASTM F 543 [208]. The removal torque-rotation diagram is shown in figure 4.44 on the right. After reaching a high initial breakaway torque (marked with asterisks), a general trend of rapidly decreasing removal torques M_{out} can be observed. The mean removal torques during the screw removal from thread number twelve to thread number three are shown in figure 4.45 on the lower left, and the mean maximum removal torques during the screw removal from thread number 15.5 to thread number six are shown in figure 4.45 on the lower right. The mean maximum removal or breakaway torques from highest to lowest were (1.16 $\pm$ 0.07) Nm for BRM grade 40, (1.09 $\pm$ 0.10) Nm for BRM grade 30, (0.73 $\pm$ 0.04) Nm for BRM grade 25, and (0.38 $\pm$ 0.05) Nm for BRM grade 15. In comparison with the insertion and removal torques of specific BRMs, it can be observed that high removal torques correlate to high insertion torques. The mean removal torques were lower than the mean insertion torques, whereas the mean maximum removal or breakaway torques were higher than the mean maximum insertion torques.

4.6.6 Breaking torque test

Breaking torque tests were conducted for five entirely discontinuous sCF-PEEK pedicle screws and five hybrid composite pedicle screws. These screws were clamped in a testing jig from thread number five to the tip in accordance with the standard ASTM F 543 [208]. A clamp was used to fix the head of the screws. The rotation speed of the testing machine *ElectroForce® 3550* from *TA Instruments, Inc.* (former *Bose Corp.*) was 0.08°/s. Figure 4.46 shows the test set-up of the breaking torque test.

The test results are shown in figure 4.47. The mean maximum torque of the sCF-PEEK pedicle screws was (2.80 $\pm$ 0.10) Nm and of the hybrid composite pedicle screws (2.48 $\pm$ 0.06) Nm. The uCF-PEEK core contributes to a reduction of approximately 11 % of the breaking torque of the hybrid composite pedicle screws compared to the breaking torque of the sCF-PEEK pedicle screws. However, for pedicle screws, torsional loads are not as critical as pull-out or bending loads, as mentioned in chapter 2.2.1. A significant torsion resistance could be maintained after reaching the breaking torque of hybrid composite pedicle screws. In contrast, the torque values of the sCF-PEEK pedicle screws sharply dropped after reaching their maximum. Whereas sCF-PEEK screws totally failed after reaching their breaking torque, structural integrity was maintained for hybrid composite pedicle screws. As mentioned before, this is of

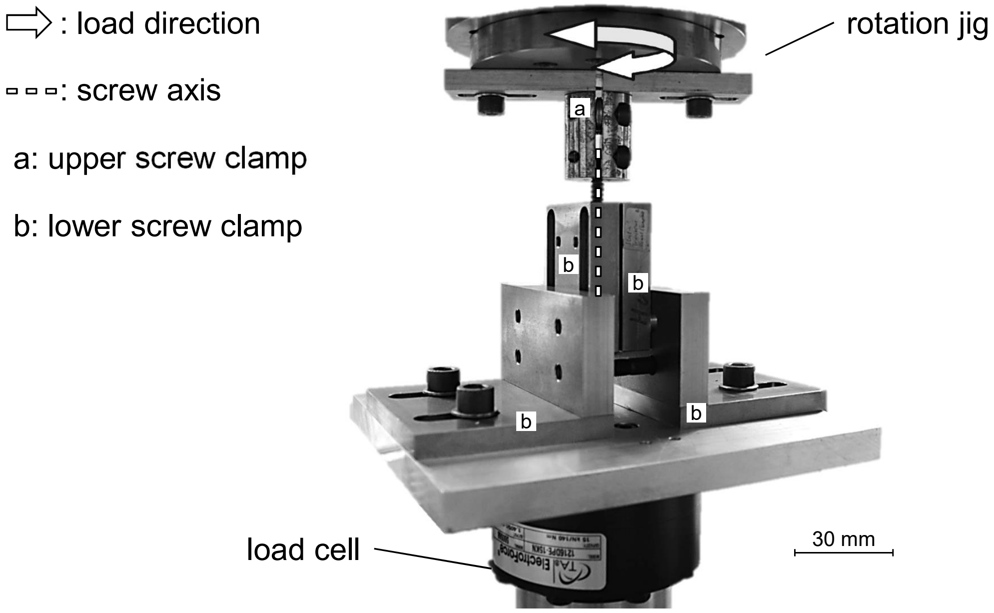

Figure 4.46.: Test set-up for breaking torque test

high importance for radiolucent composite implants (cf. chapter 4.6.2).

4.6.7 Imaging test

Imaging tests were conducted to compare the appearance of the CPSS and a metallic pedicle screw system[11] in CT scan and X-ray. Additionally, a system consisting of a metallic tulip[12] and the hybrid composite pedicle screw was examined in X-ray, named *Mix*. For the imaging tests of the CPSS, the hybrid composite pedicle screw was titanium coated, the clamp rings were marked with a tantalum wire, and two stainless steel markers were embedded in the tulip. The convolution kernels *standard* and *bone* were used for the CT images. The imaging test results can be seen in figure 4.48.

Severe artefacts can be seen in the CT images with the metallic system independently of the convolution kernel. Consequently, visibility of surrounding tissue is limited. In contrast, the CPSS system shows no artefacts in CT images. With the convolution kernel *bone*, the edges of the titanium coated hybrid composite pedicle screw and the clamp rings can clearly be seen without disturbing the visibility of surrounding tissue. The radiolucency of the CPSS is shown in the X-ray image on the right of figure 4.48. These imaging tests show that the CPSS significantly improves visibility by the prevention of artefacts in CT scan and X-ray images compared to metallic systems.

[11] *Click'X System* from *DePuy Synthes*
[12] *CD Horizon® Legacy™* from *Medtronic plc*

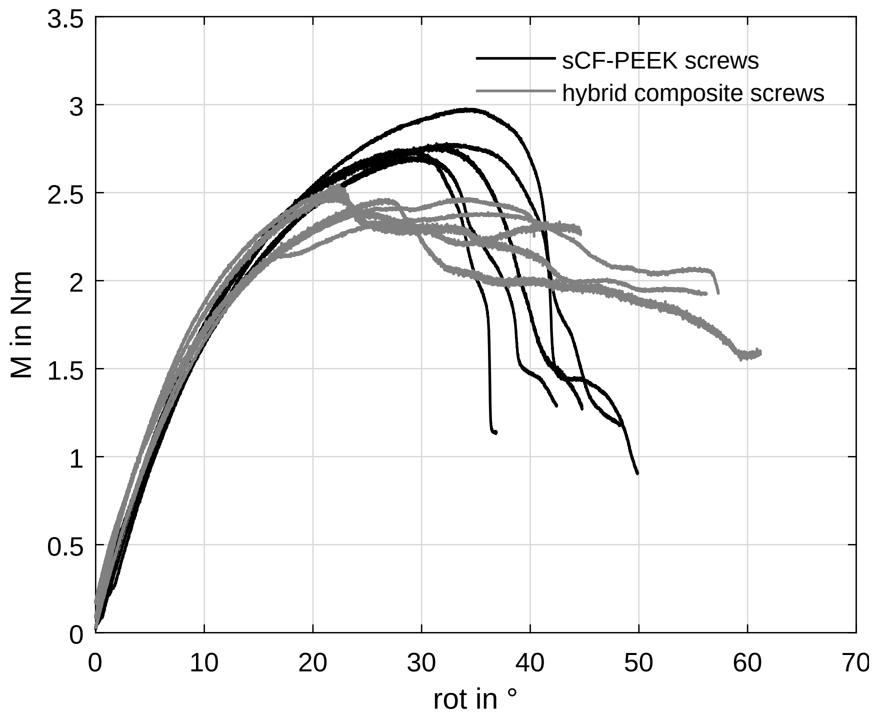

Figure 4.47.: Torque-rotation diagram for breaking torque test of sCF-PEEK and hybrid composite pedicle screws

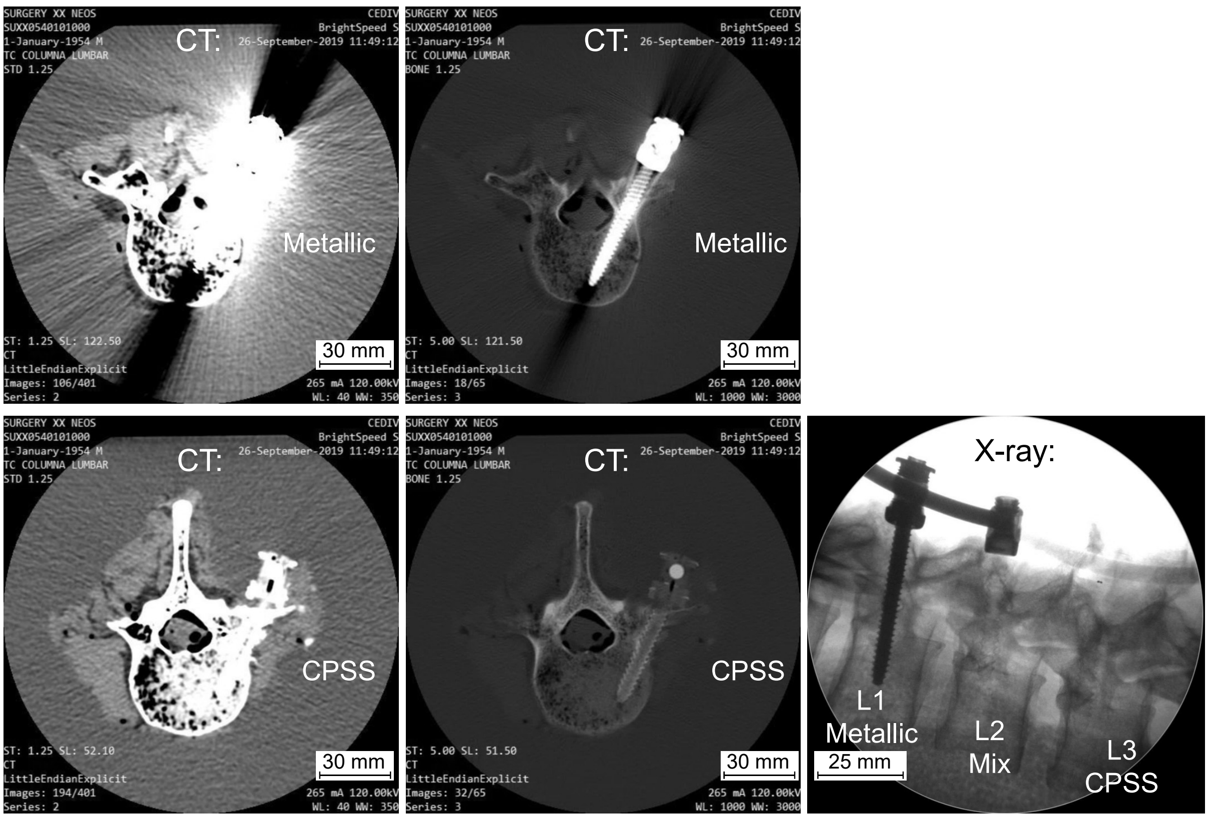

Figure 4.48.: CT scan (convolution kernels *standard* left and *bone* middle) and X-ray imaging test results (right) with different pedicle screw systems; images provided by *Neos Surgery S. L.*

5 Conclusion

TPC parts are characterised by unique properties, such as high specific mechanical properties or the possibility of remelting. Nowadays, they are used in various fields of application but significant market penetration is still missing. The majority of TPC parts can be divided into two classes: (1) discontinuous fibre reinforced mass products with a high freedom in design but moderate structural mechanical properties, and (2) continuous endless fibre reinforced products with excellent structural mechanical properties but severe design restrictions. Former research focused on the functionalisation of endless fibre composites by overmoulding. In this work, a different approach was pursued. Discontinuous short fibre reinforced material was locally reinforced by continuous unidirectional endless fibre reinforced material. In contrast to other studies, the interface between these two components was focused under the consideration of the structural mechanical properties of the hybrid structure, its manufacturability, and the possibility of mass production.

This research was based on a pedicle screw system which is an implant used for spine stabilisation and fusion. Pedicle screw breakage is one possible reason for implant failure. High forces and moments will be acting on the pedicle screw system especially if the system is implanted into the lumbar spine region. Moreover, CF-PEEK implants show distinct advantages in comparison with metallic implants. Considering these aspects, the research on a hybrid composite pedicle screw was motivated. With the concept of this hybrid composite screw, relevant structural mechanical properties could be significantly increased, and the implant stiffness could be tailored so that the applicability of composite bone screws can be extended. First biomechanical tests for certification have been conducted but the process of certification has to be pursued further on.

Biocompatible CF-PEEK is used for implants for few decades. In this work, a continuous unidirectional endless CF reinforced PEEK insert was overmoulded with discontinuous short CF reinforced PEEK material, and a high-strength interface could be established. Based on this overmoulding process, the manufacturing of the hybrid composite pedicle screws was realised. Prior to screw production, profound material characterisations were conducted to gain knowledge about physical, thermal, and structural mechanical properties of the materials used. A focus was laid on the interface characterisation between the discontinuous and continuous CF reinforced PEEK material. However, for interface strength characterisation of overmoulded structures, no standardised test method existed. Therefore, a novel specimen for interface characterisation was developed. Compared to other adapted interface characterisation specimens, this cylinder pull-out specimen showed distinct advantages, such as no influence of specimen preparation on interface strength, a simple specimen geometry and test set-up, low mould and material cost, easy manufacturability, and low rework. It is not limited to the interface characterisation between sCF-PEEK and uCF-PEEK material, but can be used for other composite or polymeric material combinations as well. Additionally, the interface between metallic inserts, and polymer or composite overmoulds can be studied. The utility patent DE202019102255.8 was successfully applied for the cylinder pull-out specimen within this research. By material and interface characterisations, a required pre-heating temperature of the endless CF-PEEK insert of at least 260 °C prior to overmoulding was determined to enable the formation of an interface with sufficient strength after overmoulding. Several methodologies were used to characterise this interface. Interface examinations by an LM, an X-ray microscope, and a stereo microscope confirm that cohesive interface formation will occur if adequate insert preparation and handling are considered. In conjunction with the adherence tests, it can be concluded that a cohesive interface has to be formed for sufficient interface strength so that superior structural mechanical properties of the hybrid structure can be achieved. If an adhesive interface between discontinuous and continuous CF reinforced PEEK is formed, interface strength will be insufficient. In this regard, micromechanical interlocking did not significantly contribute to interface strength. Due to limited scope, the molecular level of the interface was not studied but this can be complementary interesting for future works.

FE studies have shown that contact pressures due to thermal contraction contributed to the interface strength of the hybrid specimens focused in this study. Contact pressures on uCF-PEEK inserts will be higher if inserts are not pre-heated compared to inserts which are pre-heated to elevated temperatures prior to overmoulding with sCF-PEEK material. However, the interface strength of the cylinder pull-out specimens was 73 % higher provided that inserts were sufficiently pre-heated so that cohesive interface formation occurred.

For the research on the hybrid composite pedicle screw, a parametric FE model was developed in *Python*. The FE solver *Abaqus* was used for calculation. Compared to titanium pedicle screws, hybrid composite pedicle screws contributed to an increase in bone stress close to the implant. As a consequence, stress shielding can be reduced, and bone resorption can be prevented. By parametric optimisation, design recommendations were established which had to be opposed to manufacturing requirements and bone characteristics. Finally, a double shafted hybrid composite pedicle screw design was realised. According to this design, the moulds were manufactured so that the hybrid composite pedicle screw production could be approached.

The know-how, which was gained during material and interface characterisations, could be transferred to the overmoulding process of the hybrid composite pedicle screw. As a consequence, process running-in could be held low, and sufficient interface strength between the uCF-PEEK screw core and the sCF-PEEK overmould could be achieved. Different biomechanical tests were conducted to characterise the composite pedicle screw. Quasi-static pull-out tests have shown that the required pull-out force could be achieved with all BRM grades ranging from osteoporotic to high dense bone. However, the insertion of the composite screw in the high-dense BRM grades was difficult due to high friction forces between BRM and screw so that the pre-hole diameter had to be increased. This example shows that common testing standards for metallic implants cannot be directly applied for composite implants, and that new regulations have to be established. In the quasi-static bending test, hybrid composite pedicle screws showed an increase of approximately 48 % in their maximum bending moment compared to discontinuous short CF reinforced pedicle screws. Additionally, the requirement concerning the insertion torque was fulfilled because it was less than the required maximum torque of 3 Nm. No general relation between maximum insertion torque and pull-out strength could be found for composite pedicle screws. The breaking torque of the discontinuous short CF reinforced pedicle screws was approximately 11 % higher than the one of the hybrid composite screws. However, in this test, and also in the quasi-static and cyclic bending test, structural integrity could only be maintained for hybrid composite pedicle screws. Structural integrity is important for composite implants because radiolucent parts of a broken composite implant are difficult to locate within the human body. Another advantage of hybrid composite pedicle screws refers to their fatigue resistance which was superior compared to their discontinuous short CF reinforced counterparts. With the CPSS, artefacts in CT scan and X-ray could be prevented so that patients and doctors benefit from this system especially during system installation, patient follow-up, and radiotherapy.

The local reinforcement of discontinuous short fibre reinforced thermoplastics with continuous unidirectional endless fibre reinforced thermoplastics creates new fields of cost efficient structural applications. Overmoulded hybrid parts will be characterised by freedom in design, superior structural mechanical properties, and excellent fatigue resistance if sufficient interface strength is achieved. In this study, the formation of a cohesive interface between short and endless fibre reinforced PEEK was required for sufficient interface strength. The methodology developed in this work can be utilised for different applications not only in the medical but also in other industrial sectors.

A Appendix

A.1 Additional results of dynamic mechanical thermal analysis

The results of the DMTA of the specimens with their main extension perpendicular to the fibre (uCF-90) and injection direction (sCF-90) are shown in figure A.1 on the left and right. In the figure, the bending storage modulus E' and the bending loss factor $tan\ \delta$ are plotted against the temperature T.

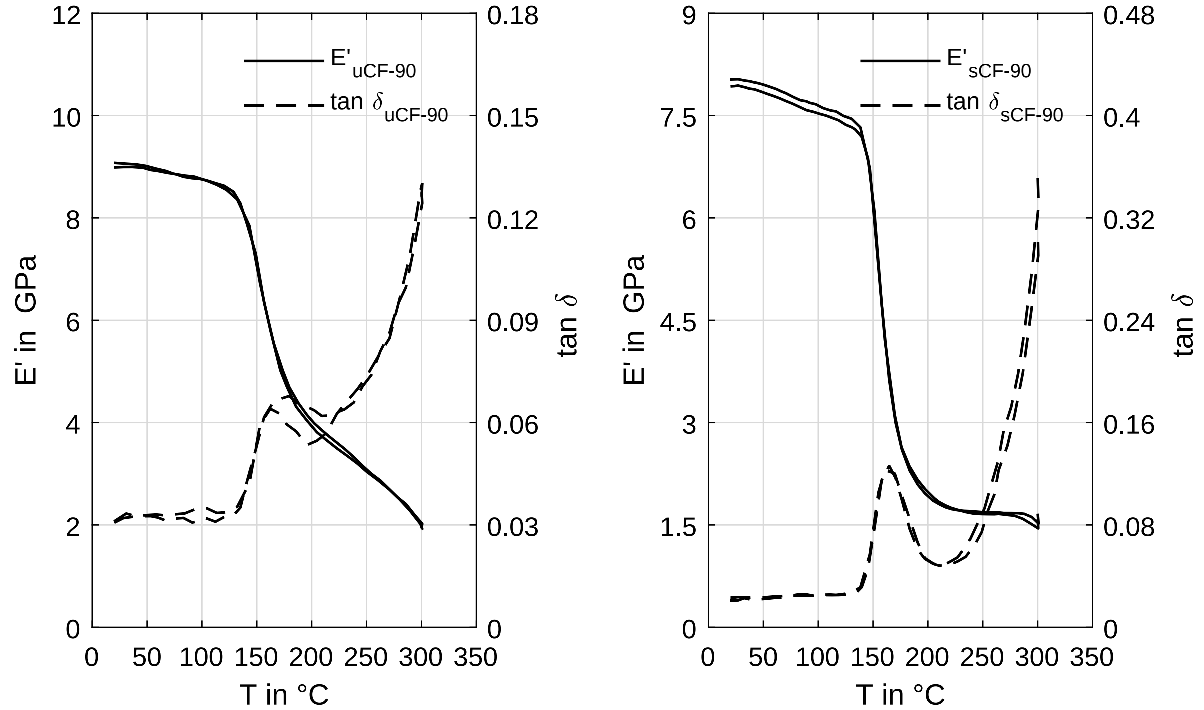

Figure A.1.: DMTA diagrams of uCF-PEEK plate specimens perpendicular to fibre direction (left) and sCF-PEEK specimens perpendicular to injection direction (right)

The comparison of the DMTA results of the sCF-90 specimens (cf. figure A.1 on the right) with the results of the sCF-0 specimens (cf. figure 4.6 on the right) confirms that the structural mechanical properties of the sCF-PEEK specimens are dependent on the process induced fibre orientation and distribution.

A.2 Additional results of parametric optimisation

The relative pull-out displacements u_{rel} dependent on the proximal and distal half angles κ_{prox} and κ_{dist} are shown in figure A.2. In this optimisation study, the proximal and distal root radii were fixed with 0.2 mm and 0.1 mm to obtain one specific surface plot. But any other value of simulated root radii could have been chosen. The results show that a higher hybrid composite pedicle screw stability can be achieved by decreasing the proximal half angle and by increasing the distal half angle.

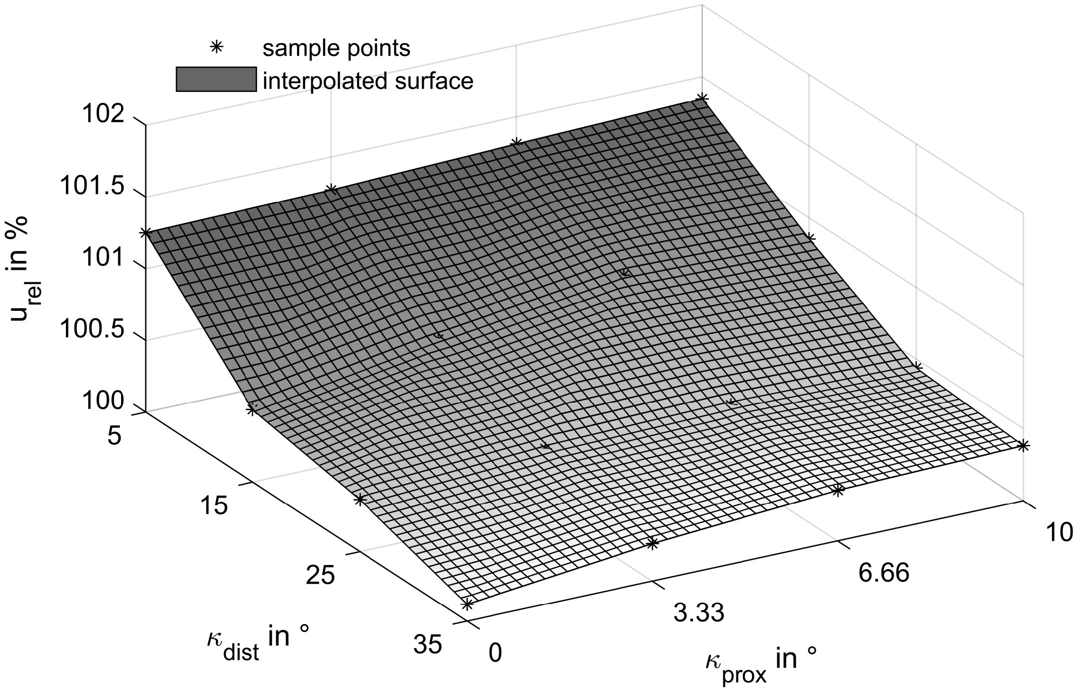

Figure A.2.: Surface plot of the relative axial screw displacements u_{rel} dependent on the half angles κ_{prox} and κ_{dist} with a fixed proximal root radius r_{prox} of 0.2 mm and a fixed distal root radius r_{dist} of 0.1 mm

Figure A.3 shows two surface plots for the lengths l_{flank}^{up} and l_{flank}^{low} of the upper and lower thread flanks. Here, the relative pull-out displacements u_{rel} were plotted for the screw shaft diameters D_i of 5 mm and 3.56 mm. But any other diameter could have been chosen. The figure shows that the influence of the screw shaft diameter on the relative displacements is higher than the influence of the lengths of the thread flanks.

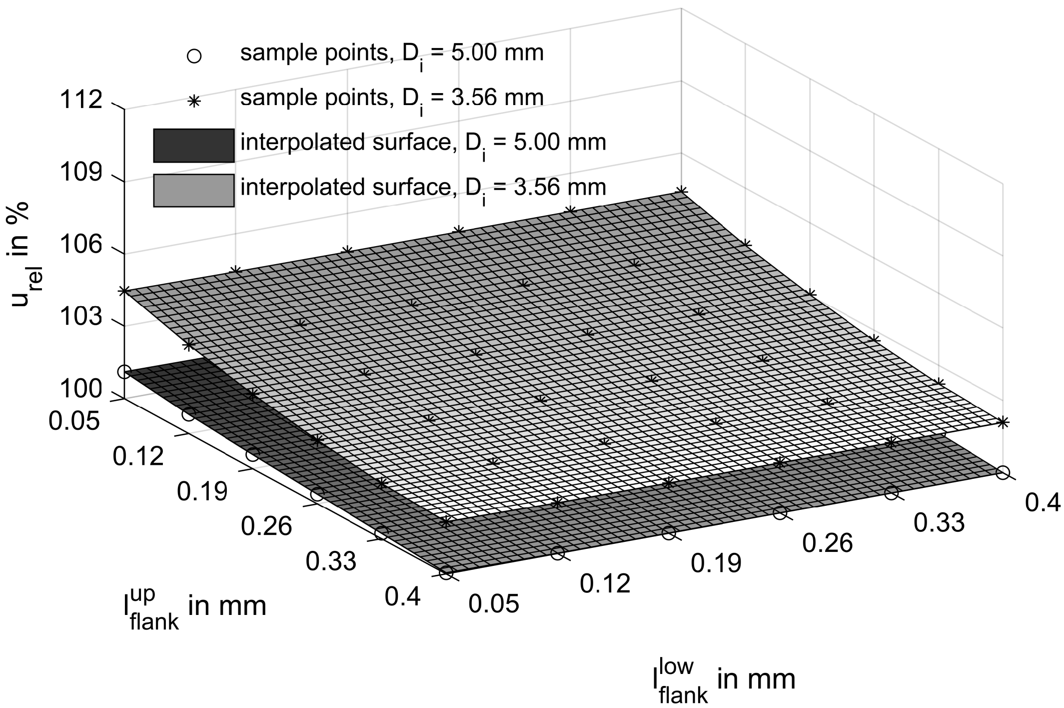

Figure A.3.: Surface plot of the relative axial screw displacements u_{rel} dependent on the thread flank lengths l_{flank}^{up} and l_{flank}^{low} and the screw shaft diameter D_i

References

[1] M. Holmes. Aerospace looks to composites for solutions. *Reinforced Plastics*, 61(4):237–241, 2017.

[2] M. Kropka, M. Muehlbacher, T. Neumeyer, and V. Altstaedt. From UD-tape to final part – a comprehensive approach towards thermoplastic composites. In *Procedia CIRP 66 – 1st Cirp Conference on Composite Materials Parts Manufacturing (Cirp-CCMPM)*, Karlsruhe, Germany, 2017.

[3] S. Epple and C. Bonten. In-situ-pultrusion – bonding of FRP-parts to PA6. In *AIP Conference Proceedings 1779*, Graz, Austria, 2016.

[4] H. Schürmann, editor. *Konstruieren mit Faser-Kunststoff-Verbunden*. Springer, 2nd edition, 2007.

[5] S. M. Kurtz, editor. *PEEK biomaterials handbook*. William Andrew, 2nd edition, 2019.

[6] M. Schulte, M. Schultheiss, E. Hartwig, H.-J. Wilke, S. Wolf, R. Sokiranski, T. Fleiter, L. Kinzl, and L. Claes. Vertebral body replacement with a bioglass-polyurethane composite in spine metastases – clinical, radiological and biomechanical results. *European Spine Journal*, 9(5):437–444, 2000.

[7] F. Ringel, Y.-M. Ryang, J. S. Kirschke, B. S. Müller, J. J. Wilkens, J. Brodard, S. E. Combs, and B. Meyer. Radiolucent carbon fiber-reinforced pedicle screws for treatment of spinal tumors: advantages for radiation planning and follow-up imaging. *World Neurosurgery*, 105:294–301, 2017.

[8] G. Tedesco, A. Gasbarrini, S. Bandiera, R. Ghermandi, and S. Boriani. Composite PEEK/carbon fiber implants can increase the effectiveness of radiotherapy in the management of spine tumors. *Journal of Spine Surgery*, 3(3):323–329, 2017.

[9] A. Nevelsky, E. Borzov, S. Daniel, and R. Bar-Deroma. Perturbation effects of the carbon fiber-PEEK screws on radiotherapy dose distribution. *Journal of Applied Clinical Medical Physics*, 18(2):62–68, 2017.

[10] A. Riveiro, R. Soto, R. Comesaña, M. Boutinguiza, J. del Val, F. Quintero, F. Lusquiños, and J. Pou. Laser surface modification of PEEK. *Applied Surface Science*, 258(23):9437–9442, 2012.

[11] F. Chen, S. Gatea, H. Ou, B. Lu, and H. Long. Fracture characteristics of PEEK at various stress triaxialities. *Journal of the Mechanical Behavior of Biomedical Materials*, 64:173–186, 2016.

[12] J. M. Toth, M. Wang, B. T. Estes, J. L. Scifert, H. B. Seim III, and A. S. Turner. Polyetheretherketone as a biomaterial for spinal applications. *Biomaterials*, 27(3):324–334, 2006.

[13] M. Athanasakopoulos, A. F. Mavrogenis, G. Triantafyllopoulos, S. Koufos, and S. G. Pneumaticos. Posterior spinal fusion using pedicle screws. *Orthopedics*, 36(7):e951–e957, 2013.

[14] A. Schwitalla, T. Spintig, I. Kallage, R. Wagner, and W. D. Müller. Polyetheretherketon (PEEK) – ein vielversprechender Werkstoff für die Zukunft. *Umwelt Medizin Gesellschaft*, 27(4):255–261, 2014.

[15] S. M. Kurtz and J. N. Devine. PEEK biomaterials in trauma, orthopedic, and spinal implants. *Biomaterials*, 28(32):4845–4869, 2007.

[16] R. K. Ponnappan, H. Serhan, B. Zarda, R. Patel, T. Albert, and A. R. Vaccaro. Biomechanical evaluation and comparison of polyetheretherketone rod system to traditional titanium rod fixation. *The Spine Journal*, 9(3):263–267, 2009.

[17] D. F. Williams and A. McNamara. Potential of polyetheretherketone (PEEK) and carbon-fibre-reinforced PEEK in medical applications. *Journal of Materials Science Letters*, 6(2):188–190, 1987.

[18] E. M. Feerick, J. Kennedy, H. Mullett, D. FitzPatrick, and P. McGarry. Investigation of metallic and carbon fibre PEEK fracture fixation devices for three-part proximal humeral fractures. *Medical Engineering and Physics*, 35(6):712–722, 2013.

[19] R. Bader, E. Steinhauser, H. Rechl, W. Siebels, W. Mittelmeier, and R. Gradinger. Kohlenstofffaserverstärkte Kunststoffe als Implantatwerkstoff. *Orthopäde*, 32:32–40, 2003.

[20] R. Hillock and S. Howard. Utility of carbon fiber implants in orthopedic surgery: literature review. *Reconstructive Review*, 4(1):23–32, 2014.

[21] R. A. Lindtner, R. Schmid, T. Nydegger, M. Konschake, and W. Schmoelz. Pedicle screw anchorage of carbon fiber-reinforced PEEK screws under cyclic loading. *European Spine Journal*, 27(8):1775–1784, 2018.

[22] M. Banghard, C. Freudigmann, K. Silmy, A. Stett, and V. Bucher. Plasma treatment on novel carbon fiber reinforced PEEK cages to enhance bioactivity. *Current Directions in Biomedical Engineering*, 2(1):569–572, 2016.

[23] E. C. Benzel, editor. *Biomechanics of spine stabilization*. Thieme Medical Publishers, Inc., 3rd edition, 2015.

[24] E. C. Teo and H. W. Ng. Evaluation of the role of ligaments, facets and disc nucleus in lower cervical spine under compression and sagittal moments using finite element method. *Medical Engineering and Physics*, 23(3):155–164, 2001.

[25] L. B. Urselmann. *Dorsale Instrumentation an der Wirbelsäule mit Pedikelschrauben – Computerassistierte orthopädische Chirurgie (CAOS) versus Konventionelle Platzierung mit Bildwandler*. Ph. D. thesis, Heinrich-Heine-Universität Düsseldorf, 2009.

[26] A. Sitiso, J. Wagner, and F. Bailly. Polyaxial pedicle screw system. US patent US2004/0158247A1, 2004.

[27] Icotec AG. VADER® pedicle system. Factsheet, September 2019.

[28] CarboFix Orthopedics Ltd. Carboclear™ pedicle screw system – a composite material spinal system. Surgical technique, July 2016.

[29] M. Heinle and D. Drummer. Measuring mechanical stresses on inserts during injection molding. *Advances in Mechanical Engineering*, 7(5):1–6, 2015.

[30] T. Härtig. *Stoffübertragung beim Spritzgießen*. Ph. D. thesis, Chemnitz University of Technology, 2013.

[31] D. F. Williams. On the mechanisms of biocompatibility. *Biomaterials*, 29(20):2941–2953, 2008.

[32] A. M. Ballo, E. A. Akca, T. Ozen, L. Lassila, P. K. Vallittu, and T. O. Närhi. Bone tissue responses to glass fiber-reinforced composite implants – a histomorphometric study. *Clinical Oral Implants Research*, 20(6):608–615, 2009.

[33] A. F. Mavrogenis, C. Vottis, G. Triantafyllopoulos, P. J. Papagelopoulos, and S. G. Pneumaticos. PEEK rod systems for the spine. *European Journal of Orthopaedic Surgery and Traumatology*, 24:111–116, 2014.

[34] T. S. Rau, editor. *Optimierungspotentiale für das Einwachsverhalten lasttragender Implantate in Knochengewebe*. University Ilmenau, 2nd edition, 2009.

[35] J. Comyn, L. Mascia, and G. Xiao. Plasma-treatment of polyetheretherketone (PEEK) for adhesive bonding. *International Journal of Adhesion and Adhesives*, 16(2):97–104, 1996.

[36] S.-W. Ha, R. Hauert, K.-H. Ernst, and E. Wintermantel. Surface analysis of chemically-etched and plasma-treated polyetheretherketone (PEEK) for biomedical applications. *Surface and Coatings Technology*, 96(2-3):293–299, 1997.

[37] L. Ponsonnet, K. Reybier, N. Jaffrezic, V. Comte, C. Lagneau, M. Lissac, and C. Martelet. Relationship between surface properties (roughness, wettability) of titanium and titanium alloys and cell behaviour. *Materials Science and Engineering C*, 23(4):551–560, 2003.

[38] S.-W. Ha, M. Kirch, F. Birchler, K.-L. Eckert, J. Mayer, E. Wintermantel, C. Sittig, I. Pfund-Klingenfuss, M. Textor, N. D. Spencer, M. Guecheva, and H. Vonmont. Surface activation of polyetheretherketone (PEEK) and formation of calcium phosphate coatings by precipitation. *Journal of Materials Science: Materials in Medicine*, 8:683–690, 1997.

[39] N. J. Hallab, K. J. Bundy, K. O'Connor, R. L. Moses, and J. J. Jacobs. Evaluation of metallic and polymeric biomaterial surface energy and surface roughness characteristics for directed cell adhesion. *Tissue Engineering*, 7(1):55–71, 2001.

[40] D. Briem, S. Strametz, K. Schröder, N. M. Meenen, W. Lehmann, W. Linhart, A. Ohl, and J. M. Rueger. Response of primary fibroblasts and osteoblasts to plasma treated polyetheretherketone (PEEK) surfaces. *Journal of Materials Science: Materials in Medicine*, 16(7):671–677, 2005.

[41] E. Wintermantel and S.-W. Ha, editors. *Medizintechnik – life science engineering*. Springer, 5th edition, 2009.

[42] E. Steinberg, E. Rath, A. Shlaifer, O. Chechik, E. Maman, and M. Salai. Carbon fiber reinforced PEEK Optima – a composite material biomechanical properties and wear/debris characteristics of CF-PEEK composites for orthopedic trauma implants. *Journal of the Mechanical Behavior of Biomedical Materials*, 17:221–228, 2013.

[43] I. M. El Fiki, F. Zaiton, and A. M. Awadalla. Role of postoperative multislice computed tomography in assessment of pedicle screw placement in spinal surgical fixation. *The Egyptian Journal of Radiology and Nuclear Medicine*, 44(1):63–70, 2013.

[44] H. M. Frost. Wolff's law and bone's structural adaptations to mechanical usage: an overview for clinicians. *The Angle Orthodontist*, 64(3):175–188, 1994.

[45] A. Gefen. Optimizing the biomechanical compatibility of orthopedic screws for bone fracture fixation. *Medical Engineering and Physics*, 24(5):337–347, 2002.

[46] K. Haase and G. Rouhi. Prediction of stress shielding around an orthopedic screw: using stress and strain energy density as mechanical stimuli. *Computers in Biology and Medicine*, 43(11):1748–1757, 2013.

[47] N. Boudeau, D. Liksonov, T. Barriere, L. Maslov, and J.-C. Gelin. Composite based on polyetheretherketone reinforced with carbon fibres, an alternative to conventional materials for femoral implant: manufacturing process and resulting structural behaviour. *Materials and Design*, 40:148–156, 2012.

[48] C.-K. Chao, J.-L. Wang, and J. Lin. Increasing bending strength and pullout strength in conical pedicle screws: biomechanical tests and finite element analyses. *Journal of Spinal Disorders and Techniques*, 21(2):130–138, 2008.

[49] S. Griza, C. E. C. de Andrade, W. W. Batista, E. K. Tentardini, and T. R. Strohaecker. Case study of Ti6Al4V pedicle screw failures due to geometric and microstructural aspects. *Engineering Failure Analysis*, 25:133–143, 2012.

[50] T. Heydt, N. Motsch, and J. Hausmann. Development of a hybrid process for the production of personalized and structurally optimized 3D-printed orthosis on site. In *2018 International Textile Conference*, Daegu, South Korea, 2018.

[51] P. Patel, T. R. Hull, R. E. Lyon, S. I. Stoliarov, R. N. Walters, S. Crowley, and N. Safronava. Investigation of the thermal decomposition and flammability of PEEK and its carbon and glass-fibre composites. *Polymer Degradation and Stability*, 96(1):12–22, 2011.

[52] J. A. Brydson, editor. *Plastics materials*, chapter "21 - Other thermoplastics containing p-phenylene groups", pages 584–612. Butterworth-Heinemann, 7th edition, 1999.

[53] S. X. Lu, P. Cebe, and M. Capel. Thermal stability and thermal expansion studies of PEEK and related polyimides. *Polymer*, 37(14):2999–3009, 1996.

[54] L. O. Dandy, G. Oliveux, J. Wood, M. J. Jenkins, and G. A. Leeke. Accelerated degradation of polyetheretherketone (PEEK) composite materials for recycling applications. *Polymer Degradation and Stability*, 112:52–62, 2015.

[55] Y. Lee and R. S. Porter. Double-melting behavior of poly(ether ether ketone). *Macromolecules*, 20(6):1336–1341, 1987.

[56] S. Z. D. Cheng, M.-Y. Cao, and B. Wunderlich. Glass transition and melting behavior of poly(oxy-1,4-phenyleneoxy-1,4-phenylenecarbonyl-1,4-phenylene). *Macromolecules*, 19(7):1868–1876, 1986.

[57] Y. Lee and R. S. Porter. Crystallization of poly(etheretherketone) (PEEK) in carbon fiber composites. *Polymer Engineering and Science*, 26(9):633–639, 1986.

[58] P. Patel, T. R. Hull, R. W. McCabe, D. Flath, J. Grasmeder, and M. Percy. Mechanism of thermal decomposition of poly(ether ether ketone) (PEEK) from a review of decomposition studies. *Polymer Degradation and Stability*, 95(5):709–718, 2010.

[59] G. da Cunha Vasconcelos, R. L. Mazur, B. Ribeiro, E. C. Botelho, and M. L. Costa. Evaluation of decomposition kinetics of poly (ether-ether-ketone) by thermogravimetric analysis. *Materials Research*, 17(1):227–235, 2014.

[60] R. Phillips, T. Glauser, and J.-A. E. Månson. Thermal stability of PEEK/carbon fiber in air and its influence on consolidation. *Polymer Composites*, 18(4):500–508, 1997.

[61] C. N. Velisaris and J. C. Seferis. Crystallization kinetics of polyetheretherketone (PEEK) matrices. *Polymer Engineering and Science*, 26(22):1574–1581, 1986.

[62] P. Patel, A. A. Stec, T. R. Hull, M. Naffakh, A. M. Diez-Pascual, G. Ellis, N. Safronava, and R. E. Lyon. Flammability properties of PEEK and carbon nanotube composites. *Polymer Degradation and Stability*, 97(12):2492–2502, 2012.

[63] R. B. Prime and J. C. Seferis. Thermo-oxidative decomposition of poly (ether ether ketone). *Journal of Polymer Science Part C: Polymer Letters*, 24(12):641–644, 1986.

[64] O. B. Searle and R. H. Pfeiffer. Victrex® poly(ethersulfone) (PES) and Victrex® poly(etheretherketone) (PEEK). *Polymer Engineering and Science*, 25(8):474–476, 1985.

[65] L. W. McKeen, editor. *Permeability properties of plastics and elastomers*, chapter "12 - High temperature/high performance polymers", pages 289–303. William Andrew, 4th edition, 2017.

[66] Victrex plc. VICTREX® PEEK 450G. Material data sheet, July 2014.

[67] R. M. Cowie, A. Briscoe, J. Fisher, and L. M. Jennings. Wear and friction of UHMWPE-on-PEEK Optima^{TM}. *Journal of the Mechanical Behavior of Biomedical Materials*, 89:65–71, 2019.

[68] P. Cebe. Annealing study of poly(etheretherketone). *Journal of Materials Science*, 23:3721–3731, 1988.

[69] B. Normand, H. Takenouti, M. Keddam, H. Liao, G. Monteil, and C. Coddet. Electrochemical impedance spectroscopy and dielectric properties of polymer: application to PEEK thermally sprayed coating. *Electrochimica Acta*, 49(17-18):2981–2986, 2004.

[70] C.-H. Rivard, S. Rhalmi, and C. Coillard. In vivo biocompatibility testing of PEEK polymer for a spinal implant system: a study in rabbits. *Journal of Biomedical Materials Research*, 62(4):488–498, 2002.

[71] E. E. Rutherford, L. J. Tarplett, E. M. Davies, J. M. Harley, and L. J. King. Lumbar spine fusion and stabilization: hardware, techniques, and imaging appearances. *Radiographics*, 27(6):1737–1749, 2007.

[72] T. Brown and Q.-B. Bao. The use of self-mating PEEK as an alternative bearing material for cervical disc arthroplasty: a comparison of different simulator inputs and tribological environments. *European Spine Journal*, 21(Suppl 5):S717–S726, 2012.

[73] S. O. Eicker, K. Krajewski, S. Payer, T. Krätzig, and M. Dreimann. First experience with carbon/PEEK pedicle screws. *Journal of Neurosurgical Sciences*, 61(2):222–224, 2017.

[74] J. R. Sarasua and P. M. Remiro. The mechanical behaviour of PEEK short fibre composites. *Journal of Materials Science*, 30(13):3501–3508, 1995.

[75] A. M. Díez-Pascual, M. Naffakh, J. M. González-Domínguez, A. Ansón, Y. Martínez-Rubi, M. T. Martínez, B. Simard, and M. A. Gómez. High performance PEEK/carbon nanotube composites compatibilized with polysulfones-I. Structure and thermal properties. *Carbon*, 48(12):3485–3499, 2010.

[76] M. Hedayati, M. Salehi, R. Bagheri, M. Panjepour, and F. Naeimi. Tribological and mechanical properties of amorphous and semi-crystalline PEEK/SiO2 nanocomposite coatings deposited on the plain carbon steel by electrostatic powder spray technique. *Progress in Organic Coatings*, 74(1):50–58, 2012.

[77] M. Q. Zhang, Z. P. Lu, and K. Friedrich. Thermal analysis of the wear debris of polyetheretherketone. *Tribology International*, 30(2):103–111, 1997.

[78] R. A. Chivers and D. R. Moore. The effect of molecular weight and crystallinity on the mechanical properties of injection moulded poly(aryl-ether-etherketone) resin. *Polymer*, 35(1):110–116, 1994.

[79] S. Yu, K. P. Hariram, R. Kumar, P. Cheang, and K. K. Aik. In vitro apatite formation and its growth kinetics on hydroxyapatite/polyetheretherketone biocomposites. *Biomaterials*, 26(15):2343–2352, 2005.

[80] J. Khoury, S. R. Kirkpatrick, M. Maxwell, R. E. Cherian, A. Kirkpatrick, and R. C. Svrluga. Neutral atom beam technique enhances bioactivity of PEEK. *Nuclear Instruments and Methods in Physics Research B*, 307:630–634, 2013.

[81] C. Díaz and G. Fuentes. Tribological studies comparison between UHMWPE and PEEK for prosthesis application. *Surface and Coatings Technology*, 325:656–660, 2017.

[82] S.-W. Ha, A. Gisep, J. Mayer, and E. Wintermantel. Topographical characterization and microstructural interface analysis of vacuum-plasma-sprayed titanium and hydroxyapatite coatings on carbon fibre-reinforced poly(etheretherketone). *Journal of Materials Science: Materials in Medicine*, 8(12):891–896, 1997.

[83] D. J. Kelsey and G. S. Springer. Composite implant for bone replacement. *Journal of Composite Materials*, 31(16):1593–1632, 1997.

[84] F. El Halabi, J. F. Rodriguez, L. Rebolledo, E. Hurtós, and M. Doblaré. Mechanical characterization and numerical simulation of polyether-ether-ketone (PEEK) cranial implants. *Journal of the Mechanical Behavior of Biomedical Materials*, 4(8):1819–1832, 2011.

[85] T. Brown, Q.-B. Bao, T. Kilpela, and M. Songer. An in vitro biotribological assessment of NUBAC, a polyetheretherketone-on-polyetheretherketone articulating nucleus replacement device. *Spine*, 35(16):E774–E781, 2010.

[86] P. Jain and M. R. Khan. Prediction of biomechanical behavior of lumbar vertebrae using a novel semi-rigid stabilization device. *Proceedings of the Institution of Mechanical Engineers Part H*, 233(8):849–857, 2019.

[87] S. Błażewicz, J. Chłopek, A. Litak, C. Wajler, and E. Staszków. Experimental study of mechanical properties of composite carbon screws. *Biomaterials*, 18(5):437–439, 1997.

[88] P. K. Vallittu, T. O. Närhi, and L. Hupa. Fiber glass-bioactive glass composite for bone replacing and bone anchoring implants. *Dental Materials*, 31(4):371–381, 2015.

[89] Z. Rasheva, G. Zhang, and T. Burkhart. A correlation between the tribological and mechanical properties of short carbon fibers reinforced PEEK materials with different fiber orientations. *Tribology International*, 43(8):1430–1437, 2010.

[90] Y. Guan, H. Bruner, N. Yoganandan, F. Pintar, and D. Maiman. Block-fixation finite element lumbar spine model to examine load-sharing, bone screw interaction, and stress in carbon fiber reinforced PEEK construct. In *Proceedings of the ASME 2009 Summer Bioengineering Conference (SBC2009)*, Resort at Squaw Creek, Lake Tahoe, CA, USA, 2009.

[91] A. Ballara, J. P. Trotignon, and J. Verdu. Skin-core structure of polyetheretherketone injection-moulded parts from DSC measurements. *Journal of Materials Science Letters*, 5:706–708, 1986.

[92] K. A. Jockisch, S. A. Brown, T. W. Bauer, and K. Merritt. Biological response to chopped-carbon-fiber-reinforced PEEK. *Journal of Biomedical Materials Research*, 26(2):133–146, 1992.

[93] Q. Q. Wang, J. J. Wu, A. Unsworth, A. Briscoe, M. Jarman-Smith, C. Lowry, D. Simpson, and S. Collins. Biotribological study of large diameter ceramic-on-CFR-PEEK hip joint including fluid uptake, wear and frictional heating. *Journal of Materials Science: Materials in Medicine*, 23(6):1533–1542, 2012.

[94] D. J. Hak, R. Fader, T. Baldini, and V. B. S. Chadayammuri. Locking screw-plate interface stability in carbon-fibre reinforced polyetheretherketone proximal humerus plates. *International Orthopaedics*, 41(9):1735–1739, 2017.

[95] A. Wang, R. Lin, C. Stark, and J. H. Dumbleton. Suitability and limitations of carbon fiber reinforced PEEK composites as bearing surfaces for total joint replacements. *Wear*, 225-229(2):724–727, 1999.

[96] R. Tognini, U. Loher, T. Peter, R. Raschle, J. Mayer, and E. Wintermantel. Fatigue properties of CF/PEEK cortical bone screws produced by composite transfer squeeze forming (CTSF). In *Proceedings of the 1999 International Conference on Composite Materials (ICCM12)*, Paris, France, 1999.

[97] M. H. Krag, B. D. Beynnon, M. H. Pope, J. W. Frymoyer, L. D. Haugh, and D. L. Weaver. An internal fixator for posterior application to short segments of

the thoracic, lumbar, or lumbosacral spine. *Clinical Orthopaedics and Related Research*, 203:75–98, 1986.

[98] G. R. Fogel, C. A. Reitman, W. Liu, and S. I. Esses. Physical characteristics of polyaxial-headed pedicle screws and biomechanical comparison of load with their failure. *Spine*, 28(5):470–473, 2003.

[99] M. F. Gornet, F. W. Chan, J. C. Coleman, B. Murrell, R. P. Nockels, B. A. Taylor, T. H. Lanman, and J. A. Ochoa. PEEK rod system for semi-rigid fixation of lumbar fusion constructs. *Journal of Biomechanical Engineering*, 133(8):1–12, 2011.

[100] D. Bomback. Spinal fusion. http://secondopinion-spine.com/spinal-procedures/spinal-fusion/, May 2018.

[101] T. Hirano, K. Hasegawa, H. E. Takahashi, S. Uchiyama, T. Hara, T. Washio, T. Sugiura, M. Yokaichiya, and M. Ikeda. Structural characteristics of the pedicle and its role in screw stability. *Spine*, 22(21):2504–2510, 1997.

[102] P. E. Chatzistergos, E. A. Magnissalis, and S. K. Kourkoulis. Numerical simulation of bone screw induced pretension: the cases of under-tapping and conical profile. *Medical Engineering and Physics*, 36(3):378–386, 2014.

[103] C. A. Lill, E. Schneider, J. Goldhahn, A. Haslemann, and F. Zeifang. Mechanical performance of cylindrical and dual core pedicle screws in calf and human vertebrae. *Archives of Orthopaedic and Trauma Surgery*, 126(10):686–694, 2006.

[104] P. E. Chatzistergos, G. Sapkas, and S. K. Kourkoulis. The influence of the insertion technique on the pullout force of pedicle screws. *Spine*, 35(9):E332–E337, 2010.

[105] American Society for Testing and Materials. ASTM F 1717: Standard test methods for spinal implant constructs in a vertebrectomy model. *ASTM International, West Conshohocken*, 2018.

[106] E. Christodoulou, S. Chinthakunta, D. Reddy, S. Khalil, T. Apostolou, P. Drees, and K. Kafchitsas. Axial pullout strength comparison of different screw designs: fenestrated screw, dual outer diameter screw and standard pedicle screw. *Scoliosis*, 10(15):1–7, 2015.

[107] P. E. Chatzistergos, E. A. Magnissalis, and S. K. Kourkoulis. A parametric study of cylindrical pedicle screw design implications on the pullout performance using an experimentally validated finite-element model. *Medical Engineering and Physics*, 32(2):145–154, 2010.

[108] C.-C. Hsu, C.-K. Chao, J.-L. Wang, S.-M. Hou, Y.-T. Tsai, and J. Lin. Increase of pullout strength of spinal pedicle screws with conical core: biomechanical tests and finite element analyses. *Journal of Orthopaedic Research*, 23(4):788–794, 2005.

[109] J. K. Biswas, T. P. Sahu, M. Rana, S. Roy, S. K. Karmakar, S. Majumder, and A. Roychowdhury. Design factors of lumbar pedicle screws under bending load: a finite element analysis. *Biocybernetics and Biomedical Engineering*, 39(1):52–62, 2019.

[110] K. Matsukawa, Y. Yato, T. Kato, H. Imabayashi, T. Asazuma, and K. Nemoto. In vivo analysis of insertional torque during pedicle screwing using cortical bone trajectory technique. *Spine*, 39(4):E240–E245, 2014.

[111] Q. H. Zhang, S. H. Tan, and S. M. Chou. Investigation of fixation screw pull-out strength on human spine. *Journal of Biomechanics*, 37(4):479–485, 2004.

[112] S.-M. Hou, C.-C. Hsu, J.-L. Wang, C.-K. Chao, and J. Lin. Mechanical tests and finite element models for bone holding power of tibial locking screws. *Clinical Biomechanics*, 19(7):738–745, 2004.

[113] G. La Rosa, C. Clienti, R. Mineo, and A. Audenino. Experimental analysis of pedicle screws. *Procedia Structural Integrity*, 2:1244–1251, 2016.

[114] Y. Amaritsakul, C.-K. Chao, and J. Lin. Biomechanical evaluation of bending strength of spinal pedicle screws, including cylindrical, conical, dual core and double dual core designs using numerical simulations and mechanical tests. *Medical Engineering and Physics*, 36(9):1218–1223, 2014.

[115] S. Pal, editor. *Design of artificial human joints & organs*. Springer Science and Business Media, 2014.

[116] J. Y. Rho, R. B. Ashman, and C. H. Turner. Young's modulus of trabecular and cortical bone material: ultrasonic and microtensile measurements. *Journal of Biomechanics*, 26(2):111–119, 1993.

[117] V. K. Goel, Y. E. Kim, T.-H. Lim, and J. N. Weinstein. An analytical investigation of the mechanics of spinal instrumentation. *Spine*, 13(9):1003–1011, 1988.

[118] M. Kutz, editor. *Standard handbook of biomedical engineering and design*, chapter "8 - Bone mechanics", pages 8.1–8.23. McGraw-Hill, 2003.

[119] M. Schünke, E. Schulte, and U. Schumacher, editors. *PROMETHEUS Lernatlas der Anatomie: Allgemeine Anatomie und Bewegungssystem*. Thieme, 4th edition, 2014.

[120] E. A. Hohn, B. Chu, A. Martin, E. Yu, C. Telles, J. Leasure, T. L. Lynch, and D. Kondrashov. The pedicles are not the densest regions of the lumbar vertebrae: Implications for bone quality assessment and surgical treatment strategy. *Global Spine Journal*, 7(6):567–571, 2017.

[121] Q. H. Zhang, S. H. Tan, and S. M. Chou. Effects of bone materials on the screw pull-out strength in human spine. *Medical Engineering and Physics*, 28(8):795–801, 2006.

[122] Y. P. Charles, H. Pelletier, P. Hydier, S. Schuller, J. Garnon, E. A. Sauleau, J.-P. Steib, and P. Clavert. Pullout characteristics of percutaneous pedicle screws with different cement augmentation methods in elderly spines: an in vitro biomechanical study. *Orthopaedics and Traumatology: Surgery and Research*, 101(3):369–374, 2015.

[123] H.-C. Chen, Y.-S. Lai, W.-C. Chen, J.-W. Chen, C.-M. Chang, Y.-L. Chen, S.-T. Wang, and C.-K. Cheng. Effect of different radial hole designs on pullout and structural strength of cannulated pedicle screws. *Medical Engineering and Physics*, 37(8):746–751, 2015.

[124] K.-S. Shih, C.-C. Hsu, S.-M. Hou, S.-C. Yu, and C.-K. Liaw. Comparison of the bending performance of solid and cannulated spinal pedicle screws using finite element analyses and biomechanical tests. *Medical Engineering and Physics*, 37(9):879–884, 2015.

[125] Q.-L. Li, C. Yun, S.-C. Li, and H.-S. Zhang. Three-dimensional finite element analysis of unilateral and bilateral pedicle screw fixation with intervertebral body fusion for degenerative lumbar instability. *International Journal of Clinical and Experimental Medicine*, 9(2):3457–3464, 2016.

[126] American Society for Testing and Materials. ASTM F 1839: Standard specification for rigid polyurethane foam for use as a standard material for testing orthopaedic devices and instruments. *ASTM International, West Conshohocken*, 2008.

[127] J. Benezech, B. Garlenq, and G. Larroque. Flexible stabilisation of the degenerative lumbar spine using PEEK rods. *Advances in Orthopedics*, 2016:1–7, 2016.

[128] K.-T. Kang, Y.-G. Koh, J. Son, J. S. Yeom, J.-H. Park, and H.-J. Kim. Biomechanical evaluation of pedicle screw fixation system in spinal adjacent levels using polyetheretherketone, carbon-fiber-reinforced polyetheretherketone, and traditional titanium as rod materials. *Composites Part B*, 130:248–256, 2017.

[129] S. M. Kurtz, T. H. Lanman, G. Higgs, D. W. MacDonald, S. H. Berven, J. E. Isaza, E. Phillips, and M. J. Steinbeck. Retrieval analysis of PEEK rods for posterior fusion and motion preservation. *European Spine Journal*, 22(12):2752–2759, 2013.

[130] C. Li, L. Liu, J.-Y. Shi, K.-Z. Yan, W.-Z. Shen, and Z.-R. Yang. Clinical and biomechanical researches of polyetheretherketone (PEEK) rods for semi-rigid lumbar fusion: a systematic review. *Neurosurgical Review*, 41(2):375–389, 2018.

[131] W.-K. Chou, A. Chien, and J.-L. Wang. Biomechanical analysis between PEEK and titanium screw-rods spinal construct subjected to fatigue loading. *Journal of Spinal Disorders and Techniques*, 28(3):E121–E125, 2015.

[132] J. K. Biswas, S. Roy, M. Rana, and S. Halder. A comparison of rigid, semi-rigid and flexible spinal stabilization devices: a finite element study. *Journal of Engineering in Medicine*, 233(12):1292–1298, 2019.

[133] C. Brecher, editor. *Advances in production technology*, chapter “10 - IMKS and IMMS – two integrated methods for the one-step-production of plastic/metal hybrid parts”, pages 131–141. Springer, 2015.

[134] U. Endemann, S. Glaser, and M. Völker. Kunststoff und Metall im festen Verbund. *Kunststoffe*, 92(11):110–113, 2002.

[135] Z. Wang, C. Lauter, B. Sanitther, A. Camberg, and T. Troester. Manufacturing and investigation of steel-CFRP hybrid pillar structures for automotive applications by intrinsic resin transfer moulding technology. *International Journal of Automotive Composites*, 2(3-4):229–243, 2016.

[136] M. Grujicic, V. Sellappan, M. A. Omar, N. Seyr, A. Obieglo, M. Erdmann, and J. Holzleitner. An overview of the polymer-to-metal direct-adhesion hybrid technologies for load-bearing automotive components. *Journal of Materials Processing Technology*, 197(1-3):363–373, 2008.

[137] C. Ochoa-Putman and U. K. Vaidya. Mechanisms of interfacial adhesion in metal-polymer composites – effect of chemical treatment. *Composites Part A*, 42(8):906–915, 2011.

[138] G. Habenicht, editor. *Kleben*. Springer, 6th edition, 2009.

[139] D. Nikolava. *Charakterisierung und Modifizierung der Grenzflächen im Polymer-Metall-Verbund*. Ph. D. thesis, Martin Luther University Halle-Wittenberg, 2005.

[140] S. Kisin. *Adhesion changes at metal-polymer interfaces: study of the copper-(acrylonitrile-butadiene-styrene) system*. Ph. D. thesis, Eindhoven University of Technology, 2006.

[141] W. Brockmann, P. L. Geiß, J. Klingen, and B. Schröder, editors. *Klebtechnik*, chapter “3 - Adhäsion”, pages 11–30. Wiley-VCH, 2005.

[142] J. Aurrekoetxea, G. Castillo, F. Cortes, M. A. Sarrionandia, and I. Urrutibeascoa. Failure of multimaterial fusion bonding interface generated during over-injection molding/thermoforming hybrid process. *Journal of Applied Polymer Science*, 102(1):261–265, 2006.

[143] M. B. Bouwman, T. Donderwinkel, E. Krämer, S. Wijskamp, and F. Costa. Over-molding – an integrated design approach for dimensional accuracy and strength of structural parts. In *Proceedings of the 3rd Annual Composites and Advanced Materials Expo (CAMX)*, Anaheim, United States, 2016.

[144] C. Ageorges, L. Yea, and M. Hou. Advances in fusion bonding techniques for joining thermoplastic matrix composites: a review. *Composites Part A*, 32(6):839–857, 2001.

[145] M. Fiorotto and G. Lucchetta. Experimental investigation of a new hybrid molding process to manufacture high-performance composites. *International Journal of Material Forming*, 6(1):179–185, 2013.

[146] P. G. de Gennes. Reptation of a polymer chain in the presence of fixed obstacles. *Journal of Chemical Physics*, 55(2):572–579, 1971.

[147] Y. H. Kim and R. P. Wool. A theory of healing at a polymer-polymer interface. *Macromolecules*, 16(7):1115–1120, 1983.

[148] R. P. Wool and K. M. O’Connor. A theory of crack healing in polymers. *Journal of Applied Physics*, 52(10):5953–5963, 1981.

[149] J.-F. Lamèthe, P. Beauchêne, and L. Léger. Polymer dynamics applied to PEEK matrix composite welding. *Aerospace Science and Technology*, 9(3):233–240, 2005.

[150] P. A. D. Rasmussen and J. M. Brown. Integral thermoset/thermoplastic composite joint. US patent US005667881A, Hughes Missile Systems Company, 1997.

[151] V. Dutschk. *Oberflächenkräfte und ihr Beitrag zu Adhäsion und Haftung in glasfaserverstärkten Thermoplasten*. Ph. D. thesis, Dresden University of Technology, 2000.

[152] J. Andrzejewski, P. Przyszczypkowski, and M. Szostak. Development and characterization of poly(ethylene terephthalate) based injection molded self-reinforced composites. Direct reinforcement by overmolding the composite inserts. *Materials and Design*, 153:273–286, 2018.

[153] G. Lucchetta, F. Marinello, and P. F. Bariani. Aluminum sheet surface roughness correlation with adhesion in polymer metal hybrid overmolding. *CIRP Annals – Manufacturing Technology*, 60(1):559–562, 2011.

[154] P. M. Charlson, C. R. Schwieters, and J. H. Souk. Laser joining of thermoplastic and thermosetting materials. US patent US4414166A, International Business Machines Corp., 1983.

[155] S. Deng, L. Djukic, R. Paton, and L. Ye. Thermoplastic-epoxy interactions and their potential applications in joining composite structures – a review. *Composites: Part A*, 68:121–132, 2015.

[156] H. Paul, M. Luke, and F. Henning. Kunststoff-Metall-Hybridverbunde – Experimentelle Untersuchungen zum Verformungs- und Versagensverhalten. *Zeitschrift Kunststofftechnik*, 10(4):117–141, 2014.

[157] S. T. Amancio-Filho and J. F. dos Santos. Joining of polymers and polymer-metal hybrid structures: recent developments and trends. *Polymer Engineering and Science*, 49(8):1461–1476, 2009.

[158] C. Zinn, M. Bobbert, C. Dammann, Z. Wang, T. Tröster, R. Mahnken, G. Meschut, and M. Schaper. Shear strength and failure behaviour of laser nano-structured and conventionally pre-treated interfaces in intrinsically manufactured CFRP-steel hybrids. *Composites Part B*, 151:173–185, 2018.

[159] J. Altmeyer, U. F. H. Suhuddin, J. F. dos Santos, and S. T. Amancio-Filho. Microstructure and mechanical performance of metal-composite hybrid joints produced by fricriveting. *Composites Part B*, 81:130–140, 2015.

[160] T. Joppich, A. Menrath, and F. Henning. Advanced molds and methods for the fundamental analysis of process induced interface bonding properties of hybrid,

thermoplastic composites. In *Procedia CIRP 66 – 1st Cirp Conference on Composite Materials Parts Manufacturing (Cirp-CCMPM)*, Karlsruhe, Germany, 2017.

[161] W. Krause, O. Geiger, F. Henning, and P. Eyerer. Development of a technology for large scale production of continuous fiber reinforced thermoplastic composites. In *Proceedings of the SPE Annual Technical Conference ANTEC*, Boston, MA, USA, 2005.

[162] K. Tanaka, K. Karasuno, N. Ryuichi, and T. Katayama. Effects of press pressure on the mechanical properties of rib root for glass fiber reinforced polypropylene composites, molded by press and injection hybrid molding. *WIT Transactions on Engineering Sciences*, 116:317–326, 2017.

[163] W. J. Cantwell, P. Davies, P. E. Bourban, P.-Y. Jar, H. Richard, and H. H. Kausch. Thermal joining of carbon fibre reinforced PEEK laminates. *Composite Structures*, 16(4):305–321, 1990.

[164] M. Gupta and K. K. Wang. Fiber orientation and mechanical properties of short-fiber-reinforced injection-molded composites: simulated and experimental results. *Polymer Composites*, 14(5):367–382, 1993.

[165] K. Tanaka, Y. Fujita, and T. Katayama. Press and injection hybrid molding of glass fiber reinforced thermoplastics. *WIT Transactions on Engineering Sciences*, 90:225–232, 2015.

[166] G. W. Ehrenstein, S. Amesöder, L. Fernández Díaz, H. Niemann, and R. Deventer. Werkstoff- und prozessoptimierte Herstellung flächiger Kunststoff-Kunststoff und Kunststoff-Metall-Verbundbauteile. In *Proceedings of the Report and Industry Colloquium 2003 of SFB 396*, Bamberg, Germany, 2003.

[167] K. Ramani and B. Moriarty. Thermoplastic bonding to metals via injection molding for macro-composite manufacture. *Polymer Engineering and Science*, 38(5):870–877, 1998.

[168] F. J. Ferfecki, M. Tanaka, S. Chung, and D. Hayduke. Performance and simulation of a thermoplastic PAEK hybrid composite system. In *Proceedings of the 3rd International Conference and Exhibition on Thermoplastic Composites*, Bremen, Germany, 2016.

[169] H. Kazan, S. Farahani, and S. Pilla. Feasibility study for manufacturing CF/Epoxy - thermoplastic hybrid structures in a single operation. *Procedia Manufacturing*, 33:232–239, 2019.

[170] B. Beck, J. Haas, and H. Tawfik. Three-dimensional fiber skeleton. *Kunststoffe International*, 2019(9):114–116, 2019.

[171] T. Menovsky, T. Asal, M. Steffens, S. Llas Vargas, P. Garcia Roig, M. Charles-Harris Ferrer, M. Serrahima Tornel, M. Gurka, and T. Becker. Clip for aneurism. US patent US2018/0008275A1, Neos Surgery S. L., 2018.

[172] M. Moumene, J. Fanger, C. M. Bartish Jr., M. J. O'Neil, A. Upal, S. Connolly, J. R. Hawkins, and M. A. Slivka. Polymeric pedicle rods and methods of manufacturing. US patent US9232968B2, DePuy Synthes Products, Inc., 2016.

[173] Invibio Ltd. PEEK-Optima specification grade LT1CA30. Material data sheet, June 2014.

[174] Victrex plc. A comprehensive review of the materials properties of VICTREX® PEEK™ high performance polymer. Material properties guide.

[175] Thyssenkrupp AG. Titan grade 5 (Ti6Al4V). Material data sheet, May 2018.

[176] American Society for Testing and Materials. ASTM F 2193: Standard specification and test methods for components used in the surgical fixation of the spinal skeletal system. *ASTM International, West Conshohocken*, 2014.

[177] Deutsches Institut für Normung e. V. DIN EN ISO 14630: Nichtaktive chirurgische Implantate – allgemeine Anforderungen. *DIN e. V., Berlin*, 2013.

[178] Deutsches Institut für Normung e. V. DIN EN 828: Kunststoffe – Verfahren zur Bestimmung der Dichte von nicht verschäumten Kunststoffen – Teil 1: Eintauchverfahren, Verfahren mit Flüssigkeitspyknometer und Titrationsverfahren. *DIN e. V., Berlin*, 2013.

[179] Victrex plc. VICTREX® PEEK 450CA30. Material data sheet, March 2016.

[180] Invibio Ltd. Endolign® composite rod grade LT3CR4. Material data sheet and certificate of analysis, December 2013.

[181] Victrex plc. VICTREX® PEEK 150P. Material data sheet, July 2014.

[182] Hexcel Corp. HexTow® AS4A carbon fiber. Product data sheet, 2016.

[183] S. Versavaud. E-mail information concerning the fibre type of VICTREX® PEEK 450CA30, 11 March 2019.

[184] Q. Wang and G. S. Springer. Moisture absorption and fracture toughness of PEEK polymer and graphite fiber reinforced PEEK. *Journal of Composite Materials*, 23(5):434–447, 1989.

[185] B. Wunderlich, editor. *Thermal analysis of polymeric materials*. Springer, 2005.

[186] A. F. Grand and C. A. Wilkie, editors. *Fire retardancy of polymeric materials*. Marcel Dekker, Inc., 2000.

[187] F. Hache, M. Delichatsios, T. Fateh, and J. Zhang. Comparison of methods for thermal analysis: Application to PEEK and a composite PEEK+CF. *Journal of Fire Sciences*, 33(3):232–246, 2015.

[188] X. Jin, M. T. Bishop, T. S. Ellis, and F. E. Karasz. A sulphonated poly(aryl ether ketone). *British Polymer Journal*, 17(1):4–10, 1985.

[189] L. H. Perng, C. J. Tsai, and Y. C. Ling. Mechanism and kinetic modelling of PEEK pyrolysis by TG/MS. *Polymer*, 40(26):7321–7329, 1999.

[190] Mettler-Toledo GmbH. Thermal analysis – MaxRes. Data sheet, October 2003.

[191] A. Haufler. E-mail information concerning the order of unidirectional endless CF-PEEK plate, 5 May 2017.

[192] Deutsches Institut für Normung e. V. DIN EN 1465: Klebstoffe – Bestimmung der Zugscherfestigkeit von Überlappungsklebungen. *DIN e. V., Berlin*, 2009.

[193] B. Thielicke. *Die Ermittlung der interlaminaren Scherfestigkeit von kohlenstoffaserverstärkten Kohlenstoffen mit dem Druck-Scherversuch im Temperaturbereich zwischen Raumtemperatur und 2000°C*. Ph. D. thesis, Fraunhofer-Institut für Werkstoffmechanik, Karlsruhe Institute of Technology, 1997.

[194] Deutsches Institut für Normung e. V. DIN EN 828: Klebstoffe – Benetzbarkeit – Bestimmung durch Messung des Kontaktwinkels und der freien Oberflächenenergie fester Oberflächen. *DIN e. V., Berlin*, 2013.

[195] American Society for Testing and Materials. ASTM D 695: Standard test method for compressive properties of rigid plastics. *ASTM International, West Conshohocken*, 2002.

[196] American Society for Testing and Materials. ASTM D 3846: Standard test method for in-plane shear strength of reinforced plastics. *ASTM International, West Conshohocken*, 2002.

[197] M. Godani, M. Gaiotti, and C. M. Rizzo. Interlaminar shear strength of marine composite laminates: tests and numerical simulations. *Composite Structures*, 112:122–133, 2014.

[198] Akro-Plastic GmbH. AKROTEK® PEEK CF 30 black. Material data sheet, February 2015.

[199] C.-L. Liu, H.-H. Chen, C.-K. Cheng, H.-C. Kao, and W.-H. Lo. Biomechanical evaluation of a new anterior spinal implant. *Clinical Biomechanics*, 13(1, Suppl 1):S40–S45, 1998.

[200] E. M. Feerick and P. McGarry. Computational study of cortical bone screw pullout using the extended finite element method (XFEM). *SIMULIA Community Conference*, 2012.

[201] J. Yang and H.-J. Xiang. A three-dimensional finite element study on the biomechanical behavior of an FGBM dental implant in surrounding bone. *Journal of Biomechanics*, 40(11):2377–2385, 2007.

[202] C.-C. Hsu, C.-K. Chao, J.-L. Wang, and J. Lin. Multiobjective optimization of tibial locking screw design using a genetic algorithm: evaluation of mechanical performance. *Journal of Orthopaedic Research*, 24(5):908–916, 2006.

[203] X. Ding, X.-H. Zhu, S.-H. Liao, X.-H. Zhang, and H. Chen. Implant-bone interface stress distribution in immediately loaded implants of different diameters: a three-dimensional finite element analysis. *Journal of Prosthodontics*, 18(5):393–402, 2009.

[204] P. S. D. Patel, D. E. T. Shepherd, and D. W. L. Hukins. The effect of screw insertion angle and thread type on the pullout strength of bone screws in normal and osteoporotic cancellous bone models. *Medical Engineering and Physics*, 32(8):822–828, 2010.

[205] J.-J. Chen and Y.-S. Shih. A study of the helical effect on the thread connection by three dimensional finite element analysis. *Nuclear Engineering and Design*, 191(2):109–116, 1999.

[206] Simulia (Dassault Systèmes SE). Abaqus analysis user's guide, 2016.

[207] W.-C. Tsai, P.-Q. Chen, T.-W. Lu, S.-S. Wu, K.-S. Shih, and S.-C. Lin. Comparison and prediction of pullout strength of conical and cylindrical pedicle screws within synthetic bone. *BMC Musculoskeletal Disorders*, 10(44):1–9, 2009.

[208] American Society for Testing and Materials. ASTM F 543: Standard specification and test methods for metallic medical bone screws. *ASTM International, West Conshohocken*, 2007.

[209] Sawbones Corporate Headquarters. Sawbones® biomechanical test materials. Material data sheet, April 2017.

[210] K. Okuyama, E. Abe, T. Suzuki, Y. Tamura, M. Chiba, and K. Sato. Can insertional torque predict screw loosening and related failures? *Spine*, 25(7):858–864, 2000.

[211] A. W. L. Kwok, J. A. Finkelstein, T. Woodside, T. C. Hearn, and R. W. Hu. Insertion torque and pull-out strengths of conical and cylindrical pedicle screws in cadaveric bone. *Spine*, 21(21):2429–2434, 1996.

Publications and conferences

Contents of this work have been published in the following journals and conference proceedings:

- Y. N. Becker, U. P. Breuer, J. Hausmann, and N. Motsch. Hybrid composite pedicle screw – finite element modelling with parametric optimization. Informatics in Medicine Unlocked, 18:1-11, 2020.
- Y. N. Becker, N. Motsch, and J. Hausmann. A new hybrid concept for CFRP pedicle screws: finite element analysis. In Proceedings of the 21st International Conference on Composite Materials (ICCM21), Xi'an, China, 20-25 August 2017.
- Y. N. Becker. Pedikelschraubensystem aus Verbundwerkstoff zum Einsatz im lumbalen Wirbelsäulenbereich. Carbon Composites Magazin, 2:48, 2018.
- Y. N. Becker. Numerical analysis of a metal-free pedicle screw system for the use in human lumbar spine. In Proceedings of the Young Researchers Symposium 2018 (YRS 2018), Kaiserslautern, Germany, 22 June 2018.
- Y. N. Becker, N. Motsch, and J. Hausmann. Numerical investigation and design optimization of a hybrid CFRP pedicle screw system. In 21st International Conference on Composite Structures (ICCS21), Bologna, Italy, 4-7 September 2018.
- Y. N. Becker, N. Motsch, and J. Hausmann. Development of a new hybrid composite pedicle screw: numerical and experimental investigation. In 9th International Conference on Composites Testing and Model Identification (CompTest), Luleå, Sweden, 27-29 May 2019.
- Y. N. Becker, N. Motsch, and U. P. Breuer. Examination of the interface strength of hybrid, overmoulded, thermoplastic composite parts. In Proceedings of the 22nd International Conference on Composite Materials (ICCM22), Melbourne, Australia, 11-16 August 2019.

Symposia

Contents of this work have been discussed at the following symposia:

- Y. N. Becker. Entwicklung eines metallfreien Pedikelschraubensystems. Carbon Composites, Gemeinsame Sitzung der AG-Thermoplastische Composites und der AG-Multi-Material-Design, Dresden, Germany, 8 May 2018.
- Y. N. Becker, N. Motsch, and J. Hausmann. Insights in the development of a new hybrid CFRP pedicle screw system: numerical investigation and design optimization. DVM Arbeitskreis “Zuverlässigkeit von Implantaten und Biostrukturen”, Berlin, Germany, 18-20 October 2018.
- Y. N. Becker. Chancen und Herausforderungen – Entwicklung eines hybriden CFK-Pedikelschraubensystems. Carbon Composites, Thementag “Herausforderung CFK in der Medizinbranche”, Duderstadt, Germany, 18 June 2019.
- Y. N. Becker. Composite pedicle screw system with a function optimized configuration. DVM Arbeitskreis “Zuverlässigkeit von Implantaten und Biostrukturen”, Rostock, Germany, 27-28 November 2019.

Student theses

Within the scope of this work, the following student theses have been supervised:

- P. Gehrke. Experimentelle und numerische Untersuchung der Anbindung von kurzfaserverstärktem CF/PEEK Spritzgussmaterial an einem UD-verstärkten CF/PEEK-Einleger. Masterarbeit, Kaiserslautern, Germany, IVW-Bericht 17-074, 2017
- S. Sathianarayanan. Dreidimensionale Designoptimierung eines neuartigen CF/PEEK Pedikelschraubensystems. Studienprojekt, Kaiserslautern, Germany, IVW-Bericht, 2018
- M. Baur. Finite Elemente Simulation zur Optimierung einer Pedikelschraube für die medizintechnische Anwendung im lumbalen Wirbelsäulenbereich. Studienarbeit, Kaiserslautern, Germany, IVW-Bericht 18-007, 2018
- J. Nikola. Charakterisierung chemischer, thermischer und mechanischer Eigenschaften von CF-PEEK. Studienarbeit, Kaiserslautern, Germany, IVW-Bericht 18-034, 2018
- R. da Silva Cirolini. Experimentelle und numerische Untersuchung eines hybriden faserverstärkten Thermoplast-Thermoplast-Verbunds. Studienarbeit, Kaiserslautern, Germany, IVW-Bericht 19-018, 2019

Curriculum vitae

Personal information

Yves Nicolas Becker

Born in Homburg (Saar), Germany

German

Secondary education

2002-2010	Saarpfalz-Gymnasium, Homburg (Saar), Germany, degree: Allgemeine Hochschulreife

Academic education

2010-2016	Mechanical engineering. Kaiserslautern University of Technology, Germany, degree: Diplom-Ingenieur (Dipl.-Ing.)
2012-2013	Mechanical engineering. Luleå University of Technology, Sweden
2014-2015	Portuguese. Pontifical Catholic University of Paraná, Curitiba, Brazil

Professional experience

2013-2016	Student assistant. Institute of Machine Elements, Gears and Transmissions. Kaiserslautern University of Technology, Germany
2015-2016	Student assistant. Institut für Verbundwerkstoffe GmbH, department "Component Development". Kaiserslautern, Germany
Since 2016	Scientific assistant. Institut für Verbundwerkstoffe GmbH, department "Component Development". Kaiserslautern, Germany

Homburg (Saar), May 2020